Charles University in Prague

Faculty of Science

Department of Biochemistry

Mgr. Kseniya Ustinova

Substrate specificity of histone deacetylases

Substrátová specifita histondeacetylas

DISSERTATION THESIS

Supervisor: RNDr. Cyril Bařinka, Ph.D.

Prague, 2020

Prohlášení

Prohlašuji, že jsem závěrečnou práci zpracovala samostatně pod vedením RNDr. Cyrila Bařinky, PhD. a všechny použité prameny jsem řádně citovala. Tato práce ani její podstatná část nebyla použita k získání jiného nebo stejného akademického titulu.

Declaration

I hereby state that I have completed this thesis as an independent work and that I have properly cited all literature and other information sources I have used. Neither this thesis nor its parts have been submitted to achieve the same or any other academic title.

V Praze / In Prague, ...

Kseniya Ustinova

Student contribution

Student Kseniya Ustinova has contributed to the advancement of knowledge in her scientific discipline - substrate specificity of histone deacetylases. She has successfully published her first-author paper. She has conducted the main part of the experiments and has written the draft of the manuscript. Moreover, she contributed to other studies focused on HDAC6 interaction with tubulin as well as on the development of highly selective HDAC6 inhibitor.

Publication 1

Skultetyova L., Ustinova K., Kutil Z., Novakova Z., Pavlicek J., Mikesova J., Trapl D., Baranova, P., Havlinova B., Hubalek M., Lansky Z., Barinka C.: **Human histone deacetylase 6 shows strong preference for tubulin dimers over assembled microtubules.** *Sci Rep* **2017**, 7:11547.

While working on this manuscript, the Ph.D. student has designed and carried out microscopy-related experiments, evaluated, and interpreted TIRF microscopy data, designed the figures, and participated in the manuscript preparation. I suggest that the student`s contribution to this manuscript is 20%.

Publication 2

Shen S., Hadley M., Ustinova K., Pavlicek J., Knox T., Noonepalle S., Tavares M.T., Zimprich Ch.A., Zhang G., Robers M.B., Bařinka C., Kozikowski A.P., Villagra A.: **Discovery of a new isoxazole-3-hydroxamate-based histone deacetylase 6 inhibitor SS-208 with antitumor activity in syngeneic melanoma mouse models.** *J Med Chem* **2019**, 62 (18): 8557-8577.

The Ph.D. student has determined, refined, and analyzed the X-ray structure of the *D.rerio* HDAC6 catalytic domain in complex with the SS-208 inhibitor. She has contributed to the writing of the manuscript. I assume that the student`s contribution to this manuscript is 20%.

In Prague, ...

RNDr. Cyril Barinka, Ph.D.

Abstract

In the cell, tubulin undergoes post-translational modifications that create functionally distinct microtubules and mark them for specialized functions. Acetylation of Lys40 of α-tubulin is one of such post-translational modifications controlled by the activity of histone deacetylase 6 (HDAC6). The Lys40 acetylation is a hallmark of stable microtubules, it protects them from mechanical aging, influences cell motility as well as axonal branching and maintenance of neuronal processes. Tubulin stands out as the most prominent physiological substrate for HDAC6. Being a multidomain cytosolic protein, HDAC6 is involved in the myriad of cellular processes and is a promising target for the treatment of cancer and neurodegenerative diseases. The understanding of the mechanisms of HDAC6 interactions with its substrates, especially with tubulin, can open avenues for the development of new treatment strategies exploiting highly selective HDAC6 inhibitors.

In this thesis, we have investigated the molecular basis of tubulin recognition by HDAC6. We provided a detailed kinetic analysis showing the HDAC6 deacetylation rate of free tubulin is 1500-fold faster than microtubules. Additionally, we have shown that amino acids of the flexible Lys40 loop (except P1 and P-1) make a minor contribution to the substrate recognition by HDAC6, while the more important role can be assigned to residues at the longitudinal and lateral interactions between tubulin dimers. Moreover, we visualized the direct binding of HDAC6 to microtubules and qualitatively/quantitatively mapped HDAC6 binding to microtubules. Here we identified the N-terminus of HDAC6 to be the microtubule-binding domain (MBD), showing that HDAC6/tubulin (microtubules) interactions are driven by ionic (electrostatic) forces. Interestingly, while HDAC6 binding to microtubules is not dependent on its deacetylation activity, the presence of MBD enhances tubulin deacetylation more that 100-folds. Our results thus provide mechanistic underpinnings on the recognition of tubulin/microtubules by HDAC6.

Using our biochemical and X-ray crystallography expertise, we have also contributed to the development of SS-208, an HDAC6-specific inhibitor harboring an isoxazole moiety as a zinc-binding group. This inhibitor is highly specific for HDAC6 and only modestly potent against HDAC1. *In vivo* studies revealed that SS-208 impairs tumor growth by mediating immune-related tumor destruction rather than by the direct cytotoxic effect on tumor cells.

Abstrakt

Tubulin v buňce podléhá posttranslačním modifikacím, jež vytvářejí funkčně odlišné mikrotubuly a označují je pro specializované funkce. Jednou z takovýchto posttranslačních modifikací je acetylace Lys40 α-tubulinu, která je řízena aktivitou histondeacetylasy 6 (HDAC6). Acetylace Lys40 je charakteristickým znakem stabilních mikrotubulů. Chrání je před mechanickým stárnutím, ovlivňuje pohyblivost buněk, jakož i větvení axonů a stabilizaci dendritů. Tubulin vyniká jako nejvýznamnější fyziologický substrát pro HDAC6. HDAC6 je multidoménovým cytosolickým proteinem podílejícím se na nesčetných buněčných procesech a je slibným cílem léčby rakoviny a neurodegenerativních chorob. Pochopení mechanismů interakce HDAC6 s jeho substráty, zejména s tubulinem, může otevřít cestu pro vývoj nových léčebných strategií využívajících vysoce selektivní inhibitory HDAC6.

V této práci jsme zkoumala molekulární podstatu jak HDAC6 rozpoznává tubulin. Naše detailní kinetická analýza ukazuje, že deacetylace volného tubulinu pomocí HDAC6 je 1500krát rychlejší než deacetylace mikrotubulů. Dále jsme ukázali, že na rozdíl od aminokyselin podílejících se na podélných a laterálních interakcích mezi tubulinovými dimery, aminokyseliny flexibilní smyčky obsahující Lys40 (s výjimkou míst P1 a P-1) příliš nepřispívají k rozpoznávání substrátu pomocí HDAC6. Kromě toho jsme ukázali přímou vazbu HDAC6 na mikrotubuly a kvalitativně i kvantitativně tuto vazbu zmapovali. Také jsme identifikovali N-konec HDAC6 jako doménu vázající se na mikrotubuly (MBD), a ukázali, že interakce HDAC6 s tubulinem (mikrotubuly) jsou řízeny iontovými (elektrostatickými) silami. Je zajímavé, že zatímco vazba HDAC6 na mikrotubuly nezávisí na jeho deacetylační aktivitě, přítomnost MBD zvyšuje deacetylaci tubulinu více než 100krát. Naše výsledky tak poskytují základní informace o mechanismu rozpoznávání tubulinu resp. mikrotubulů pomocí HDAC6.

Naše zkušenosti s biochemickými metodami a rentgenovou krystalografií jsme se také využili při vývoji specifického inhibitoru pro HDAC6 (SS-208), jenž obsahuje skupinu vázající zinek na bázi hydroxamátu isoxazolu. Tento inhibitor je vysoce specifický pro HDAC6 asoučasně slabě inhibuje HDAC1. Experimenty *in vivo* ukázaly, že SS-208 omezuje růst nádoru tím, že podporuje protinádorovou imunitní reakci, aniž by vykazoval přímý cytotoxický efekt vůči nádorovým buňkám.

Acknowledgment

First and foremost I want to express my gratitude to my supervisor Cyril Bařinka. It has been an honor to be his Ph.D. student. He took me to his laboratory knowing that I must learn everything from scratch. Being strict but fair and with lots of patience to me, he managed to make me a skillful student. Moreover, I appreciate his willingness to dedicate his time so generously. Under his great lab management, the laboratory has evolved into a very friendly community sharing not only work but leisure – team-buildings became memorable events and a source of funny stories.

I am grateful to the many people with whom I have had the pleasure to work during this and other related projects. I would also like to extend my thanks to all members of our laboratory. They have been a source of good advice as well as fun and support. I would like to thank Bara for showing that there are no unsolvable situations, Kuba and Jana M. for their great sense of humor, Zorka and Zsofka for their support and advice. I have had a pleasure to work with Jana N., Péťa, Shivam and Iva.

I am also pleased to say thank you to Verena who was always side-by-side with me – in Ph.D. studies as well as in personal life. With her encouragement and continuous optimism, these five years became much brighter for me. Further, I would like to give special thanks to Tania and Lena for the unconditional acceptance of me and the wonderful moments we shared.

And my biggest thanks to my family for all love, support, and encouragement you have given to me through this research. I am grateful to my mom for her care, investment in my education, giving me the opportunities and experiences that have made me who I am. I am grateful for the presence of my brother Sasha in Prague for the last year of my studies.

Once again, I would like to appreciate the invaluable help and assistance that all people mentioned above provided me during my study.

Abbreviations

α-TAT	alpha-tubulin N-acetyltransferase
BUZ	binding of ubiquitin zinc finger
CTCL	cutaneous T-cell lymphoma
CYLD	cylindromatosis tumor suppressor protein
DD1	first deacetylase domain
DD2	second deacetylase domain
DMB	dynein motor binding site
EGF	epidermal growth factor
ERα	estrogen receptors α
GSK3β	glycogen synthase kinase 3 beta
HATs	histone acetyltransferases
HDAC1	histone deacetylase 1
HDAC6	histone deacetylase 6
HDACs	histone deacetylases
Hsp90	heat shock protein 90
K40	lysine 40
MAPK	mitogen-activated protein kinase
MAPs	microtubule-associated proteins
MBD	microtubule-binding domain
MST	Microscale Thermophoresis
NES	nuclear export signal
NF-kB	nuclear factor-kB
NLS	nuclear localization signal
p300	histone acetyltransferase p300
p53	p53 tumor suppressor protein
PTCL	peripheral T-cell lymphoma
PD-L1	programmed death receptor ligand 1
PD-1	programmed death receptor 1
Prx	peroxiredoxin
PTMs	post-translational modifications
RanBPM	Ran-binding protein M
PDB	Protein Data Bank
p97	AAA-ATPase chaperone p97
SAHA	suberoylanilide hydroxamic acid, Vorinostat
SE14	serine-glutamate tetradecapeptide
TIRF microscopy	total internal reflection fluorescence microscopy
TSA	Trichostatin A
US FDA	United States Food and Drug Administration
ZBG	zinc binding group

Table of Contents

1 Introduction

1.1 Histone deacetylases – historical overview

Histone deacetylases (HDACs) are an important class of enzymes catalyzing the removal of the acetyl group from ε-N-acetyl-lysine residues of histones causing the increase in their positive charge and subsequently increasing the binding between histones and DNA. The name of this class was suggested by Taunton et al., (1) who have discovered the first representative of the HDAC family. He hypothesized that these enzymes are involved in the alteration of histone acetylation status and this hypothesis has been confirmed experimentally later (2). With the discovery of many non-histone substrates, HDACs became also known as lysine deacetylases – KDACs. The name "HDACs" is remaining the most common and will be used throughout this thesis. Together with histone acetyltransferases (HATs) (EC 2.3.1.48), HDACs (EC 3.5.1.98) form a fine-tuned system (3,4). involved in epigenetic regulation, cell cycle progression, and cell development (5).

HDACs are grouped into four classes based on their sequence homology to yeast histone deacetylases. Nowadays, 10 HDAC members are identified in *Saccharomyces cerevisiae*, 11 members – in *Caenorhabditis elegans,* and 18 members – in humans (6). Class I, II (IIa and IIb), and IV are zinc-dependent enzymes, while the class III is NAD+ dependent (7) (**Figure 1**).

Class I HDACs are Rpd3-like proteins of around 55 kDa molecular weight (HDAC1, HDAC2, HDAC3, and HDAC8) exclusively found in the nucleus as they harbor a nuclear localization signal (NLS) (8,9). The exception is HDAC3 that has both a nuclear export signal (NES) and NLS. Class II are Hda1-like proteins of molecular weight around 110 kDa which are divided into two subclasses based on their domain organization. The class IIa (HDAC4, HDAC5, HDAC7, HDAC9) shuttles between the cytoplasm and the nucleus. This translocation is controlled by calmodulin-dependent kinase-mediated phosphorylation (10,11). Additionally, the class IIa exerts weaker deacetylation activity compared to other family members (12). Members of the class IIb are predominantly localized to the cytoplasm and deacetylate non-histone substrates. The members of this subclass are HDAC6 (the major focus of this work) and HDAC10. The class III comprises the NAD + -dependent Sir2-like proteins (SIRT1, SIRT2, SIRT3, SIRT4, SIRT5, SIRT6, and SIRT7) that have distinct catalytic mechanisms from zinc-dependent HDACs. The class IV contains only a single member, HDAC11 – the smallest HDAC isoform discovered by Gao et al in 2002 (13) that shuttles between the nucleus and the cytoplasm. Its sequence similarity with other HDACs is limited, however, HDAC11 contains conserved residues in the catalytic core similar to class I and II HDACs (13).

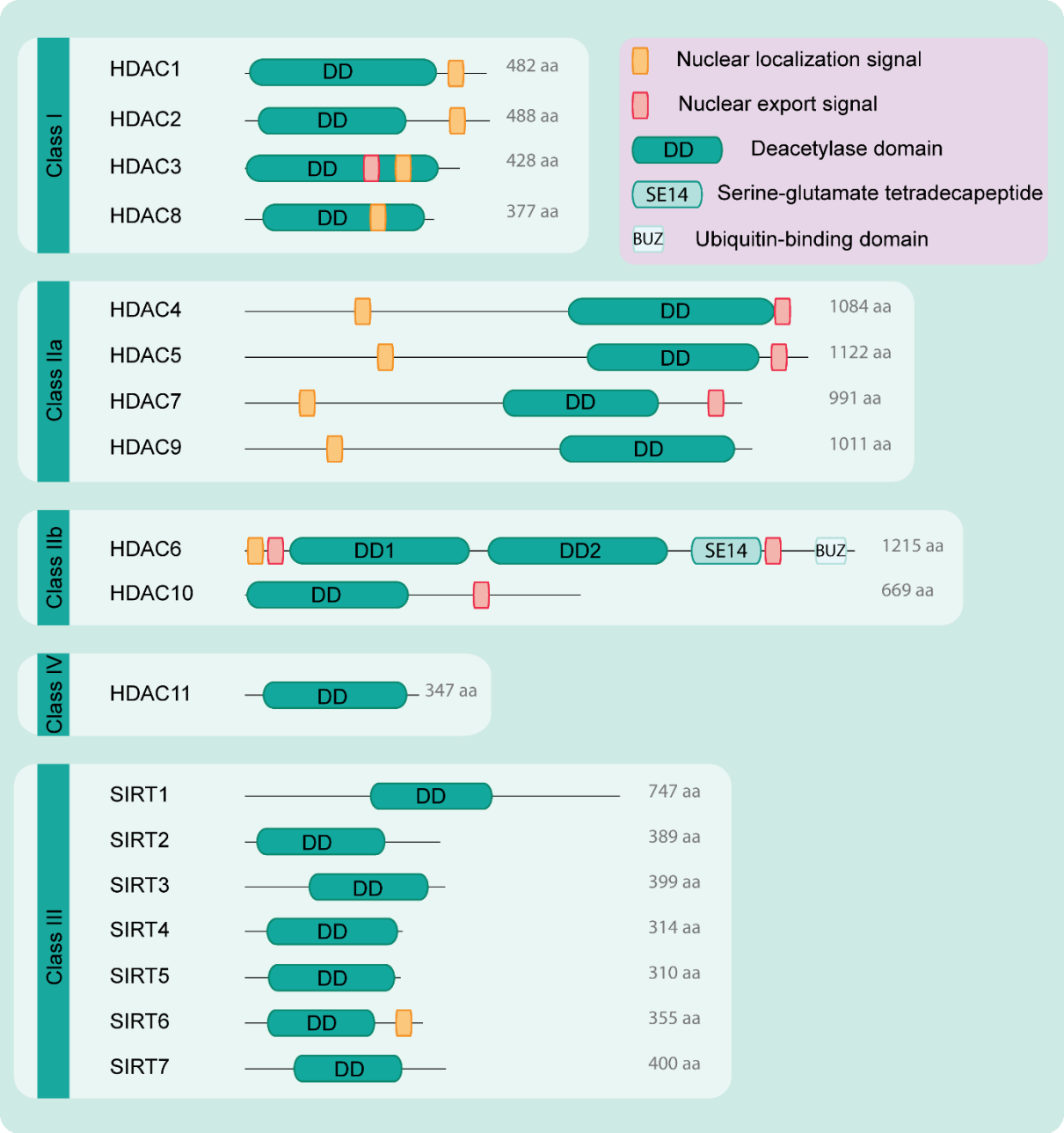

Figure 1. Schematic representation of domain structure of human HDAC isoenzymes. Classes I, II, and IV are zinc-dependent enzymes. Class III is represented by sirtuins, which activity depends on nicotinamide adenine dinucleotide. Most HDACs possess a single deacetylase domain, a nuclear localization signal (NLS) (translocates proteins into nucleus) and/or nuclear export signal (prevents the accumulation of the protein in the nucleus). The exception is HDAC6 comprising two tandem deacetylase domains (DD1 and DD2). Ser-Glu-containing tetradecapeptide (SE14) region ensures stable anchorage of HDAC6 in the cytoplasm. HDAC6 contains a high affinity ubiquitin-binding zinc finger domain (BUZ).

In our studies, we have focused on HDAC6 – a unique representative of the HDAC family with two homologous catalytic domains. HDAC6 affects the function of cytoplasmic proteins and is thus an important regulator of many signaling pathways that are linked to cancer.

The *HDAC6* gene is located on the X-chromosome p11.22-23 locus and is composed of 28 exons (14,15). The translation of this gene leads to the production of HDAC6 protein of 131 kDa. HDAC6 is a 1215 amino acid protein discovered in 1999 by Verdel and Khochbin (mouse HDAC6) (16) followed by the discovery of its human ortholog by Grozinger et al., (17). It is a unique family member harboring duplication of class I/II HDAC-homology domain that became a hallmark of HDAC6 while searching for its orthologs from other species including *Drosophila melanogaster*, *C.elegans* and *Arabidopsis thaliana* (18,19). Distinct from its orthologs, human HDAC6 has the SE14-domain at the C-terminus. A more detailed description of the HDAC6 domain organization is discussed in the next chapter.

While undergoing alternative splicing, two isoforms of HDAC6 can be found in the cell - HDAC6p131 and HDAC6p114. The HDAC6p131 has been chosen as the canonical sequence of HDAC6. The HDAC6p114 is a protein with a molecular mass of 114 kDa. It is missing the first 152 amino acid residues and is required for transforming growth factor-β1-activated gene expression associated with epithelial-mesenchymal transition (20).

According to the tissue-based map of the human proteome, expression levels of HDAC6 are high in testis, breast, and skin (21). HDAC6 expression can be transcriptionally affected under certain conditions. Estrogen up-regulates HDAC6 expression in estrogen receptor-positive breast cancer cells causing an estrogen-induced increase in cell motility (22). Furthermore, HDAC6 expression can be induced upon oncogenic Ras transformation and is required for efficient tumorigenesis (23).

1.1.1 HDAC6 domain organization and function

The N-terminal domain of human HDAC6 (EC 3.5.1.98) is the intrinsically disordered region present in orthologs across various species (amino acids 1-83). It shows a high degree of phylogenetic conservation. However, the function of the N-terminal domain remains unknown. It harbors an NLS (amino acids 14-59) and regulates HDAC6 nuclear import (Figure 2). Moreover, HDAC6 contains two leucine-rich NES (NES1, NES2) that determine and govern its constant cytoplasmic localization (Figure 2). NES1 is placed at the amino terminus of human HDAC6 at the residues 67-76 and is conserved in the mouse ortholog of HDAC6 (amino acids 55-104) (24). NES2 is sited at amino acid residues 1049-1058 of human HDAC6. NES2 is less conserved and nonfunctional in the mouse ortholog of HDAC6 (25). The control of the subcellular localization of HDAC6 has an impact on the HDAC6 functions. Verdel et al., have shown that the mutation in the NES1 arrested mouse HDAC6 shuttle to the cytoplasm, causing its accumulation in the nucleus (24). It was hypothesized that the post-translational modifications (PTMs) of amino acids around the NES motif might play the role in masking the NES and inducing its nucleus accumulation.

Furthermore, nuclear/cytoplasm shuttling of HDAC6 might be regulated by the acetylation status of two clusters of lysine residues located at the N-terminus. Acetylation of these clusters by histone acetyltransferase p300 (p300) can regulate tubulin deacetylase activity of HDAC6 as well as its nuclear import (26). The acetylation of two lysine clusters and even only the second lysine cluster abolishes the nuclear localization signal, resulting in the retention of HDAC6 in the cytoplasm. The interaction of importin-α with the N-terminal part of HDAC6 blocks the acetylation of lysine clusters at N-terminus and influences the nuclear/cytoplasm shuttling of HDAC6 (26).

HDAC6 is a unique member of the class IIb mammalian HDAC as HDAC6 contains two homologous deacetylase domains. The interplay between these two domains is required for efficient substrate deacetylation. Scientists have been investigating the role of each catalytic domain of HDAC6 for many years, interrogating their function and activity. It is not clear yet what is the exact role of each catalytic domain. Experiments with inactive mutants of each domain did not give simple but rather opposite answers. Grozinger et al., 1999 showed that both domains have independent catalytic activity towards histone substrates. Several years later, in 2003 and 2006 Zhang et al., disproved original findings by showing that HDAC6 activity depends on cooperation between the two catalytic domains. Following the discovery of α-tubulin as an HDAC6 substrate, the role of both catalytic domains has been evaluated (27). Original experiments showed that both deacetylase domains are required for the tubulin deacetylase activity of HDAC6 (28,29). However, the follow up studies assigned tubulin deacetylase activity of HDAC6 to the second deacetylase domain (30,31).

The first deacetylase domain (DD1) (amino acids 84-440) exerts its activity on peptide substrates containing C-terminal acetylated lysines (32). The H216A mutation (the DD1 inactive mutant) did not influence HDAC6 activity on α-tubulin and histone substrates showing its minimal role in the deacetylation of these substrates. The second deacetylase domain (DD2) (479-835 amino acids) is the major deacetylase domain, suggested to be crucial for HDAC6 activity on various substrates - α-tubulin, histone substrates *in vitro*, survivin, heat shock protein 90 (Hsp90), cortactin, β-catenin, etc. The DD2 inactive mutant (H611A) showed a total absence of deacetylase activity on the same substrates, suggesting it to be critical for the deacetylation of α-tubulin and histones.

A glutamate-rich linker between two catalytic domains (amino acids 441-478) is involved in dynein motor binding (the dynein motor binding site (DMB)) (33). HDAC6 functions as a linker between ubiquitinated/misfolded proteins and the dynein molecular motor. It is hypothesized that HDAC6 may control a motor-dependent cargo transport due to its presumed interaction with the p150-glued-complex through the DMB site (27). The other approach to the understanding of the role of a linker was its modification (29). Mutations in the linker – addition or deletion of 5 amino acid residues had a great impact on HDAC6 activity - decreasing it. The most pronounced loss of the enzyme activity was observed when the linker region (411-478 amino acids) was deleted.

The SE14 domain (serine-glutamate tetradecapeptide, amino acids 884-1022) is a unique intrinsically disordered region of HDAC6 present only in humans, but not in other HDAC6 orthologs.

It harbors eight Ser-Glu-containing tetradecapeptide repeats (SE14) between the catalytic domain and the ubiquitin-binding zinc finger domain (34). The SE14 domain is responsible for the cytoplasmic localization of HDAC6. This domain affects neither deacetylation activity nor the ubiquitin-binding activity of HDAC6 (25).

The C-terminal zinc finger - hydrolase-like ubiquitin-binding domain BUZ (binding of ubiquitin zinc finger, amino acids 1131-1192) is interacting with mono/poly-ubiquitylated proteins (35-37) thus regulating the degradation of proteins (38).

Figure 2. Domain organization of HDAC6. Schematic representation of HDAC6 domain organization. NLS – nuclear localization signal, NES1 – the first nuclear export signal, DD1 – deacetylase domain 1, DMB – dynein motor binding site, DD2 – deacetylase domain 2, SE14 – Ser-Glu containing tetradecapeptide repeat, NES2 – the second nuclear export signal, BUZ – ubiquitin-binding – zinc-finger domain. The numbers correspond to the individual domains within the amino acid sequence.

Elucidating structure-function relationships of multiple domains of HDAC6 can provide deeper insights into protein functions and intracellular signaling pathways HDAC6 is involved in.

1.1.2 Structural studies of HDAC6

Up to date, there is no crystal structure of the full-length HDAC6 available. Multidomain proteins are usually difficult to crystalize. Another obstacle is disordered regions of the protein – it will be less likely to self-organize into a crystal. A typical approach involves the crystallization of domains separately. The first attempts were made to crystallize structured domains of HDAC6 such as catalytic domains and the ZnF-domain. The first crystal structure of HDAC6 was published in 2008 by Dong group who have successfully crystallized the C-terminal ubiquitin-binding zinc-finger domain of human HDAC6 (Protein Data Bank (PDB): 3C5K). Further, this group has successfully crystalized the HDAC6 zinc-finger domain (BUZ) with a ubiquitin C-terminal peptide RLRGG in 2009 (PDB: 3GV4) and also, in complex with ubiquitin in 2010 (PDB: 3PHD). The domain contains conserved amino acids (11 cysteine and 10 histidine residues) that bind three zinc ions. Binding to the substrate elicits conformational changes in amino acids Arg-1155 and Tyr-1156. Therefore, these two amino acids are assumed to be gatekeepers that switch between “open” and “closed” conformation depending on ubiquitin binding (Figure 3) (39).

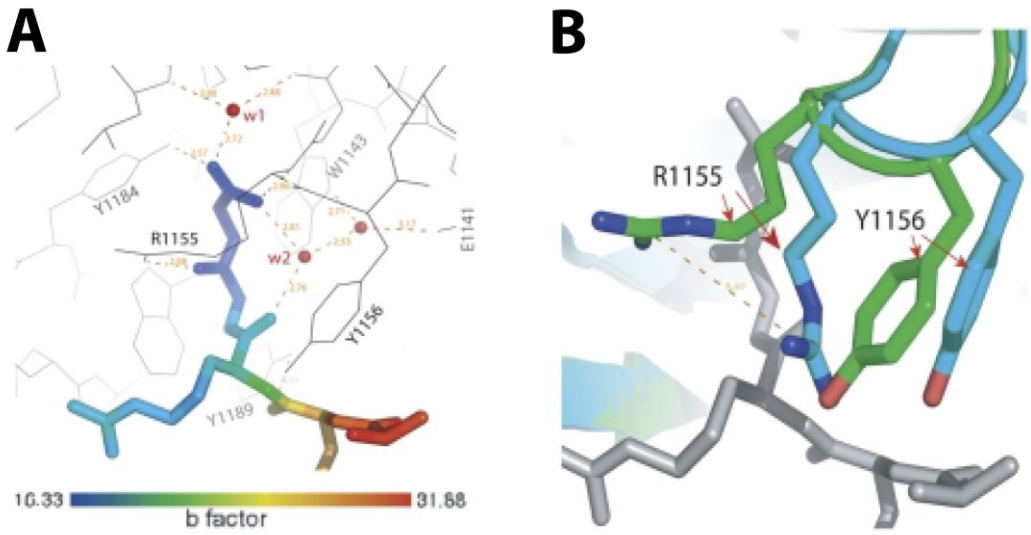

Figure 3. Structure of the HDAC6 BUZ-UBP domain and ubiquitin C-terminal peptide complex. A. The visualization of the hydrogen bond network in the complex structure of HDAC6 BUZ-UBP and RLRGG peptide. The peptide is colored by B-factors. Water molecules are shown in red. **B.** An overlay of the unoccupied (*green*) occupied with RLRGG peptide (*cyan*) ubiquitin-binding site of the HDAC6 BUZ-UBP domain. The RLRGG peptide is shown in *gray*. These are obvious differences in the Arg-1155 and Tyr-1156 conformations. The image is taken from (39).

A crystal structure of HDAC6 catalytic domains has been determined by Hai et al., in 2016. The crystal structure of DD1 and DD2 from *Danio rerio* (zebrafish) HDAC6 revealed domain organization, but in the absence of the HDAC6/substrate complex (40) molecular mechanisms of HDAC6 interactions with its substrates remain unknown (40). Further, Hai et al. have reported the crystal structure of the HDAC6 second catalytic domain DD2 from *Homo sapiens* (human) that has a high similarity of the active site to DD2 from *D.rerio*. Additionally, it has been shown that DD2 has broad enzymatic activity (endo- and exo-acetyllysine peptide substrates), while DD1 is more specific for exo-acetyllysine peptide substrates (40).

Further structural studies are mainly focused on the design, synthesis, and structural characterization of HDAC6 specific inhibitors. More than 40 structures of HDAC6 catalytic domains with inhibitors have been solved and are deposited in the Protein Data Bank (PDB) nowadays. However, all these discovered inhibitors are mainly pan-inhibitors and highly selective HDAC6 inhibitors with good pharmacologic properties are still to be discovered.

1.2 HDAC6 function

HDAC6 interacts with various proteins involved in cell migration, cell proliferation and death, sperm motility, intracellular trafficking, cell signaling, immune response, transcription, the degradation of misfolded proteins and aggregates, and stress response pathways.

HDAC6 exerts deacetylase enzymatic activities mainly on non-histone substrates in cells such as tubulin, Hsp90, cortactin substrates, and many others (41). Furthermore, it can deacetylate histones *in vitro*. Recently, several novel HDAC6-interacting proteins were described – AAA-ATPase chaperone p97 (p97) (37), mDia2 (42), ubiquitin, survivin, nuclear factor-kB (NF-kB) and the p150 glued component of the dynein-dynactin protein complex (27). Even though HDAC6 has been discovered over 20 years ago, its major function and mechanism of action remain unclear. One main difficulty in unraveling physiological functions of HDAC6 is the fact that only several physiological substrates have been identified so far. Some well-studied functions of HDAC6 will be discussed in this chapter.

1.2.1 Cellular function of HDAC6

It has been found that HDAC6 influences aggresome formation and the aggregation of misfolded proteins via inducing the expression of heat shock proteins, as it participates in the control of cellular response pathways (43). HDAC6 deacetylase activity, as well as ubiquitin-binding activity, are crucial for the aggresome formation. The cells lacking HDAC6 are not able to form aggresomes and tend to accumulate misfolded proteins (33). Kawaguchi et al, have shown that HDAC6 serves as a link between ubiquitinated/misfolded proteins and dynein-motors. They have shown that HDAC6 can bind dynein motor proteins and can attach misfolded protein cargoes to dynein for transport to aggresomes (33). Another study has shown that the phosphorylation of HDAC6 at the serine-22 by Leucine-rich repeat kinase 2 increases its interaction with dynein and also increases the recruitment of ubiquitinated proteins to aggresomes (44).

HDAC6 assists in ubiquitinated misfolded protein clearance via stimulating their recruitment to aggresomes. This is a cellular protecting mechanism from apoptosis caused by misfolded protein-induced stress. HDAC6 is implicated in the ubiquitin/proteasome system control. It is known that HDAC6 interacts with the chaperone p97 and its cofactor phospholipase A2-activating protein - proteins that are involved in the ubiquitin signaling pathway (37). The chaperone p97 interacts with HDAC6 and regulates the accumulation of polyubiquitinated proteins by the dissociation of the HDAC6/ubiquitin complex. Boyault et al. came up with the hypothesis that p97 and HDAC6 might have opposite effects: p97 increases the rate of protein degradation, while HDAC6 induces the aggregation of ubiquitinated proteins (35). Ubiquitous, nucleocytoplasmic protein Ran-binding protein M (RanBPM) serves as an activator of apoptotic pathways (45). RanBPM is an essential component required for the aggresome formation. The LisH/CTLH domain of RanBPM forms

a complex with HDAC6. This interaction leads to the inhibition of HDAC6 deacetylation activity and therefore serves as a regulator of the aggresome formation (46,47).

Additionally, HDAC6 is a regulator of cell motility – invasive motility of fibroblasts (27) and carcinoma cells (22). Its overexpression in cancer cells promotes cell migration and metastasis. For this reason, HDAC6 inhibitors are promising anti-cancer drugs as they hinder invasive motility by inhibiting tubulin deacetylation and increasing the total focal adhesion area (48). HDAC6 activity is critical for the microtubule-dependent motility and promotes growth factor-induced motility of cells (27). HDAC6 is involved in modulation of sperm motility by alteration of α-tubulin acetylation status in sperm axoneme (49). Also, HDAC6 can influence cell motility through an actin-dependent manner – by regulating cortactin acetylation that consequently affects the F-actin binding affinity of cortactin (50).

Moreover, HDAC6 regulates mitochondrial trafficking in neurons. Specific inhibition of HDAC6 increased the level of acetylated tubulin and increased mitochondrial transport. It could be explained by an increased affinity of motor proteins to acetylated microtubules (51). It has been recently discovered that HDAC6 can deacetylate Miro1 at lysine 105 – a protein that links mitochondria to motor proteins. This causes a decrease in axonal mitochondrial transport (52). Therefore, HDAC6 has a broad spectrum of functions and can influence cellular cytoskeleton that consequently causes changes in intracellular trafficking.

Survivin belongs to an Inhibitor of apoptosis protein family of antiapoptotic proteins. It is conserved in its function across evolution in vertebrates and invertebrates. Survivin has increased expression in breast cancer cells. The acetylation of survivin is a regulatory mechanism of its stability, subcellular localization, and interaction with other proteins. In the cytoplasm, survivin inhibits caspase activation with further blocking of programmed cell death. In the nucleus, survivin promotes cell division by the regulation of cytokinesis. Acetylation of survivin at lysine 129 by CREB-binding protein promotes its migration from the cytoplasm to the nucleus. The deacetylation of survivin by HDAC6 causes its depletion from the nucleus (53).

1.2.2 Acetylation of the cytoskeleton

Posttranslational modifications represent an elegant mechanism of modulation protein functions and their enzymatic activity without changing protein levels in the cell. In the human proteome acetylation of lysines in proteins is one of the major post-translational modifications (PTMs) (54). The reversible acetylation of proteins plays a crucial role in diverse biological processes important for normal cell functioning. In the cell, the acetylation status of proteins is regulated by two enzyme families with opposite activities – HATs (writers) and HDACs (erasers). Most of HDACs localize to the nucleus, HDAC6 and HDAC10 are found in the cytoplasm, while some sirtuins are mitochondrial proteins. Altered acetylation/deacetylation dynamics leads to cellular disorders, including for example cancer.

All cytoskeletal components of the cell may be regulated by reversible acetylation:

- actin filaments – three major actin isoforms can be acetylated. The acetylation of the lysine residue 61 in gamma actin increases the stability of actin stress fibers (55). Also, the Arp2/3 complex, crucial for the nucleation of actin, is acetylated in its 6 subunits (56). Being acetylated by p300, cortactin is translocated to the cell periphery. Consequently binding of cortactin to actin is reduced (50,57). The contraction of muscles, especially actomyosin filament activity, is also influenced by acetylation. The acetylation of the muscle LIM protein increases the calcium sensitivity of myofilaments (58);
- microtubules – a tight connection between actin-network and microtubule-network is mediated by the RhoA effector Dia. Dia can affect microtubule orientation, stability, and acetylation level (59). Recently it has been discovered that Src homology region 2 (SH2)-containing protein tyrosine phosphatase 2 downregulates RhoA-Dia signaling, triggering microtubule destabilization, and HDAC6-mediated deacetylation (60);
- intermediate filaments – the most abundant protein in the third type of cytoskeletal element is vimentin. It is also affected by acetylation on its several lysine residues. It has been reported that the deacetylation of vimentin at lysine120 by SIRT5 is involved in metastasis (61).

Lysine acetylation has been reported to regulate protein stability. It may be caused by the fact the acetylation of lysine competes with lysine ubiquitination. Smad7 stability is influenced by lysine acetylation, while HDAC1- or SIRT1-dependent deacetylation increases Smad7 ubiquitination and degradation (62,63). HDAC-mediated deacetylation influences the stability of the p53 tumor suppressor protein (p53), Runt-related transcription factor 3. The transcription factors Gata-1 and MYC are also more stable due to lysine acetylation (64). The acetylation of E3 ubiquitin ligase Mdm2 is an example of an indirect influence of lysine acetylation. Acetylation of Mdm2 causes is inactivation and consequently stabilizes p53 (65).

Recently it has been discovered that the acetylation status of disordered protein regions can regulate liquid-liquid phase separation of these proteins. It was reported that acetylation serves as a switch of stress granules assembly. The phenomenon was described for HDAC6 deacetylation of a DEAD box ATP-dependent RNA helicase DDX3X, a component of stress granules (66).

1.2.3 Posttranslational modifications of HDAC6

Moreover, PTMs of HDAC6 such as acetylation/deacetylation, phosphorylation may affect its function. The phosphorylation of HDAC6 is well studied and is regulated by several kinases. Serine 22 of HDAC6 is phosphorylated by glycogen synthase kinase 3 beta (GSK-3β) (67) that is linked to increased HDAC6 activity and microtubule depolymerization. Phosphorylation of Ser458 by casein kinase 2 has an impact on HDAC6 interaction with dynein as well as on aggresome formation (68). HDAC6 Tyr570 is phosphorylated by the epidermal growth factor receptor and it inhibits its tubulin

deacetylase activity (69). Extracellular signal-regulated kinase 1 is responsible for Thr1031 phosphorylation (70) and Ser1035 (70) phosphorylation of HDAC6. G protein-coupled receptor kinase 2 phosphorylates HDAC6 at Ser1060, Ser1062, and Ser1069 (71).

Recently, it has been discovered that HDAC6 acetylation has an impact on its activity and subcellular localization. Liu et al. have shown that p300 acetylates HDAC6 on five clusters of residues. Acetylation of HDAC6 lysines in the N-terminal nuclear localization signal region (patch B) (Lys51, Lys52, Lys53, Lys 55, Lys 57, Lys 58) significantly decreased tubulin deacetylase activity of HDAC6, decreased HDAC6 mediated cell motility, and anchored HDAC6 in the cytoplasm by blocking its interaction with importin-α (26). The role of lysine acetylation of HDAC6 in the mechanism of HDAC6 interaction with tubulin is detailed in the manuscript that is a part of this thesis (72).

Although many acetylation sites have been discovered so far, there are likely more to be identified. All evidence mentioned above shows that lysine acetylation plays an important role in cellular functions, protein-protein interactions, and regulatory mechanisms. Identification of new acetylation sites can shed light on many regulatory mechanisms and cellular processes.

1.3 Substrate specificity of HDAC6

HDAC6 exerts its deacetylase/enzymatic activity mainly on non-histone substrates such as tubulin, Hsp90, and cortactin (41). Furthermore, it can deacetylate histones *in vitro*. As tubulin is the main physiological substrate of HDAC6, the interaction of tubulin and HDAC6 will be detailed in this chapter.

1.3.1 Tubulin as HDAC6 substrate

Tubulin was the first non-histone substrate of HDAC6 identified by several research groups (27,28,73). The discovery of tubulin as a substrate has opened a room for testing either HDAC6 activity or HDAC6 inhibition on tubulin as a substrate in biochemical assays (28,29). It has been reported that β-tubulin interacts with HDAC6 *in vitro* and *in vivo* (28). The tubulin dimers (α-tubulin and β-tubulin) polymerize into tubular filaments called microtubules and numerous microtubules assemble into a cellular network as a part of the cytoskeleton. Microtubule-based functions are diverse, including intracellular transport, spindle formation, shape maintenance, cell polarity, migration, and signal transduction (74). Individual tubulin subunits and microtubules undergo various post-translational modifications that define the structure and stability of the cytoskeleton. The most conserved modification of microtubules, that is present from Chlamydomonas to mammals, is the acetylation of lysine 40 (K40) in the α-tubulin subunit (74), being a hallmark of stable microtubules (Figure 5) (75,76). K40 is located in the microtubule lumen as it was shown from the high-resolution structure of microtubule (77).

Deacetylation at K40 of α-tubulin is mediated by HDAC6 and is supposed to be important for microtubule dynamics. Deacetylation of microtubules is often correlated with their depolymerization meaning that HDAC6 mainly deacetylates free tubulin. HDAC6 overexpression causes the hypoacetylation of α-tubulin in cells (27). Additionally, the acetylation of microtubules may influence the behavior of microtubule-associated proteins (MAPs). Microtubule acetylation state increases the transport of cellular cargo by molecular motors kinesin-1 and dynein (78,79). Microtubule-severing protein katanin preferentially cuts microtubules rich in acetylation and these breaks are mainly co-localized with highly-acetylated regions of microtubules (80). In this way, HDAC6 is indirectly influencing crosstalk between various MAPs and microtubules and potentially is affecting different signaling pathways.

The acetylation state of K40 is regulated by two types of enzymes: acetyltransferases MEC17/α-tubulin N-acetyltransferase (α-TAT) (81,82), ARD1-NAT1 (83), and GCN5 (84) and deacetylases HDAC6 (27), SIRT2, and HDAC5. However, in mammalian cells, two main enzymes regulate the level of α-tubulin acetylation - α-TAT and HDAC6 (Figure 4).

α-TAT acetylates microtubules more efficiently than tubulin dimers. Microtubules are acetylated 4-6 times faster by α-TAT compared to tubulin with the respective acetylation rate (k_{cat}) $615 \pm 34 \times 10^{-6}$ s-1 and $98 \pm 1.8 \times 10^{-6}$ s-1. α-TAT K_m values are 1.6 ± 0.36 μM and 2.0 ± 0.16 μM for

microtubules and tubulin, respectively (85). Despite being identified 8 years earlier than α-TAT, HDAC6 is not well studied. It is known that HDAC6 is the major tubulin deacetylase as HDAC6 knockout mice exert a hyperacetylated tubulin phenotype (86). On the contrary to α-TAT, HDAC6 has a preference for the deacetylation of tubulin dimers rather than microtubules as the deacetylation rate of tubulin is over 1,500-fold higher than that of microtubules. K_m value for tubulin deacetylation is 0.23 μM. α-TAT diffusively scans the lumen of microtubules with no preference to "+ / -" tips of microtubules and acetylates K40. In contrast, HDAC6 binds microtubules from the outer surface of microtubules without any preference to "+ / -" tips. Therefore, α-TAT and HDAC6 have opposing substrate preferences and different patterns of interaction with microtubules.

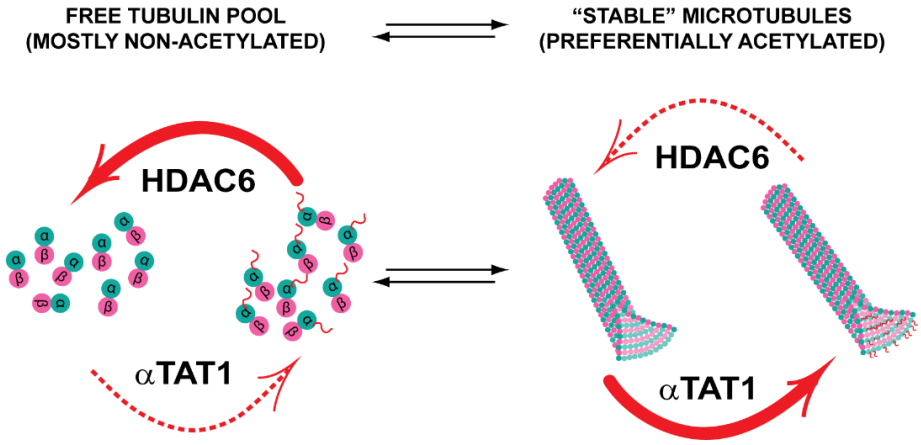

Figure 4. Opposing substrate preferences of two main enzymes regulating the level of α-tubulin acetylation - α-TAT and HDAC6. HDAC6 shows a preference for the deacetylation of tubulin dimers rather than microtubules, while α-TAT shows opposite preference. Thus, it is likely that the pool of free tubulin in the cell is mostly in the non-acetylated state. Stable microtubules with long lifespans are highly acetylated by αTAT1. Both HDAC6 and αTAT1 thus serve as "timers" to set the clocks gauging microtubule age based on their acetylation status.

Except for K40, there are many other lysine acetylation sites on α-tubulin identified by proteome studies - TUBA1C (K60, K112, K326), TUBA4A (K163, K164, K311, K394, K370, and K401), while K58 is acetylated in β-tubulin isoforms TUBB3, TUBB2C, and TUBB5 (56). Further, additional acetylation in β-tubulin was identified - K154, K174, and K252. The K252 acetylation has been observed only on free tubulin dimers but not on microtubules. It has been hypothesized that the K252 acetylation may inhibit tubulin polymerization (87).

Cells use PTMs as an elegant tool to manipulate the structure and functions of microtubules. The acetylation of K40 of α-tubulin is the main modification that localizes to the lumen of microtubules. The acetylation mark is added by αTAT1 and removed by HDAC6, however, structural insights into the effect of this modification on microtubule properties are not understood. In the manuscript, which is the part of the dissertation thesis, we partially elucidate the mechanism of HDAC6 – tubulin/microtubule interactions.

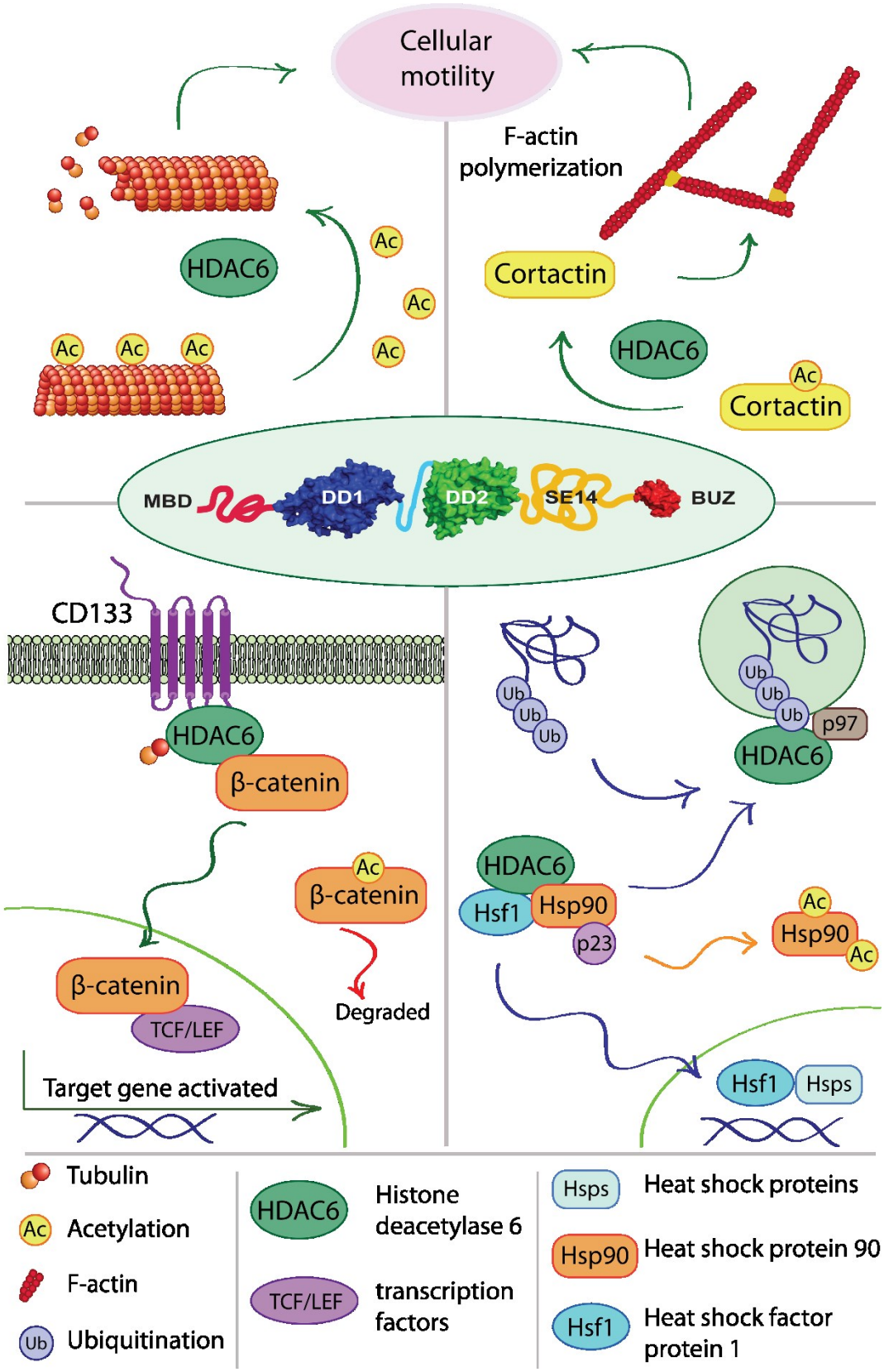

Figure 5. The major HDAC6 substrates. The role of cortactin and α-tubulin acetylation is shown in the upper part of the figure. The deacetylation of cortactin by HDAC6 leads to its association with F-actin (upper right panel), and the deacetylation of α-tubulin (upper left panel) causes an increase in microtubule dynamics, allowing mobility and cell division. The lower left panel is the schematic representation of HDAC6-mediated stabilization of β-

catenin, the central regulator of canonical Wnt signaling. HDAC6 binds to membrane glycoprotein CD133 and stabilizes the β-catenin that in the nucleus promotes the activation of its target genes. Downregulation of CD133 or HDAC6 results in increased β-catenin acetylation and its further degradation. The lower right panel - in the presence of HDAC6, Hsp90 binds multiple client proteins, including Hsf1. HDAC6 binding to ubiquitinated protein aggregates induces the release of Hsp90 and client proteins. Hsf1 undergoes nuclear translocation inducing of other heat shock proteins to serve as chaperones for client proteins.

1.3.2 Other HDAC6 substrates

Nowadays, several HDAC6 cytosolic substrates are known, although plenty of them is yet to be discovered. The second discovered substrate of HDAC6 is Hsp90 (88-90). Both HDAC6 deacetylase and ubiquitin-binding domains are essential for the interaction and efficient deacetylation of Hsp90 (88). The Hsp90 chaperone activity is regulated by the acetylation status of its lysines (91). It has been reported that the deacetylation of lysine 294 disrupts Hsp90 interaction with cochaperone p23 and a glucocorticoid receptor (88). HDAC6 inhibition causes Hsp90 hyperacetylation (88) and blocks Hsp90, AhR, p23, XAP-2 chaperone complex formation (92).

Another well studied HDAC6 substrate is cortactin, an F-actin binding protein. HDAC6-regulated acetylation of cortactin induces its binding to F-actin (Figure 5). HDAC6 deacetylates lysine patches in both repeat region of cortactin. The first patch is comprised of K124, K189, K198, and K272, while the second patch contains three lysines (K161, K309, and K319). Thereby the alteration of the "charge patch" enhances binding of cortactin to F-actin. Cortactin/F-actin interaction triggers F-actin polymerization and branching. Cortactin is mainly localized in the leading edge of migrating cells, where active actin assembly occurs (93). Cortactin hyperacetylation impairs cell motility via hindering its localization to membrane ruffles (50). Therefore, HDAC6 influences not only microtubule-based cell motility but additionally actin-based cell motility by changing the charge of cortactin and its F-actin binding ability (50).

HDAC6 deacetylates β-catenin, a key player in the Wnt-signaling pathway in development and cancerogenesis (Figure 5) (94). Additionally, β-catenin interacts with E-cadherin and is involved in cell-cell adherens junctions (95). HDAC6 deacetylates β-catenin at the position lysine 49 that is conserved in β-catenin from *Drosophila* to humans (94). Epidermal growth factor (EGF) induces HDAC6 translocation to the plasma membrane with subsequent deacetylation of β-catenin. The deacetylation of β-catenin at lysine 49 reduces phosphorylation of β-catenin at serine 45 by casein kinase 1, therefore, promoting its nuclear localization and accumulation (94). Serine 45 phosphorylation is crucial for β-catenin degradation, and its mutations are tightly connected with colon cancer (96). This evidence shows that HDAC6, being a link between EGF and Wnt-signaling pathway, is involved in tumor formation.

HDAC6 is a regulator of the antioxidants Peroxiredoxin I (Prx I) and Peroxiredoxin II (Prx II), which are responsible for cellular protection from free radical accumulation. Hyperacetylation of Prx increases its reducing activity (H_2O_2) and increases the ability to form high-molecular-mass

complexes (97). At the same time, the deacetylation of these proteins initiates apoptosis, meaning that HDAC6 is involved in stress response regulation.

Several major HDAC6 substrates are known and well-studied up to date, however, there are many more potential substrates to be discovered. The identification of new HDAC6 interacting partners, protein complexes, in which HDAC6 is involved, may help us to understand regulatory mechanisms in which HDAC6 is involved.

1.4 HDAC6 in pathologies

HDAC6 is involved in various important cellular processes via interaction with proteins and protein deacetylation. Such broad functions of HDAC6 suggest its involvement in the main physiological and pathophysiological states. HDAC6 is often overexpressed or deregulated in cancer cells, neurodegenerative diseases, and inflammatory disorders. For this reason, HDAC6 became an attractive therapeutic target in the range of diseases.

1.4.1 HDAC6 as a target for cancer therapy

HDAC6 has become an attractive target for cancer therapy as it is involved in carcinogenic processes. Deregulation of HDAC6 correlates with tumorigenesis and HDAC6 serves as a marker for disease prognosis.

The abnormal expression of HDAC6 has been reported in a variety of cancer cell lines and mouse tumor models. Expression profiling in MCF-7 cells showed the HDAC6 gene to be an estrogen-regulated gene (98). Estrogen receptors α (ERα) plays a critical role in the development of breast cancer (99). The estrogen-mediated up-regulation of HDAC6 indicates the correlation between HDAC6 expression levels and cancer cell metastasis. HDAC6 overexpression increases the motility of cancer cells. It has been shown that expression levels of HDAC6 mRNA in invasive breast cancer correlated with tumor size (tumors measuring < 2 cm), ERα protein, and progesterone receptor protein expression (100). It has been reported that ER-positive patients with high levels of HDAC6 expression showed improved survival during selective estrogen-receptor modulating treatment with tamoxifen (22). HDAC6 up-regulation occurs in oral squamous cell lines correlating with primary tumor stage (101), in primary acute myeloid leukemia blasts, in some myeloblastic cell lines (102) and also can be caused by oncogenic Ras transformation (23). It has been reported that HDAC6 overexpression in colon cancer is associated with poor prognosis. HDAC6 inhibition may suppress colon cancer metastasis and invasion (103).

HDAC6 can be considered as a hallmark of the malignant transformation. It has been found that HDAC6 inactivation by genetic ablation makes cells more resistant to oncogenic transformation as well as reduces tumor growth *in vitro* and *in vivo*. Anchorage-independent proliferation enables cancer cells to survive by escaping anoikis, a programmed cell death caused by the deficiency of cell adhesion to the surrounding basement membrane and extracellular matrix. HDAC6 knockdown in cancer cell lines inhibited their anchorage-independent growth (23). Therefore, HDAC6 is suggested to be required for growth factor-induced activation of mitogen-activated protein kinase (MAPK) and phosphatidylinositol-3-kinase signaling cascades (23). As the RAS/MAPK signaling pathway is known to be required for tumorigenesis, HDAC6 pharmacological inhibition could potentially confer an anti-tumor effect.

Cylindromatosis tumor suppressor protein (CYLD) is a deubiquitinating enzyme that regulates cell proliferation through inhibition of NF-κB signaling. It has been reported that CYLD-mediated

HDAC6 inhibition reduces the cytokinesis rate and causes the cell cycle delay. CYLD N-terminal CAP-Gly domains interact with HDAC6 catalytic domains, inducing α-tubulin acetylation and CYLD translocation to the perinuclear region. Additionally, CYLD can interact with HDAC6 in the midbody, regulating the cytokinesis rate in a deubiquitinase-independent manner (104). The understanding of the HDAC6 role in this process is important as the abnormal cell-cycle progression through G1 phases and cytokinesis are both hallmarks of cancer cell proliferation.

The TP53 gene is encoding the p53 transcription factor – the best known tumor-suppressor gene. Tumors having p53 mutated or deleted are less sensitive to chemotherapy (105). It has been reported that p53 expression is differentially regulated by HDAC6 depending on p53 mutations. P53 protein stability and its activity as a tumor suppressor are strongly dependent on the acetylation status of its lysine residues 381 and 382. It has been reported that HDAC6 can deacetylate p53 thus regulating its stability and its activity. It affected the complex Hsp90/p53 by inactivating Hsp90, disrupting the complex and p53 release (106).

Additionally, HDAC6 regulates gene expression of tumor-associated antigens, programmed death receptor-1 (PD-1), and programmed death receptor ligand-1 (PD-L1), which are central targets in cancer immunotherapy. The inhibition of HDAC6 mimics anti-tumor effects: cell cycle arrest in the G1 phase and increased expression of tumor associated antigens and MHC class I, as well as the delay in tumor growth (107). These results suggest that HDAC6 inhibition has increased tumor-specific immunogenic signals, which is a goal of many anti-cancer therapies. The immunoregulatory role of HDAC6 needs to be further investigated and new selective HDAC6 inhibitors are needed to improve antitumor immunity.

All this evidence suggests HDAC6 is an important component of cancer cell invasion and metastasis. Consequently, HDAC6 inhibition with subsequent blocking of tumor angiogenesis and apoptosis triggering can be a promising cancer treatment strategy.

1.4.2 HDAC6 in neurodegenerative disorders

Neurodegenerative disorders such as Alzheimer's, Parkinson's, Huntington diseases, amyotrophic lateral sclerosis, and prion diseases are associated with the pathogenic aggregation of proteins. 'Protein conformational diseases' can be caused by HDAC6-mediated accumulation of misfolded and ubiquitinated proteins (35) as well as by pathogenic consequences of aggresome formation (33).

Alzheimer's disease is a chronic disease, the cause of 60-70% of dementia cases. One of the main brain areas affected by Alzheimer's disease is the hippocampus, which is essential for memory formation and memory events (108). This disease is characterized by "tau tangles" (abnormal forms of the tau protein that stick/adhere to other tau proteins inside the neuron) and β-amyloid plaques. In comparison to a normal brain, HDAC6 expression in the brain suffering from Alzheimer's disease increased by 52% in the cortex and by 91% in the hippocampus (109). The tau protein stabilizes

the cytoskeleton of neurons. HDAC6 has been shown to co-localize with tau tangles. Moreover, tau acted as an inhibitor of HDAC6 deacetylase activity, causing an increase in tubulin acetylation, and as well as an inhibitor of the aggresome pathway (110). Further, it has been reported that the excess of tau may prevent the induction of autophagy by inhibiting proteasome function (110). In a mouse model for Alzheimer's disease, the reduction of endogenous HDAC6 protein levels led to learning ability and memory amelioration (111). Therefore, HDAC6 inhibition can be a promising strategy in the therapy of Alzheimer's disease.

Parkinson`s disease is another neurodegenerative disease in which HDAC6 is involved. A progressive degeneration together with the presence of Lewy bodies are the hallmarks of the disease. The Lewy bodies are insoluble inclusions made of α-synuclein. It has been found that HDAC6 accumulates in the Lewy bodies inside nerve cells in Parkinson's disease suggesting its involvement in neurodegenerative disorders (33). HDAC6 deficiency hinders the formation of protein aggregates of α-synuclein, increases the level of α-synuclein in the nucleus, and consequently triggers apoptosis in various cell types (112). HDAC6 is playing a cytoprotective role while decreasing the amount of α-synuclein oligomers in neurons (113). Parkin is a ubiquitin E3 ligase linked to Parkinson`s disease. HDAC6 controls the reversible recruitment of parkin to the centrosome in response to the reversal of proteasome inhibition. HDAC6 forms a complex with motor proteins to efficiently transport the HDAC6/parkin complex. Therefore, HDAC6 serves as a proteasome inhibition sensor and directs parkin trafficking in the cell (114).

Huntington disease is the consequence of the expansion of CAG trinucleotide repeats that encode glutamine homopolymeric tracts. Typically, the huntingtin protein contains more than 39 glutamines that are largely insoluble and accumulate in inclusion bodies. HDAC6 protein, as well as its enzymatic activity, are required for the autophagic clearance of mutant huntingtin aggregates (115). The inhibition of HDAC6 activity by non-selective inhibitors Vorinostat (suberoylanilide hydroxamic acid (SAHA)) and trichostatin A (TSA) significantly increased intracellular transport of brain-derived neurotrophic factor (79).

Mitochondrial transport is crucial for innate neuronal function. The abnormal mitochondrial transport, which is typical for Alzheimer's disease and Parkinson's disease, is associated with the misregulation of HDAC6 by GSK-3β (51). It has been discovered that HDAC6 regulates the transport of mitochondria in neurons, and its inhibition promoted mitochondrial transport in hippocampal neurons. The regulation of HDAC6 can affect cellular transport of proteins as well as organelles through the alteration of tubulin acetylation. Moreover, the HDAC6 mediated deacetylation of Miro1 protein, which serves as a linker between motor proteins and mitochondria, decreases mitochondrial transport (52). The reduction of mitochondrial movement is consonant with HDAC6 increased activity in the hippocampus during Alzheimer's disease.

Charcot–Marie–Tooth disease is the most common inherited disorder of the peripheral nervous system causing progressive degeneration of the motor and sensory nerves which leads to muscle

weakness, deformities of hands, and feet. As HDAC6 is connected with the regulation of mitochondrial axonal transport, it could serve as a potential target for the therapy. Three inhibitors (ACY-738, ACY-775, and ACY-1215) being selective for HDAC6, increased innervation of neuromuscular junctions and amended the motor and sensory nerve conduction.

1.5 HDAC inhibitors

Nowadays, HDAC inhibitors are considered to be promising drugs the treatment of inflammatory diseases, cancer, and neurodegenerative disorders such as Parkinson's and Alzheimer's disease. HDAC6 inhibitors were originally used in cancer treatment. Later, Hahnen et al have shown that HDAC inhibitors might be a promising strategy for the treatment of neurodegenerative disorders (116). Valproic acid, marketed under trade names Depakene, Depakote, and Divalproex, was used in psychiatry as a mood stabilizer and in neurology as anti-epileptics.

1.5.1 Structure of HDAC active cavity

Early efforts to develop HDAC inhibitors were not so successful as neither the isoform selectivity nor the mechanism of action of HDAC inhibitors was known. Solving a crystal structure of an HDAC homolog from the hyperthermophilic bacterium *Aquifex aeolicus* in complex with TSA and SAHA inhibitors in 1999 facilitated the design and comprehension of inhibitory mechanisms of HDAC inhibitors, forming a basis for the development of novel HDAC inhibitors.

The HDAC homolog shares 35.2% identity with human HDAC1 having similar critical active site residues and has deacetylase activity for histones (117). The structure revealed that the active site contains: i) a zinc ion, positioned near the bottom of the pocket and a water molecule; ii) two charge-relay systems - aspartate and histidine residues; iii) a tyrosine residue - coordinates the acetyl oxygen of the transition state. Chelation of the zinc ion blocks HDAC enzymatic activity. A hydrophobic pocket of HDACs is delineated by aromatic and glycine residues.

The catalytic domains of HDACs from different species contain numerous conserved amino acids suggesting a common mechanism of deacetylation. The catalytic center is a tube-like hydrophobic pocket formed by an open alpha/beta fold with seven loops. Additionally, the catalytic domain contains variable loops that are responsible for the specific substrate recognition. They facilitate the insertion of the substrate to the catalytic site. These four loops (L1-4) are extremely variable in size and conformation between HDACs that may explain the importance of HDAC surface interactions with their substrates and subsequently their substrate selectivity.

In class IIa HDACs two cysteine residues and a histidine residue in the loop L1 and a cysteine residue in the loop L2 coordinate the zinc ion, reducing the flexibility of these loops. (118). In the loop L2 common for HDACs of Class I and II, conserved residue D101 (in the case of HDAC8) is enhancing substrate specificity of the enzyme (119). It has been determined from crystal structures of HDACs class IIa that the aspartate residue (HDAC4 – D759, HDAC5 – D789, HDAC7 – D626, HDAC9 – D739) is at the entrance to the active tunnel similar to HDAC8. For HDACs class IIb HDAC6 harbors aspartate in both catalytic domains (D172 and D567) and HDAC10 – D91 (120). The mutation in aspartate results in loss of the enzyme activity (121). Therefore, the diverse and flexible loops at the rim of the catalytic pocket create a changeable/diverse interface for the interaction with various substrates and interacting partners.

1.5.2 Classification of HDAC inhibitors

According to the pharmacophore model of HDAC inhibitors proposed by Miller, inhibitors should contain a cap (binds at the edge of the active tunnel), a chelator (interacts with zinc ion at the bottom of the active tunnel), and a linker (between the cap and the chelator) (Figure 6) (122). The inhibitor caps can vary in the chemical nature, orientation and can interact with different flexible loops of the rim. Therefore, a small cap region of inhibitors (for example, SAHA) does not contribute to binding, while large caps can significantly improve binding to a target HDAC.

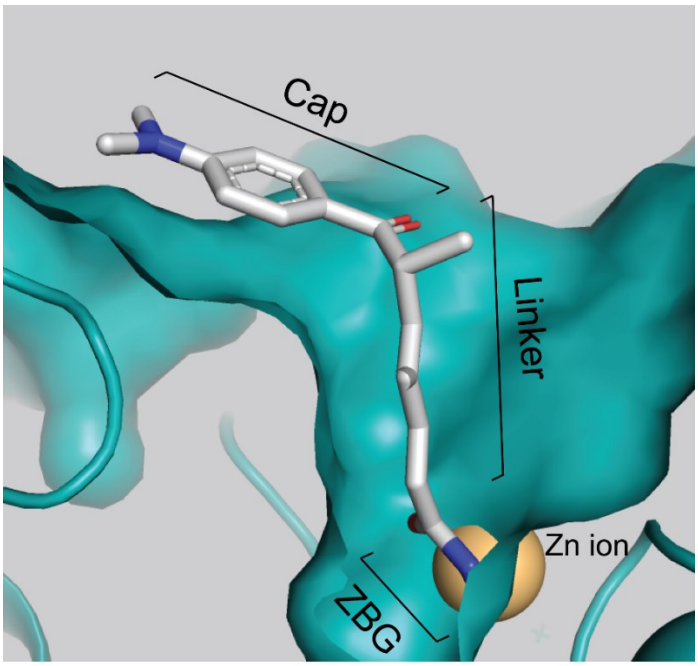

Figure 6. Visualization of trichostatin A HDAC6 complex (PDB: 5WGI). Structural components of the HDAC6 inhibitor are marked – the cap region, the linker region, and the zinc-binding group (ZBG). The zinc ion is represented by an orange sphere.

"Classical" HDAC inhibitors act exclusively on class I, II, and class IV HDACs by binding to the zinc-containing catalytic domain of the HDACs. These HDAC inhibitors can be divided into several classes depending on the chemical moiety that binds to the zinc ion (Figure 7):

- **hydroxamic acids** (hydroxamates), such as **trichostatin A (TSA)**, SAHA, Belinostat, Panobinostat, Dacinostat, Resminostat, Givinostat, and many others. Tubacin is a highly selective HDAC6 inhibitor (30). They inhibit class I and II HDACs. These inhibitors will be discussed in more detail in the following chapter.
- **cyclic tetrapeptides -** such as trapoxin B, Apicidin, Depsipeptide FR901228, FK228, Romidepsin, Isostax – have nanomolar HDAC inhibitory activity. Depsipeptide FK228 is effective in models of lymphoma and leukemia (123,124).
- **benzamides**, Mocetinostat, Tacedinaline (CI-994) (125) and Entinostat (MS-275) (126) are less active inhibitors having Ki in the micromolar range. These two inhibitors exert *in vivo*

activity against tumors in different models. MS-275 inhibited the tumor growth in mice using xenograft orthotopic models of undifferentiated sarcoma and Ewing's sarcoma (127). Moreover, MS-275 strongly inhibited the growth of human tumor cell lines through HDAC inhibition (128). This suggests that MS-275 exerts strong antitumor efficacy against human cancers.

- **electrophilic ketones** (epoxyketones) – these inhibitors chemically modify a nucleophile in the active site with the epoxy group eliminating or reducing ketone.
- **short chain carboxylic acids** such as phenylbutyrate, valproic acid, Pivanex, Phenylacetate. They mainly work as inhibitors of class I HDACs.
- **hybrid molecules** – the class contains both a cyclic peptide and an aliphatic hydroxamate. Representatives - cyclic hydroxamic-acid-containing peptide (CHAP31) (129) and CHAP50 (130). These compounds inhibit HDACs in the nanomolar range. The optimal linker found contains 5 methylene units (131). Trapoxin A and B - the hybrid cyclic tetrapeptides with an epoxyketone-containing amino acid.

Additionally, EnVivo Pharmaceuticals has discovered a class I HDAC inhibitor EVP-0334. It is CNS-penetrant, orally bioavailable, and is applied for the treatment of the cognitive deficits. EVP-0334 has been used in phase I clinical trials for Alzheimer's disease treatment since 2010 (132). However, neither structure nor clinical trajectory for this inhibitor has been disclosed.

Five HDAC inhibitors (2 non-hydroxamate molecules and 3 hydroxamate acid-based molecules) have recently been approved by the U.S. Food and Drug Administration (FDA) (Table 1) (133). Vorinostat (SAHA) exerts antineoplastic activity and was the first compound approved for the treatment of cutaneous T-cell lymphoma (CTCL) by the US FDA in 2006. Romidepsin was approved as an anticancer agent in CTCL in 2009 and peripheral T-cell lymphoma (PTCL) in 2011. Non-hydroxamate inhibitor valproic acid was used for acute myeloid leukemia (134) and now is used for the treatment of epilepsy and migraine prophylaxis. Belinostat (PXD101) is an antineoplastic agent that inhibits tumor cell proliferation by inducing apoptosis. It was approved in 2014 by the US FDA to treat peripheral T-cell lymphoma. In 2015 Panobinostat is a non-selective HDAC inhibitor and antineoplastic agent. It is approved for usage with the anti-cancer drug bortezomib and the corticoid dexamethasone for the treatment of multiple myeloma. All three inhibitors are effectively used nowadays for cancer treatment, however, they inhibit the activity of several HDAC isoforms consequently causing adverse effects such as pancytopenia, thrombocytopenia, anemia, leucopenia, neutropenia, lymphopenia.

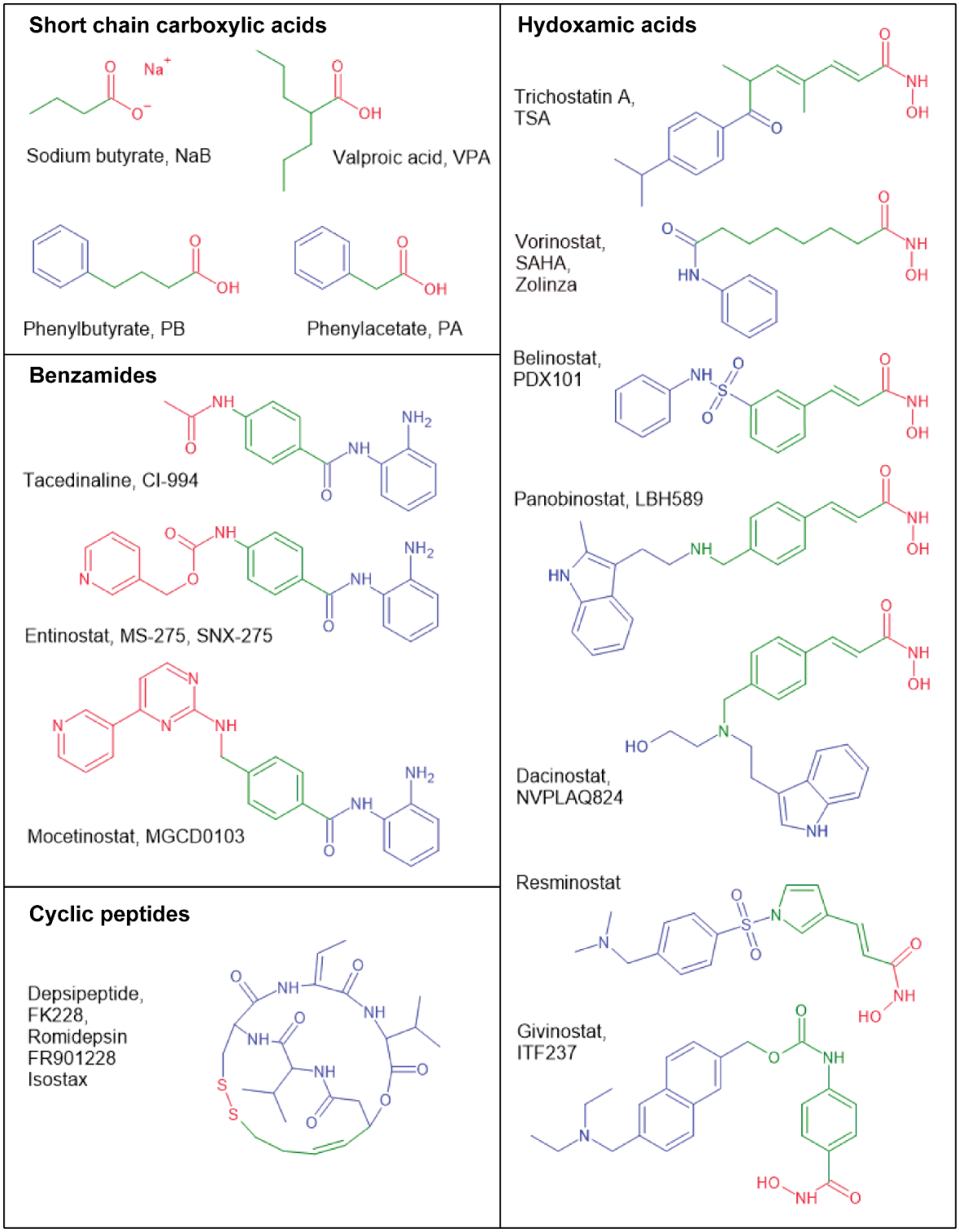

Figure 7. Chemical structure of four major classes of HDAC inhibitors: short chain carboxylic acids, benzamides, cyclic peptides, and hydroxamic acids. Different structural parts of the inhibitors are marked in color - the cap (blue), the linker (green), and the zinc-binding group (red).

Table 1. HDAC inhibitors approved by the United States Food and Drug Administration

Chemical name	FDA approved indication	Classification	Structure	IC50	Ref.
Vorinostat SAHA Zolinza®	CTCL*	hydroxamate	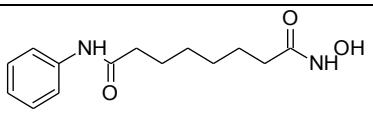	HDAC1 – 33 nM HDAC2 – 96 nM HDAC3 – 20 nM HDAC6 – 33 nM HDAC8 – 540 nM	(135)
Panobinostat LBH-589 Farydak®	CTCL*	hydroxamate	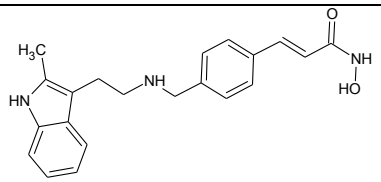	HDACs – 5 nM	(136)
Belinostat PXD101 Beleodaq®	Multiple melanoma	hydroxamate	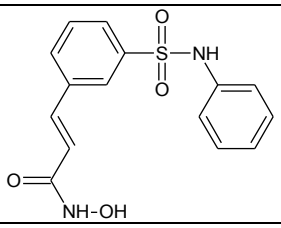	HDACs – 27 nM	(137)
Romidepsin FK228 Istodax®	CTCL* PTCL**	Cyclicpeptide	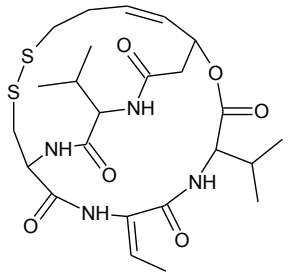	HDAC1 – 36 nM HDAC2 – 47 nM	(138)
Valproic acid Depacon®	Seizures Bipolar disorder Epilepsy Migraine	Carboxylate	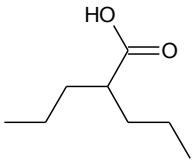	HDAC1 – 0.7 mM HDAC2 – 0.8 mM HDAC3 – 1 mM HDAC4 – 1.5 mM HDAC5 – 1 mM HDAC7 – 1.3 mM HDAC6 – > 20 mM HDAC10 – > 20 mM	(139)
Entinostat MS-275	On trial	Benzamide	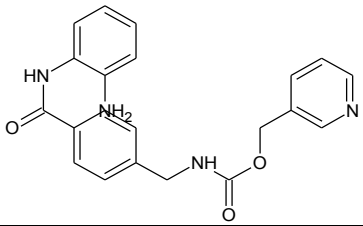	HDAC1 – 510 nM HDAC3 – 1.7 μM	(140)

* CTCL - cutaneous T-cell lymphoma; ** PTCL - peripheral T-cell lymphoma.

The development of isoform-specific HDAC inhibitor with CNS permeability and stability became an attainable goal nowadays. Available HDAC inhibitors have adverse side effects, the clinical toxicity, and affect gene expression and therefore cell-cycle progression. HDAC inhibitors have adverse drug reactions such as hepatotoxicity, teratogenicity, and pancreatitis in the case of VPA (Valproic acid) (133). Romidepsin bears adverse effects like thrombocytopenia, changes in cardiac

electrical conduction, and anemia (133). Hydroxamates cause bone marrow toxicity or thrombocytopenia. The common problem of these inhibitors is their poor pharmacokinetic properties such as fast clearance and off-target interactions.

HDAC inhibitors block the activity of HDAC isoforms subsequently causing the alteration of the acetylation status of various transcription factors, transcriptional co-regulators, and nonhistone effector molecules. This can promote or decrease gene transcription (*HSP90, Ku70, MKP-1, NF-κB, PCNA, p53, RB, Runx, SF1 Sp3, STAT, etc*). Revealing exact mechanisms of gene expression regulation and transcriptional factors acetylation by HDACs could lead to the design of selective inhibitors that would regulate a defined pathway, rather than trigger a cascade of response reactions in the cell. It will provide a better understanding of drug combinations with HDAC inhibitors.

Nowadays, new strategies are being applied for the development of new classes of HDAC inhibitors to improve their therapeutic effect and minimize adverse effects. The combination of HDAC inhibitors with proteasome inhibitors, hormonal therapy, tyrosine kinase inhibitors, DNA-hypomethylating agents has shown preclinical promise. HDAC inhibitors exert synergistic or additive antitumor effects with various chemotherapeutic agents. Additionally, new drug delivery strategies such as liposome encapsulation of an HDAC inhibitor LAQ824 have been developed. Furthermore, the combination of immune checkpoint inhibitors with HDAC inhibitors is considered to be a breakthrough in cancer treatment (141). All these strategies hold much promise and the fate of HDAC inhibitors will be defined in years to come.

1.5.3 Hydroxamic acid-based inhibitors

Most HDAC inhibitors contain hydroxamic acid – a functional group chelating the active-site zinc ion (ZBG) (142). Hydroxamates exert the highest zinc binding affinity among all HDAC inhibitors and are found to be the most active inhibitors (131). Carbonyl and hydroxyl oxygen atoms coordinate the zinc ion in a bidentate manner, although a monodentate chelating mode is observed in HDAC6 complexes with phenylhydroxamate-based inhibitors.

The ZBG of these inhibitors is represented by a hydroxamic acid moiety – binds zinc ion at the bottom of the active-site cavity. The essential characteristic of hydroxamic acid-based molecules is a four–six carbon hydrophobic methylene spacer, which occupies the hydrophobic channel. They contain a hydrophobic cap that interacts with amino acids at the rim of the catalytic pocket and the linker between the spacer and the cap. The linker can contribute to inhibitor binding when it favorably occupies the active tunnel (143). While HDACs have a conserved structure of active tunnel, the width of the tunnel differs between HDAC isoforms. Via homology modeling, it has been discovered that compared to HDAC1, the second HDAC6 catalytic domain has a much wider active tunnel rim. This knowledge was used for the design of new inhibitors with bulky and/or branched cap groups (144). Recent studies have shown that the linker chirality can increase inhibitor selectivity toward HDAC6 (145).

Additionally, the development and modification of the spacer group – thiazole, oxazole influenced the selectivity of inhibitors (146).

There were made attempts to increase the selectivity of inhibitors towards HDAC6 to reduce the dosage of inhibitors and consequently reduce adverse effects. For this reason, SAHA analogs with the modified linker have been synthesized and tested. Modification of SAHA to C5-benzyl SAHA increased inhibitor dual selectivity for HDAC6 / HDAC8 8- to 21- fold (135). The knowledge that linker modification can change isoform selectivity allows us to develop isoform-selective HDAC inhibitors.

Recently, by the application of the strategy of linker modification, a new HDAC6-selective inhibitor SS-208 has been discovered. This novel HDAC6 inhibitor contains the isoxazole-3-hydroxamate moiety as a hydrophobic linker and a zinc-binding group. It is shown that the introduction of isoxazole to inhibitor structure may increase its affinity as well as decrease the toxicity and generally improve the pharmacokinetic profile (147). The hydroxamate group of SS-208 coordinates the active-site zinc ion in a bidentate manner while all phenylhydroxamate-based inhibitors in HDAC6 complexes have a monodentate coordination mode. SS-208 is an HDAC6-selective inhibitor with an IC_{50} of 12 nM, whereas it inhibits other HDAC isoforms with IC_{50} values in the low micromolar range. SS-208 has anti-tumor activity in a mouse melanoma model. The results of this work are detailed in the manuscript that is a part of this thesis. These findings suggest that the design and development of isoform-selective HDAC6 inhibitors may become a successful way to overcome the limitations of inhibitors such as dosage and adverse effects.

2 Results

2.1 List of publications

Skultetyova L., Ustinova K., Kutil Z., Novakova Z., Pavlicek J., Mikesova J., Trapl D., Baranova, P., Havlinova B., Hubalek M., Lansky Z., Barinka C.: **Human histone deacetylase 6 shows strong preference for tubulin dimers over assembled microtubules.** *Sci Rep* **2017**, 7:11547.

Ustinova K., Novakova Z., Saito M., Meleshin M., Mikesova J., Kutil Z., Baranova P., Havlinova B., Schutkowski M., Matthias P., Barinka C.: **The disordered N-terminus of HDAC6 is a microtubule-binding domain critical for efficient tubulin deacetylation.** *J Biol Chem* **2020**, 295:2614-2628.

Shen S., Hadley M., Ustinova K., Pavlicek J., Knox T., Noonepalle S., Tavares M.T., Zimprich Ch.A., Zhang G., Robers M.B., Bařinka C., Kozikowski A.P., Villagra A.: **Discovery of a new isoxazole-3-hydroxamate-based histone deacetylase 6 inhibitor SS-208 with antitumor activity in syngeneic melanoma mouse models.** *J Med Chem* **2019**, 62 (18): 8557-8577.

2.2 Human histone deacetylase 6 shows strong preference for tubulin dimers over assembled microtubules

Background and motivation of the study

PTMs of tubulin are the mechanisms of regulation of tubulin/microtubule function and dynamics in the cell. Mainly, PMTs occur on polymerized microtubules affecting microtubule organization and interaction with other cellular components. Generally, PTMs occur at the unstructured C-terminal tails of tubulin, but lysine 40 of α-tubulin (K40) is in the flexible loop that is exposed to the microtubule lumen (74). Acetylation of K40 is one of the most conserved PTMs and is controlled by opposite activities of tubulin acetyltransferase and HDAC6. Acetylation of K40 is a hallmark of microtubule aging and prevents microtubules from the mechanical breakage (76). Moreover, the lysine acetylation of tubulin itself may influence sperm motility, fertility, cell signaling, cell cycle progression, intracellular transport, neurodegenerative diseases.

Although HDAC6 was discovered more than 20 years ago, the information about HDAC6 deacetylation of different tubulin isoforms is missing. The majority of prior studies used either only partially purified HDAC6 and orthologs and truncated variants of human HDAC6. Consequently, available information on HDAC6 substrate preferences was limited and quite often contradictory. In this work, we used highly purified human full-length HDAC6 and tubulin to biochemically characterize the deacetylation activity of HDAC6. Additionally, we investigated HDAC6s interaction with microtubules using Total internal reflection fluorescence (TIRF) microscopy.

Summary of the work

Using recombinant properly folded highly-active human full-length HDAC6 and tubulin isolated from pig brains, we conducted fluorescent microscopy measurements and biochemical deacetylation assays.

By the TIRF-microscopy we were the first to directly visualize HDAC6/microtubule interaction (Figure 1A). Our data revealed fast kinetics of HDAC6 binding to microtubules and quantification of the HDAC6 signal on microtubules pointed towards the uniform distribution of HDAC6 along the whole microtubule length. HDAC6 likely binds to the outer surface of microtubules with no preference for the microtubule tips (Figure 1B), rather than diffusing into the microtubule lumen via open tips as reported for α-TAT. HDAC6 binding to microtubules in the presence of HDAC6 inhibitor Nexturastat A was not affected suggesting that HDAC6 deacetylation activity is not required for the efficient binding to microtubules.

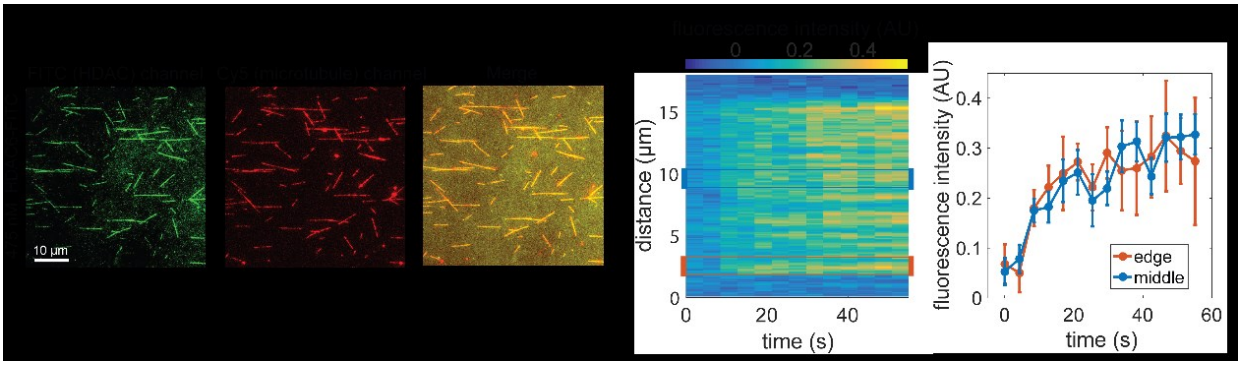

Figure 1. Interaction of HDAC6 with microtubules. A. FITC-labeled HDAC6 (green) interacts directly with microtubules (red) immobilized on a coverslip surface. Fluorescent signals of microtubules and HDAC6 co-localize along the whole length of microtubules (yellow). **B, C.** GFP-HDAC6 fusion binds uniformly along the whole length of the microtubules - a uniform increase in GFP fluorescence intensity was observed. The kymograph in Panel B depicts averaged (background subtracted) GFP fluorescence intensity of 4 microtubules of the same length (approximately 12 µm) after the addition of HDAC6-GFP in the timespan from 0 to 60 seconds. Panel C shows the averaged GFP signal (±s.d.) over time at the edge of the microtubules (orange line) and in the middle (blue line). 1.5 µm regions used for the averaging are indicated in the kymograph B) by orange and blue rectangles.

We also provided the missing quantitative and qualitative data on HDAC6 enzymatic preferences for different tubulin forms. The comparison of the HDAC6 deacetylation efficiency of tubulin polymeric forms with distinctly different geometries (microtubules, Zn-sheets, and Dolastatin-10 rings) with free tubulin dimers points to the decrease in the deacetylation efficiency 1,500-fold, 750-fold, and 100-fold, respectively (Figure 2A). As the surface of the lumen and thus K40 is exposed in the case of Zn-sheets and Dolastatin-10 rings, and the deacetylation rates differ substantially, we concluded that residues forming both lateral and longitudinal contacts within the tubulin polymer lattices are critical for tubulin deacetylation by HDAC6.

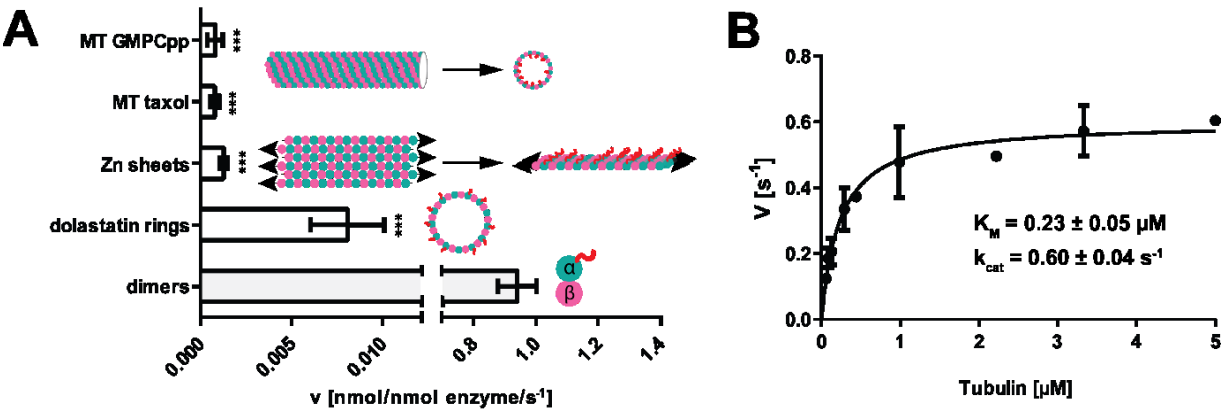

Figure 2. HDAC6 deacetylation of free tubulin dimers and tubulin polymeric forms. A. HDAC6 shows increased deacetylation activity on tubulin dimers over zinc sheets, Dolastatin-10 rings, and taxol/GMPCPP-stabilized microtubules. The data were obtained using Western blot quantification. Free tubulin dimers are deacetylated 100- to 1,500-fold more efficiently than are tubulin polymeric forms. α-tubulin and β-tubulin are

shown as blue and pink spheres, respectively, and the acetyl group as a red ribbon. **B.** Steady-state kinetics of tubulin dimer deacetylation by HDAC6. Michaelis-Menten constants (K_m and k_{cat}) were calculated from non-linear regression fit using the GraphPad program.

The αK40 loop derived peptides of different lengths were deacetylated by HDAC6 with a negative correlation between the peptide length and deacetylation rates. The peptides were deacetylated 12- to 200-fold less efficiently compared to tubulin dimers. Our data show that amino acids of the αK40 loop have a somewhat limited contribution to substrate binding and recognition. On the contrary, structural features outside the αK40 loop such as lateral and longitudinal interfaces contribute to substrate binding and recognition.

Overall, this study offers a deeper understanding of HDAC6 mediated tubulin deacetylation in the cell. We provide a detailed kinetic analysis of tubulin deacetylation by HDAC6 (Figure 2B). Furthermore, we show that the deacetylation of tubulin by HDAC6 requires complex interactions with the substrate. Understanding this complex interaction might form a basis for the design and discovery of selective inhibitors targeting tubulin deacetylation. This knowledge further strengthens the theory of the correlation between tubulin acetylation and microtubule age and will help to understand the complex system of post-translational modifications in cells.

My contribution

I have designed microscopy-related experiments, collected, evaluated, and interpreted TIRF microscopy data, and participated in the manuscript preparation.

SCIENTIFIC REPORTS

OPEN

Human histone deacetylase 6 shows strong preference for tubulin dimers over assembled microtubules

Received: 2 March 2017
Accepted: 29 August 2017
Published online: 14 September 2017

Lubica Skultetyova[1,2], Kseniya Ustinova[1], Zsofia Kutil[1], Zora Novakova[1], Jiri Pavlicek[1], Jana Mikesova[1], Dalibor Trapl[1], Petra Baranova[1], Barbora Havlinova[1], Martin Hubalek[3], Zdenek Lansky[1] & Cyril Barinka[1]

Human histone deacetylase 6 (HDAC6) is the major deacetylase responsible for removing the acetyl group from Lys40 of α-tubulin (αK40), which is located lumenally in polymerized microtubules. Here, we provide a detailed kinetic analysis of tubulin deacetylation and HDAC6/microtubule interactions using individual purified components. Our data unequivocally show that free tubulin dimers represent the preferred HDAC6 substrate, with a K_M value of 0.23 μM and a deacetylation rate over 1,500-fold higher than that of assembled microtubules. We attribute the lower deacetylation rate of microtubules to both longitudinal and lateral lattice interactions within tubulin polymers. Using TIRF microscopy, we directly visualized stochastic binding of HDAC6 to assembled microtubules without any detectable preferential binding to microtubule tips. Likewise, indirect immunofluorescence microscopy revealed that microtubule deacetylation by HDAC6 is carried out stochastically along the whole microtubule length, rather than from the open extremities. Our data thus complement prior studies on tubulin acetylation and further strengthen the rationale for the correlation between tubulin acetylation and microtubule age.

Tubulin post-translational modifications (PTMs) provide mechanisms enabling highly conserved α/β-tubulin dimers to form microtubules (MTs) endowed with different functional properties. The best studied PTMs, collectively called the "tubulin code", include detyrosination, glutamylation, glycylation, polyamination, phosphorylation, and acetylation[1–6]. Whereas the majority of PTMs are found within the unstructured C-terminal tubulin tails decorating the outer surface of microtubules, acetylation at the Lys40 side chain of the α-tubulin subunit (αK40) stands out due to its presumed localization within the microtubule lumen[7]. This αK40 acetylation is a hallmark of long-lived stable microtubules and can affect sperm motility, fertility, cell signaling, and cell cycle progression[8–10]. Additionally, microtubule acetylation may be a regulatory step for intracellular kinesin/dynein-mediated transport[11–13] and, consequently, has been implicated in the pathologies of a variety of human neurodegenerative diseases. At the same time, intraluminal positioning of the flexible loop harboring αK40 understandably brings about questions concerning the accessibility of this site for relevant modifying enzymes.

The acetylation status of αK40 is defined by the opposing activities of tubulin acetyl transferases, most notably the mammalian α-tubulin N-acetyltransferase 1 (αTAT1) and its ortholog MEC-17 from *C. elegans*[9,14], and lysine deacetylases, namely histone deacetylase 6 (HDAC6) and SIRT2[15–17]. Although HDAC6 and SIRT2 may interact and function together, several studies indicate that HDAC6, not SIRT2, is the major tubulin deacetylase[18,19]. A recent report[20] suggests that the two deacetylases might have both overlapping and distinct tubulin deacetylase activities depending on the specific structural contexts of αK40, as well as the physiological state of the cell. Of note, several additional acetylation sites in tubulin have been identified to date[21–23], but their functional role and the characterization of the enzymes responsible require further research in this direction.

[1]Institute of Biotechnology CAS, BIOCEV, Prumyslova 595, 252 50, Vestec, Czech Republic. [2]Department of Biochemistry, Faculty of Natural Science, Charles University, Albertov 6, Prague 2, Czech Republic. [3]Institute of Organic Chemistry and Biochemistry of the Academy of Sciences of the Czech Republic, Flemingovo n. 2, 166 10, Prague 6, Czech Republic. Correspondence and requests for materials should be addressed to C.B. (email: cyril.barinka@ibt.cas.cz)

HDAC6, a member of the class IIb zinc-dependent histone deacetylases, stands out as a structurally and functionally unique member of the HDAC family due to its complex domain organization and atypical predominantly cytosolic localization. HDAC6 harbors the tandem catalytic domains DD1 and DD2, a cytoplasm-anchoring serine/glutamate-rich repeat motifs, and the C-terminal ubiquitin binding domain, which is implicated in sequestering misfolded polyubiquitinated protein aggregates and transporting them to the aggresome[24]. Several post-translational modifications, including phosphorylation, acetylation, and S-nitrosylation, have been shown to regulate HDAC6 deacetylase activity, nucleus/cytoplasm shuttling, and interactions with physiological partners[25–28]. Given the broad repertoire of HDAC6 substrates and interaction partners (e.g., heat-shock protein 90, cortactin, peroxiredoxin, β-catenin, dynein)[29–33], it is not surprising that the enzyme is involved in many (patho) physiological processes, including cell motility and metastasis, cell signaling, protein folding and degradation, and inflammation. Consequently, targeting HDAC6 is a viable strategy for the treatment of various disorders, such as neurodegenerative diseases, multiple myelomas, and solid malignancies[34–37].

Despite the fact that HDAC6 was identified as the major tubulin deacetylase more than 10 years ago, there is a surprising nearly total absence of qualitative/quantitative data concerning HDAC6 preferences for different tubulin forms. Moreover, when available, these findings are relatively contentious and somewhat difficult to reconcile. Finally, the majority of studies have used either partially purified HDAC6 and/or tubulin preparations, or orthologs and truncated variants of human HDAC6, as these are more readily available in the amounts required for biochemical/structural studies. In their seminal paper, Hubbert *et al*., described for the first time the way in which HDAC6 functions as a tubulin deacetylase. *In vitro* experiments using mouse HDAC6 revealed that the enzyme deacetylates assembled microtubules, but not free tubulin[15]. This notion was subsequently challenged by several reports showing that both free heterodimers and assembled MTs can serve as HDAC6 substrates, but no quantitative data to evaluate substrate preferences were presented[16, 17, 38]. In this report, we exploited a bottom-up biochemical approach using purified full-length human HDAC6 and tubulin to assess HDAC6 substrate preferences and shed light on the structural features that govern HDAC6/tubulin interactions. We also directly visualized HDAC6/tubulin interactions, suggesting that the enzyme binds preferentially to the external face of assembled microtubules.

Results

Expression and characterization of full-length human HDAC6. The HEK293T-based mammalian system was selected for heterologous HDAC6 expression to secure the closest semblance to the native wild-type HDAC6 protein existing in human cells/tissues. Using a combination of affinity and size-exclusion chromatography, we were able to obtain homogenous preparation of untagged human HDAC6 (Fig. 1a) with yields of approximately 2 mgs per liter of original cell culture.

Previous reports have pointed out the influence of PTMs (namely acetylation and phosphorylation) on HDAC6 deacetylase activity[25, 26, 39–41]. To determine whether any such "activity-altering" PTMs existed in our HDAC6 preparation, the protein was analyzed using liquid chromatography-tandem mass spectrometry (LC-MS/MS). The deconvolution of the MS/MS spectra revealed the absence of any known (or unreported) PTM, thus excluding the possibility of our *in vitro* experiments being impacted by HDAC6 PTMs (data not shown).

To assess the deacetylase activity of untagged HDAC6, we determined its kinetic parameters in comparison to several commercially available substrates (Fig. 1b). K_M values were in the low micromolar range (3.7–11.3 μM) and turnover numbers (k_{cat}) ranged from 0.9–2.2 s^{-1}, in good agreement with data reported in the literature[42, 43]. Furthermore, using the same substrate set, we also verified that the attachment of N-terminal tags (either HALO- or GFP-tags) does not influence HDAC6 deacetylation activity (Supplementary Fig. S1). Finally, HDAC6 was profiled against suberoylanilide hydroxamic acid (SAHA), trichostatin (TSA), and nexturastat A (Nex A), with IC_{50} values of 3.8, 0.16, and 2.9 nM, respectively, also in the range reported in scientific literature[44–47] (Fig. 1c).

Overall, the above-mentioned characteristics confirm that our HDAC6 is a homogenous, properly folded, highly-active full-length enzyme well suited for the presented biochemical experiments.

HDAC6 prefers tubulin dimers to microtubules. Several earlier studies assessed the deacetylation activity of HDAC6 on tubulin and polymerized microtubules[15–17, 38, 48]; however, these studies predominantly used orthologs of human HDAC6 (mouse, zebrafish), their truncated (or tagged and modified) variants, and/or unpurified (or partly purified) assay components. To the best of our knowledge, none of the prior studies attempted to quantify deacetylase preferences of the full-length human HDAC6 for free tubulin versus assembled MTs. For our biochemical experiments, we took advantage of the fact that tubulin isolated from porcine brain tissue is highly acetylated, with the αK40 acetylation levels comprising 36% of the total tubulin (Supplementary Fig. S2).

We directly compared the catalytic activity of human HDAC6 on free tubulin dimers against its activity on paclitaxel- and GMPCPP-stabilized MTs (Fig. 2). Using highly-purified components, we showed that free tubulin dimers are the preferred HDAC6 substrate. At a 1 μM substrate concentration, the deacetylation rate was 0.6 mol/mol*s and 0.0004 mol/mol*s for tubulin dimers and stabilized MTs, respectively; in other words, the deacetylation rate was approximately 1,500-fold higher for αβ-tubulin dimers. Importantly, deacetylation rates on both paclitaxel- and GMPCPP-stabilized MTs were virtually identical, suggesting that substantially slower deacetylation of assembled MTs does not result from the compound interference, but is rather linked to either tubulin lattice packing or the limited accessibility of the luminal αK40 loop.

Contacts within polymer lattices inhibit tubulin deacetylation by HDAC6. Unlike other known microtubule PTMs, which are positioned at the external surface of MTs, αK40 is confined to the MT lumen. Consequently, the substantially lower MT deacetylation rates (as compared to tubulin dimers) could simply result from hindered accessibility of the αK40 loop by the enzyme. Additional factors, such as the transition from curved (free tubulin) to straight (microtubules) tubulin dimer conformations or the blockage of HDAC6/tubulin

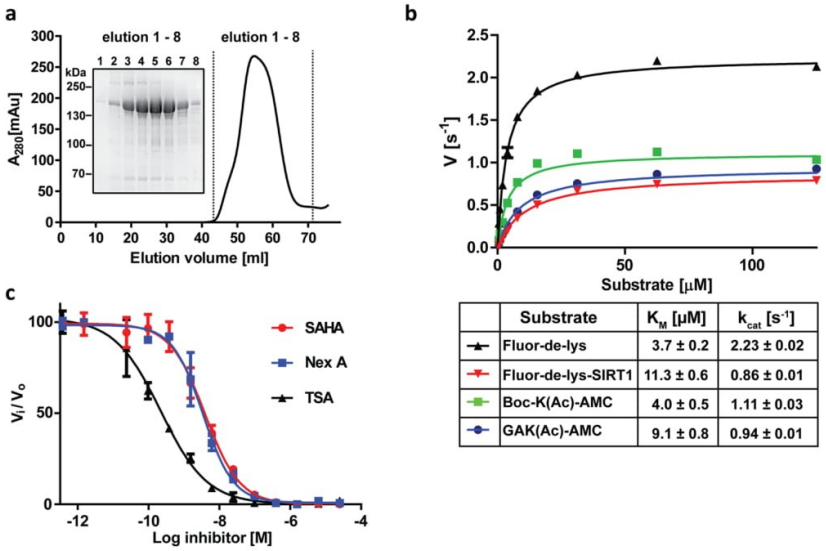

	Substrate	K_M [μM]	k_{cat} [s^{-1}]
▲	Fluor-de-lys	3.7 ± 0.2	2.23 ± 0.02
▼	Fluor-de-lys-SIRT1	11.3 ± 0.6	0.86 ± 0.01
■	Boc-K(Ac)-AMC	4.0 ± 0.5	1.11 ± 0.03
●	GAK(Ac)-AMC	9.1 ± 0.8	0.94 ± 0.01

Figure 1. Purification and characterization of full length HDAC6. (**a**) Elution profile of human HDAC6 from a Superdex 16/600 HR200 size-exclusion column (SEC) and reducing SDS-PAGE analysis of HDAC6 fractions from the SEC, documenting monodispersity and >95% purity of the final enzyme preparation, respectively. (**b**) Steady-state kinetics of HDAC6 on commercial fluorogenic peptide substrates GAK(Ac)-AMC, Boc-K(Ac)-AMC, FLUOR-DE-LYS, and FLUOR-DE-LYS-SIRT1. Michaelis-Menten constants (K_M and k_{cat}) for individual peptides, calculated from non-linear regression fit using the GraphPad program, are shown in the embedded table. Data represent mean values ± s.d. (n = 3). **(c)** IC50 values for SAHA (3.8 nM), Nexturastat A (2.9 nM), and Trichostatin A (0.16 nM) were determined using a fluorometric assay with 10 μM (Ac)GAK(Ac)-AMC as a substrate. Data are plotted as mean values ± s.d. from three independent experiments (n = 3).

interaction interfaces by longitudinal/lateral contacts within the polymer lattice, may also play a role. To distinguish between the above-mentioned scenarios, we assessed HDAC6 deacetylation activity using microtubules, Zn-sheets, and Dolastatin-10 rings, three tubulin polymeric forms with distinctly different geometries (Fig. 2).

Dolastatin-10 induces single-walled tubulin rings by curving individual protofilaments such that their luminal surface becomes accessible on the exterior of the ring[49]. In Zn-sheets, protofilaments of alternating polarity are arrayed in parallel and the "luminal" surface, as would be defined in microtubules, is exposed to the solution[50]. All tubulin polymers were deacetylated substantially (100- to 1,500-fold) slower than were free dimers (Fig. 2). As the "luminal" surface harboring the αK40 loop is exposed in both Zn-sheets and Dolastatin-10 rings, lower deacetylation rates cannot be simply attributed to the inaccessibility of the αK40 within the lumen of assembled MTs. Instead, we argue that it is the presence of both lateral and longitudinal contacts within the tubulin polymer lattices that negatively influences deacetylation by HDAC6, as documented by 100- and 750-fold slower deacetylation rates observed for Dolastatin-10 rings and Zn-sheets, respectively.

Structural features outside the αK40 loop of αβ-tubulin are important for HDAC6 interactions. We first turned our attention to HDAC6 recognition of the isolated αK40 loop to answer the following questions: (i) is the "isolated" sequence of the αK40 loop recognized by HDAC6; (ii) what is the minimum sequence length to be processed/recognized; and (iii) is there a difference in deacetylation rates between the αK40 loop in the form of a free peptide and within the context of an αβ-tubulin dimer?

To this end, we synthesized a series of peptides of different lengths derived from the human α-tubulin sequence that are centered around acetylated αK40 (T3–T19). Next, using a deacetylation assay followed by high-performance liquid chromatography (HPLC) analysis, we determined the kinetic parameters of HDAC6 against acetylated αK40-derived peptides (Fig. 3). The K_M values for the peptides were in the high micromolar range (88 μM to 328 μM for T9 and T15, respectively), revealing relatively low affinity of HDAC6 for the isolated αK40 sequences. At the same time, K_M values for all tubulin-derived peptides were very similar and there was no clear trend showing increasing affinity with the extension of the peptide sequence. Consequently, it is likely that within the isolated αK40 loop sequence, there is a limited contribution of residues beyond the P_1 and P_{-1} positions to substrate binding/recognition. We also noticed a negative correlation between the peptide length and deacetylation rates, with the shortest T3 tripeptide being deacetylated 20-fold more efficiently when compared to the T19 sequence (Fig. 3a).

We then used the same experimental setup to directly compare deacetylation rates of the αK40 loop in its "free" peptidic form and in the context of αβ-tubulin dimers at a 3 μM concentration. Interestingly, free peptides were deacetylated approximately 12- to 200-fold less efficiently than were tubulin dimers (Fig. 3c). Additionally,

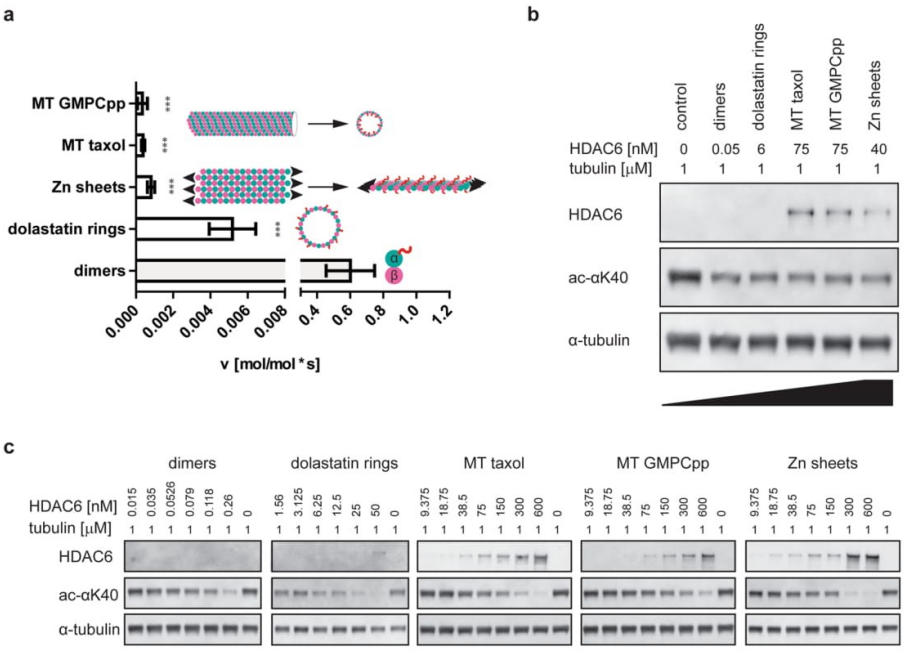

Figure 2. HDAC6 shows strong preference for tubulin dimers over polymeric forms. (**a**) Deacetylation activity of HDAC6 on tubulin polymers (zinc sheets, Dolastatin-10 rings, and taxol/GMPCPP-stabilized microtubules [MT]) and tubulin dimers was determined using Western blot quantification. Results clearly show that free dimers are deacetylated 100- to 1,500-fold more efficiently than are tubulin polymeric forms. Data represent mean values ± s.d. ($n \geq 3$; ***$p < 0.001$). Organization of tubulin in polymers is illustrated in schemes embedded in the graph, with α-tubulin and β-tubulin shown as blue and pink spheres, respectively, and the acetyl group as a red ribbon. (**b**,**c**) Representative Western blots illustrating distinct HDAC6 deacetylase activity on tubulin dimers and polymeric tubulin forms. Individual substrates (1 μM) were incubated with indicated concentrations of HDAC6 for 1 h at 37 °C. Protein samples were separated by SDS-PAGE, electrotransferred to a polyvinylidene difluoride (PVDF) membrane and acetylation levels quantified using an αK(Ac)40-specific fluorescence signal normalized to the amount of total tubulin detected by rabbit polyclonal anti-α tubulin antibody.

we determined the kinetic parameters of HDAC6 for free tubulin to be $K_M = 0.23 \pm 0.05\,\mu M$ and $k_{cat} = 0.6\,s^{-1}$ (Fig. 3d), revealing that the dramatically higher (>6,000-fold) HDAC6 catalytic efficacy (K_M/k_{cat}) for the natively-folded tubulin, as compared to free peptides, stems mostly from the increase in binding affinity, rather than from the increase in reaction speed. These results suggest that sequences and/or structural features outside the αK40 loop contribute to HDAC6/tubulin interactions. Such additional interaction sites might include lateral/longitudinal interfaces buried within tubulin polymeric lattices, as revealed by experiments where different MT polymers were used as substrates (see above).

HDAC6 binds and deacetylates microtubules without a preference for microtubule tips. Given the relatively slow, but clearly distinguishable deacetylation of MTs by HDAC6, we asked how the enzyme accesses the αK40 loop in the MT lumen. Non-exclusive options would involve entering the MT lumen via open tips, through bends and breaks in the MT lattice, or by deacetylation of the αK40 loop "protruding" from the external microtubule face.

To this end, we first investigated the localization and kinetics of HDAC6 interactions with assembled MTs using total internal reflection fluorescence (TIRF) microscopy. Rhodamine-labeled paclitaxel-stabilized MTs were immobilized on a cover slip, probed with either GFP-HDAC6, or FITC-HALO-HDAC6 fusions, and then directly visualized using a Nikon Ti-E microscope equipped with H-TIRF System (Fig. 4). The kinetics of HDAC6 binding to MTs were quite fast, with all MTs fully decorated in less than a minute. Based on signal distribution analysis during HDAC6 binding to the MTs, we did not detect any preferential binding to MT tips. Instead, we observed uniformly-distributed interactions along the MT length throughout the whole experiment, up until the time that the binding equilibrium was established. The rapid binding kinetics and even signal distribution suggest that HDAC6 does not enter the microtubule lumen from the open tips, but rather binds to and interacts with the external face of MTs.

Given the observed interactions of HDAC6 with the outer MT surface, we wondered whether HDAC6 binding to MTs is also translated into stochastic, rather than open-end favored, MT deacetylation. To answer this

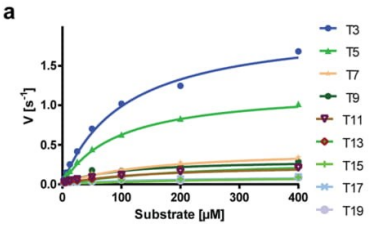

b

Peptide	Sequence	V_{max} (s^{-1})	K_M (μM)
T3	Abz-D{K-Ac}T--NH2	2.03 ± 0.10	105 ± 13
T5	Abz-SD{K-Ac}TI--NH2	1.21 ± 0.03	93 ± 6
T7	Abz-PSD{K-Ac}TIG--NH2	0.44 ± 0.02	149 ± 12
T9	Abz-MPSD{K-Ac}TIGG--NH2	0.31 ± 0.04	88 ± 28
T11	Abz-QMPSD{K-Ac}TIGGG--NH2	0.25 ± 0.01	141 ± 19
T13	Abz-GQMPSD{K-Ac}TIGGGD--NH2	0.32 ± 0.03	223 ± 39
T15	Abz-DGQMPSD{K-Ac}TIGGGDD--NH2	0.12 ± 0.01	328 ± 64
T17	Abz-PDGQMPSD{K-Ac}TIGGGDDS--NH2	0.10 ± 0.01	153 ± 45
T19	Abz-QPDGQMPSD{K-Ac}TIGGGDDSF--NH2	0.10 ± 0.03	228 ± 139

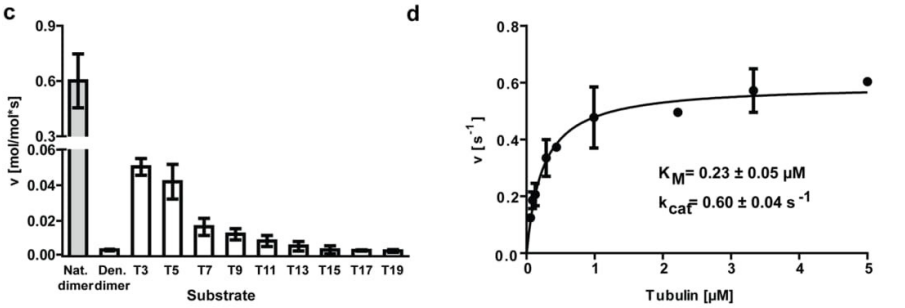

Figure 3. Structural features outside the αK40 loop are required for efficient substrate deacetylation by HDAC6. (**a**,**b**) Michaelis-Menten kinetics for peptides derived from the Lys40 of α-tubulin (αK40) loop (3-mer to 19-mer; T3 through T19) were determined *in vitro* using an HPLC-based assay (**a**). Corresponding kinetic parameters derived from the non-linear regression fit of experimental data, together with peptide sequences, are shown in (**b**). High micromolar K_M values indicate low affinity of HDAC6 for tested peptides, with limited contribution of residues that do not directly neighbor the central acetyllysine for the overall HDAC6 affinity/specificity. (**c**) Comparison of HDAC6 deacetylation rates using various substrates (natively-folded αβ-tubulin dimers, denatured tubulin dimers, peptides T3 through T19) at identical 3 μM concentrations. Deacetylation rates were determined using an HPLC assay for peptides and Western blotting quantification for tubulin dimers. Natively folded tubulin dimers are deacetylated 50- to 800-fold more efficiently than are either denatured tubulin dimers or "isolated" αK40 loop-derived peptides, suggesting that interactions/structural features outside the αK40 loop are required for efficient HDAC6/tubulin interactions. Data are presented as mean values ± s.d. (n = 3). (**d**) Steady-state kinetics of tubulin dimer deacetylation by HDAC6. Michaelis-Menten constants (K_M and k_{cat}) were calculated from non-linear regression fit using the GraphPad program. Data represent mean values ± s.d. (n = 3).

question, taxol-stabilized MTs (1 μM) were deacetylated using 2 μM HDAC6 in the BRB80 buffer, and the time course of deacetylation was then evaluated side-by-side both via fluorescence microscopy and biochemically (Fig. 5). The fluorescence microscopy and the parallel quantitative Western blotting revealed that the αK40 acetylation decreased over time, with only 10–15% of the original acetylation levels remaining after 120 minutes. More importantly, we observed that the extent of the deacetylation by HDAC6 was uniform along the whole MT length, as evidenced by the constant ratio of the immunofluorescence signal between the αK40 and total tubulin at microtubule tips, and the distance of 10 μm towards the MT center (Fig. 5a). Surprisingly, the spatio-temporal pattern of MT deacetylation appears to differ from the opposite reaction carried out by tubulin acetyltransferase, which favors open MT tips as the site of action[51–53].

Discussion

Although it has been known for more than a decade that HDAC6 is the primary deacetylase responsible for the removal of the acetylation mark at the αK40 position of tubulin, there are surprisingly few quantitative data characterizing human HDAC6 as tubulin deacetylase. Our report thus fills this gap by offering a detailed biochemical analysis of tubulin deacetylation by full-length human HDAC6, which reveals a strong preference for tubulin dimers over assembled microtubules. Additionally, we show that although isolated peptides derived from the αK40 loop are deacetylated by the enzyme, the structural context of native tubulin outside the loop is critical for highly efficient deacetylation. Finally, we directly visualized HDAC6/tubulin interactions for the first time, suggesting predominant HDAC6 binding to the external surface of assembled MTs.

The present study employed a bottom-up approach, where individual, isolated components were first purified and then combined and examined in a panel of biochemical and biophysical experiments. To this end, we cloned, expressed, and purified to homogeneity several human HDAC6 constructs, together with the corresponding control proteins in HEK293T cells. When we compared the activity of our HDAC6 preparations to the activities of recombinant proteins produced in *E. coli* or baculovirus systems (commercially available and/or reported in literature) our HEK293T-expressed enzymes were typically more active on equivalent substrates[42,43,48]. As the

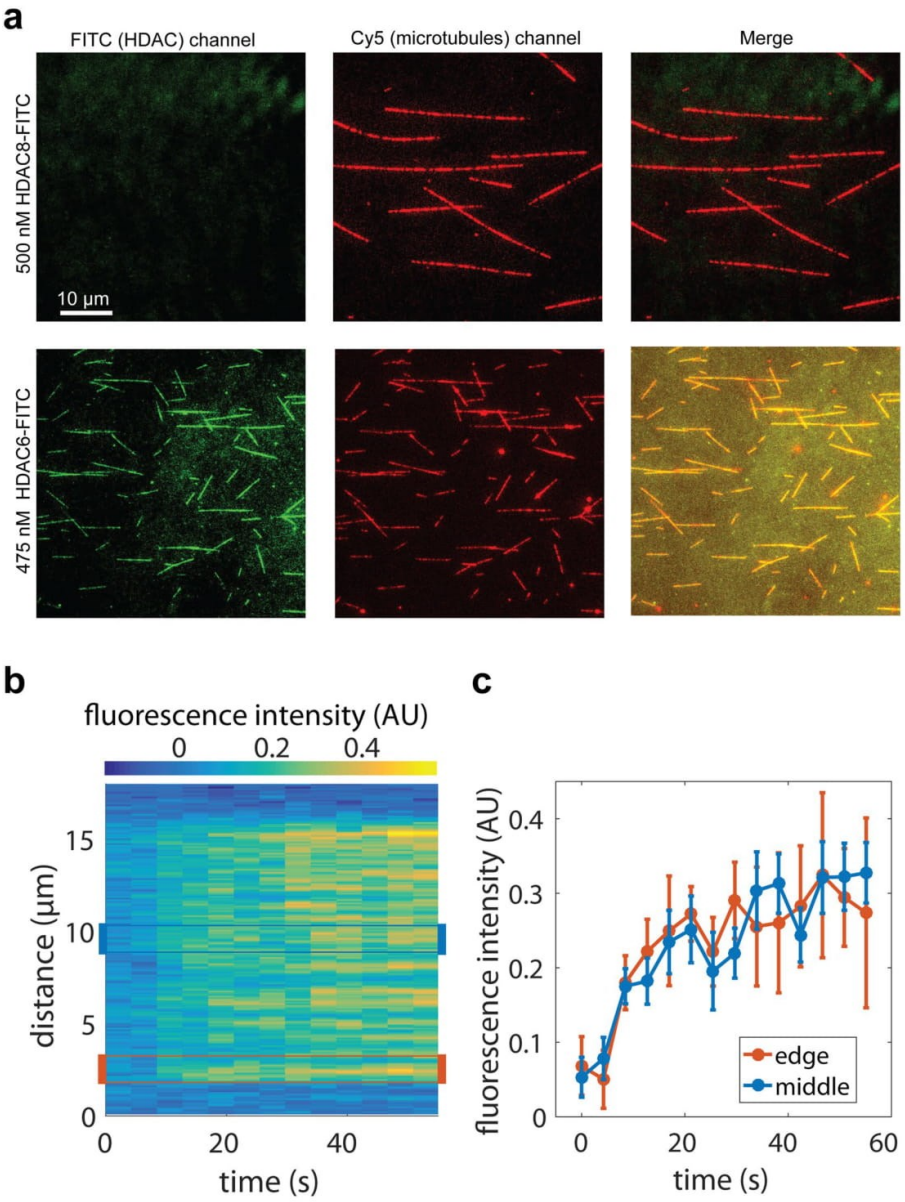

Figure 4. Interaction of HDAC6 with microtubules visualized by TIRF microscopy. (**a**) HDAC6 interacts directly with microtubules. Cy5-labeled microtubules were immobilized on a glass coverslip surface. Micrographs show microtubules (red) in the presence of 500 nM HDAC8-FITC (green; negative control, upper panel) or 475 nM FITC-labeled HDAC6 (green; lower panel). In the presence of FITC-labeled HDAC6, fluorescent signals of microtubules and HDAC6 co-localize along the whole length of microtubules (yellow). (**b**,**c**) HDAC6-GFP binds uniformly along the whole length of the microtubules. GFP-HDAC6 fusion was added to surface-immobilized microtubules and visualized in the 488 channel using TIRF microscopy. Uniform increase in GFP fluorescence intensity was observed along the whole length of microtubules. The kymograph in Panel B depicts averaged (background subtracted) GFP fluorescence intensity of 4 microtubules of the same length (approximately 12 µm) after the addition of HDAC6-GFP in the timespan from 0 to 60 seconds. The right panel shows the averaged GFP signal (±s.d.) over time at the edge of the microtubules (orange line) and in the middle (blue line). The regions (width of 1.5 µm) used for the averaging are indicated in the kymograph (**b**) by orange and blue rectangles.

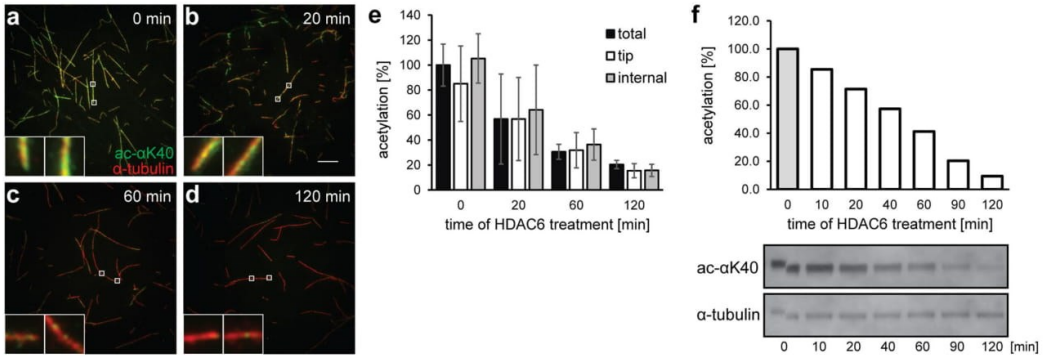

Figure 5. Stochastic, time-dependent deacetylation of assembled microtubules by HDAC6. *In vitro* assembled microtubules (1 μM) were treated with 2 μM human HDAC6 in BRB80 buffer. Deacetylation reactions were terminated at defined time points by the addition of 10 μM SAHA, and the acetylation of αK40 was quantified in parallel by indirect immunofluorescence microscopy (**a**–**e**) and Western blotting (**f**). (**a**–**e**) Indirect immunofluorescence microscopy was used to visualize the spatial distribution of αK40 acetylation signals along the length of microtubules at the given time points (upper right corner). Microtubules were immobilized on poly-L-lysine coverslips and probed with anti-αK(Ac)40 (green) and anti-α-tubulin (red) antibodies. The staining intensity of acetylated αK40 decreases over the time and the decrease parallels changes observed in the concomitant biochemical experiment. Additionally, the signal decrease is uniform over the whole length of the microtubules (see insets and panel e), suggesting that deacetylation of MTs by HDAC6 does not spread from the open tips, but is rather stochastic throughout the MT length. The left insets show microtubule tips and the right insets show the internal parts of microtubules positioned 10 μm from the tip. (**e**) Shows averaged intensity of the signal originating from a whole microtubule (total), the tip, and an area positioned 10 μm from the tip (internal). Bar = 10 μm. (**f**) Protein samples were electrotransferred to a PVDF membrane following SDS-PAGE separation, and then acetylation levels were quantified using an αK40-specific fluorescence signal normalized to the amount of total tubulin detected by rabbit polyclonal anti-α tubulin antibody. The decrease parallels changes observed in the concomitant immunofluorescence microscopy experiment.

increased activity cannot be linked to post-translation modifications, which are absent from our samples, a more likely explanation would be a higher percentage of enzymatically competent molecules in our HDAC6 preparations, which are thus more suitable for the present biochemical experiments.

Next, we evaluated the *in vitro* HDAC6 activity using a panel of different substrates. At the peptide level, HDAC6 deacetylates αK40-derived peptides with relatively low affinity (high micromolar K_M values) and k_{cat} values in the range of 0.1–2 s^{-1}. For comparison, SIRT2 deacetylates the T9 peptide somewhat less efficiently ($k_{cat} = 0.144 \pm 0.005\ s^{-1}$ and $k_{cat}/K_M = 894 \pm 100\ M^{-1}s^{-1}$)[17], whereas αTAT1 has no activity on the T19 peptide[54]. The HDAC6 deacetylation of the T3–T19 peptide series clearly shows that amino acids beyond positions P_{-1} and P_{+1} around the central lysine are not critical for the recognition of the target peptidic substrates by HDAC6. These results are consistent with our unpublished data, as well as with reports mapping substrate specificity of HDAC6, which show that the enzyme is rather promiscuous at the peptide level, with few positional amino acid preferences[55]. A mechanistic explanation of these biochemical observations was recently provided by the crystal structure of HDAC6 complexes with tubulin/histone-derived peptides, which revealed that HDAC6/peptide contacts are limited to the recognition of the scissile acetyllysine, namely direct and water-mediated contacts with the acetyllysine amide and carbonyl groups, respectively[56].

There is a clear difference between recognition and deacetylation of peptidic substrates and tubulin. Understandably, the recognition pattern of tubulin dimers by HDAC6 is considerably more complex than that of short peptides. This was supported in the current study by the substantially lower Michaelis constant ($K_M = 0.23$ μM) of the deacetylation reaction using tubulin dimers as a substrate (Fig. 3d). Additionally, overall catalytic efficacy (k_{cat}/K_M) was 2.6 $\mu M^{-1}s^{-1}$ and 0.00044 $\mu M^{-1}s^{-1}$ for tubulin dimers and the T19 peptide, respectively, revealing a striking 6,000-fold preference for native tubulin dimers as a substrate. Furthermore, in contrast to tubulin dimers isolated from porcine brains in a natively-folded state (confirmed by its ability to polymerize into MTs), when thermally-denatured tubulin was used as a substrate, its deacetylation rate by HDAC6 was much slower, more in the range of the deacetylation rates of free peptides (Fig. 3c), implying that the secondary/tertiary structural features, rather than simple linear amino acid motifs, outside the αK40 loop are critical for interactions with HDAC6. Our study points towards residues at the longitudinal/lateral interfaces of tubulin, which are buried in tubulin polymers, as being critical for free tubulin recognition/deacetylation. Although HDAC6/tubulin interactions are not fully understood, a study by Miyake *et al.*, provided some mechanistic explanation by showing that in addition to residues located at the rim of the HDAC6 tunnel leading to the catalytic site, a uniquely-positioned H25 α-helix and Trp459 and Asn460 residues in a flexible loop joining helices H20 and H21 are critical for tubulin deacetylation. At the same time, substitutions at these positions have a limited effect on the deacetylation of peptidic substrates, indicating that the capacity to use/bind tubulin as a substrate, rather than the catalytic potential of HDAC6, is impaired[48].

The quantitative data reported here demonstrate that free tubulin dimers are deacetylated by full-length human HDAC6 approximately 1,500-fold more efficiently than are assembled MTs. Similar preferences were also noticed by Miyake *et al.*, who showed that the truncated *Danio rerio* enzyme prefers free tubulin over MTs, although in that study, the difference in the deacetylation rate was only approximately 2.5-fold. This paper, which is to the best of our knowledge the only other report providing quantitative data on HDAC6 preferences for individual tubulin forms, suggests that there are substantial differences in tubulin deacetylation among individual HDAC6 orthologs and likely also between full-length proteins and constructs truncated beyond the tandem catalytic domains. Detailed studies concerning the impact of these and other variables (presence/absence of accessory proteins, post-translational modifications on HDAC6/tubulin) will be required to understand and reconcile intriguing discrepancies in HDAC6 substrate preferences (from an absolute preference for MTs to favoring free heterodimers) that have been reported in prior *in vivo/in vitro* studies[15–17,38,42,48,57].

Although HDAC6 is the major tubulin deacetylase, interactions between MTs and HDAC6 have not yet been visualized. Our study thus offers the first direct visualization of HDAC6 binding to the MT surface. The reported flush-in experiment, where the chamber with surface-immobilized MTs was injected with the GFP-HDAC6 fusion and binding kinetics quantified by TIRF microscopy, reveals that kinetics of HDAC6 binding to MTs are relatively fast. The initial increase in the fluorescence signal was observed within 10 seconds following the flush-in and the signal plateau was reached approximately 30 seconds later (Fig. 4). Such kinetics, together with the even distribution of the signal along the whole MT length within the monitored time period, strongly suggest that HDAC6 binds to the outer MT surface rather than diffusing into the MT lumen via open tips. This observation does not formally exclude the possibility of HDAC6 entering and binding/functioning within the lumenal cavity of MTs, but this would likely happen with considerably slower kinetics. It should also be noted that HDAC6 deacetylase activity is not required for HDAC6 binding to MTs, as the TIRF assay in the presence of the HDAC6 inhibitor Nexturastat A gave virtually indistinguishable binding curves (data not shown).

Biochemical or physiological implications of HDAC6 binding to the external surface of MTs are unclear at present. For example, such interactions can help with targeting and concentrating the enzyme at the site of its action, and binding can help HDAC6 to access the αK40 either via the open MT ends and/or through fluctuations/defects in the MT lattice observed in previous studies[58–60]. Alternatively, the binding of HDAC6 can influence the stability of MTs[61,62] and/or the dynamic properties of MTs[16]. Further structural and biological studies are required to provide more insight into these outstanding issues.

It has been shown that αTAT1 enters MT lumen in order to acetylate αK40[2,51,63], and that acetylation starts at the open tips of MTs, followed by the acetylation mark progressively spreading by longitudinal diffusion of αTAT1 in the MT lumen. Alternatively, αTAT1 can enter MT lumen via structural defects in the MT lattice. Irrespective of the mode of αTAT1 entry into the MT lumen, assembled MTs are a preferred substrate for αTAT1[51–53]. In contrast, our study reveals stochastic deacetylation of MTs by HDAC6 without any tip preferences (Fig. 5), and a similar deacetylation pattern was reported for the tandem catalytic domain construct of *D. rerio* HDAC6[48]. The underlying cause for spatial differences in αK40 acetylation and deacetylation reactions by αTAT1 and HDAC6, respectively, remains unknown at present.

Overall, our study adds another piece of information to the complex puzzle of how tubulin acetylation status is controlled by the opposing activities of αTAT1 and HDAC6, as previously suggested by others[48,64]. To this end, our data complement these findings concerning the αTAT1/tubulin interplay, and provide further rationale for the correlation between tubulin acetylation and microtubule age. As HDAC6 prefers free tubulin dimers with a velocity of >0.6 mol/mol*s, it is tempting to speculate that the pool of free tubulin dimers within cells should be mostly non-acetylated. Once MTs are formed, however, these become preferred substrates for αTAT1 and are therefore preferentially acetylated. At the same time, MTs are only inefficiently deacetylated by HDAC6. Consequently, given the inverse preferences of HDAC6 and αTAT1 for free tubulin and MTs, respectively, in the context of long-lived stable MTs, the equilibrium is clearly shifted towards acetylated αK40 (Fig. 6). Finally, ongoing investigations in our laboratory are focused on building up the complexity of our experimental system by evaluating certain variables encountered *in vivo*, such as post-translational modifications, HDAC6/tubulin interaction partners, and MT dynamics, with the aim of describing and dissecting their individual contributions and mutual interplay in relation to tubulin deacetylation by HDAC6.

Methods

Chemicals and peptides. If not stated otherwise, all chemicals were purchased from Sigma-Aldrich (St. Louis, MO, USA). Peptides were synthesized commercially by KareBay (Monmouth Junction, NJ, USA) at >90% purity and their identities were confirmed by analytical LC-MS (data not shown).

Expression plasmids. The sequence encoding human HDAC6 (NP_006035.2, UniProtKB - Q9UBN7) was used as a template for cloning all HDAC6 variants used in this report. In general, a nucleotide sequence encoding a given variant was PCR amplified with a set of desired primer pairs and inserted into the pDONR221 plasmid using the BP recombination reaction (Invitrogen, Carlsbad, CA, USA), according to the manufacturer's protocol. The identity of the resulting entry clone was confirmed by Sanger sequencing. Expression plasmids were generated via LR recombination reaction between the entry clone and a required destination vector, which typically introduced a TEV-cleavable tag at the N-terminus of the HDAC6 variant to simplify purification and/or visualization of the resulting fusion. Schematic representations of constructs used in this study are shown in Supplementary Fig. S1.

Large-scale expression of HDAC6 variants. All HDAC6 variants were expressed using HEK-293/T17 cells following transient transfection mediated by linear polyethylene imine (PEI) (Polysciences Inc., Warrington, PA, USA). To this end, the suspension culture of HEK-293/T17 cells was grown in 2 L Erlenmeyer flasks in Free

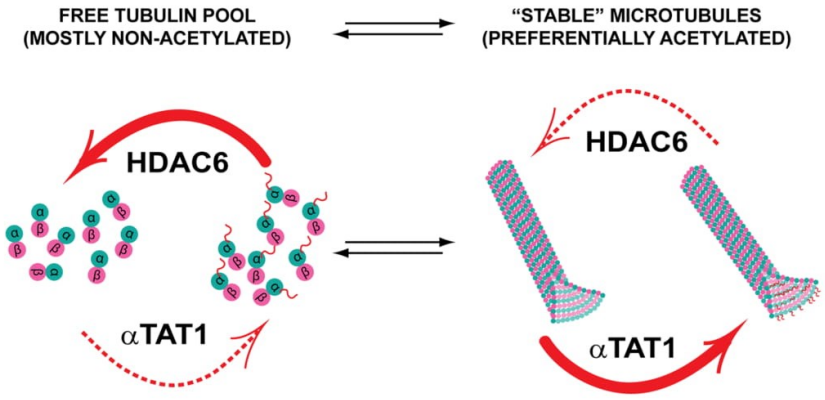

Figure 6. High acetylation levels of stable microtubules are linked to opposing substrate preferences of HDAC6 and αTAT1. HDAC6 prefers free tubulin as a substrate, whereas αTAT1 is 5-fold more active on assembled microtubules (preferences shown as thick red arrows). Consequently, it is likely that within the cell, the pool of free tubulin is mostly in the non-acetylated state. Once microtubules are assembled, however, they become preferentially acetylated by αTAT1. For dynamic microtubules, their lifetime may be too short to become extensively acetylated, whereas stable microtubules with long lifespans have a much higher probability of being fully acetylated by αTAT1. Both HDAC6 and αTAT1 thus serve as "timers" to set the clocks gauging microtubule age based on their acetylation status.

Style F17 medium (Thermo Fisher Scientific) supplemented by 0.1% Pluronic F-68 (Invitrogen) and 2 mM L-glutamine at 110 rpm under a humidified 5% CO_2 atmosphere at 37 °C. For large-scale expression, 0.7 mg of an expression plasmid was diluted in 17.5 ml of PBS, to which 2.1 ml of 1 mg/ml PEI was added. The mixture was vortexed briefly, incubated for 10 min at room temperature, and then added to 350 ml of cells at a concentration of 4×10^6 cell/ml. Four hours post-transfection, the cell suspension was diluted by an equal volume of ExCell serum-free medium. Cells were harvested 72 h post transfection by centrifugation at 500 × g for 5 min, then the cell pellet was frozen in liquid nitrogen and stored at −80 °C until further use.

Purification of HDAC6 variants. The cell pellet was lysed by sonication (24 W/1 min) in ice-cold lysis buffer (100 mM Tris-HCl, 10 mM NaCl, 5 mM KCl, 2 mM $MgCl_2$, 10% glycerol; pH 8.0) supplemented with benzonase (1 U/ml; Merck, Darmstadt, Germany) and protease inhibitor coctail (Roche, Basel, Switzerland). To further assist cell lysis, Igepal-630 was added to the cell lysate to a final concentration of 0.2% (v/v) and the mixture was incubated for 20 min on ice. NaCl was added to a final concentration of 150 mM. The lysate was then cleared by centrifugation at 40,000 × g for 30 min at 4 °C and the supernatant was loaded onto a Strep-Tactin column (IBA, Gottingen, Germany) equilibrated in the lysis buffer. Following the washing step with the lysis buffer, the fusion protein was eluted using 50 mM Tris-HCl, 150 mM NaCl, 10 mM KCl, 10% glycerol and 3 mM desthiobiotin (pH 8.0). The eluted fusion protein was concentrated to approximately 1 mg/ml and (if desired) the N-terminal tag was cleaved by the addition of the 1:20 (w/w) TEV protease overnight at 4 °C. The HDAC6 protein was then separated from tags and the TEV protease by size exclusion chromatography using the Superdex 16/600 HR200 column (GE Healthcare Bio-Sciences, Little Chalfont, UK) with 30 mM HEPES, 140 mM NaCl, 10 mM KCl, 3% glycerol, and 0.25 mM TCEP (AMRESCO, Solon, OH, USA), with a pH 7.4 adjusted with NaOH, as a mobile phase. The purified protein was concentrated to approximately 1 mg/ml and aliquots were flash frozen in liquid nitrogen and stored at −80 °C until further use.

Fluorometric assays. Deacetylation activity of HDAC6 variants was determined using acetyl-Gly-Ala-(acetyl-Lys)-AMC (GAK(Ac) -AMC; Bachem, Bubendorf, Switzerland), Boc-(acetyl-Lys)-AMC (Boc-K(Ac)-AMC; Bachem) and Fluor-de-Lys (Enzo Life Sciences, Plymouth Meeting, PA, USA) substrates. In general, a given HDAC6 variant was incubated with a substrate in a reaction buffer comprised of 50 mM HEPES, 140 mM NaCl, 10 mM KCl, 1 mg/ml bovine serum albumin (BSA), and 1 mM TCEP, at a pH 7.4 adjusted with NaOH (total volume 20 µl). This incubation occurred in 384-well plates for 30 min with vigorous shaking at 37 °C. The reaction was stopped by addition of 20 µl of trypsin solution (2 mg/ml trypsin, 20 mM Tris-HCl, 150 mM NaCl, 1 mM EDTA; pH 7.4 adjusted with NaOH). Following the 15-min incubation at 37 °C, a fluorescence signal of released aminomethylcoumarin was quantified using a CLARIOstar fluorimeter (BMG Labtech GmbH, Ortenberg, Germany) with excitation/emission wavelengths set at 365/440 nm, respectively. The data were fitted using the GraphPad Prism software (GraphPad Software, San Diego, CA, USA) and kinetic values were calculated by non-linear regression analysis.

HPLC-based assays. Individual fluorophore-labeled peptides were incubated with HDAC6 at 37 °C for 30 min in an assay buffer comprised of 50 mM HEPES, 140 mM NaCl, 10 mM KCl, 2 mg/ml BSA, and 1 mM TCEP, at a pH 7.4 adjusted with NaOH. The reaction was quenched by the addition of acetic acid to a final concentration

of 0.5%, and reaction products were quantified by means of RP-HPLC (Shimadzu, HPLC Prominence system) on the column Kinetex® 2.6 µm XB-C18 100 Å, 100 × 3 mm (Phenomenex, Torrance, CA, USA).

Determination of inhibition constant. The inhibition constants for SAHA (Selleckchem, Houston, TX, USA), Trichostatin A, and Nexturastat A (gift from A. Villagra and A. Kozikowski from George Washington University, USA, and University of Illinois at Chicago, USA, respectively) were determined using the slightly modified fluorogenic assay described above. Briefly, the tested compounds were preincubated with 0.3 nM human recombinant HDAC6 at 37 °C for 15 min, and then the deacetylation reaction was started by addition of 10 µM GAK(Ac)-AMC. After a 120-min incubation at 37 °C, the reaction was stopped by the addition of trypsin solution. Following the 15-min incubation at 37 °C, a fluorescence signal of released aminomethylcoumarin was quantified using a CLARIOstar fluorimeter with excitation/emission wavelengths set at 365/440 nm, respectively. The data were fitted using the GraphPad Prism software and IC_{50} values were calculated by non-linear regression analysis. The inhibitor and enzyme-free controls were defined as 100% and 0% HDAC6 activity, respectively.

Isolation of tubulin from porcine brains. Tubulin isolation from pig brain tissue was carried out according to an established protocol (details in the supplementary material)[65]. The concentration of the final tubulin preparation was determined based on the absorbance at 280 nm. Supernatant containing purified tubulin was flash frozen in aliquots using liquid nitrogen and stored at −80 °C.

Determination of αK40 acetylation levels. Five µg of porcine tubulin were diluted in 100 µl of 50 mM ammonium bicarbonate (pH 8.5) and then digested with GluC (V8) protease (Roche) for 10 hours at a ratio of 1:100. After complete evaporation on speedvac, the sample was dissolved in 15 µl of 0.1% formic acid, 10% dimethylsulfoxide in water. Acetylated and non-acetylated versions of the peptide HGIQPDGQMPSDKTIGGGDDSFNTFFSE with isotopically-labeled isoleucine (heavy peptides) was added into the mixture of the same concentration. Three µl of the sample were analyzed on the UltiMate 3000 RSLCnano system (Dionex, Sunnyvale, CA, USA) coupled to a TripleTOF 5600 mass spectrometer with a NanoSpray III source (AB Sciex, Framingham, MA, USA). The peptides were trapped and desalted with 2% acetonitrile in 0.1% formic acid at a flow rate of 5 µl/min on the Acclaim PepMap100 column (5 µm, 2 cm × 100 µm ID, Thermo Scientific). Eluted peptides were separated by the Acclaim PepMap100 analytical column (3 µm, 25 cm × 75 µm ID, Thermo Scientific) using a 70-min elution gradient at a constant flow of 300 nl/min, with mobile phase A being 0.1% formic acid and mobile phase B being 0.1% formic acid in acetonitrile. Extracted ion chromatogram of the αK40 containing identified peptides, either acetylated or nonacetylated, in light and heavy forms, were generated and the area of relevant peaks of charge state 3 was recorded. The area of light peptides was normalized to the heavy peptide area, and the percentage of acetylated versus non-acetylated peptides was calculated.

Labeling of HALO-HDAC6 fusions. The HALO-HDAC6 variants were labeled via covalent modification of the HALO fusion partner using the HaloTag-FITC ligand. The HALO-HDAC6 fusion (1 mg/ml) was incubated with a 5 molar excess of the ligand overnight at 4 °C. The unbound labels were removed by size exclusion chromatography using the Superdex 10/300 HR200 column with 30 mM HEPES, 140 mM NaCl, 10 mM KCl, 3% glycerol, and 0.25 mM TCEP, at pH 7.4 adjusted with NaOH, as a mobile phase, and labeled fusions were concentrated to approximately 1 mg/ml, aliquoted, and then snap-frozen in liquid nitrogen.

Preparation of tubulin polymers. To obtain taxol-stabilized microtubules, tubulin at a concentration of 4.4 mg/ml was polymerized for 30 min at 37 °C in BRB80 buffer supplemented with 4.8% DMSO, 4 mM $MgCl_2$, and 1 mM GTP, after which BRB80 with 20 µM paclitaxel was added. For GMPCPP-stabilized microtubules, tubulin at a concentration of 0.25 mg/ml was incubated for 2 h at 37 °C in BRB80 buffer supplemented with 1 mM $MgCl_2$ and 1 mM GMPCPP (Jena Bioscience, Jena, Germany). Dolastatin-10 rings resulted from the polymerization of 2.2 mg/ml tubulin for 40 min at room temperature with 40 µM dolastatin-10 in 80 mM PIPES (pH 6.9), 50 mM KCl, 1 mM EGTA, 1 mM $MgCl_2$, and 1 mM DTT. After the polymerization, all abovementioned polymers were pelleted at 30,000 × g for 40 min at 37 °C and the pellet was suspended in warm BRB80 with 20 µM taxol to the required concentration. Zn-sheets were prepared via 2 h incubation of 3 mg/ml tubulin at 37 °C in 80 mM MES, 200 mM NaCl, 3 mM GTP, 1.25 mM $MgSO_4$, 1.25 mM $ZnSO_4$, and 0.025 mg/ml pepstatin, adjusted to a pH of 5.5 with NaOH. Zn-sheets were then stabilized by the addition of paclitaxel to a final concentration of 31.5 µM. Zn-sheets were pelleted at 30,000 × g for 40 min at 37 °C and the pellet was suspended in a warm solution of 80 mM MES, 200 mM NaCl, 1.25 mM $MgSO_4$, and 20 µM taxol, adjusted to a of pH 5.5 with NaOH.

Microtubule binding assay. Microtubules and flow cells were prepared as described previously[66]. Briefly, taxol-stabilized microtubules were polymerized from tubulin purified from pig brains using a 1:30 ratio of Alexa-647-labeled tubulin to unlabeled tubulin, at a concentration of 2 µM and 1 mM GMPCPP in BRB80. Microscope chambers were constructed of silanized coverslips, with parafilm used to space them to form channels of 0.1-mm thickness, 3-mm width, and 18-mm length. Silanization was performed as described previously[67]. Microtubules were immobilized to the glass surface of a flow cell covered with anti-β-tubulin antibodies (Sigma-Aldrich, St. Louis, MO, USA, #T7816, 20 µg/ml in PBS), and then GFP-labeled HDAC6 was flushed into the flow cell at a final concentration of 300 nM. All experiments were carried out in a buffer consisting of BRB50, 1 mM TCEP, 0.5 mg/ml casein, 10 µM paclitaxel, 20 mM D-glucose, 110 µg/ml glucose oxidase, and 20 µg/ml catalase.

TIRF microscopy. Binding experiments were visualized using TIRF microscopy. Experiments were carried out using a Nikon Ti-E microscope equipped with H-TIRF System, 60x oil immersion 1.49 NA TIRF objective and Andor Ixon Ultra EMCCD camera (Andor Technology, Belfast, UK) controlled by NIS Elements software (Nikon). Alexa-647-labeled microtubules and GFP-labeled HDAC6 in microtubule binding assays were

visualized sequentially by switching between 640 nm and 488 nm excitation lasers. The image acquisition rate was 0.5 frames per second for sequential dual-color imaging, and image analysis was performed using Fiji[68] and MatLab (MathWorks).

Deacetylation of tubulin dimers and polymers. Using a fluorescence peptide-based assay, we first verified that small molecule components (e.g., taxol, GMPCPP, Dolastatin-10, Zn^{2+} ions) do not interfere with HDAC6 deacetylase activity at levels above the highest concentrations used in our assays (data not shown). Deacetylation reactions in a total volume of 20 µl were performed in BRB80 buffer (experiments with Zn sheets were performed in 80 mM MES, 200 mM NaCl, and 1.25 mM $MgSO_4$, adjusted to pH 5.5 with NaOH) supplemented with 1 mM TCEP and 0.5 mg/ml BSA, at 37 °C for 30 min in the case of dimers; for microtubules, the reaction was continuous and aliquots were usually harvested at 0.5, 1, 2, and 3 h. Prior to the reaction, HDAC6 was diluted to the required concentrations in the BRB80 buffer supplemented with TCEP and BSA, and the reaction was started by the addition of tubulin dimers/microtubules. Colchicine (40 µM) and paclitaxel (10 µM) were added to reaction mixtures of free tubulin dimers and microtubules, respectively. For assays with denatured tubulin dimers, the mixture of free tubulin dimers was incubated for 20 min at 95 °C, then cooled and deacetylated as native substrates. The deacetylation reaction was stopped by the addition of 20 µl of 2x Laemmli buffer and boiling samples at 95 °C for 5 min.

SDS-PAGE, Western blotting, and data analysis. Samples were loaded onto a 4–20% gradient PAGE gel (GenScript, Piscataway, NJ, USA) at 150 ng of tubulin per lane, and then run in MOPS-SDS running buffer at 160 V for 45 mins. Gels were electrotransferred onto a PVDF membrane that was subsequently blocked with 5% (w/v) BSA in TBS. The level of tubulin acetylation at αK40 was determined using a monoclonal anti-acetylated tubulin antibody[69] (Sigma, T7451, 0.3 µg/ml); a secondary goat anti-mouse antibody conjugated to Alexa Fluor 488 (Life Technologies, A11029, dilution 0.4 µg/ml) and normalized to the amount of total tubulin detected by rabbit polyclonal anti-α tubulin antibody (Abcam, Cambridge UK, ab18251, 1 µg/ml); and a secondary donkey anti-rabbit antibody conjugated to Alexa Fluor 568 (Life Technologies, USA, A10042, 0.4 µg/ml). HDAC6 was visualized using a custom-made anti-HDAC6 polyclonal rabbit sera at 1:5,000 dilution. Fluorescence intensity was measured by Typhoon FLA9500 imager (GE Healthcare Bio-Sciences) and quantified using Quantity One 1-D Analysis Software (Bio-Rad, Hercules, CA, USA). Data analysis of enzyme kinetics and statistical analysis using one-way ANOVA with Tukey's post hoc tests were performed using Graph Pad Prism software.

Indirect immunofluorescence microscopy. Deacetylation experiments were also visualized using indirect immunofluorescence microscopy. Deacetylation reactions were terminated by the addition of 10 µM SAHA, and the mixture of microtubules and HDAC6 was applied to a glass slide pretreated by poly-L-lysine. The following steps were carried out in PBS supplemented with 10 µM taxol at room temperature. Coverslips were washed with PBS and blocked with 0.5% BSA for 20 min. Coverslips were then incubated with anti-acetylated tubulin monoclonal antibody (10 µg/ml) and rabbit polyclonal anti-α tubulin antibody (2.5 µg/ml) for 20 min. Following the washing step, goat anti-mouse antibody conjugated to Alexa Fluor 488 and goat anti-rabbit antibody conjugated to Alexa Fluor 594 were applied for 20 min. After the final wash, coverslips were mounted in VectaShield medium (Vector Laboratories), and images were obtained using the Nikon Eclipse Ti fluorescence microscope equipped with a 100x immersion oil objective and additive 2.5x lens magnification (Nikon), as well as with the ORCA-flash 4.0 digital CMOS camera (Hamamatsu Photonics, Japan). Images were processed using Adobe Photoshop software and the signal intensity was quantified using Fiji.

Data availability. All data generated or analysed during this study are included in this published article (and its Supplementary Information files).

References

1. Gundersen, G. G. & Bulinski, J. C. Distribution of tyrosinated and nontyrosinated alpha-tubulin during mitosis. *J Cell Biol* **102**, 1118–1126 (1986).
2. Edde, B. *et al.* Posttranslational glutamylation of alpha-tubulin. *Science* **247**, 83–85 (1990).
3. Redeker, V. *et al.* Polyglycylation of tubulin: a posttranslational modification in axonemal microtubules. *Science* **266**, 1688–1691 (1994).
4. L'Hernault, S. W. & Rosenbaum, J. L. Chlamydomonas alpha-tubulin is posttranslationally modified by acetylation on the epsilon-amino group of a lysine. *Biochemistry* **24**, 473–478 (1985).
5. Song, Y. *et al.* Transglutaminase and polyamination of tubulin: posttranslational modification for stabilizing axonal microtubules. *Neuron* **78**, 109–123, doi:https://doi.org/10.1016/j.neuron.2013.01.036 (2013).
6. Eipper, B. A. Properties of rat brain tubulin. *J Biol Chem* **249**, 1407–1416 (1974).
7. Nogales, E., Wolf, S. G. & Downing, K. H. Structure of the alpha beta tubulin dimer by electron crystallography. *Nature* **391**, 199–203, doi:https://doi.org/10.1038/34465 (1998).
8. Tran, A. D. *et al.* HDAC6 deacetylation of tubulin modulates dynamics of cellular adhesions. *Journal of cell science* **120**, 1469–1479, doi:https://doi.org/10.1242/jcs.03431 (2007).
9. Kalebic, N. *et al.* alphaTAT1 is the major alpha-tubulin acetyltransferase in mice. *Nat Commun* **4**, 1962, doi:https://doi.org/10.1038/ncomms2962 (2013).
10. Jeong, S. G. & Cho, G. W. The tubulin deacetylase sirtuin-2 regulates neuronal differentiation through the ERK/CREB signaling pathway. *Biochem Biophys Res Commun* **482**, 182–187, doi:https://doi.org/10.1016/j.bbrc.2016.11.031 (2017).
11. Dompierre, J. P. *et al.* Histone deacetylase 6 inhibition compensates for the transport deficit in Huntington's disease by increasing tubulin acetylation. *The Journal of neuroscience: the official journal of the Society for Neuroscience* **27**, 3571–3583, doi:https://doi.org/10.1523/JNEUROSCI.0037-07.2007 (2007).
12. Reed, N. A. *et al.* Microtubule acetylation promotes kinesin-1 binding and transport. *Curr Biol* **16**, 2166–2172, doi:https://doi.org/10.1016/j.cub.2006.09.014 (2006).

13. Chen, S., Owens, G. C., Makarenkova, H. & Edelman, D. B. HDAC6 regulates mitochondrial transport in hippocampal neurons. *PloS one* **5**, e10848, doi:https://doi.org/10.1371/journal.pone.0010848 (2010).
14. Akella, J. S. *et al.* MEC-17 is an alpha-tubulin acetyltransferase. *Nature* **467**, 218–222, doi:https://doi.org/10.1038/nature09324 (2010).
15. Hubbert, C. *et al.* HDAC6 is a microtubule-associated deacetylase. *Nature* **417**, 455–458, doi:https://doi.org/10.1038/417455a (2002).
16. Matsuyama, A. *et al. In vivo* destabilization of dynamic microtubules by HDAC6-mediated deacetylation. *The EMBO journal* **21**, 6820–6831 (2002).
17. North, B. J., Marshall, B. L., Borra, M. T., Denu, J. M. & Verdin, E. The human Sir2 ortholog, SIRT2, is an NAD + -dependent tubulin deacetylase. *Molecular cell* **11**, 437–444 (2003).
18. Bobrowska, A., Donmez, G., Weiss, A., Guarente, L. & Bates, G. SIRT2 ablation has no effect on tubulin acetylation in brain, cholesterol biosynthesis or the progression of Huntington's disease phenotypes *in vivo*. *PloS one* **7**, e34805, doi:https://doi.org/10.1371/journal.pone.0034805 (2012).
19. Zhang, Y. *et al.* Mice lacking histone deacetylase 6 have hyperacetylated tubulin but are viable and develop normally. *Molecular and cellular biology* **28**, 1688–1701, doi:https://doi.org/10.1128/MCB.01154-06 (2008).
20. Skoge, R. H. & Ziegler, M. SIRT2 inactivation reveals a subset of hyperacetylated perinuclear microtubules inaccessible to HDAC6. *J Cell Sci* **129**, 2972–2982, doi:https://doi.org/10.1242/jcs.187518 (2016).
21. Choudhary, C. *et al.* Lysine acetylation targets protein complexes and co-regulates major cellular functions. *Science* **325**, 834–840, doi:https://doi.org/10.1126/science.1175371 (2009).
22. Chu, C. W. *et al.* A novel acetylation of beta-tubulin by San modulates microtubule polymerization via down-regulating tubulin incorporation. *Mol Biol Cell* **22**, 448–456, doi:https://doi.org/10.1091/mbc.E10-03-0203 (2011).
23. Huan, Y. *et al.* Epigenetic Modification Agents Improve Gene-Specific Methylation Reprogramming in Porcine Cloned Embryos. *PLoS One* **10**, e0129803, doi:https://doi.org/10.1371/journal.pone.0129803 (2015).
24. Ouyang, H. *et al.* Protein aggregates are recruited to aggresome by histone deacetylase 6 via unanchored ubiquitin C termini. *J Biol Chem* **287**, 2317–2327, doi:https://doi.org/10.1074/jbc.M111.273730 (2012).
25. Han, Y. *et al.* Acetylation of histone deacetylase 6 by p300 attenuates its deacetylase activity. *Biochem Biophys Res Commun* **383**, 88–92, doi:https://doi.org/10.1016/j.bbrc.2009.03.147 (2009).
26. Liu, Y., Peng, L., Seto, E., Huang, S. & Qiu, Y. Modulation of histone deacetylase 6 (HDAC6) nuclear import and tubulin deacetylase activity through acetylation. *J Biol Chem* **287**, 29168–29174, doi:https://doi.org/10.1074/jbc.M112.371120 (2012).
27. Okuda, K., Ito, A. & Uehara, T. Regulation of Histone Deacetylase 6 Activity via S-Nitrosylation. *Biol Pharm Bull* **38**, 1434–1437, doi:https://doi.org/10.1248/bpb.b15-00364 (2015).
28. Lafarga, V., Aymerich, I., Tapia, O., Mayor, F. Jr. & Penela, P. A novel GRK2/HDAC6 interaction modulates cell spreading and motility. *EMBO J* **31**, 856–869, doi:https://doi.org/10.1038/emboj.2011.466 (2012).
29. Kovacs, J. J. *et al.* HDAC6 regulates Hsp90 acetylation and chaperone-dependent activation of glucocorticoid receptor. *Mol Cell* **18**, 601–607, doi:https://doi.org/10.1016/j.molcel.2005.04.021 (2005).
30. Zhang, X. *et al.* HDAC6 modulates cell motility by altering the acetylation level of cortactin. *Mol Cell* **27**, 197–213, doi:https://doi.org/10.1016/j.molcel.2007.05.033 (2007).
31. Parmigiani, R. B. *et al.* HDAC6 is a specific deacetylase of peroxiredoxins and is involved in redox regulation. *Proc Natl Acad Sci USA* **105**, 9633–9638, doi:https://doi.org/10.1073/pnas.0803749105 (2008).
32. Li, Y., Zhang, X., Polakiewicz, R. D., Yao, T. P. & Comb, M. J. HDAC6 is required for epidermal growth factor-induced beta-catenin nuclear localization. *J Biol Chem* **283**, 12686–12690, doi:https://doi.org/10.1074/jbc.C700185200 (2008).
33. Kawaguchi, Y. *et al.* The deacetylase HDAC6 regulates aggresome formation and cell viability in response to misfolded protein stress. *Cell* **115**, 727–738 (2003).
34. Seidel, C., Schnekenburger, M., Dicato, M. & Diederich, M. Histone deacetylase 6 in health and disease. *Epigenomics* **7**, 103–118, doi:https://doi.org/10.2217/epi.14.69 (2015).
35. Li, G., Jiang, H., Chang, M., Xie, H. & Hu, L. HDAC6 alpha-tubulin deacetylase: a potential therapeutic target in neurodegenerative diseases. *J Neurol Sci* **304**, 1–8, doi:https://doi.org/10.1016/j.jns.2011.02.017 (2011).
36. Simoes-Pires, C. *et al.* HDAC6 as a target for neurodegenerative diseases: what makes it different from the other HDACs? *Mol Neurodegener* **8**, 7, doi:https://doi.org/10.1186/1750-1326-8-7 (2013).
37. Aldana-Masangkay, G. I. & Sakamoto, K. M. The role of HDAC6 in cancer. *J Biomed Biotechnol* **2011**, 875824, doi:https://doi.org/10.1155/2011/875824 (2011).
38. Zhao, Z., Xu, H. & Gong, W. Histone deacetylase 6 (HDAC6) is an independent deacetylase for alpha-tubulin. *Protein and peptide letters* **17**, 555–558 (2010).
39. Du, Y., Seibenhener, M. L., Yan, J., Jiang, J. & Wooten, M. C. aPKC phosphorylation of HDAC6 results in increased deacetylation activity. *PloS one* **10**, e0123191, doi:https://doi.org/10.1371/journal.pone.0123191 (2015).
40. Williams, K. A. *et al.* Extracellular signal-regulated kinase (ERK) phosphorylates histone deacetylase 6 (HDAC6) at serine 1035 to stimulate cell migration. *The Journal of biological chemistry* **288**, 33156–33170, doi:https://doi.org/10.1074/jbc.M113.472506 (2013).
41. Watabe, M. & Nakaki, T. Protein kinase CK2 regulates the formation and clearance of aggresomes in response to stress. *Journal of cell science* **124**, 1519–1532, doi:https://doi.org/10.1242/jcs.081778 (2011).
42. Zou, H., Wu, Y., Navre, M. & Sang, B. C. Characterization of the two catalytic domains in histone deacetylase 6. *Biochemical and biophysical research communications* **341**, 45–50, doi:https://doi.org/10.1016/j.bbrc.2005.12.144 (2006).
43. Schultz, B. E. *et al.* Kinetics and comparative reactivity of human class I and class IIb histone deacetylases. *Biochemistry* **43**, 11083–11091, doi:https://doi.org/10.1021/bi0494471 (2004).
44. Lai, M. J. *et al.* Synthesis and biological evaluation of 1-arylsulfonyl-5-(N-hydroxyacrylamide)indoles as potent histone deacetylase inhibitors with antitumor activity *in vivo*. *J Med Chem* **55**, 3777–3791, doi:https://doi.org/10.1021/jm300197a (2012).
45. Wagner, F. F. *et al.* Potent and selective inhibition of histone deacetylase 6 (HDAC6) does not require a surface-binding motif. *Journal of medicinal chemistry* **56**, 1772–1776, doi:https://doi.org/10.1021/jm301355j (2013).
46. Bergman, J. A. *et al.* Selective histone deacetylase 6 inhibitors bearing substituted urea linkers inhibit melanoma cell growth. *Journal of medicinal chemistry* **55**, 9891–9899, doi:https://doi.org/10.1021/jm301098e (2012).
47. Giannini, G. *et al.* N-Hydroxy-(4-oxime)-cinnamide: a versatile scaffold for the synthesis of novel histone deacetylase [correction of deacetilase] (HDAC) inhibitors. *Bioorganic & medicinal chemistry letters* **19**, 2346–2349, doi:https://doi.org/10.1016/j.bmcl.2009.02.029 (2009).
48. Miyake, Y. *et al.* Structural insights into HDAC6 tubulin deacetylation and its selective inhibition. *Nat Chem Biol* **12**, 748–754, doi:https://doi.org/10.1038/nchembio.2140 (2016).
49. Moores, C. A. & Milligan, R. A. Visualisation of a kinesin-13 motor on microtubule end mimics. *J Mol Biol* **377**, 647–654, doi:https://doi.org/10.1016/j.jmb.2008.01.079 (2008).
50. Wolf, S. G., Mosser, G. & Downing, K. H. Tubulin conformation in zinc-induced sheets and macrotubes. *J Struct Biol* **111**, 190–199, doi:https://doi.org/10.1006/jsbi.1993.1049 (1993).
51. Szyk, A. *et al.* Molecular basis for age-dependent microtubule acetylation by tubulin acetyltransferase. *Cell* **157**, 1405–1415, doi:https://doi.org/10.1016/j.cell.2014.03.061 (2014).

52. Friedmann, D. R., Aguilar, A., Fan, J., Nachury, M. V. & Marmorstein, R. Structure of the alpha-tubulin acetyltransferase, alphaTAT1, and implications for tubulin-specific acetylation. *Proc Natl Acad Sci USA* **109**, 19655–19660, doi:https://doi.org/10.1073/pnas.1209357109 (2012).
53. Taschner, M., Vetter, M. & Lorentzen, E. Atomic resolution structure of human alpha-tubulin acetyltransferase bound to acetyl-CoA. *Proc Natl Acad Sci USA* **109**, 19649–19654, doi:https://doi.org/10.1073/pnas.1209343109 (2012).
54. Li, W. *et al*. Molecular basis of the acetyltransferase activity of MEC-17 towards alpha-tubulin. *Cell Res* **22**, 1707–1711, doi:https://doi.org/10.1038/cr.2012.154 (2012).
55. Riester, D., Hildmann, C., Grunewald, S., Beckers, T. & Schwienhorst, A. Factors affecting the substrate specificity of histone deacetylases. *Biochem Biophys Res Commun* **357**, 439–445, doi:https://doi.org/10.1016/j.bbrc.2007.03.158 (2007).
56. Hai, Y. & Christianson, D. W. Histone deacetylase 6 structure and molecular basis of catalysis and inhibition. *Nat Chem Biol* **12**, 741–747, doi:https://doi.org/10.1038/nchembio.2134 (2016).
57. Zhang, Y. *et al*. HDAC-6 interacts with and deacetylates tubulin and microtubules *in vivo*. *The EMBO journal* **22**, 1168–1179, doi:https://doi.org/10.1093/emboj/cdg115 (2003).
58. Li, H., DeRosier, D. J., Nicholson, W. V., Nogales, E. & Downing, K. H. Microtubule structure at 8 A resolution. *Structure* **10**, 1317–1328 (2002).
59. Meurer-Grob, P., Kasparian, J. & Wade, R. H. Microtubule structure at improved resolution. *Biochemistry* **40**, 8000–8008 (2001).
60. Howes, S. C., Alushin, G. M., Shida, T., Nachury, M. V. & Nogales, E. Effects of tubulin acetylation and tubulin acetyltransferase binding on microtubule structure. *Molecular biology of the cell* **25**, 257–266, doi:https://doi.org/10.1091/mbc.E13-07-0387 (2014).
61. Asthana, J., Kapoor, S., Mohan, R. & Panda, D. Inhibition of HDAC6 deacetylase activity increases its binding with microtubules and suppresses microtubule dynamic instability in MCF-7 cells. *The Journal of biological chemistry* **288**, 22516–22526, doi:https://doi.org/10.1074/jbc.M113.489328 (2013).
62. Purev, E., Neff, L., Horne, W. C. & Baron, R. c-Cbl and Cbl-b act redundantly to protect osteoclasts from apoptosis and to displace HDAC6 from beta-tubulin, stabilizing microtubules and podosomes. *Molecular biology of the cell* **20**, 4021–4030, doi:https://doi.org/10.1091/mbc.E09-03-0248 (2009).
63. Ly, N. *et al*. alphaTAT1 controls longitudinal spreading of acetylation marks from open microtubules extremities. *Sci Rep* **6**, 35624, doi:https://doi.org/10.1038/srep35624 (2016).
64. Skoge, R. H., Dolle, C. & Ziegler, M. Regulation of SIRT2-dependent alpha-tubulin deacetylation by cellular NAD levels. *DNA Repair (Amst)* **23**, 33–38, doi:https://doi.org/10.1016/j.dnarep.2014.04.011 (2014).
65. Geuens, G. *et al*. Ultrastructural colocalization of tyrosinated and detyrosinated alpha-tubulin in interphase and mitotic cells. *J Cell Biol* **103**, 1883–1893 (1986).
66. Braun, M. *et al*. Adaptive braking by Ase1 prevents overlapping microtubules from sliding completely apart. *Nat Cell Biol* **13**, 1259–1264, doi:https://doi.org/10.1038/ncb2323 (2011).
67. Hyman, A. A. Preparation of marked microtubules for the assay of the polarity of microtubule-based motors by fluorescence. *J Cell Sci Suppl* **14**, 125–127 (1991).
68. Schindelin, J. *et al*. Fiji: an open-source platform for biological-image analysis. *Nat Methods* **9**, 676–682, doi:https://doi.org/10.1038/nmeth.2019 (2012).
69. Piperno, G. & Fuller, M. T. Monoclonal antibodies specific for an acetylated form of alpha-tubulin recognize the antigen in cilia and flagella from a variety of organisms. *J Cell Biol* **101**, 2085–2094 (1985).

Acknowledgements

We thank Verena Puttrich for help with the TIRF microscopy, Petr Man for MS analysis, A. Villagra/A. Kozikowski for the gift of Nexturastat A, T. Moravec for electron microscopy, and M. Kuchar for the synthesis of HALO-reactive probes. This work was supported by the Czech Science Foundation (grants No 15-19640 S to C.B. and No 15-17488 S to Z.L., respectively), the CAS (RVO: 86652036), and the "BIOCEV" project (CZ.1.05/1.1.00/02.0109) from the ERDF. L.S. acknowledges support from GAUK (grant no. 796313). We acknowledge the use of The Centre of Imaging Methods core facility, Faculty of Science, Charles University, supported by the MEYS CR (LM2015062 Czech-BioImaging).

Author Contributions

L.S. - design, acquisition, and interpretation of kinetic data, manuscript writing; K.U. and Z.L. - design, acquisition, and interpretation of TIRF data; Z.K., J.M., Z.N. - design, acquisition, and interpretation of kinetic experiments; J.P., D.T., P.B., B.H. - design, cloning and purification of HDAC6 constructs, M.H. - MS quantification; C.B. - conception and design of the project, manuscript writing. All authors reviewed the manuscript.

Additional Information

Supplementary information accompanies this paper at doi:10.1038/s41598-017-11739-3

Competing Interests: The authors declare that they have no competing interests.

Publisher's note: Springer Nature remains neutral with regard to jurisdictional claims in published maps and institutional affiliations.

2.3 The disordered N-terminus of HDAC6 is a microtubule-binding domain critical for efficient tubulin deacetylation

Background and motivation of the study

Although tubulin is the main physiological substrate of HDAC6, it is still not known how exactly HDAC6 recognizes and interacts with it. Mapping HDAC6 interactions with tubulin offers an insight into the functionality of the enzyme and provides a mechanistic understanding of physiological processes that are based on tubulin acetylation.

In the previous study, we have visualized the direct binding of human full-length HDAC6 to stabilized microtubules. HDAC6 is binding to microtubules uniformly with no preference for the tips and with fast kinetics. Furthermore, we have provided quantitative data on HDAC6 deacetylation of different tubulin forms showing the preference of HDAC6 for free tubulin compared to polymerized microtubules. We hypothesized that domains beyond the tandem catalytic domains may contribute to HDAC6 recognition, interaction, and deacetylation of tubulin. Therefore, we set up to map the molecular basis of the interactions between HDAC6 and different tubulin forms by a set of biophysical and biochemical methods. This knowledge can provide basic information on the recognition of tubulin and microtubules by HDAC6 and on the influence on microtubules polymerization. Furthermore, it can be useful in the design and development of inhibitors specifically targeting the HDAC6/tubulin system.

Summary of the work

By using heterologous protein expression, site-directed mutagenesis, biochemical and biophysical methods, we identified the N-terminal disordered domain of HDAC6 to be a microtubule-binding domain and functionally characterized it to the single-molecule level.

A set of truncated HDAC6 construct has been cloned, expressed, and purified and their correct fold and enzymatic activity were verified. Further, we have assayed these constructs for their binding to microtubules. The affinity of human full-length HDAC6 for microtubules is $appK_D$ = 135 ± 9 nM. Additionally, the interaction mode of HDAC6 with microtubules at the single-molecule level was estimated revealing two predominant interaction modes: static binding (binding/unbinding) and one-dimensional diffusion.

We have determined that catalytic domains of HDAC6 are not involved in HDAC6 binding to microtubules. Neither an inactive HDAC6 mutant nor HDAC6 in a complex with the Nexturastat A inhibitor showed any difference in the affinity to microtubules. Furthermore, observed interaction mode was similar to native HDAC6 suggesting a crucial role of other domain(s) of HDAC6 in binding to microtubules. Using TIRF microscopy we showed that catalytic domains of HDAC6 do not bind to microtubules, while constructs comprising the N-terminal domain interact with microtubules. The

determination of the affinity of the N-terminal domain revealed that it is primarily responsible for HDAC6 interactions with microtubules with an apparent dissociation constant of 98 ± 9 nM. The pelleting assay has supported our previous findings.

Figure 1. Sequence alignment of HDAC6 N-terminal domains from different species. Microtubule-binding motifs of HDAC6 span positively charged patches comprising residues Lys-32 to Lys-37 (patch A) and Lys-51 to Lys-58 (patch B).

The N-terminal domain, being an MBD, was functionally characterized to the single-molecule level. The exact amino acids involved in this interaction were identified - two positively charged patches comprising residues Lys-32 to Lys-58 (Figure 1). Acetylation mimicking Lys to Gln HDAC6 mutants (the patch A and B) showed a lower binding affinity for microtubules. The more pronounced effect was observed in the case of mutation in patch B (KQ PB). These findings were supported by studies using matching synthetic peptides. Peptides of the wild-type sequence (P-WT), a mutation in patch A (P KQ PA), patch B (P KQ PB), and in both sites (P KQ PAB) had the same affinity for microtubules as HDAC6 mutants (Figure 2A). Obtained data confirmed that this motif is responsible for the microtubule binding with no influence of other HDAC6 domains. It was shown that HDAC6 binding to microtubules is mediated by electrostatic interactions between the negatively charged microtubule surface and positively charged HDAC6 lysine patches.

The MBD of HDAC6 is essential not only for interactions with microtubules but also for interactions with tubulin dimers. Using Microscale Thermophoresis (MST), the affinity of MBD to tubulin dimers was determined - $appK_D$ value of 577 ± 102 nM (Figure 2B). Furthermore, the deacetylation of tubulin dimers by truncated constructs of HDAC6 revealed a 50- to 120-fold lower deacetylation efficiency when MBD was missing (Figure 2C). These *in vitro* data were supported by *in vivo* studies where HDAC6 KO cells were transfected with HDAC6 truncated constructs and the acetylation levels of cellular tubulin quantified. In agreement with *in vitro* experiments, *in vivo* experiments showed the same activity pattern, suggesting that MBD (patch B) is a critical contributor to HDAC6 deacetylase activity.

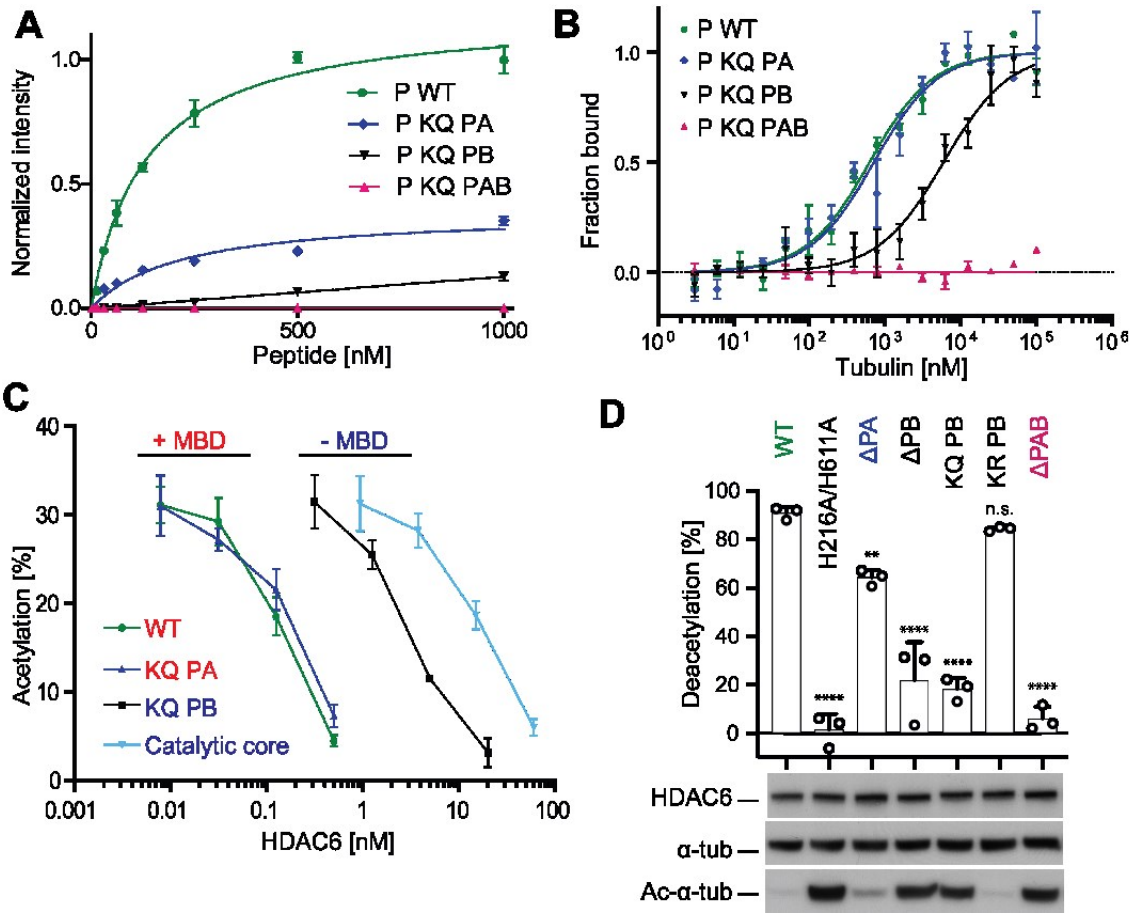

Figure 2. The MBD domain patches are critical for binding and deacetylation of tubulin/microtubules. A. The apparent dissociation constants ($appK_D$) for HDAC6 MBD-derived peptides (P WT, WT; KQ PA, patch A; KQ PB, patch B; KQ PAB, combined patch A/B) was calculated from binding isotherms of TIRF microscopy experiments. The apparent dissociation constant for the P WT was 131 ± 5 nM. Acetylation mimicking Lys to Gln peptides (the patch A and B) showed a lower binding affinity for microtubules. The more pronounced effect was observed in the case of peptide KQ PB. No binding was observed for the KQ PAB peptide. **B.** The binding affinity of HDAC6 MBD–derived peptides for free tubulin dimers was quantified using MST. Calculated apparent $appK_D$ values were 577 ± 102 nM, 665 ± 181 nM, and 5898 ± 800 nM for the WT (P WT), patch A mutant (P KQ PA), and patch B mutant (P KQ PB), respectively. No binding was observed for the double mutant (P KQ PAB). **C.** The deacetylation activity of HDAC6 variants on free tubulin dimers. Much higher (40- to150-fold) concentrations of variants with mutated/missing MBD (-MBD, blue) are required for efficient deacetylation of tubulin compared with variants with WT sequences (+MBD, red). **D.** *In vivo* deacetylase activity of HDAC6 variants in HEK293T HDAC6 KO cells. While the expression of all variants was similar, the tubulin deacetylation level significantly increased in the case of HDAC6 mutants with the native patch B and the K/R mutant.

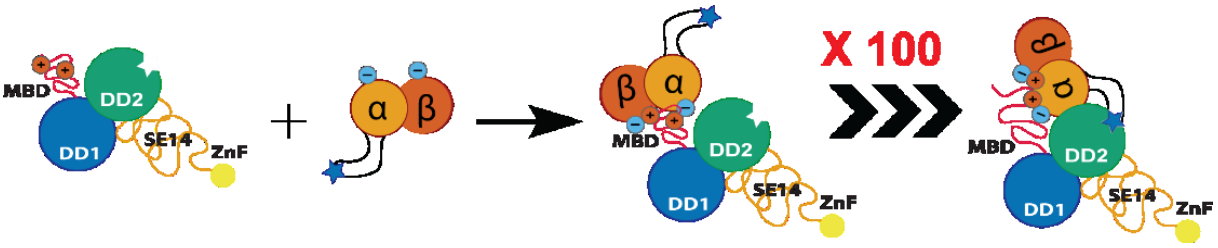

Figure 3. Mechanism of substrate deacetylation by HDAC6. MBD of HDAC6 interacts with tubulin via ionic interactions thus increasing the local concentration of the binary HDAC6/tubulin complex, resulting in 100-fold faster tubulin deacetylation.

In summary, a crosstalk between the MBD and the catalytic domains is critical for recognition and efficient deacetylation of free tubulin dimers both *in vitro* and *in vivo* (Figure 2D). The N-terminal domain increases HDAC6 deacetylase activity against free tubulin by more than 100-fold. These findings show the critical role of domains outside the catalytic core in the modulation of HDAC6 deacetylase activity. It may lead to new strategies in the selective inhibition of substrate deacetylation by HDAC6.

My contribution

I planned experiments, performed site-directed mutagenesis, expressed, purified proteins and analyzed them by SEC, performed and analyzed MST measurements, performed and analyzed TIRF microscopy measurements, analyzed CD data, and wrote the draft of the manuscript.

JBC ARTICLE

The disordered N-terminus of HDAC6 is a microtubule-binding domain critical for efficient tubulin deacetylation

Received for publication, September 25, 2019, and in revised form, January 14, 2020 Published, Papers in Press, January 17, 2020, DOI 10.1074/jbc.RA119.011243

Kseniya Ustinova[‡§], Zora Novakova[‡], Makoto Saito[¶‖1], Marat Meleshin[**], Jana Mikesova[‡], Zsofia Kutil[‡], Petra Baranova[‡], Barbora Havlinova[‡], Mike Schutkowski[**], Patrick Matthias[¶‖], and Cyril Barinka[‡2]

From the [‡]Institute of Biotechnology of the Czech Academy of Sciences, BIOCEV, Prumyslova 595, 252 50 Vestec, Czech Republic, [§]Department of Biochemistry, Faculty of Natural Science, Charles University, Albertov 6, Prague 2, Czech Republic, [¶]Friedrich Miescher Institute for Biomedical Research, 4058 Basel, Switzerland, [**]Department of Enzymology, Institute of Biochemistry and Biotechnology, Charles Tanford Protein Center, Martin Luther University, Halle-Wittenberg, 06120 Halle/Saale, Germany, and [‖]Faculty of Sciences, University of Basel, 4031 Basel, Switzerland

Edited by John M. Denu

Histone deacetylase 6 (HDAC6) is a multidomain cytosolic enzyme having tubulin deacetylase activity that has been unequivocally assigned to the second of the tandem catalytic domains. However, virtually no information exists on the contribution of other HDAC6 domains on tubulin recognition. Here, using recombinant protein expression, site-directed mutagenesis, fluorimetric and biochemical assays, microscale thermophoresis, and total internal reflection fluorescence microscopy, we identified the N-terminal, disordered region of HDAC6 as a microtubule-binding domain and functionally characterized it to the single-molecule level. We show that the microtubule-binding motif spans two positively charged patches comprising residues Lys-32 to Lys-58. We found that HDAC6-microtubule interactions are entirely independent of the catalytic domains and are mediated by ionic interactions with the negatively charged microtubule surface. Importantly, a crosstalk between the microtubule-binding domain and the deacetylase domain was critical for recognition and efficient deacetylation of free tubulin dimers both *in vitro* and *in vivo*. Overall, our results reveal that recognition of substrates by HDAC6 is more complex than previously appreciated and that domains outside the tandem catalytic core are essential for proficient substrate deacetylation.

Acetylation at the N^{ϵ} group of lysines is a major posttranslational modification found on most proteins of the human proteome (1). Both histones and nonhistone proteins are targets of the acetylation/deacetylation machinery. Lysine acetylation has been implicated in diverse biological functions, including metabolic stress response, inflammation, chromatin assembly, DNA repair and recombination, circadian rhythm, as well as immune surveillance, neurological development, and brain function (2–7). At the molecular level, the protein acetylation status is regulated by opposing activities of histone acetyltransferases (writers) and histone deacetylases (HDACs)[3] (erasers). In addition to enzymatic acetylation by histone acetyltransferases, nonenzymatic acetylation by metabolic intermediates/end products (such as acetyl-CoA) has been reported (8). In contrast, the removal of acetyl groups is more tightly regulated by substrate specificities of individual HDACs and their spatiotemporal distribution within the cell. Among 11 zinc-dependent HDACs, class I and IV enzymes are primarily located in the nucleus, class IIa enzymes are shuttling between the nucleus and cytosol, and class IIb enzymes, including HDAC6, are mainly localized to the cytosol (9).

HDAC6 stands out as a structurally and functionally unique lysine deacetylase, and it represents an attractive target for therapeutic interventions in cancer (10) and neuropathologies (11, 12). Structurally, human HDAC6 consists of five domains: (i) the N-terminal domain (amino acids 1–87), (ii) tandem deacetylase domains DD1 (amino acids 88–440), (iii) DD2 (amino acids 480–855) connected by a glutamate-rich linker, (iv) the Ser-Glu–containing repeated tetrapeptide domain (SE) (amino acids 856–1108), and (v) the C-terminal ubiquitin-binding zinc finger domain (ZnF) (amino acids 1109–1215) (see Fig. 2*A*). Recently, X-ray structures of both catalytic domains of zebrafish HDAC6 as well as the ZnF and DD2 domains of human HDAC6 have been reported (13, 14). Functionally, DD2 and ZnF are also characterized in the greatest detail. The DD2 is primarily responsible for the

This work was supported by Czech Science Foundation Grant 15–19640S; Czech Academy of Sciences RVO: 86652036 (to C. B.); European Regional Development Fund CZ.1.05/1.1.00/02.0109; and Ministry of Education, Youth and Sports Grants LM2015043, LM2015062, and CZ.02.1.01/0.0/0.0/16_013/0001775 (to C. B.). This work was also supported by the Grant Agency of Charles University Project 1558218 (to K. U.) and by the Novartis Research Foundation (to P. M.). The authors declare that they have no conflicts of interest with the contents of this article.

This article contains Figs. S1–S14, Table S1, Video S1, and method description S15.

[1] Supported in part by a fellowship from the Nakajima Foundation. Present address: Broad Institute of MIT and Harvard, Cambridge, MA 02142.

[2] To whom correspondence should be addressed: Institute of Biotechnology v.v.i., Laboratory of Structural Biology, Prumyslova 595, 252 50 Vestec, Czech Republic. Tel.: 420-325-873-777; E-mail: cyril.barinka@ibt.cas.cz.

[3] The abbreviations used are: HDAC, histone deacetylase; SE, Ser-Glu tetradecapeptide repeat; ZnF, zinc finger domain; NES, nuclear export signal; MT, microtubule; PTM, posttranslational modification; MAP, microtubule-associated protein; TIRF, total internal reflection fluorescence; FL, full length; NexA, Nexturastat A; MBD, microtubule-binding domain; MST, microscale thermophoresis; GMPCPP, guanosine-5′-[(α,β)-methyleno]triphosphate; ACN, acetonitrile; TCEP, tris(2-carboxyethyl)phosphine; RT, room temperature; DMF, *N*,*N*-dimethylformamide; DIPEA, *N*,*N*-diisopropylethylamine; DCM, dichloromethane; UPLC, ultra-performance liquid chromatography; Fmoc, *N*-(9-fluorenyl)methoxycarbonyl; AMC, 7-amino-4-methylcoumarin.

deacetylation of a host of HDAC6 physiological substrates, including tubulin, heat shock protein 90, cortactin, and β-catenin. The ZnF domain binds ubiquitin with high affinity (15), and this nonenzymatic function of HDAC6 plays a critical role in protein clearance and degradation via the aggresome pathway (16) and also in influenza virus infection (17). Physiological functions of remaining HDAC6 domains are much less studied. The N-terminal domain comprises nuclear localization signals and nuclear export signals (NES), with the former being the subject of acetylation/deacetylation cycles that control nucleus/cytoplasmic shuttling of HDAC6 (18). The DD1 domain has negligible deacetylase activity against substrates with an internal acetyl lysine but has been shown to deacetylate peptides featuring acetyl lysine at their C terminus as well as intrinsically disordered regions of several target proteins (19, 20). Finally, the SE domain has been reported to be implicated in the HDAC6 cytoplasmic anchoring and interactions with the microtubule (MT) network (21).

Localized predominantly to the cytoplasm, HDAC6 acts on a plethora of cytosolic proteins, with tubulin being the most prominent and the best-studied HDAC6 physiological substrate (14, 22–26). Tubulin acetylation at Lys-40 of the α-subunit (αK40) is a hallmark of stable MTs and protects long-lived MTs against mechanical aging (27). The αK40 acetylation belongs to a host of tubulin posttranslational modifications (PTMs), including (de)tyrosination, glutamylation, glycylation, polyamination, and phosphorylation (28). Note that unlike the luminal localization of αK40, the majority of the tubulin PTMs are localized to unstructured, negatively charged C-terminal tails decorating the outer surface of MTs (29). Not only are the C-hooks the prime sites for the display of the tubulin code PTMs but they also critically impact MTs interactions and function of a variety of the microtubule-associated proteins (MAPs) (30), modification enzymes (31), and molecular motors (32).

Prior biological studies revealed that HDAC6 could influence MT dynamics and stability, including regulation of focal adhesion turnover (33), the function of mitotic apparatus (34), and axonal stability (35). These studies also indicate that HDAC6 can function as a MAP and the above processes can be influenced by HDAC6/tubulin interactions, sometimes irrespective of its deacetylase activity, although no mechanistic explanation has been offered for these findings (36). At the same time, there are virtually no data describing qualitative or quantitative interactions between HDAC6 and free tubulin and MTs, including the importance of HDAC6 domains beyond the tandem catalytic core for tubulin recognition and deacetylation by HDAC6. This study uncovers the N-terminal domain of HDAC6 as a component critical for binding and efficient deacetylation of tubulin. As a general extension, our findings suggest that recognition of other physiological substrates by HDAC6 might also be more complex than previously appreciated, and that domains outside the tandem catalytic core can play important roles for HDAC6 deacetylase activity *in vivo*.

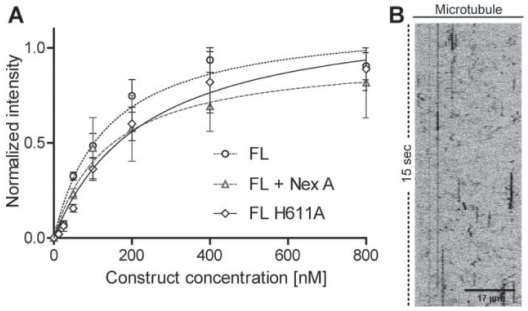

Figure 1. Ensemble and single-molecule interactions between HDAC6 and stabilized MTs. *A*, saturation binding curve representing HDAC6 binding affinity to MTs. MTs were immobilized on the glass surface and the dilution series of GFP-HDAC6 FL (FL), GFP-HDAC6 FL H611A (FL H611A), and GFP-HDAC6 FL in the presence of 1.6 μM Nexturastat A, an HDAC6-specific inhibitor (FL + NexA), was added to the channel. The fluorescence signal of the MT-bound HDAC6 was quantified using TIRF microscopy. Apparent dissociation constants ($appK_D$), calculated from binding isotherms, are 135 ± 9.2 nM, 233 ± 15.2 nM, and 141 ± 19.5 nM, respectively. Data represent mean values ± S.D.; $n = 3$. *B*, the kymograph representing the mode of interactions between GFP-HDAC6 FL fusion and stabilized MTs at the single-molecule level, visualized by TIRF microscopy. Both static binding-unbinding events (*straight lines*) and fast nondirectional diffusion interactions are observed.

Results

Expression and characterization of HDAC6 mutants

All HDAC6 mutants used in this study were expressed in HEK293T cells and purified to apparent homogeneity by the combination of Strep-Tactin affinity chromatography and size-exclusion chromatography. Relative molecular weight and purity of the final preparations were verified by SDS-PAGE (Fig. S1). For total internal reflection fluorescence (TIRF) microscopy experiments, GFP was fused at the N terminus of HDAC6 mutants, and the presence of the tag did not have any effect on HDAC6 deacetylase activity (37). Additionally, the CD spectra for each mutant correlated well with the predicted secondary structure content (Fig. S2). Overall, all proteins used in this report are thus correctly folded and enzymatically active (when harboring the DD1-DD2 catalytic core that comprises the tandem catalytic domains DD1 (amino acids 75–440) and DD2 (amino acids 480–855)).

HDAC6 binds microtubules with nanomolar affinity

Our recent study showed that HDAC6 full length (FL) binds double stabilized MTs uniformly along their entire length with fast kinetics (37). To obtain more detailed and quantitative insights into HDAC6/MT interactions, we used TIRF microscopy to determine HDAC6/MT affinity as well as the mode of HDAC6/MT interactions at the single-molecule level. We first determined HDAC6 FL affinity for MTs by incubating immobilized MTs with increasing concentrations of GFP-HDAC6 fusions (ranging from 12.5 nM–1 μM) and quantifying fluorescence signal of the bound fusion. The resulting binding isotherm reveals high affinity with an apparent dissociation constant of $appK_D = 135 \pm 9.2$ nM (Fig. 1*A*).

We next examined the mode of HDAC6 binding to MTs using single-molecule measurements. Kymograph analyses revealed two predominant interaction modes: static binding (binding/unbinding) and one-dimensional diffusion (Fig. 1*B*;

see Video S1). At the same time, the HDAC6 diffusion rate along MTs is too fast be precisely quantified in our experimental setup with the shortest exposure time of 30 ms, thus preventing the assessment of the proportion of molecules in each interaction mode class.

The above-mentioned measurements (and all additional experiments dealing with MT/HDAC6 interactions) were carried out in BRB50, unless stated otherwise. Although the ionic strength of BRB50 is somewhat lower compared with "physiological ionic strength" of the BRB80 buffer, the use of low ionic strength buffers is a standard practice in studies investigating interactions between MTs and MAPs and molecular motors, where buffers down to BRB12 (12 mM PIPES) are typically used (38–40).

HDAC6 deacetylase activity is not required for MT binding

To determine whether HDAC6 binding to MTs depends on its deacetylase activity, we repeated the binding experiment (i) using the catalytically inactive H611A mutant and (ii) in the presence of Nexturastat A (NexA), a nanomolar HDAC6 inhibitor. Although the use of the H611A catalytically inactive mutant directly uncouples the HDAC6 deacetylation activity from MT binding, it does not block potential interactions between the αK40 loop and HDAC6 DD2. On the other hand, NexA binding to the active-site of DD2 (and DD1) would sterically block the αK40 side-chain insertion into the HDAC6 active-site tunnel. Consequently, if HDAC6/αK40 interactions were critical for MT binding, one could expect more pronounced effects of the latter. Using both experimental approaches, however, we did not observe any significant effect of DD2 inhibition/inactivation on HDAC6 microtubule-binding affinity and the mode of interaction (Fig. S3). This observation reveals that HDAC6 binding to MTs is independent of its catalytic function, and there is no/negligible contribution from the αK40 motif toward HDAC6 interactions (Fig. 1*A*).

The N-terminal part of HDAC6 is a microtubule-binding domain

To identify domain(s) responsible for interactions with stabilized MTs, we performed an extensive deletion mutagenesis study using a panel of truncated HDAC6 mutants (Fig. 2*A*; Fig. S1). Surprisingly, the construct comprising the tandem deacetylation domains that are sufficient to effectively deacetylate a wide variety of substrates (14, 22, 41–45), including tubulin, did not interact with stabilized MTs. Instead, only mutants harboring the N-terminal domain (amino acids 1–87), either isolated or in combination with other HDAC6 domains, were capable of MT binding (Fig. 2*B*). Clearly, the N-terminal part of HDAC6, but not the tandem catalytic core (DD1-DD2), is necessary and sufficient to bind MTs and henceforth denoted the microtubule-binding domain (MBD).

Using TIRF microscopy, we compared the affinity and the interaction mode of the isolated catalytic core of HDAC6 and two other constructs harboring the N terminus: the HDAC6 MBD and the HDAC6 MBD-DD2 mutant (Fig. 2*C*). These experiments yielded virtually identical apparent dissociation constants for two constructs 98 ± 9.3 nM and 140 ± 2.7 nM, respectively. It reveals that the N-terminal MBD is primarily responsible for HDAC6 affinity toward MTs without any obvious contribution of other domains.

Because the pelleting assay is a gold standard in the field, this method was used independently to corroborate direct HDAC6 binding to MTs. To this end, stabilized MTs were incubated with various HDAC6 mutants. Both the supernatant and pelleted fraction were analyzed for the presence of MTs and/or HDAC6 mutants by SDS-PAGE. Overall, the pelleting assay fully reproduced major findings from the TIRF microscopy that (i) the duplicated catalytic core does not interact appreciably with MTs and (ii) the N-terminal domain is necessary and sufficient for MT binding (Fig. 2*D*).

HDAC6 microtubule-binding motifs span amino acids Lys-32 to Lys-37 and Lys-51 to Lys-58

The sequence analysis of the microtubule-binding domain of human HDAC6 revealed the presence of two lysine/arginine-rich patches (patch A and B comprising amino acids Lys-32 to Lys-37 and Lys-51 to Lys-58, respectively) (Fig. 3*A*) that in principle can be involved in ionic interactions with the negatively charged MTs surface.

The lysine residues at both patches were shown to be acetylated *in vivo* by acetyltransferase p300, and their acetylation status is linked to HDAC6 nucleocytoplasmic shuttling (18). We hypothesized that *N*-acetylation at the two patches could, in addition to its control over the HDAC6 nuclear import, also influence HDAC6/MT interactions. To test this notion, lysines at both patches were mutated to glutamines to mimic lysine acetylation. Mutants harboring the mutated MBD were purified, and their affinity for stabilized MTs determined. Compared with the WT sequence, mutants mimicking lysine acetylation at patches A and B showed 40- and >150-fold weaker affinity for stabilized MTs, respectively, pointing toward more pronounced involvement of patch B in mediating HDAC6 interactions with MTs. Additionally, the combined patch AB acetylation mimic mutant failed to bind MTs altogether (Fig. 3*B*).

Using the synthetic peptide corresponding to amino acids Ser-31 to Leu-59 of HDAC6 (P-WT) and its acetylation mimics (P-KQ PA, P-KQ PB, P-KQ PAB) (Fig. S13), we corroborated and extended principal findings of the above TIRF-binding experiments where recombinant proteins were used (Fig. 3*A*; Figs. S4 and S12). The P-WT peptide derived from the native N terminus bound to stabilized MTs with an apparent dissociation constant of 131 ± 5.1 nM, whereas the marked decrease in binding affinity was observed for each of patch A (P-KQ PA) and B (P-KQ PB) mutants. Finally, no binding was observed for the doubly mutated P-KQ PAB variant (Fig. 3*C*). Peptide-based data pinpointed the Ser-31 to Leu-59 sequence as a key MT-interacting motif with a submicromolar affinity for stabilized MTs and confirmed the dominant contribution of patch B for MTs binding (Fig. 3*C*).

Furthermore, in competition experiments, the Ser-31 to Leu-59 peptide, but not its acetylation mimic variant, was able to completely abolish interactions between MTs and the GFP-HDAC6 fusion, thus verifying the specificity of HDAC6/MT interactions (Fig. 4).

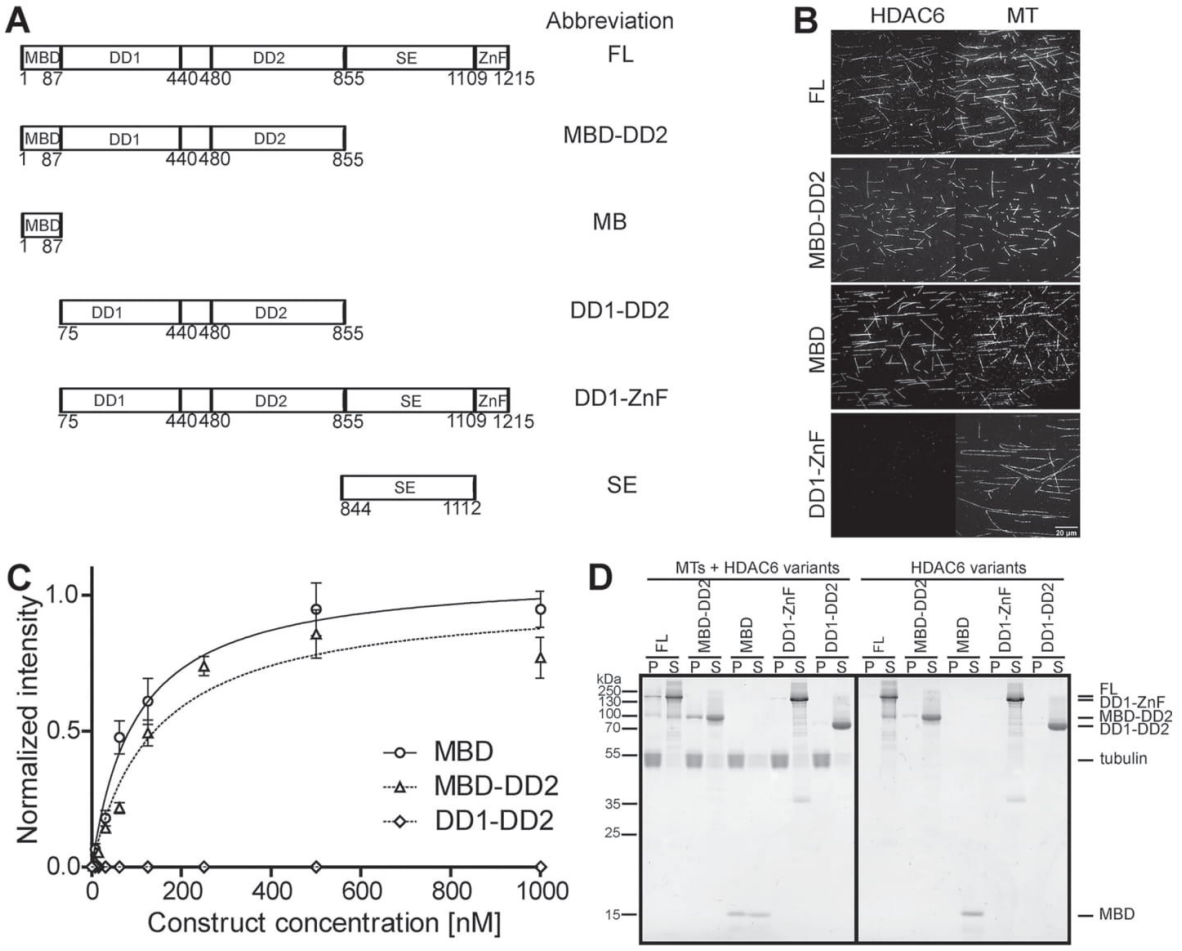

Figure 2. The HDAC6 N-terminal domain is necessary and sufficient to mediate interactions with stabilized MTs. *A*, schematic representation of truncated HDAC6 constructs. All constructs were produced as N-terminally tagged GFP fusions or with the unmodified N terminus. *B*, HDAC6 interaction with MTs. Alexa Fluor 647–labeled MTs were immobilized on the glass surface, and different GFP-HDAC6 fusions (500 nM) injected to the channel. GFP-HDAC6 fusion binding to MTs was visualized in the 488 nm channel, and the Alexa Fluor 647–labeled MTs in the 640 nm channel. Although HDAC6 constructs harboring the N terminus were uniformly distributed along MTs, no binding was observed for the DD1-ZnF mutant missing the MBD. *C*, interactions of individual HDAC6 mutants with stabilized MTs. MTs were immobilized on the glass surface and the dilution series of GFP-HDAC6 MBD (MBD), GFP-HDAC6 MBD-DD2 (MBD-DD2), and GFP-HDAC6 DD1-DD2 (DD1-DD2) were added to the channel. The fluorescence signal of the MT-bound HDAC6 mutants was quantified using TIRF microscopy and respective apparent dissociation constants ($appK_D$) calculated from binding curves using the GraphPad program. Apparent dissociation constants for MBD and MBD-DD2 were calculated to be 98 ± 9.3 nM and 140 ± 2.7 nM, respectively. No binding was observed for the catalytic core. Data represent mean values ± S.D.; $n = 3$. *D*, pelleting assay using Taxol-stabilized MTs. HDAC6 constructs of final concentration 1 μM were mixed with MTs of final concentration 0.5 μM (or without MTs as controls), samples centrifuged, supernatant (*S*), and pellet (*P*) fractions separated and visualized by SDS-PAGE. Only constructs containing the MBD were found in the pellet fraction bound to MTs.

Tubulin-negative charges are essential for MT recognition by HDAC6

The fast, one-dimensional diffusion kinetics observed at the single-molecule level suggest that HDAC6/MT interactions can be mediated by electrostatic forces between the negatively charged MT surface and positively charged motif(s) of HDAC6, as reported for several MAPs (31, 46, 47). To test this hypothesis, we first examined the influence of salt concentration on HDAC6 binding to MTs by performing the TIRF-binding assay in buffers of different ionic strengths ranging from BRB80 (80 mM PIPES) to BRB10 (10 mM PIPES). The fluorescence signal quantification of HDAC6 bound to MTs revealed the strong dependence of HDAC6/MTs interactions on salt concentration, with the highest signal observed for BRB10 and binding virtually absent in BRB80 at the HDAC6 concentration used (100 nM) (Fig. 5*A*).

We next examined whether the presence of C-terminal unstructured acidic tails on MTs is required for HDAC6 binding. The C-terminal tails were removed by treatment with the nonspecific protease subtilisin and their absence verified by MS (Fig. 5*B*; Fig. S5). The mixture of untreated and subtilisin-treated MTs was then immobilized on coverslips and binding of GFP-HDAC6 fusions assayed by TIRF microscopy. Although HDAC6 avidly bound to native, nontreated MTs, there was a

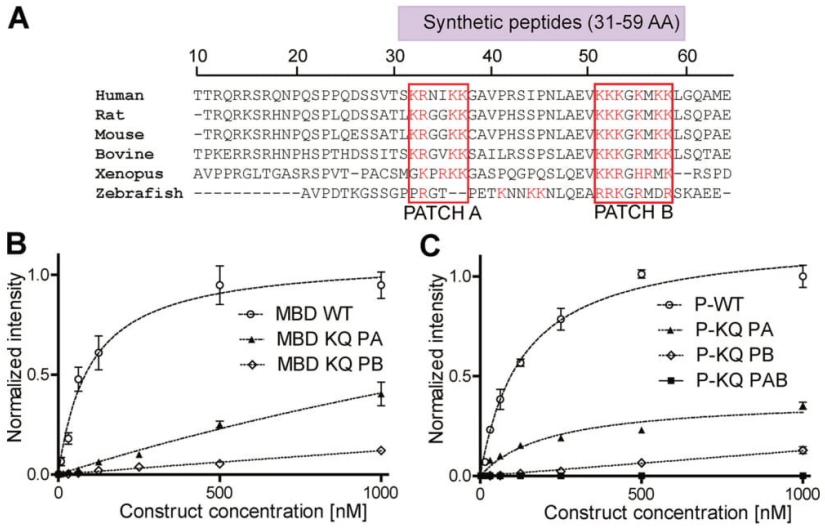

Figure 3. Positively charged patches of the MBD domain are critical for HDAC6 binding to MTs. *A*, sequence alignment of HDAC6 N-terminal domains from different species. Microtubule-binding motifs of HDAC6 span positively charged patches comprising residues Lys-32 to Lys-37 (patch A) and Lys-51 to Lys-58 (patch B). The *purple box* above the sequence alignment denotes the position of HDAC-derived synthetic peptides used in this study (amino acids 31–59). *B* and *C*, interactions of the HDAC6 MBD with stabilized MTs at the protein (*B*) and peptide (*C*) levels. MTs were immobilized on the glass surface and the dilution series of (*B*) GFP-MBD fusions (MBD WT, WT; MBD KQ PA, patch A; and MBD KQ PB, patch B mutants) or (*C*) corresponding FITC-labeled synthetic peptides (P-WT, WT; KQ PA, patch A; KQ PB, patch B; KQ PAB, combined patch A/B) were added to the channel. The fluorescence signal of the MT-bound proteins/peptides was quantified using TIRF microscopy and respective apparent dissociation constants ($appK_D$) calculated from binding isotherms. The apparent dissociation constant for the GFP-MBD WT and corresponding FITC-labeled P-WT was calculated to be 98 ± 9.3 nM and 131 ± 5.1 nM, respectively. Acetylation mimicking Lys to Gln mutants of the patch A and B, revealed a substantially lower binding affinity for MTs, with more pronounced effects observed in the case of patch B mutants. No binding was observed for the KQ PAB double mutant. Experimental points represent mean values ± S.D.; $n = 3$.

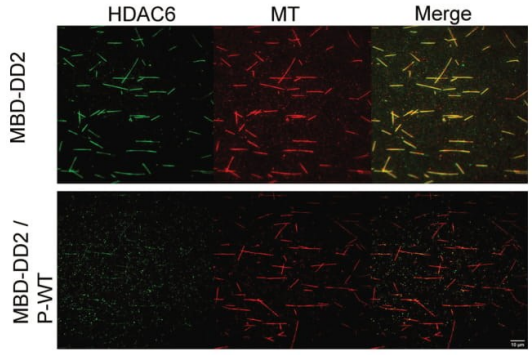

Figure 4. The MBD-derived peptide (P-WT) competes with HDAC6 for MT binding. Alexa Fluor 647–labeled MTs were immobilized on the glass surface. The 100 nM GFP-MBD-DD2 fusion either alone (MBD-DD2) (*upper panel*) or together with the 1000 nM unlabeled synthetic P-WT peptide (MBD-DD2/P-WT; *lower panel*) were injected to the channel. The P-WT peptide outcompetes GFP-MBD-DD2 binding to MTs, confirming the critical importance of the N terminus of HDAC6 for interactions with MTs. GFP-MBD-DD2 binding to MTs was visualized in the 488 nm channel and superimposed with the Alexa Fluor 647 signal of MTs.

complete absence of the GFP signal from MTs lacking C-terminal tails (Fig. 5*C*). Collectively, these findings show that HDAC6/MTs interactions are mediated by ionic interactions between negatively charged MT surface and lysine patches of HDAC6 N-terminal domain.

MBD is critical for efficient tubulin deacetylation in vitro

Based on the above experimental data, it is apparent that the MBD endows HDAC6 with MAP-like properties. At the same time, as free tubulin dimers are the physiological substrate of HDAC6 (14, 37), we set out to examine the importance of the MBD on HDAC6 deacetylase activity *in vitro* and *in vivo*. Using microscale thermophoresis (MST), we first quantified interactions between free tubulin dimers and HDAC6 mutants and HDAC6-derived MBD peptides, because to the best of our knowledge no such direct quantification has ever been reported. All tested mutants comprising the WT MBD interacted with free tubulin dimers, whereas no HDAC6/tubulin interactions were observed for mutants lacking MBD. Unfortunately, as we were not able to reach the upper plateau of the signal, the corresponding values of dissociation constants could not be calculated (Fig. S6). At the same time, quantification of interactions between tubulin and HDAC6-derived MBD peptides revealed $appK_D$ values of 577 ± 102, 665 ± 181, and 5898 ± 800 nM for P-WT, P-KQ PA, and P-KQ PB peptides, respectively, with no interaction signal observed for the KQ PAB peptide (Fig. 6).

Identification of the MBD interaction with free tubulin motivated us to examine whether the presence of the domain also influences the HDAC6 deacetylase activity. To this end, we assessed the deacetylation activity of the HDAC6 FL and its truncated/mutated constructs against several substrates, including a fluorescent Ac-GAK-AMC peptide, the αK40 loop-derived peptide, and free tubulin dimers, a preferred physiological substrate *in vitro* (Fig. 7). When short peptidic substrates were used, we did not observe any substantial difference in kinetic parameters between the constructs (Fig. S7), suggesting that domains beyond the catalytic tandem deacetylase core (and likely only the C-terminal deacetylation domain) do not

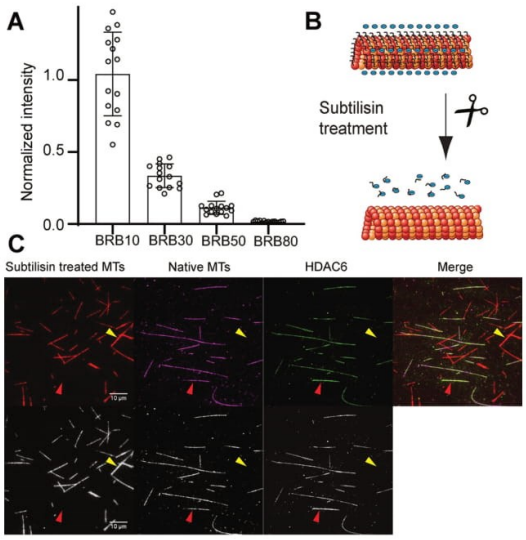

Figure 5. HDAC6/MT interactions are mediated by electrostatic interactions with negatively charged tubulin surface. *A*, influence of salt concentration on HDAC6 FL binding to MTs. The GFP-HDAC6 FL fusion (100 nM) was incubated with immobilized MTs in buffers of increasing ionic strength (10 mM PIPES (BRB10) through 80 mM PIPES (BRB80)) and the amount of the GFP-HDAC6 FL fusion bound to MTs was quantified using TIRF microscopy and normalized to the mean fluorescence signal in the BRB10 buffer. The HDAC6 FL binding to MTs is strongly modulated by ionic strength with the GFP-HDAC6 signal extremely weak in BRB80. Data represent mean values ± S.D.; $n = 3$. *B*, schematic representation of subtilisin treatment of MTs. *C*, tubulin C-terminal tails are required for HDAC6 FL binding. Native (rhodamine-labeled; *violet*) and subtilisin-treated (Alexa Fluor 647–labeled; *red*) MTs were simultaneously attached to a glass coverslip and probed with GFP-labeled HDAC6 FL (250 nM) in the BRB50 buffer. Although the GFP-HDAC6 FL fusion co-localizes with native MTs (*red arrow*), interactions are absent in the case of MTs missing C-terminal tails (*yellow arrow*). Color images are shown in the *top row*; the *bottom row* displays the same images in *greyscale*.

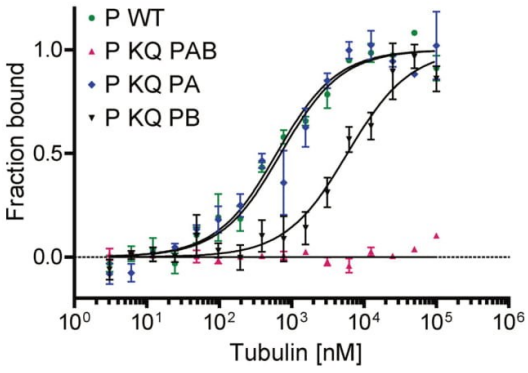

Figure 6. The MBD is essential for HDAC6 interactions with free tubulin dimers. Binding affinity between HDAC6 MBD–derived peptides and free tubulin dimers was quantified using MST. FITC-labeled peptides (100 nM) were titrated by a dilution series of tubulin dimers (100 μM–3 nM). MST curves were fitted using the MO.Affinity software (NanoTemper, Munich, Germany) and calculated apparent $appK_D$ values were 577 ± 102 nM, 665 ± 181 nM and 5898 ± 800 nM for the WT (P WT), patch A mutant (P KQ PA), and patch B mutant (P KQ PB), respectively. No binding was observed for the patch A/B double mutant (P KQ PAB). Experimental data points represent mean values ± S.D.; $n = 3$.

contribute to the recognition of peptidic substrates (Fig. 7*C*). To the contrary, when free tubulin was used as a substrate, deacetylation rates by constructs lacking (or having mutated) MBD were 50- to 120-fold (or 20-fold, respectively) lower compared with constructs having the WT MBD (Fig. 7*A* and *B*).

To support the kinetic data and to underscore the importance of the MBD interactions with tubulin, but not small peptidic substrates, we carried out competition experiments in which deacetylation of tubulin or short peptidic substrates was assayed in the presence of HDAC6-derived MBD peptides (for examples of Western blots and HPLC chromatograms used for calculations/quantifications, see Fig. S8). Although the WT peptide inhibited tubulin deacetylation by HDAC6 FL in a concentration-dependent manner, it had no effect on either tubulin deacetylation by the DD1-DD2 variant or on deacetylation of short peptidic substrates by both HDAC6 FL and DD1-DD2 (Fig. 7*C*).

Taken together, our kinetic data thus parallel binding experiments with both free tubulin dimers and MTs, revealing that the presence of the MBD is also critical for efficient deacetylation of tubulin, but not of short peptidic substrates.

MBD is required for efficient tubulin deacetylation in the cellular environment

In the final set of experiments, we extended our *in vitro* findings into more complex cellular environment. To this end, we prepared a set of HDAC6 mutants with a truncated/modified MBD (Fig. 8*A*), and their activity was tested in HEK293T-HDAC6 KO cells (20). The catalytically inactive HDAC6 (H216A/H611A) double mutant was used as an additional control.

Although HDAC6 FL and its mutants were equally expressed in cells, tubulin αK40 acetylation levels were different (Fig. 8*B*; Fig. S14). In line with our *in vitro* observations, HDAC6 mutants FL_Δ_PA and FL_Δ_PB showed less deacetylase activity on tubulin (Fig. 8*B*, *lanes 2, 4*, and *5*). The patch B is likely to have more significant contribution to the activity (Fig. 8*B*, *lanes 4* and *5*), and furthermore, the FL_PB(K/Q) mutant (the patch B acetyl mimic neutralizing the positive charge) shows decreased activity, similar to its deletion (Fig. 8*B*, *lanes 5* and *6*). In contrast, the FL_PB(K/R) mutant (nonacetylated but retaining the overall positive charge) still has catalytic activity, which is comparable with that of HDAC6 FL (Fig. 8*B*, *lanes 2* and *7*). Thus, it appears that the positive charge of patch B plays an important role in tubulin αK40 deacetylation in cells. Two N-terminal domain deletion mutants (amino acids 45–1215 and amino acids 62–1215 designated HD6_Δ2–44 and HD6_Δ2–61, respectively), which are the human versions of the *Danio rerio* constructs used for crystallization (14), also exhibit less activity, in good agreement with the observations above (Fig. 8*B*, *lanes 9* and *10*). Previous reports showed that the HDAC6 N-terminal region contains a nuclear localization signal (amino acids 14–58) and an NES (amino acids 67–76) (21); we therefore tested the cellular localization of all HDAC6 mutants to rule out that the differential deacetylase activity observed might be because of changes in subcellular localization. As shown in Fig. 8*C*, all mutants equally localize to the cytosol, and thus it is unlikely that mutation leads unintended localization of HDAC6 to the nucleus and a subsequent decrease of tubulin deacetylation (Fig. 8*C*). In summary, we revealed that these two N-terminal lysine/arginine-rich patches (patch A and patch B) are

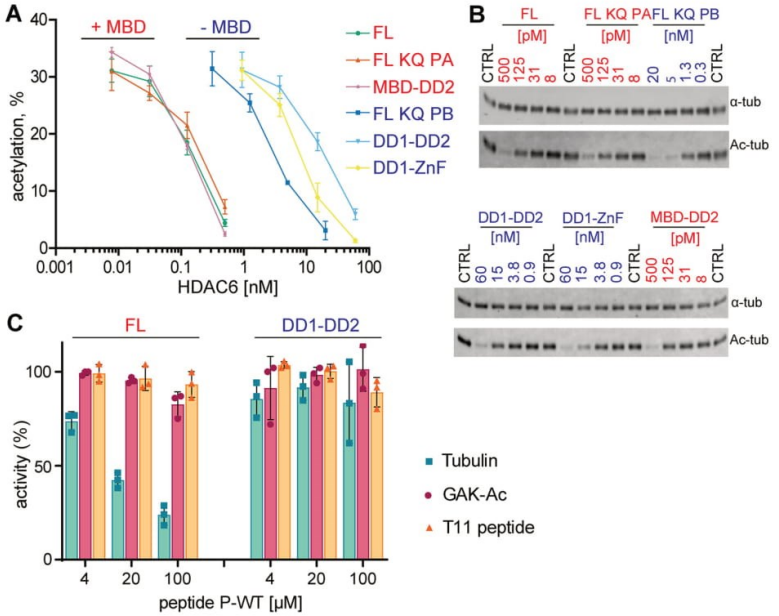

Figure 7. The MBD of HDAC6 is critical for deacetylation of tubulin, but not small peptidic substrates. *A*, deacetylation activity of HDAC6 variants on free tubulin dimers. Optimized dilution series of HDAC6 variants (the WT, deleted, and mutated MBD) were incubated with free tubulin and αK40 acetylation determined by quantitative Western blotting. Much higher (40- to150-fold) concentrations of variants with mutated/missing MBD (−MBD, *blue*) are required for efficient deacetylation of tubulin compared with variants with WT sequences (+MBD, *red*). *B*, examples of Western blotting used for calculations/quantifications shown in (*A*). *C*, deacetylation activity of WT HDAC6 and its DD1/DD2 mutants against tubulin and short-peptidic substrates (T11, GAK-Ac) were evaluated in the presence of the peptide P-WT, derived from the MBD of HDAC6. Peptide P-WT competes with deacetylation of tubulin by HDAC6 protein in a concentration-dependent manner but does not influence deacetylation efficacy of HDAC6 FL toward short peptides or the DD1-DD2 variant toward any substrate.

important for the catalytic activity on tubulin, and also confirmed that positively charged residues are necessary for the patch B function.

Discussion

Within the past decade, our comprehension of structural and functional aspects of HDAC6 has expanded rapidly. Understandably, major efforts have been invested into studying the DD2 and ZnF domains, which have a compact three-dimensional fold and fairly well-defined physiological functions (13, 14, 26, 48). Much less is known about the contribution(s) of the DD1 domain toward HDAC6 function (20), and there is virtually no information concerning the physiological role(s) of intrinsically disordered N-terminal and SE domains. In this report, we identified the N-terminal part of HDAC6 as an MBD that is critical for tubulin recognition and efficient deacetylation by HDAC6.

The N-terminal domain/extension of HDAC6 is present in orthologs across various species. It shows a high degree of phylogenetic conservation and pronounced cationic character (Fig. S9) with the calculated pI of the human sequence to be pI = 10.5 (amino acids 1–75). Because the electrostatic potential of tubulin/MT surface is highly negative (Fig. S10), it is plausible that ionic attraction forces are critical to high-affinity interactions between HDAC6 (the MBD) and tubulin/MTs. Several lines of evidence presented here support this conclusion. In addition to human HDAC6, interactions between MTs and HDAC6 orthologs from zebrafish and mouse were evaluated. In line with human HDAC6 data, both full-length orthologs avidly bind Taxol/GMPCPP double-stabilized MTs (Fig. S11). It is also interesting to note that in eukaryotic cells, the HDAC6 mutant in which the patch B lysines were replaced by arginines (FL_PB(K/R)) has deacetylase activity virtually identical to the WT protein (Fig. 8). The findings above suggest that the overall charge, rather than the exact sequence, is critical for tubulin/MT interactions. This notion is further supported by the use of the scrambled 31–59 peptide (a scrambled sequence of the MBD), which binds to MTs with the same affinity as the parent WT peptide (Fig. S12). Finally, it shall be noted that in addition to patches A and B analyzed here, three additional clusters of positively charged lysines (Lys-553, Lys-555; Lys-849, Lys-853, Lys-854; and Lys-872, Lys-873), which are subject to acetylation by p300, have been identified in the HDAC6 sequence (18). However, as these additional sites are located in the DD2 and SE domains of HDAC6 and neither of these domains is capable of mediating HDAC6/MTs interactions, their acetylation can play a role in HDAC6 physiological functions other than MT/tubulin binding/deacetylation. As disordered regions in various proteins have been associated with phase separation or condensate formation (49), it is possible to speculate that this property might also contribute to the enhanced affinity of HDAC6 for MTs.

Note that although the presence of the unmodified MBD significantly increases the deacetylation rate of tubulin, the domain is not essential for HDAC6 deacetylase activity on all

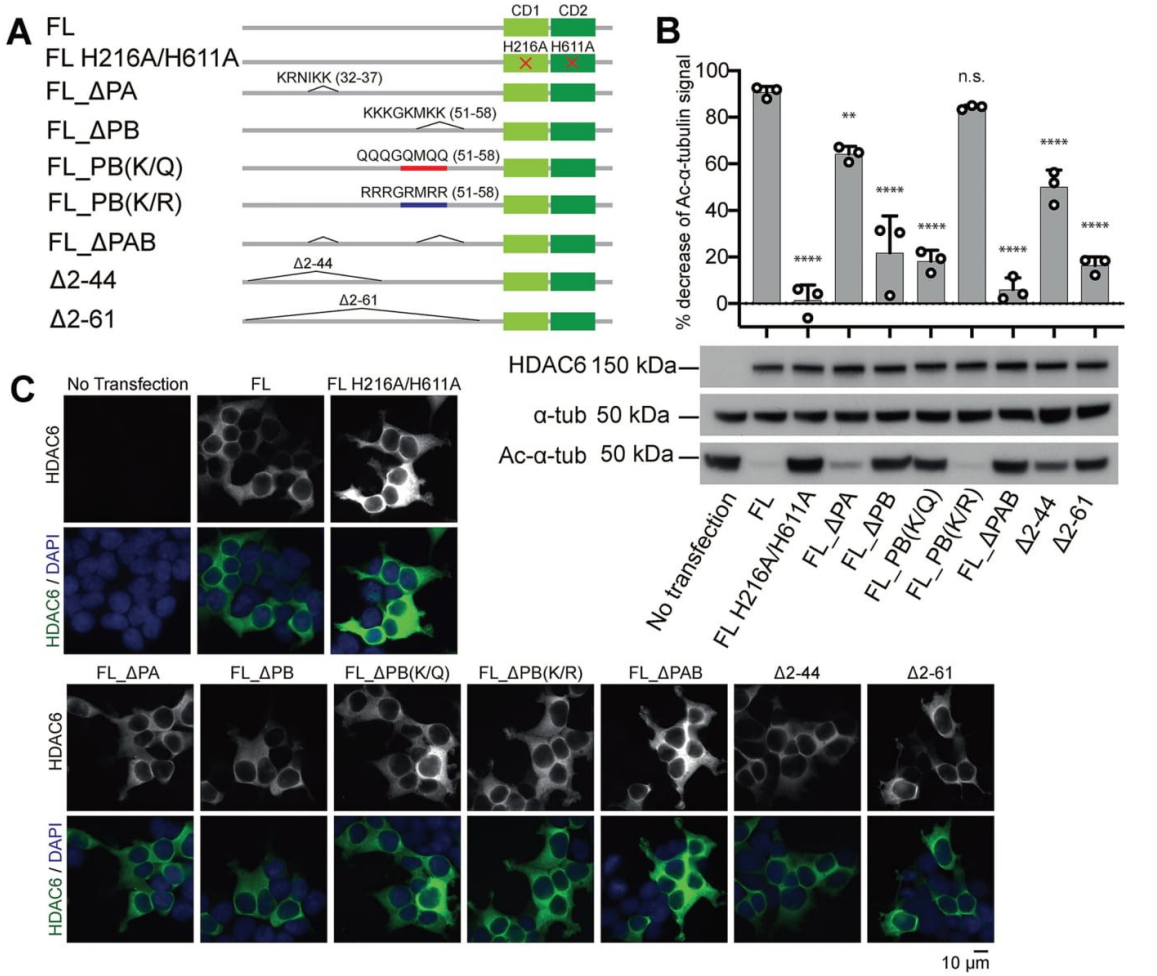

Figure 8. *In vivo* deacetylase activity and localization of HDAC6 mutants in HEK293T HDAC6 KO cells. *A*, panel of HDAC6 mutants used for transfection of HEK293T-KO cells. HDAC6 harbors two lysine/arginine rich patches (patch A and patch B) in its N-terminal domain (amino acids 1–86). FL_PB(K/Q) is a neutralized mutant of patch B, whereas FL_PB(K/R) is a positive-charge retention mutant. FL_H216A/H611A is a catalytic-dead mutant. HD6_Δ2–44 and HD6_Δ2–61 are human constructs corresponding to *D. rerio* HDAC6 constructs (drHD6_Δ1–24 and drHD6_Δ1–39, respectively) previously used for crystallization and tubulin deacetylation assays (Miyake *et al.* (14)). *B*, analysis and quantification of tubulin acetylation levels in transfected HEK293T-HDAC6 KO cells using Western blotting. HDAC6 FL or mutants in pcDNA3 vector were transiently expressed in HEK293T-HDAC6 KO cells, and tubulin αK40 acetylation level was tested by immunoblotting. Although the expression of all variants was approximately similar, the acetylation level significantly decreased in the case of HDAC6 mutants with the native patch B and the K/R mutant (FL_PB(K/R). The result is normalized by the expression levels of α-tubulin and HDAC6. *, $p < 0.05$; **, $p < 0.01$; ***, $p < 0.001$; and ****, $p < 0.0001$ by one-way analysis of variance. *C*, subcellular localization of HDAC6 FL and mutants. The indicated HDAC6 constructs were transiently expressed in HEK293T-HDAC6 KO cells. Localization of HDAC6 was assessed by immunofluorescence microscopy. All HDAC6 mutants localize to the cytoplasm and no re-localization to the nucleus was observed. *Scale bar*, 10 μm.

substrates tested so far, including tubulin and microtubules (13, 14, 26, 37). Additionally, other HDAC6 structural features outside the MBD, such as the helix H25 and the loop H20–H21 of the DD2, are critical for deacetylation of αK40 on α-tubulin, but not in the context of short peptides (14). These findings demonstrate the recognition complexity of physiological substrates by HDAC6 that warrant further studies. Another distinction shall be made between *binding to* and *deacetylation of* tubulin/MTs by HDAC6 N-terminal mutants. For example, using stabilized MTs as a substrate, we observed a weak deacetylase activity of HDAC6 mutants lacking the MBD (14, 37), yet not its binding to the MT surface. At the same time, it is clear that for the deacetylation reaction to proceed, the enzyme must recognize (and interact with) its cognate substrate. This apparent discrepancy can be explained by temporal resolution and sensitivity of experimental techniques used. The MT deacetylation in cells is easily followed with the anti-AcK40 antibody by Western blotting or fluorescent microscopy as the end point signal at various time intervals. On the other hand, in the case of real-time TIRF microscopy, longer residence time, and ideally also higher concentration (more molecules) of fluorophores, is needed to obtain a detectable signal. We believe that the presence of the MBD allows GFP-HDAC6 fusions to stay attached to the MT surface for a longer period that can be easily moni-

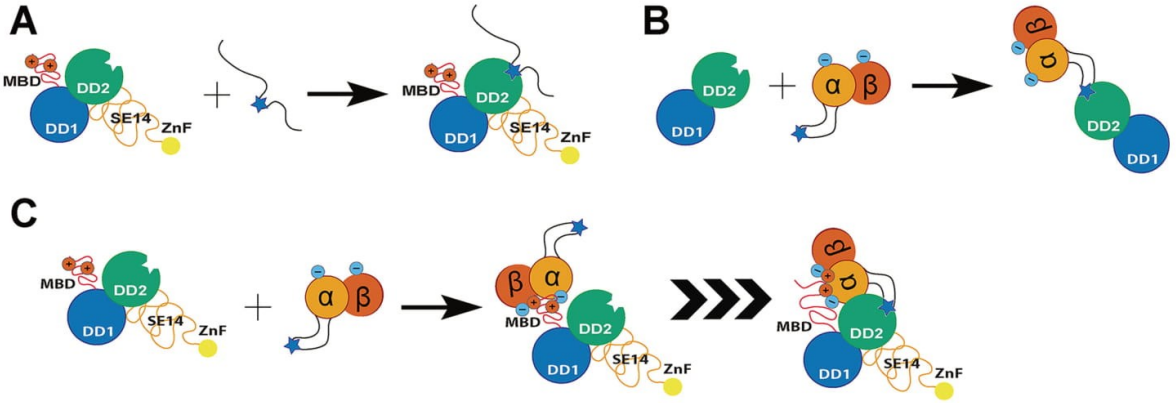

Figure 9. Mechanism of substrate deacetylation by HDAC6. *A*, short peptides, such as the 11-mer peptide derived from the αK40 loop of α-tubulin (acetylated lysine K40 denoted by a *star*), are directly recognized and deacetylated by the catalytic domain DD2 in a single step. However, the overall catalytic efficiency of the deacetylation is low due to suboptimal recognition/binding of the peptide by HDAC6 (high K_m values). *B*, HDAC6 mutants missing the MBD bind and deacetylate tubulin dimers in a single step and with similar efficacy to that for short peptides. *C*, tubulin deacetylation by HDAC6 FL is enhanced ~100-fold compared with mutants missing the MBD. Our data suggest that the MBD of HDAC6 first interacts with tubulin via ionic interactions, thus increasing the local concentration of the binary HDAC6/tubulin complex, which results in a 100-fold faster tubulin deacetylation.

tored up to the single-molecule level. On the other hand, interactions between MTs and HDAC6 mutants missing the MBD are very transient (and infrequent) and thus cannot be directly visualized by TIRF microscopy.

Apart from acetylation, HDAC6 is a target of additional posttranslational modifications including ubiquitinylation and phosphorylation and also a subject to alternative splicing (50, 51). Thirty-three alternatively spliced mRNA variants of human HDAC6 are predicted to exist (52) although the evidence for the existence of the translated protein species *in vivo* is missing. In fact, only one of the splice variants, denoted hHDAC6bApr07, was partially characterized at the protein level. This variant starts at the position 152 of the HDAC6 FL, lacking thus the MBD and a part of DD1, and retains a weak tubulin deacetylase activity. Moreover, it has been suggested that the truncated variant could differ from the full-length HDAC6 in the activation of gene expression, although the mechanism has not been studied (51). Apparently, in addition to lowered tubulin deacetylase activity, HDAC6 variants with the missing or posttranslationally modified N terminus might have other disparate physiological functions and be differentially regulated under various (patho)physiological conditions.

Numerous kinases target HDAC6 and regulate its deacetylase activity toward physiological substrate(s), ultimately influencing diverse cellular functions. G protein–coupled receptor kinase 2 (phosphorylates HDAC6 at positions Ser-1060, Ser-1062, and Ser-1069) (53), extracellular signal-regulated kinase (Thr-1031, Ser-1035) (54), p38α (54), protein kinase Cζ (50), protein kinase CK2 (Ser-458) (55), Aurora protein kinase A (56), and glycogen synthase kinase 3β (Ser-22) (57) were all shown to positively modulate HDAC6 tubulin deacetylase activity *in vitro*/*in vivo*, whereas HDAC6 phosphorylation by epidermal growth factor receptor kinase (Tyr-570) (58) has the opposite effect. Ser-22, the target residue of glycogen synthase kinase 3β, is the only characterized phosphorylation site residing within the N-terminal domain of HDAC6, whereas the other phosphorylated residues are distributed throughout DD1, DD2, and SE domains. Seen through the prism of findings presented here, it is not clear how the introduction of a negatively charged phosphate group at the MBD could contribute to increased HDAC6 deacetylation activity against tubulin. In general, mechanisms of HDAC6 activation/inhibition by phosphorylation events are not well-characterized and warrant further studies in the future.

The SE domain, together with the NES, is responsible for the cytoplasmic retention of HDAC6 and it has been reported to bind MTs with low affinity *in cellulo* (21). Our *in vitro* reconstitution experiments, however, do not support the notion of direct SE/tubulin interactions (Fig. 2). It is thus likely that observed binding of SE to MTs in the cellular milieu can either be mediated by an unknown MAP or, alternatively, dependent on unidentified PTM(s) within the SE domain that is missing from our recombinant enzyme.

Based on our findings reported here, we proposed a molecular mechanism of tubulin deacetylation by HDAC6 and compared it to the deacetylation of short peptides (Fig. 9). For short peptides with internal lysine, the target sequence is directly recognized and deacetylated by the DD2 in a single step. Because the recognition process (limited complementary interfaces) is not very effective, high concentrations of a peptidic substrate, reflected in high millimolar K_m values, are needed for efficient deacetylation. On the other hand, in the case of tubulin deacetylation, HDAC6 is first attracted to tubulin via nonspecific ionic interactions of its disordered MBD, increasing thus the local concentration of the binary HDAC6/tubulin complex that is then deacetylated much more efficiently.

Collectively, we identified the N-terminal domain of HDAC6, denoted the MBD, as a component critical for facilitating HDAC6 interactions with MTs as well as enhancing HDAC6 deacetylase activity against free tubulin by more than 100-fold. From the data reported here, it is obvious that substrate recognition by HDAC6 is more complex than previously appreciated, and these findings shall be considered when mutated/truncated constructs are used in biological experi-

ments. It will also be interesting to see whether the MBD and/or domains outside the catalytic core can modulate deacetylation of other HDAC6 physiological substrates. Finally, our findings open new avenues in the design of HDAC6-specific compounds that could selectively block deacetylation of only a single (or a limited set) of its physiological substrates.

Experimental procedures

Chemicals

If not stated otherwise, all chemicals were purchased from Sigma-Aldrich. Alexa Fluor 647 NHS Ester (A37573) and NHS-Rhodamine (46406) were purchased from Thermo Fisher Scientific. Nexturastat A was a kind gift from Alan Kozikowski, StarWise Therapeutics LLC (Madison, WI).

Cloning and site-directed mutagenesis

Full-length WT human HDAC6 (UniProtKB: NP_006035.2, Q9UBN7) was used as a template for the cloning of all HDAC6 truncated/mutated constructs. Truncated mutants were PCR amplified using corresponding sets of gene-specific primers (Table S1) and cloned into the pDONR221 donor vector via the BP recombination reaction according to the manufacturer protocol (Invitrogen). The identity of each donor clone was verified by Sanger sequencing and the sequence encoding a given HDAC6 construct inserted into the desired expression vector by the LR recombinant reaction. Site-directed mutagenesis was carried out by the standard QuikChange protocol using matching pairs of complementary mutagenic primers (Table S1) and the original pMM322_HDAC6 plasmid as a template (37). The identity of all HDAC6 expression clones was verified using Sanger sequencing, and their schematic representations are shown in Fig. 2.

HDAC6 expression and purification

All HDAC6 mutants were expressed in HEK293T17 cells and purified to near homogeneity by the combination of Strep-Tactin affinity and size-exclusion chromatography essentially as described previously (19, 37). Briefly, HEK293T17 cells were grown in Gibco FreeStyle F17 Expression Medium (Thermo Fisher Scientific) supplemented with 0.1% Pluronic F-68 (Invitrogen) and 2 mM L-glutamine at 110 rpm under a humidified 5% CO_2 atmosphere at 37 °C. Linear polyethyleneimine (Polysciences Inc., Warrington, PA) was used to mediate transient transfection. Four h post transfection, the cell suspension was diluted by the addition of an equal volume of ExCell293 Serum-Free Medium and cells were harvested 72 h post transfection by centrifugation at 500 × *g* for 5 min. The cell pellet was snap-frozen in liquid nitrogen and stored at −80 °C.

For purification, cell pellets were lysed in 50 mM Tris, 150 mM NaCl, 10 mM KCl, 10% glycerol, 0.2% Nonidet P-40, pH 8.0, supplemented with a mixture of protease inhibitors (Roche) followed by incubation for 30 min on ice. Cell lysate was cleared by centrifugation at 40,000 × *g* for 30 min at 4 °C, the supernatant loaded on a Strep-Tactin column (IBA, Göttingen, Germany) and then eluted with the lysis buffer containing 2 mM desthiobiotin. If desired, the N-terminal tag was cleaved by tobacco etch virus protease (1:20 ratio (w/w)) overnight at 4 °C. The final purification step included size-exclusion chromatography on Superose 6 column (GE Healthcare Life Sciences). Purified proteins were concentrated to 1 mg/ml and flash-frozen in liquid nitrogen until further use.

Fluorimetric assay

The deacetylation activity of HDAC6 constructs was determined as described previously (37). Briefly, HDAC6 constructs were incubated with 2-fold serial dilutions of the substrate acetyl-Gly-Ala-(acetyl-Lys)-AMC (Bachem, Bubendorf, Switzerland) in the reaction buffer (50 mM HEPES, 140 mM NaCl, 10 mM KCl, 0.2 mg/ml BSA, 1 mM TCEP, pH 7.4) in 384-well plates for 30 min at 37 °C in total volume of 20 μl. The reaction was quenched by adding 10 μl trypsin solution (4 mg/ml trypsin) and incubating 15 min at 37 °C. Subsequently, the aminomethylcoumarin (AMC) fluorescence signal was detected by a CLARIOstar fluorimeter (BMG Labtech GmbH, Ortenberg, Germany) (λ_{ex} = 365 nm, λ_{em} = 440 nm). The GraphPad Prism software (GraphPad Software, San Diego, CA) was used for data analysis and fitting.

HPLC-based deacetylation assay

A 2-aminobenzoyl–labeled 11-mer peptide derived from the α-tubulin sequence (Abz-QMPSDK(Ac)TIGGG-NH_2) was used as a substrate in the RP-HPLC setup. Reaction mixtures comprised the peptide in the concentration range of 0.8–400 μM and 20 nM HDAC6 construct in an assay buffer comprising 50 mM HEPES, 140 mM NaCl, 10 mM KCl, 0.2 mg/ml BSA, 1 mM TCEP, pH 7.4. Reactions were incubated for 60 min at 37 °C, quenched by the addition of 0.5% acetic acid, and centrifuged at 2000 × *g* at 37 °C for 15 min to remove precipitated BSA and HDAC6. Reactions were analyzed by RP-HPLC (Shimadzu, HPLC Prominence system) using a Kinetex 2.6 μm XB-C18 100 Å column (100 × 3 mm; Phenomenex, Torrance, CA). The mobile phase A was 5% acetonitrile (ACN) with 0.1% (v/v) trifluoroacetic acid (TFA), and the mobile phase B was 95% ACN with 0.1% (v/v) TFA. The separation of the reaction product from the acetylated substrate was performed in a 12-min linear gradient from 10 to 35% of eluent B at a flow rate of 0.6 ml/min. The excitation/emission wavelengths were set to 320/420 nm, respectively, to monitor the fluorescence of the reaction product. The amount of the reaction product was quantified from the peptide calibration curve. The data were fitted using the GraphPad Prism software (GraphPad Software, San Diego, CA), and kinetic values were calculated through nonlinear regression analysis.

Pelleting assay

A pelleting assay was run in a similar way to already-published co-sedimentation assays (59) with several modifications, described below. Working stocks of HDAC6 constructs were precleared by centrifugation at 30,000 × *g* for 45 min at 30 °C prior to combining the binding reaction with MTs. Binding reactions were kept at 32 °C throughout the whole procedure. In a 40-μl reaction mix, Taxol-stabilized MTs in a final concentration of 0.5 μM were combined with HDAC6 and its constructs of final concentration 1 μM in BRB50 supplemented with 0.01% C12E8 detergent, 10 μM Taxol, and 0.5 mM TCEP.

After a 5-min incubation, the reaction was centrifuged at 30,000 × *g* for 45 min without using any cushion. The whole supernatant was taken and mixed with 5 μl of 4× concentrated Laemmli sample buffer, whereas the pellet was directly dissolved in 20 μl of Laemmli sample buffer. Samples were heated at 95 °C for 5 min, and protein separation by SDS-PAGE in 13% Tris-glycine gels followed. Proteins were visualized in gel by Coomassie Brilliant Blue G-250 staining. Photograph of the gel was processed in Adobe Photoshop software.

Tubulin isolation from porcine brains

Tubulin isolation from pig brain tissue was carried out according to the established protocol (60) as described previously (37). The final tubulin stock was stored in the BRB80 buffer at the 20 mg/ml concentration as determined from absorbance readings at λ_{280} using NanoDrop One Microvolume UV-Vis Spectrophotometer (Thermo Scientific).

Tubulin labeling

Tubulin was diluted in a polymerization buffer (1 mM GTP, 3.5 mM $MgCl_2$, 30% glycerol, BRB80 buffer, pH 6.9) at a final concentration of 30 μM and left to polymerize for 1 h at 37 °C. MTs were centrifuged through pre-warmed high-pH cushion (0.1 mM HEPES, 1 mM EGTA, 1 mM $MgCl_2$, 60% glycerol, pH 8.6) at 150,000 × *g* for 30 min. Resuspended MTs were labeled through NHS coupling with Alexa Fluor 647 NHS ester or rhodamine NHS ester at a 10-molar excess of the dye to tubulin for 1 h at 37 °C. Two volumes of a stop solution (2× BRB80, 40% glycerol, 100 mM glutamate) were added and incubated for 5 min to terminate the labeling. The labeled MTs were pelleted through a low pH cushion (BRB80, 60% glycerol, pH 6.9), resuspended in an ice-cold BRB80 buffer, and left for 70 min on ice to induce depolymerization. Following the two cycles of polymerization and depolymerization tubulin concentration was determined from the absorbance at λ_{280} nm, the labeled tubulin aliquoted at 4 mg/ml and snap-frozen in liquid nitrogen. For TIRF experiments, the Alexa Fluor 647– or rhodamine-labeled tubulin was mixed with unlabeled tubulin at 1:30 ratio.

Microtubule polymerization

Tubulin (2.5 μM) in the polymerization buffer (BRB80 buffer, 1 mM GMPCPP (Jena Bioscience, Jena, Germany), 1 mM $MgCl_2$) was incubated on ice for 5 min and then for 2 h at 37 °C. The sample was centrifuged at 14,000 × *g* for 30 min at RT, the supernatant carefully discarded and the pelleted MTs dissolved in the BRB80 buffer supplemented with 1 μM Taxol (total volume 100 μl). The double-stabilized MTs were stored at room temperature until further use.

Microtubule subtilisin treatment

Double-stabilized MTs were digested by incubating with subtilisin (1:50 w/w ratio) for 60 min at 30 °C (61). The reaction was quenched by the addition of 5 mM phenylmethylsulfonyl fluoride (PMSF) and incubation 1 h at RT. The sample was then centrifuged at 14,000 × *g* for 30 min at RT, and pelleted MTs were dissolved in BRB80 buffer (supplemented with 1 μM Taxol) and stored at RT. The removal of the C-terminal tails was verified by the MS analysis (Fig. S5).

Total internal reflection fluorescence microscopy

TIRF microscopy was performed using a Nikon Ti-E microscope equipped with an H-TIRF System (Nikon, Japan), a 60× oil immersion 1.49 NA TIRF objective and an Andor iXon Ultra EMCCD camera (Andor Technology, Belfast, UK) controlled by the NIS Elements software (Nikon, Japan). Visualization was done by sequential dual-color imaging (switching between 488 nm and 640 nm excitation lasers to detect the GFP-HDAC6 fusion and Alexa Fluor 647–labeled MTs, respectively). Additionally, rhodamine-labeled MTs (detected at 561 nm) were used as nontreated controls in the experiments with subtilisin-treated MTs. The image acquisition rate was 1 frame per 0.4–0.5 s. For the determination of HDAC6 single-molecule movement mode, we used Nikon Ti-E microscope with N-SIM and N-STORM modules (Nikon, Japan), Nikon CFI HP Apo TIRF 100× oil objective, NA 1.49, an Andor iXon Ultra DU897 camera (Andor Technology, Oxon, UK) controlled by the NIS Elements software (Nikon, Japan). The image acquisition rate was increased one frame per 30 ms. Image analysis was carried out using Fiji (62, 63).

TIRF-based evaluation of HDAC6/MTs affinity

MTs and flow cells were prepared as described previously (37, 64). Briefly, microscope chambers were built from silanized coverslips (Corning Cover Glass Product) prepared as described previously (65). Parafilm was used to space glasses to form channels of ~0.1-mm thickness, 3-mm width, and 18-mm length. MTs were attached to the glass surface in each chamber via anti-β-tubulin antibodies (Sigma-Aldrich, T7816, 20 μg/ml in PBS). Subsequently, various concentrations of GFP-HDAC6 fusion constructs were added to the chamber in the binding buffer (BRB50, 0.5 mM TCEP, AMRESCO, Solon, OH), 0.5 mg/ml casein, 10 μM paclitaxel, 0.001% $C_{12}E_8$ (dodecyloctaglycol), 20 mM D-glucose, 110 μg/ml glucose oxidase, and 20 μg/ml catalase. The fluorescent signal of the GFP-HDAC6 fusion was determined by completely co-localizing with the signal of labeled MTs. Experimental data were processed with Fiji and binding curves fitted with the GraphPad Prism software using the nonlinear regression model. Experimental data points represent mean values ± S.D.; $n = 3$. Details of data processing and fitting, including calculations of apparent $appK_D$ values, are described in the supporting information (see method description S15).

Deacetylation of tubulin dimers

Deacetylation reactions were performed essentially as described previously (37). Briefly, tubulin dimers (1 μM) were incubated with optimized concentrations of HDAC6 constructs in a reaction buffer (BRB80, 1 mM TCEP, 0.2 mg/ml BSA, 80 μM colchicine) for 30 min at 37 °C in the total volume of 20 μl. Five microliters of TFA (5%) was used to quench the reaction. The deacetylation reaction was stopped by the addition of 20 μl of 5× Laemmli buffer and boiling samples at 95 °C for 5 min.

SDS-PAGE, Western blotting, and data analysis

Protein samples were resolved by SDS-PAGE in a 10% polyacrylamide gel at 150 V for 90 min. For immunoblotting, the gel

was transferred to a PVDF membrane using the Bio-Rad Trans-Blot Turbo Transfer System (Hercules, CA) under standard conditions. The membrane was blocked with 5% BSA dissolved in TBS. Monoclonal anti-acetylated tubulin antibody (Sigma, T7451, 0.3 μg/ml) with the combination of secondary antibody goat anti-mouse antibody conjugated to Alexa Fluor 488 were used for the detection of acetylated αK40 tubulin. Total tubulin was detected by rabbit polyclonal anti-α-tubulin antibody (Abcam, Cambridge, MA; ab18251; 1 μg/ml) and the secondary donkey anti-rabbit antibody conjugated to Alexa Fluor 568. The fluorescent signal was detected on a Typhoon FLA9500 imager (GE Healthcare Life Sciences) and quantified using Quantity One 1-D Analysis Software (Bio-Rad).

Microscale thermophoresis

Two-fold dilution series in the final volume of 10 μl were prepared from nonlabeled tubulin in the BRB50 buffer with 0.1% (v/v) Tween 20. A GFP-HDAC6 fusion was diluted in the same buffer, and an equal amount was added to the dilution series (100 μM–3 nM) of tubulin to the final concentration of 100 nM. The reactions were incubated at room temperature for 5 min. Reactions were centrifuged at 13,000 $\times$ *g* for 5 min 4 °C. Monolith NT.115 Capillaries standard (NanoTemper, Munchen, Germany) and machine Monolith NT.115 (NanoTemper, Munchen, Germany) were used for the measurement. Excitation power was set to 30 and 40% and MST power was set to 40 and 60% for FITC-labeled synthetic peptides and GFP-fusions, respectively. The results were processed with MO.Affinity Analysis and GraphPad Prism. For data analysis, the change in sample fluorescence upon IR-laser activation is monitored by calculating the ratio between the fluorescence after a given MST-on time (F1) and the fluorescence prior to IR laser activation (F0). A model for calculating apparent $appK_D$ value is implemented in the control software of the MST instrument and is derived from the law of mass action: $f(\text{concentration}) = U + (B - U) * (C + Tc + appK_D - \text{Sqrt}(C + Tc + appK_D)\wedge 2)/2*Tc$, where U is response value of unbound state (F0), B is response value of bound state (F1), $appK_D$ is dissociation constant, Tc is final concentration of a fluorescent molecule, C is concentration of the ligand molecule.

Cell-based HDAC6 localization and activity test

To construct expression vectors for expression of HDAC6 functional mutants, pcDNA3-hsHDAC6 was amplified with appropriate sets of primers, and the PCR product was self-ligated to generate internal deletions and obtain a mutated plasmid. Each mutated plasmid was transfected into HEK293T-HDAC6 KO cells, which were established in the previous work (Saito *et al.* 20) with Lipofectamine 2000 (Life Technologies). After 2 days, cells were subjected to immunoblotting or immunofluorescence.

For immunoblotting, cells were washed by ice-cold PBS and lysed in Triton lysis buffer (50 mM Tris, pH 8.0, 150 mM NaCl, 1 mM EDTA, 0.1% Triton X-100 and cOmplete EDTA-free Protease Inhibitors (Roche)) for analysis. The extracted cytosol fraction was boiled for 10 min in SDS-PAGE sample buffer and separated in 4–12% NuPAGE gels (Invitrogen). Proteins were transferred onto PVDF membranes (Immobilon-P, Millipore), proved with specific primary antibody for overnight and secondary antibody for 1 h under 5% nonfat dry milk in TBS blocking conditions and detected with Amersham Biosciences ECL Western blotting reagent (GE Healthcare). Primary antibodies were as follows: anti-α-tubulin (DM1A) (Sigma-Aldrich, T9026), anti-(K(Ac)40)-α-tubulin (Enzo, NY; BML, SA452–0100), and anti-human-HDAC6 was developed in Barinka Laboratory, Institute of Biotechnology CAS (clone 2H3G1). Secondary antibodies were as follows: Amersham Biosciences ECL Mouse IgG, HRP-linked whole Ab from sheep (GE Healthcare, NA931V), Amersham Biosciences ECL Rabbit IgG, HRP-linked whole Ab from donkey (GE Healthcare, NA934V).

For immunofluorescence, cells on a coverglass were washed with ice-cold PBS, then fixed with 4% paraformaldehyde. After permeabilization with 0.5% Triton X-100 in PBS for 10 min, the cells were incubated with specific primary and secondary antibodies in 10% goat serum blocking buffer, then mounted with ProLong Gold Antifade Reagent with DAPI (Cell Signaling Technology, 8961). Images were captured by Axio Imager Z1 microscope (Zeiss, Germany). Primary antibody was as follows: anti-human-HDAC6 was developed in Barinka Laboratory (clone 2H3G1). Secondary antibody was as follows: Alexa Fluor 488 Goat anti-Mouse IgG (H+L) Secondary Antibody (Invitrogen, A11001).

Peptide synthesis

Chemicals and general methods—Most of the Fmoc-protected amino acids were purchased from GL Biochem Ltd (Shanghai, China). *N*,*N*-dimethylformamide (DMF), piperidine, ethyl (hydroxyimino)cyanoacetate (OxymaPure), TentaGel R RAM resin (0.18 mmol/g), and *N*-α-(9-fluorenylmethyloxycarbonyl)-*N*-α-(2,4-dimethoxybenzyl)-glycine were purchased from Iris Biotech (Marktredwitz, Germany). *N*,*N*-diisopropylethylamine (DIPEA), TFA, and dichloromethane (DCM) were purchased from Carl Roth (Karlsruhe, Germany). For HPLC separations solvents consisting of water (solvent A) and ACN (solvent B), both containing 0.1% TFA, were used.

UPLC-MS analysis was performed using Waters ACQUITY UPLC-MS system (Milford, MA) with a Waters ACQUITY-UPLC-MS-BEH C18; 1.7 μM (2.1 $\times$ 50 mm; 30 Å) column. As a mobile phase, 0.1% formic acid in H_2O (solvent A) and 0.1% formic acid in ACN (solvent B) solutions were used. A typical gradient from 95:5 (v/v) of H_2O:ACN to 5:95 (v/v) of H_2O:ACN in 6 min was used for most of the runs. Data analysis was performed using Waters MassLynx software. Purification of peptides was done on Shimadzu LC System with a Phenomenex Kinetex^{TM} 5 μm XB-C18 (250 $\times$ 21.1 mm, 100 Å) column using different gradients of 0.1% TFA in H_2O (solvent A) and 0.1% TFA in ACN (solvent B) solutions.

Solid-phase peptide synthesis—The peptides were synthesized using Fmoc-based solid-phase peptide synthesis with automated microwave peptide synthesizer Liberty Blue (CEM Corporation, Matthews, NC). The coupling of amino acids was performed with DIC/OxymaPure at 90 °C for 2 min. All coupling steps were performed twice. Fmoc deprotection was accomplished with 10% piperazine solution in ethanol: *N*-methyl-2-pyrrolidone (1:9. v/v) containing 0.1 M of *N*-hydroxybenzotriazole at 90 °C for 1 min. To avoid side reactions

and improve synthesis efficiency, all methionine residues were replaced by norleucine and some glycine residues were incorporated as *N*-2,4-dimethoxybenzyl protected derivatives.

FITC labeling

FITC labeling was performed on the resin using FITC (3 eq) and DIPEA (6 eq) in DMF for 3 h.

Global deprotection

After the synthesis, the resin was washed several times with DCM, MeOH, DCM before TFA treatment. Then it was incubated with TFA-H_2O-TIPS (92.5:5:2.5, v/v/v) solution for 2–4 h, filtered and the volatiles were removed *in vacuo*. The residue was dissolved in ACN-H_2O solution and purified with HPLC. Fractions containing pure peptide (as judged by UPLC-MS) were frozen and lyophilized affording pure peptide.

N-terminal modification was performed with 2-aminobenzoic acid (4 eq), *O*-(benzotriazol-1-yl)-*N*,*N*,*N*′,*N*′-tetramethyluronium hexafluorophosphate (4 eq) and DIPEA (8 eq) at room temperature in DMF for 1 h. Alternatively, acetylation was performed using acetic anhydride/DIPEA/DMF (1:2:7, v/v) mixture.

Data availability

All data generated or analyzed during this study are included in this published article (and its supporting information files).

Author contributions—K. U. and C. B. conceptualization; K. U., M. Saito, M. M., J. M., P. B., M. Schutkowski, P. M., and C. B. resources; K. U. and C. B. data curation; K. U., M. Saito, M. M., J. M., P. B., B. H., and C. B. formal analysis; K. U., M. Saito, J. M., P. B., M. Schutkowski, P. M., and C. B. supervision; K. U., M. Saito, J. M., P. B., M. Schutkowski, P. M., and C. B. funding acquisition; K. U. and C. B. validation; K. U., Z. N., M. Saito, M. M., J. M., Z. K., P. B., B. H., M. Schutkowski, P. M., and C. B. investigation; K. U., M. Saito, M. M., J. M., P. B., M. Schutkowski, P. M., and C. B. methodology; K. U., M. Saito, M. M., J. M., P. B., B. H., M. Schutkowski, P. M., and C. B. writing-original draft; K. U. and C. B. project administration; K. U., M. Saito, M. M., J. M., P. B., M. Schutkowski, P. M., and C. B. writing-review and editing.

Acknowledgments—We thank I. Jelinkova for the excellent technical assistance, M. Hubalek for MS analysis, and A. Kozikowski for the gift of Nexturastat A. We acknowledge the Imaging Methods Core Facility at BIOCEV, institution supported by the Czech-BioImaging large RI projects (LM2015062 and CZ.02.1.01/0.0/0.0/16_013/0001775, funded by MEYS CR) and the Biophysics facility of CMS supported by MEYS CR (LM2015043) for their support with obtaining scientific data presented in this article.

References

1. Hansen, B. K., Gupta, R., Baldus, L., Lyon, D., Narita, T., Lammers, M., Choudhary, C., and Weinert, B. T. (2019) Analysis of human acetylation stoichiometry defines mechanistic constraints on protein regulation. *Nat. Commun.* **10,** 1055 CrossRef Medline
2. Guan, J. S., Haggarty, S. J., Giacometti, E., Dannenberg, J. H., Joseph, N., Gao, J., Nieland, T. J., Zhou, Y., Wang, X., Mazitschek, R., Bradner, J. E., DePinho, R. A., Jaenisch, R., and Tsai, L. H. (2009) HDAC2 negatively regulates memory formation and synaptic plasticity. *Nature* **459,** 55–60 CrossRef Medline
3. Villagra, A., Cheng, F., Wang, H. W., Suarez, I., Glozak, M., Maurin, M., Nguyen, D., Wright, K. L., Atadja, P. W., Bhalla, K., Pinilla-Ibarz, J., Seto, E., and Sotomayor, E. M. (2009) The histone deacetylase HDAC11 regulates the expression of interleukin 10 and immune tolerance. *Nat. Immunol.* **10,** 92–100 CrossRef Medline
4. Gräff, J., Rei, D., Guan, J. S., Wang, W. Y., Seo, J., Hennig, K. M., Nieland, T. J., Fass, D. M., Kao, P. F., Kahn, M., Su, S. C., Samiei, A., Joseph, N., Haggarty, S. J., Delalle, I., and Tsai, L. H. (2012) An epigenetic blockade of cognitive functions in the neurodegenerating brain. *Nature* **483,** 222–226 CrossRef Medline
5. Jakovcevski, M., and Akbarian, S. (2012) Epigenetic mechanisms in neurological disease. *Nat. Med.* **18,** 1194–1204 CrossRef Medline
6. Falkenberg, K. J., and Johnstone, R. W. (2014) Histone deacetylases and their inhibitors in cancer, neurological diseases and immune disorders. *Nat. Rev. Drug Discov.* **13,** 673–691 CrossRef Medline
7. Zhao, S., Xu, W., Jiang, W., Yu, W., Lin, Y., Zhang, T., Yao, J., Zhou, L., Zeng, Y., Li, H., Li, Y., Shi, J., An, W., Hancock, S. M., He, F., *et al.* (2010) Regulation of cellular metabolism by protein lysine acetylation. *Science* **327,** 1000–1004 CrossRef Medline
8. Wang, M. M., You, D., and Ye, B. C. (2017) Site-specific and kinetic characterization of enzymatic and nonenzymatic protein acetylation in bacteria. *Sci. Rep.* **7,** 14790 CrossRef Medline
9. Clocchiatti, A., Florean, C., and Brancolini, C. (2011) Class IIa HDACs: From important roles in differentiation to possible implications in tumourigenesis. *J. Cell Mol. Med.* **15,** 1833–1846 CrossRef Medline
10. Lernoux, M., Schnekenburger, M., Dicato, M., and Diederich, M. (2018) Anti-cancer effects of naturally derived compounds targeting histone deacetylase 6-related pathways. *Pharmacol. Res.* **129,** 337–356 CrossRef Medline
11. Li, G., Jiang, H., Chang, M., Xie, H., and Hu, L. (2011) HDAC6 α-tubulin deacetylase: A potential therapeutic target in neurodegenerative diseases. *J. Neurol. Sci.* **304,** 1–8 CrossRef Medline
12. Kozikowski, A. P., Shen, S., Pardo, M., Tavares, M. T., Szarics, D., Benoy, V., Zimprich, C. A., Kutil, Z., Zhang, G., Bainka, C., Robers, M. B., Van Den Bosch, L., Eubanks, J. H., and Jope, R. S. (2019) Brain penetrable histone deacetylase 6 inhibitor SW-100 ameliorates memory and learning impairments in a mouse model of fragile X syndrome. *ACS Chem. Neurosci.* **10,** 1679–1695 CrossRef Medline
13. Hai, Y., and Christianson, D. W. (2016) Histone deacetylase 6 structure and molecular basis of catalysis and inhibition. *Nat. Chem. Biol.* **12,** 741–747 CrossRef Medline
14. Miyake, Y., Keusch, J. J., Wang, L., Saito, M., Hess, D., Wang, X., Melancon, B. J., Helquist, P., Gut, H., and Matthias, P. (2016) Structural insights into HDAC6 tubulin deacetylation and its selective inhibition. *Nat. Chem. Biol.* **12,** 748–754 CrossRef Medline
15. Boyault, C., Gilquin, B., Zhang, Y., Rybin, V., Garman, E., Meyer-Klaucke, W., Matthias, P., Müller, C. W., and Khochbin, S. (2006) HDAC6-p97/VCP controlled polyubiquitin chain turnover. *EMBO J.* **25,** 3357–3366 CrossRef Medline
16. Hao, R., Nanduri, P., Rao, Y., Panichelli, R. S., Ito, A., Yoshida, M., and Yao, T. P. (2013) Proteasomes activate aggresome disassembly and clearance by producing unanchored ubiquitin chains. *Mol. Cell* **51,** 819–828 CrossRef Medline
17. Banerjee, I., Miyake, Y., Nobs, S. P., Schneider, C., Horvath, P., Kopf, M., Matthias, P., Helenius, A., and Yamauchi, Y. (2014) Influenza A virus uses the aggresome processing machinery for host cell entry. *Science* **346,** 473–477 CrossRef Medline
18. Liu, Y., Peng, L., Seto, E., Huang, S., and Qiu, Y. (2012) Modulation of histone deacetylase 6 (HDAC6) nuclear import and tubulin deacetylase activity through acetylation. *J. Biol. Chem.* **287,** 29168–29174 CrossRef Medline
19. Kutil, Z., Skultetyova, L., Rauh, D., Meleshin, M., Snajdr, I., Novakova, Z., Mikesova, J., Pavlicek, J., Hadzima, M., Baranova, P., Havlinova, B., Majer, P., Schutkowski, M., and Barinka, C. (2019) The unraveling of substrate specificity of histone deacetylase 6 domains using acetylome peptide microarrays and peptide libraries. *FASEB J.* **33,** 4035–4045 CrossRef Medline

20. Saito, M., Hess, D., Eglinger, J., Fritsch, A. W., Kreysing, M., Weinert, B. T., Choudhary, C., and Matthias, P. (2019) Acetylation of intrinsically disordered regions regulates phase separation. *Nat. Chem. Biol.* **15,** 51–61 CrossRef Medline
21. Bertos, N. R., Gilquin, B., Chan, G. K., Yen, T. J., Khochbin, S., and Yang, X. J. (2004) Role of the tetradecapeptide repeat domain of human histone deacetylase 6 in cytoplasmic retention. *J. Biol. Chem.* **279,** 48246–48254 CrossRef Medline
22. Hubbert, C., Guardiola, A., Shao, R., Kawaguchi, Y., Ito, A., Nixon, A., Yoshida, M., Wang, X. F., and Yao, T. P. (2002) HDAC6 is a microtubule-associated deacetylase. *Nature* **417,** 455–458 CrossRef Medline
23. Matsuyama, A., Shimazu, T., Sumida, Y., Saito, A., Yoshimatsu, Y., Seigneurin-Berny, D., Osada, H., Komatsu, Y., Nishino, N., Khochbin, S., Horinouchi, S., and Yoshida, M. (2002) *In vivo* destabilization of dynamic microtubules by HDAC6-mediated deacetylation. *EMBO J.* **21,** 6820–6831 CrossRef Medline
24. Zhang, Y., Li, N., Caron, C., Matthias, G., Hess, D., Khochbin, S., and Matthias, P. (2003) HDAC-6 interacts with and deacetylates tubulin and microtubules in vivo. *EMBO J.* **22,** 1168–1179 CrossRef Medline
25. Zhao, Z., Xu, H., and Gong, W. (2010) Histone deacetylase 6 (HDAC6) is an independent deacetylase for α-tubulin. *Protein Pept. Lett.* **17,** 555–558 CrossRef Medline
26. Zou, H., Wu, Y., Navre, M., and Sang, B. C. (2006) Characterization of the two catalytic domains in histone deacetylase 6. *Biochem. Biophys. Res. Commun.* **341,** 45–50 CrossRef Medline
27. Portran, D., Schaedel, L., Xu, Z., Théry, M., and Nachury, M. V. (2017) Tubulin acetylation protects long-lived microtubules against mechanical ageing. *Nat. Cell Biol.* **19,** 391–398 CrossRef Medline
28. Verhey, K. J., and Gaertig, J. (2007) The tubulin code. *Cell Cycle* **6,** 2152–2160 CrossRef Medline
29. Janke, C. (2014) The tubulin code: Molecular components, readout mechanisms, and functions. *J. Cell Biol.* **206,** 461–472 CrossRef Medline
30. Alushin, G. M., Musinipally, V., Matson, D., Tooley, J., Stukenberg, P. T., and Nogales, E. (2012) Multimodal microtubule binding by the Ndc80 kinetochore complex. *Nat. Struct. Mol. Biol.* **19,** 1161–1167 CrossRef Medline
31. Garnham, C. P., Vemu, A., Wilson-Kubalek, E. M., Yu, I., Szyk, A., Lander, G. C., Milligan, R. A., and Roll-Mecak, A. (2015) Multivalent microtubule recognition by tubulin tyrosine ligase-like family glutamylases. *Cell* **161,** 1112–1123 CrossRef Medline
32. Sirajuddin, M., Rice, L. M., and Vale, R. D. (2014) Regulation of microtubule motors by tubulin isotypes and post-translational modifications. *Nat. Cell Biol.* **16,** 335–344 CrossRef Medline
33. Tran, A. D., Marmo, T. P., Salam, A. A., Che, S., Finkelstein, E., Kabarriti, R., Xenias, H. S., Mazitschek, R., Hubbert, C., Kawaguchi, Y., Sheetz, M. P., Yao, T. P., and Bulinski, J. C. (2007) HDAC6 deacetylation of tubulin modulates dynamics of cellular adhesions. *J. Cell Sci.* **120,** 1469–1479 CrossRef Medline
34. Nahhas, F., Dryden, S. C., Abrams, J., and Tainsky, M. A. (2007) Mutations in SIRT2 deacetylase which regulate enzymatic activity but not its interaction with HDAC6 and tubulin. *Mol. Cell Biochem.* **303,** 221–230 CrossRef Medline
35. Chang, J., Baloh, R. H., and Milbrandt, J. (2009) The NIMA-family kinase Nek3 regulates microtubule acetylation in neurons. *J. Cell Sci.* **122,** 2274–2282 CrossRef Medline
36. Zilberman, Y., Ballestrem, C., Carramusa, L., Mazitschek, R., Khochbin, S., and Bershadsky, A. (2009) Regulation of microtubule dynamics by inhibition of the tubulin deacetylase HDAC6. *J. Cell Sci.* **122,** 3531–3541 CrossRef Medline
37. Skultetyova, L., Ustinova, K., Kutil, Z., Novakova, Z., Pavlicek, J., Mikesova, J., Trapl, D., Baranova, P., Havlinova, B., Hubalek, M., Lansky, Z., and Barinka, C. (2017) Human histone deacetylase 6 shows strong preference for tubulin dimers over assembled microtubules. *Sci. Rep.* **7,** 11547 CrossRef Medline
38. Hinrichs, M. H., Jalal, A., Brenner, B., Mandelkow, E., Kumar, S., and Scholz, T. (2012) Tau protein diffuses along the microtubule lattice. *J. Biol. Chem.* **287,** 38559–38568 CrossRef Medline
39. Seitz, A., Kojima, H., Oiwa, K., Mandelkow, E. M., Song, Y. H., and Mandelkow, E. (2002) Single-molecule investigation of the interference between kinesin, tau and MAP2c. *EMBO J.* **21,** 4896–4905 CrossRef Medline
40. Thiede, C., Lakämper, S., Wessel, A. D., Kramer, S., and Schmidt, C. F. (2013) A chimeric kinesin-1 head/kinesin-5 tail motor switches between diffusive and processive motility. *Biophys. J.* **104,** 432–441 CrossRef Medline
41. Gao, Y. S., Hubbert, C. C., and Yao, T. P. (2010) The microtubule-associated histone deacetylase 6 (HDAC6) regulates epidermal growth factor receptor (EGFR) endocytic trafficking and degradation. *J. Biol. Chem.* **285,** 11219–11226 CrossRef Medline
42. Huo, L., Li, D., Sun, X., Shi, X., Karna, P., Yang, W., Liu, M., Qiao, W., Aneja, R., and Zhou, J. (2011) Regulation of Tat acetylation and transactivation activity by the microtubule-associated deacetylase HDAC6. *J. Biol. Chem.* **286,** 9280–9286 CrossRef Medline
43. Kovacs, J. J., Murphy, P. J., Gaillard, S., Zhao, X., Wu, J. T., Nicchitta, C. V., Yoshida, M., Toft, D. O., Pratt, W. B., and Yao, T. P. (2005) HDAC6 regulates Hsp90 acetylation and chaperone-dependent activation of glucocorticoid receptor. *Mol. Cell* **18,** 601–607 CrossRef Medline
44. Parmigiani, R. B., Xu, W. S., Venta-Perez, G., Erdjument-Bromage, H., Yaneva, M., Tempst, P., and Marks, P. A. (2008) HDAC6 is a specific deacetylase of peroxiredoxins and is involved in redox regulation. *Proc. Natl. Acad. Sci. U.S.A.* **105,** 9633–9638 CrossRef Medline
45. Zhang, X., Yuan, Z., Zhang, Y., Yong, S., Salas-Burgos, A., Koomen, J., Olashaw, N., Parsons, J. T., Yang, X. J., Dent, S. R., Yao, T. P., Lane, W. S., and Seto, E. (2007) HDAC6 modulates cell motility by altering the acetylation level of cortactin. *Mol. Cell* **27,** 197–213 CrossRef Medline
46. Lefevre, J., Chernov, K. G., Joshi, V., Delga, S., Toma, F., Pastre, D., Curmi, P. A., and Savarin, P. (2011) The C terminus of tubulin, a versatile partner for cationic molecules binding of tau, polyamines, and calcium. *J. Biol. Chem.* **286,** 3065–3078 CrossRef Medline
47. Wang, Q., Crevenna, A. H., Kunze, I., and Mizuno, N. (2014) Structural basis for the extended CAP-Gly domains of p150(glued) binding to microtubules and the implication for tubulin dynamics. *Proc. Natl. Acad. Sci. U.S.A.* **111,** 11347–11352 CrossRef Medline
48. Hard, R. L., Liu, J., Shen, J., Zhou, P., and Pei, D. (2010) HDAC6 and Ubp-M BUZ domains recognize specific C-terminal sequences of proteins. *Biochemistry* **49,** 10737–10746 CrossRef Medline
49. Alberti, S., Gladfelter, A., and Mittag, T. (2019) Considerations and challenges in studying liquid-liquid phase separation and biomolecular condensates. *Cell* **176,** 419–434 CrossRef Medline
50. Du, Y., Seibenhener, M. L., Yan, J., Jiang, J., and Wooten, M. C. (2015) aPKC phosphorylation of HDAC6 results in increased deacetylation activity. *PLoS One* **10,** e0123191 CrossRef Medline
51. Zhuang, Y., Nguyen, H. T., Lasky, J. A., Cao, S., Li, C., Hu, J., Guo, X., Burow, M. E., and Shan, B. (2010) Requirement of a novel splicing variant of human histone deacetylase 6 for TGF-β1-mediated gene activation. *Biochem. Biophys. Res. Commun.* **392,** 608–613 CrossRef Medline
52. Thierry-Mieg, D., and Thierry-Mieg, J. (2006) AceView: A comprehensive cDNA-supported gene and transcripts annotation. *Genome Biol.* **7,** Suppl. 1, S12 CrossRef Medline
53. Lafarga, V., Aymerich, I., Tapia, O., Mayor, F., Jr., and Penela, P. (2012) A novel GRK2/HDAC6 interaction modulates cell spreading and motility. *EMBO J.* **31,** 856–869 CrossRef Medline
54. Williams, K. A., Zhang, M., Xiang, S., Hu, C., Wu, J. Y., Zhang, S., Ryan, M., Cox, A. D., Der, C. J., Fang, B., Koomen, J., Haura, E., Bepler, G., Nicosia, S. V., Matthias, P., Wang, C., Bai, W., and Zhang, X. (2013) Extracellular signal-regulated kinase (ERK) phosphorylates histone deacetylase 6 (HDAC6) at serine 1035 to stimulate cell migration. *J. Biol. Chem.* **288,** 33156–33170 CrossRef Medline
55. Watabe, M., and Nakaki, T. (2011) Protein kinase CK2 regulates the formation and clearance of aggresomes in response to stress. *J. Cell Sci.* **124,** 1519–1532 CrossRef Medline
56. Pugacheva, E. N., Jablonski, S. A., Hartman, T. R., Henske, E. P., and Golemis, E. A. (2007) HEF1-dependent Aurora A activation induces disassembly of the primary cilium. *Cell* **129,** 1351–1363 CrossRef Medline

57. Chen, S., Owens, G. C., Makarenkova, H., and Edelman, D. B. (2010) HDAC6 regulates mitochondrial transport in hippocampal neurons. *PLoS One* **5,** e10848 CrossRef Medline
58. Deribe, Y. L., Wild, P., Chandrashaker, A., Curak, J., Schmidt, M. H. H., Kalaidzidis, Y., Milutinovic, N., Kratchmarova, I., Buerkle, L., Fetchko, M. J., Schmidt, P., Kittanakom, S., Brown, K. R., Jurisica, I., Blagoev, B., Zerial, M., Stagljar, I., and Dikic, I. (2009) Regulation of epidermal growth factor receptor trafficking by lysine deacetylase HDAC6. *Sci. Signal.* **2,** ra84 CrossRef Medline
59. Kellogg, E. H., Howes, S., Ti, S. C., Ramírez-Aportela, E., Kapoor, T. M., Chacón, P., and Nogales, E. (2016) Near-atomic cryo-EM structure of PRC1 bound to the microtubule. *Proc. Natl. Acad. Sci. U.S.A.* **113,** 9430–9439 CrossRef Medline
60. Castoldi, M., and Popov, A. V. (2003) Purification of brain tubulin through two cycles of polymerization-depolymerization in a high-molarity buffer. *Protein Expr. Purif.* **32,** 83–88 CrossRef Medline
61. Redeker, V., Melki, R., Promé, D., Le Caer, J. P., and Rossier, J. (1992) Structure of tubulin C-terminal domain obtained by subtilisin treatment. The major α and β tubulin isotypes from pig brain are glutamylated. *FEBS Lett.* **313,** 185–192 CrossRef Medline
62. Rueden, C. T., Schindelin, J., Hiner, M. C., DeZonia, B. E., Walter, A. E., Arena, E. T., and Eliceiri, K. W. (2017) ImageJ2: ImageJ for the next generation of scientific image data. *BMC Bioinformatics* **18,** 529 CrossRef Medline
63. Schindelin, J., Arganda-Carreras, I., Frise, E., Kaynig, V., Longair, M., Pietzsch, T., Preibisch, S., Rueden, C., Saalfeld, S., Schmid, B., Tinevez, J. Y., White, D. J., Hartenstein, V., Eliceiri, K., Tomancak, P., and Cardona, A. (2012) Fiji: An open-source platform for biological image analysis. *Nat. Meth.* **9,** 676–682 CrossRef Medline
64. Braun, M., Lansky, Z., Fink, G., Ruhnow, F., Diez, S., and Janson, M. E. (2011) Adaptive braking by Ase1 prevents overlapping microtubules from sliding completely apart. *Nat. Cell Biol.* **13,** 1259–1264 CrossRef Medline
65. Hyman, A. A. (1991) Preparation of marked microtubules for the assay of the polarity of microtubule-based motors by fluorescence. *J. Cell Sci. Suppl.* **14,** 125–127 CrossRef Medline

2.4 Rational discovery of a new isoxazole-3-hydroxamate-based histone deacetylase 6 inhibitor SS-208 with antitumor activity in syngeneic melanoma mouse models

Background and motivation of the study

Selective HDAC6 inhibitors are considered as potential therapeutic agents for the treatment of various neurological disorders. Nowadays, partially selective HDAC6 inhibitors, ricolinostat (ACY-1215), and citarinostat (ACY-241) are used in clinical trials as monotherapy or combinatorial therapy for multiple myeloma, lymphoma, breast cancer, and melanoma. The combination of a selective HDAC6 inhibitor Nexturastat A and PD-1 immune blockade led to the marked improvement in an antitumor immune response inhibiting tumor growth (148). However, there are concerns that HDAC inhibition may evoke unwanted off-target effects and toxicity. Given the limited selectivity of current HDAC6-specific compounds, it is required to find HDAC6-selective inhibitors with better selectivity and good pharmacologic properties to be used in the combination therapy of cancers or chronic neurological diseases.

Summary of the work

I. A series of HDAC6 inhibitors were designed, synthesized and their inhibitory activity evaluated. The inhibitor **1a** harboring an isoxazole-3-hydroxamate zinc-binding group showed potent HDAC6 inhibitory activity, unlike its analogs **1b** and **1c**, harboring alkylhydroxamate and phenylhydroxamate zinc-binding groups, respectively. Structure-activity relationship approach was used to modify the cap moiety of 1a resulting in compound **7b**, termed SS-208, with high potency and selectivity for HDAC6 that was used for further investigation.

II. SS-208 was crystallized with the second catalytic domain of *D.rerio* HDAC6. We determined an X-ray structure of the HDAC6/inhibitor complex (Figure 1). Analysis of the HDAC6/SS-208 complex revealed bidentate coordination of the zinc ion, in the form of a typical five-membered chelate complex. The hydroxamate C=O group accepts a hydrogen bond from the hydroxyl group of Y745, while the N-O- group interacts with the residues H573 and H574. It has been determined that interactions between the 3,4-dichlorophenyl cap and the L1 pocket, formed by the side chains of H463, P464, F583, and L712, are important for SS-208 selectivity for HDAC6.

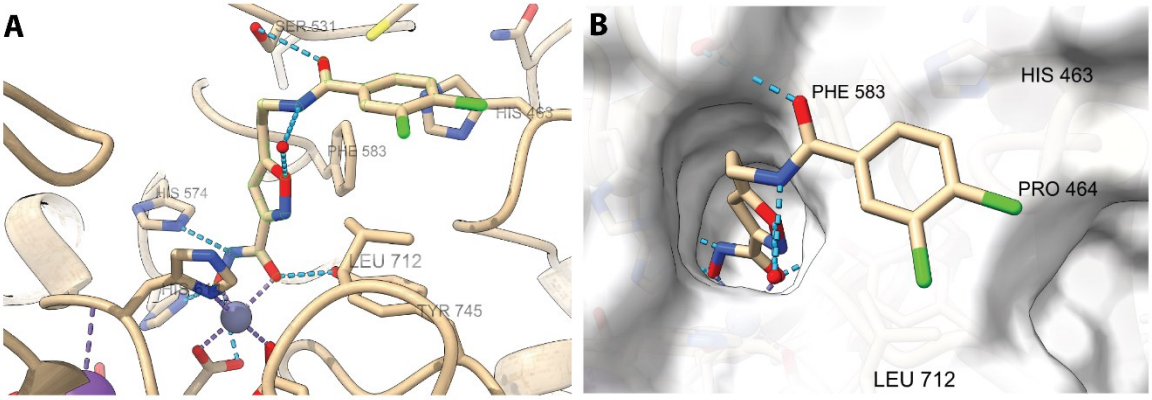

Figure 1. Crystal structure of the HDAC6 catalytic domain (DD2) in the complex with the inhibitor SS-208. **A.** The visualization of interactions of HDAC6 residues within the active site tunnel with SS-208. HDAC6 residues, as well as the inhibitor, are represented as sticks with atoms of carbon (beige), oxygen (red), nitrogen (blue), and chlorine (green). The active-site zinc ion (grey sphere) and water molecules (red spheres), H-bonds (dashed lines) are also displayed. **B.** Interactions between the capping moiety and the "L1-loop pocket" of HDAC6 formed by side chains of H463, P464, F583, and L712. The surface of HDAC6 is shown as a semitransparent surface.

III. ADMET (absorption, distribution, metabolism, excretion, and toxicity) profiling of the SS-208 inhibitor revealed the inhibitor to be Ames-negative, with no significant inhibition in the hERG (human Ether-à-go-go related gene) assay, and to be metabolically more stable than its precursor **1a**. In melanoma cells, SS-208 causes minimal cell death, comparable to other HDAC6 inhibitors – Nexturastat A and Tubastatin A and elevates acetylation levels of α-tubulin. The SS-208 inhibitor also affects STAT3 Y705 phosphorylation, mediated by IL-6, and downregulates PD-L1 expression. Consequently, SS-208 attenuates tumor growth in a murine SM1 syngeneic melanoma mouse model. It also caused increased infiltration of CD8+ T cells and Natural Killer cells as well as the elevation of the M1 and M2 macrophage ratio in the tumor microenvironment.

Therefore, the replacement of phenyl-hydroxamate for the isoxazole-3-hydroxamate improved HDAC6 selectivity and resulted in a 100-fold increase in HDAC6 selectivity. This is a promising feature regarding ongoing efforts in the development of HDAC6-selective inhibitors.

My contribution

I have determined, refined, and analyzed the X-ray structure of the *D.rerio* HDAC6 catalytic domain in complex with the SS-208 inhibitor (PDB: 6R0K) and participated in the manuscript preparation.

Journal of Medicinal Chemistry

Article

Cite This: J. Med. Chem. XXXX, XXX, XXX−XXX

pubs.acs.org/jmc

Discovery of a New Isoxazole-3-hydroxamate-Based Histone Deacetylase 6 Inhibitor SS-208 with Antitumor Activity in Syngeneic Melanoma Mouse Models

Sida Shen,[§,¶] Melissa Hadley,[†] Kseniya Ustinova,[∥,○] Jiri Pavlicek,[∥] Tessa Knox,[†] Satish Noonepalle,[†] Mauricio T. Tavares,[§,▽] Chad A. Zimprich,[⊥] Guiping Zhang,[#] Matthew B. Robers,[⊥] Cyril Bařinka,[∥] Alan P. Kozikowski,[*,‡] and Alejandro Villagra[*,†]

[†]Department of Biochemistry and Molecular Medicine, The George Washington University, Washington, District of Columbia 20052, United States

[‡]StarWise Therapeutics LLC, University Research Park, Inc., Madison, Wisconsin 53719, United States

[§]Department of Medicinal Chemistry and Pharmacognosy, College of Pharmacy, University of Illinois at Chicago, Chicago, Illinois 60612, United States

[∥]Laboratory of Structural Biology, Institute of Biotechnology of the Czech Academy of Sciences, Prumyslova 595, 252 50 Vestec, Czech Republic

[⊥]Promega Corporation, Madison, Wisconsin 53711, United States

[#]Bontac Bio-Engineering (Shenzhen) Co., Ltd, Shenzhen, Guangdong 518102, China

[○]Department of Biochemistry, Faculty of Natural Science, Charles University, Albertov 6, 128 43 Prague 2, Czech Republic

Supporting Information

ABSTRACT: Isoxazole is a five-membered heterocycle that is widely used in drug discovery endeavors. Here, we report the design, synthesis, and structural and biological characterization of SS-208, a novel HDAC6-selective inhibitor containing the isoxazole-3-hydroxamate moiety as a zinc-binding group as well as a hydrophobic linker. A crystal structure of the *Danio rerio* HDAC6/SS-208 complex reveals a bidentate coordination of the active-site zinc ion that differs from the preferred monodentate coordination observed for HDAC6 complexes with phenylhydroxamate-based inhibitors. While SS-208 has minimal effects on the viability of murine SM1 melanoma cells in vitro, it significantly reduced in vivo tumor growth in a murine SM1 syngeneic melanoma mouse model. These findings suggest that the antitumor activity of SS-208 is mainly mediated by immune-related antitumor activity as evidenced by the increased infiltration of CD8+ and NK+ T cells and the enhanced ratio of M1 and M2 macrophages in the tumor microenvironment.

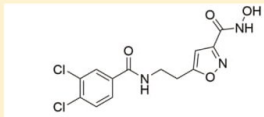

HDAC6 (IC_{50}) = 12 nM HDAC7 (IC_{50}) = 8340 nM
HDAC1 (IC_{50}) = 1390 nM HDAC8 (IC_{50}) = 1230 nM
HDAC4 (IC_{50}) = 19500 nM HDAC9 (IC_{50}) = 38200 nM
HDAC5 (IC_{50}) = 6910 nM HDAC11 (IC_{50}) = 5120 nM

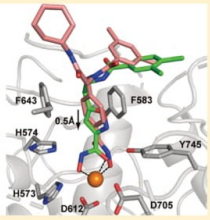

■ INTRODUCTION

Malignant melanoma represents the most aggressive and the deadliest form of cutaneous cancer with increasing incidence, high metastasis, rapid disease progression, poor prognosis, and high mortality.[1,2] Patients with metastatic melanoma have poor prognosis with a 5 year survival rate of less than 10%.[3] A few targeted agent therapies have recently become available for metastatic melanoma. For instance, BRAF inhibitors (i.e., dabrafenib) and MEK1/2 inhibitors (trametinib) have been approved as monotherapy or combined approach for the treatment of melanoma with mutation.[4] However, the clinical benefit of these therapies is limited due to the rapid development of resistance associated with the activation of alternative pro-oncogenic pathways.[4] Within the last five years, immunotherapy has revolutionized the treatment of patients with advanced-stage melanoma. Antibodies that block the negative co-stimulatory receptors CTLA-4 (ipilimumab),[5,6] and programmed cell death-1 (PD-1) (nivolumab and pembrolizumab)[7−9] have been approved based on significantly longer overall survival in clinical trials compared to other therapies. The objective response rates of these immune checkpoint blockades are around 20−30%,[10] while primary, adaptive, and acquired resistance to immunotherapy is common and may be related to the lack of recognition by T-cells.[11,12] Novel aiming to overcome these limitations, especially the resistance mechanisms originated in other components of the tumor microenvironment (TME) are still highly needed to improve current available therapeutics.[13−16]

Received: June 13, 2019
Published: August 15, 2019

DOI: 10.1021/acs.jmedchem.9b00946
J. Med. Chem. XXXX, XXX, XXX−XXX

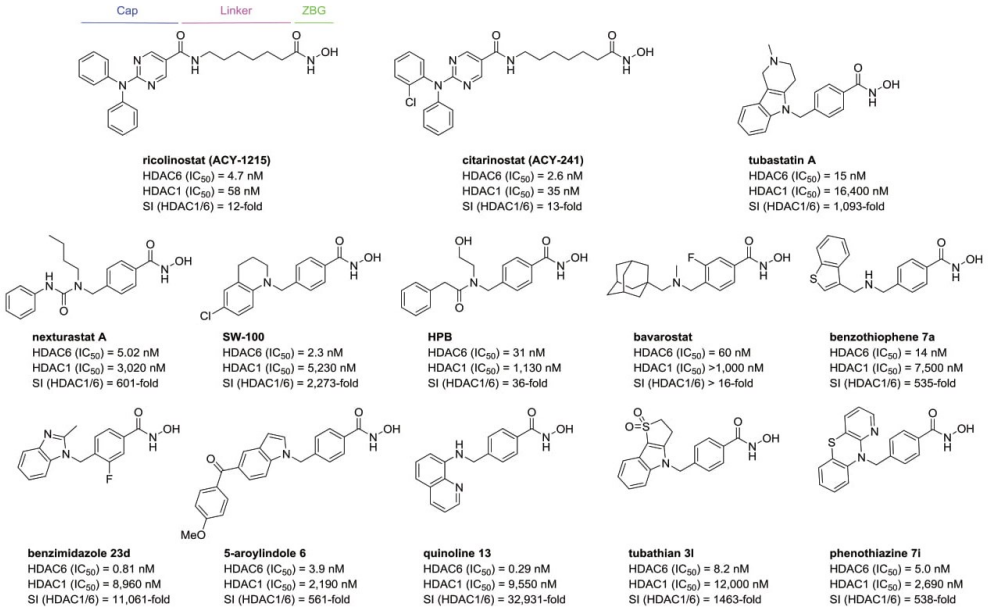

Figure 1. Structures of recent published HDAC6 inhibitors.

Histone deacetylases (HDACs) are a family of proteins involved in the epigenetic regulation of target genes through deacetylating lysine ε-amino groups on histone tails to promote a status of DNA condensation and transcriptional silencing.[17] Furthermore, HDACs have been found to modify other nonhistone proteins, and these modifications can influence a variety of cellular functions without modifying the acetylation of the chromatin acetylation status.[18−20] HDACs have been proven to be promising therapeutic targets for the treatment of cancer based on the successful launch of five HDAC inhibitors (vorinostat, romidepsin, panobinostat, belinostat, and chidamide) which are relatively nonselective.[21,22] In general, broad-spectrum HDAC inhibitors (pan-HDACis) are involved in chromosome remodeling, cell cycle arrest, apoptosis, and cytotoxicity in transformed cancer cells.[23,24] In addition to these effects, there is growing evidence to demonstrate that the treatment with HDACis increases differentiation antigen expression, enhances major histocompatibility complex (MHC) class I and II surface expression, and elevates immunogenicity in terms of increased expression of CD25, CD40, or CD80.[25,26] It has been reported that pan-HDACis can upregulate the expression of PD-L1 and PD-L2 in human and murine melanoma cells.[27] Therefore, pan-HDACis show the ability to possess antitumor activity through inhibiting proliferation and improving immune responses.[28] However, phase I/II clinical trials of pan-HDACis (vorinostat, panobinostat, and quisinostat) with melanoma patients only exhibited limited efficacy and tolerability as single agents, while hematological toxicity, fatigue, nausea, and laboratory abnormalities occurred as frequent adverse events.[26] Important concerns regarding the toxicity of pan-HDACis are rising because their broad inhibition may result in unwanted off-target effects that eventually impair their clinical profile. Thus, there is an emerging interest in the development and investigation of selective HDACis to better understand the molecular mechanisms mediating the antitumor effects.[29] So far, there are few subtype-selective or isoform-selective inhibitors that are noncytotoxic and better tolerated, and that effectively impair tumor growth in preclinical models.[30−35]

Eighteen known mammalian HDACs have been identified, which can be classified into four subgroups according to their homology to yeast enzymes: class I (HDAC1, 2, 3, and 8), class IIa (HDAC4, 5, 7, and 9), class IIb (HDAC6 and HDAC10), class III or sirtuins (SIRT 1−7), and class IV (HDAC11).[36] Class I, II, and IV HDACs require Zn^{2+} (zinc ion) as a cofactor to exert their hydrolytic activity and are also referred to as the conventional HDACs. On the other hand, SIRT 1−7 are dependent on nicotinamide adenine dinucleotide for their activity.[37] In comparison with other HDAC family members, HDAC6 is relatively unique. It contains two tandem deacetylase catalytic domains (CD1 and CD2) and is primarily localized to the cytosol, and its preferred substrates include a variety of nonhistone proteins, such as α-tubulin, cortactin, HSP-90, and HSF-1.[38,39] Moreover, only CD2 exhibits catalytic activity with broad specificity.[40] Intriguingly, according to a patent survey based on the recent efforts on the synthesis and applications of HDACis from 2013 to 2017, most patents focused on the discovery of new HDAC6 inhibitors (HDAC6is).[41] Up to date, two partially selective HDAC6is, ricolinostat (ACY-1215)[42] and citarinostat (ACY-241),[43] have been advanced into clinical trials for different types of cancer, such as multiple myeloma, lymphoma, breast cancer, and melanoma, through monotherapy or a combination approach. Moreover, selective HDAC6is have been considered as potential therapeutic agents for the treatment of various neurological disorders.[44−46]

HDAC6 promotes the proliferation and metastasis of melanoma cells, and knockdown of HDAC6 decreases proliferation and induces the G1-cell cycle arrest of melanoma cells.[28,47] Moreover, it was found that HDAC6 increases the

DOI: 10.1021/acs.jmedchem.9b00946
J. Med. Chem. XXXX, XXX, XXX−XXX

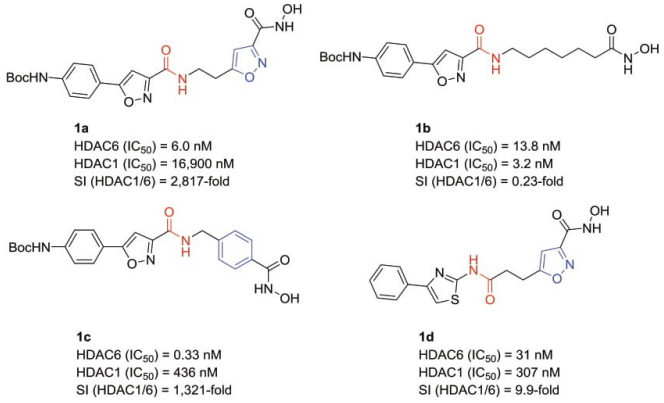

Figure 2. Structures of isoxazole-3-hydroxamate HDAC inhibitors **1a–d**.

protein level of tyrosine-protein phosphatase nonreceptor type 1 (PTPN1), which is responsible for promoting proliferation, colony formation, and migration while decreasing the apoptosis of melanoma cells through activating extracellular signal-regulated kinase 1/2 (ERK1/2).[48] A preclinical study of ricolinostat showed that this partially selective HDAC6i-impaired proliferation and induced apoptosis of BRAF-mutant melanoma A375 cells.[49] Notably, the combination treatment of BRAF inhibitor vemurafenib and ricolinostat displayed a synergetic effect in BRAF-mutant melanoma cells partially through the induction of endoplasmic reticulum stress and inactivation of ERK.[49] In addition to the effects on survival, we have found that HDAC6 is a modulator of the expression of specific tumor-associated antigens, MHC class I, and costimulatory molecules in melanoma.[28] In previous works, we reported that either selective pharmacological inhibition or genetic abrogation of HDAC6 plays a critical role in the immune checkpoint blockade by downregulating the expression of PD-L1, which exhibits an opposite effect relative to class I and pan-HDACis.[50] Also, we recently found that the combination of a selective HDAC6i, nexturastat A (NextA), and PD-1 immune blockade resulted in significant improvement in antitumor immune responses leading to the further reduction of tumor growth compared to monotherapy.[51] Taken together, all the preclinical and clinical stage studies indicate that HDAC6 inhibition shows potential to become a promising approach for melanoma therapy. However, neither ricolinostat nor citarinostat can be considered to be highly selective HDAC6is because of their 10-fold enzymic selectivity against the class I isoform, HDAC1 (Figure 1).[52,53] Therefore, there is a need for the advancement of drug candidates with higher selectivity and good pharmacologic attributes.

A typical HDACi structure contains a zinc-binding group (ZBG) that coordinates the active-site Zn^{2+} at the deep bottom of the substrate pocket, a linker to occupy the hydrophobic channel, and a capping group (cap) to interact with residues at the rim of the catalytic cavity. Recent results suggest that the connecting unit (CU) region that links the cap with the linker and ZBG may strongly impact the ligand's selectivity toward HDAC6.[54] The phenylhydroxamate moiety has been recognized as a useful ZBG as well as a hydrophobic linker in the discovery of selective HDAC6is (Figure 1).[31,34,55−64] The majority of recent advancements has concentrated on the development of hydroxamate analogues bearing a phenyl or pyrimidyl ring.[65,66] Meanwhile, minimal effort has gone into developing linkers containing five-membered heteroaromatics such as thiazole and oxazole.[67,68] Isoxazole is a five-membered heterocycle which contains two heteroatoms, one oxygen, and one nitrogen atom, in adjacent positions. Two double bonds contribute to the unsaturated character of the molecule. The structural features of isoxazole make it suitable for multiple noncovalent interactions, including hydrogen bonding (N and O as acceptors) and $\pi-\pi$ stacking.[69] We note that the isoxazole moiety is a central part of multiple compounds aimed at a wide spectrum of biological targets, and the inclusion of isoxazole in a structure may contribute to its increased efficacy, decreased toxicity, and improved pharmacokinetic profile.[70] Herein, we report the discovery of SS-208, a novel isoxazole-3-hydroxamate-based, selective HDAC6i, its structural characterization in a complex with the catalytic domain 2 of *Danio rerio* HDAC6 (drHDAC6), and the in vivo efficacy results in a syngeneic mouse model of melanoma.

■ RESULTS AND DISCUSSION

Chemistry. In our prior work, we identified an isoxazole-3-hydroxamate-based hit **1a**, which demonstrates potent HDAC6 inhibitory activity and modest potency against HDAC1, a member of class I HDACs,[71] unlike its corresponding alkylhydroxamate (**1b**) and phenylhydroxamate (**1c**) analogues. Moreover, the compound **1d** incorporating the reverse direction of the amide CU dramatically loses selectivity (Figure 2).[71−73] However, the nonideal physicochemical properties of **1a** [topological polar surface area (TPSA) = 168.82, MW = 457.44, calculated by SwissADME[74] and short half-lives ($t_{1/2}$) in microsomal stability studies (mouse: 16 min; human: 85 min, determined by Pharmaron, Inc., Irvine, CA) constitute an obstacle for its advance into in vivo studies. Notably, **1a** was incubated with two strains of *Salmonella typhimurium* (TA97A and TA1537) by Pharmaron in the presence and absence of mammalian microsomal enzymes (S9 mix) to evaluate the mutagenicity potential of the hydroxamate moiety.[75] The results in Table S1 indicate that **1a** is Ames-negative under the testing conditions, which encouraged us to pursue further structural tuning in order to discover more druggable isoxazole-3-hydroxamate-based HDAC6is.

DOI: 10.1021/acs.jmedchem.9b00946
J. Med. Chem. XXXX, XXX, XXX−XXX

To improve the physicochemical properties of this series of compounds, we started our optimization by replacing the Boc-protected phenylisoxazole cap with simple monocyclic and bicyclic aromatic rings (**7a–d**), while keeping the same ethylamide and isoxazole-3-hydroxamate moieties to maintain close structural similarity to **1a**. The synthetic routes to analogues **7a–d** as shown in Scheme 1 started from 3-butyn-1-ol (**2a**) and led to the preparation of the same 1-amino-3-butyne intermediate **4** through a Mitsunobu reaction using phthalimide/Ph_3P/diethyl azodicarboxylate (DEAD). Subsequent deprotection and acylation with the appropriate acyl chlorides provided the alkyne intermediates **5a–d**. The acetylenic moieties in **5a–d** were transformed into the isoxazole esters **6a–d** by 1,3-dipolar cycloaddition with a nitrile oxide generated in situ from ethyl 2-chloro-2-(hydroximino)acetate and a base under microwave conditions.[76] These esters upon treatment with aqueous NH_2OH/NaOH solution efficiently afforded the desired hydroxamic acids **7a–d** bearing aromatic caps.

Given the wide rim of the HDAC6 substrate pocket, aryl caps bearing a sterically bulky moiety are usually preferred to enhance inhibitor affinity and specificity via interactions with the residues forming the surface.[55,64,77,78] Therefore, we further investigated the replacement of the cap and amide CU in **1a** with bicyclic and tricyclic caps. To prepare the indole-capped analogue **11a** illustrated in Scheme 2, 1,3-dipolar cycloaddition of 5-hexyn-1-ol (**2b**) and ethyl 2-chloro-2(hydroximino)-acetate was conducted to establish the key isoxazole ester **8a** from the beginning. Subsequently, **8a** underwent bromination with CBr_4/Ph_3P, N-alkylation under Cs_2CO_3/*N*,*N*-dimethylformamide (DMF) conditions, and transformation into the desired hydroxamate analogue **11a** in the presence of aqueous NH_2OH/NaOH solution. The synthetic routes to **11b–c** started from 4-chloroaniline (**12**), which was first converted to

Scheme 1. Synthetic Route to Compounds 7a–d[a]

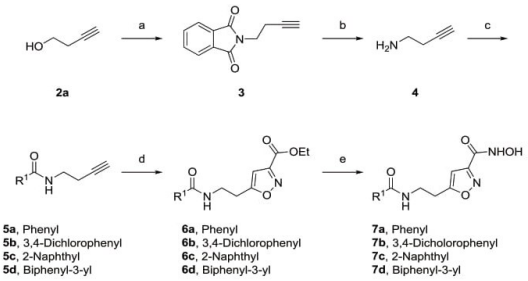

[a](a) Phthalimide, Ph_3P, DEAD, tetrahydrofuran (THF), 0 °C to rt, yield: 93%; (b) hydrazine monohydrate, MeOH, rt; (c) ArCOCl, TEA, dichloromethane (DCM), 0 °C, yields: 52–90% over two steps; (d) ethyl 2-chloro-2-(hydroxyimino)acetate, $NaHCO_3$, EtOAc, 100 °C (MW), yields: 49–78%; (e) NH_2OH (aq, 50%), NaOH, THF/MeOH (1:1), 0 °C to rt, yields: 10–43%.

Scheme 2. Synthetic Routes to Compounds 11a–d[a]

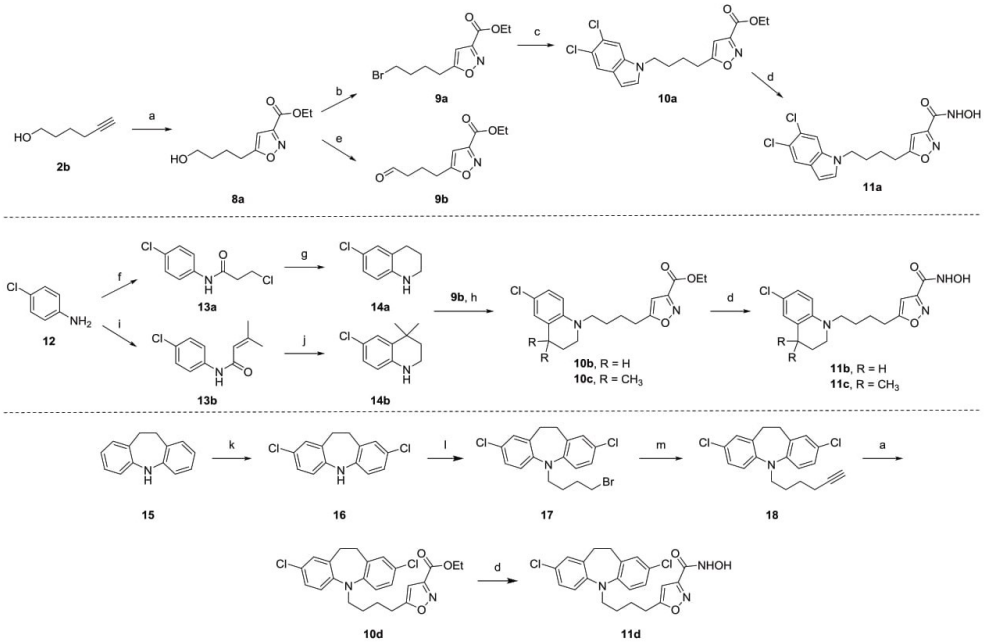

[a](a) Ethyl 2-chloro-2-(hydroximino)acetate, $NaHCO_3$, EtOAc, 100 °C (MW), yields: 67–87%; (b) CBr_4, Ph_3P, DCM, rt, yield: 89%; (c) 5,6-dichloro-1*H*-indole, Cs_2CO_3, DMF, 80 °C, 80%; (d) NH_2OH (aq, 50%), NaOH, THF/MeOH (1:1), 0 °C to rt, yields: 34–94%; (e) PCC, DCM, rt, yield: 88%; (f) 3-chloropropanoyl chloride, acetone, reflux, yield: 54%; (g) (i) $AlCl_3$, 140 °C (neat), (ii) $LiAlH_4$, THF, 0 °C to reflux, yield: 70% over two steps; (h) **9b**, $NaBH(OAc)_3$, AcOH/EtOH, rt, yields: 42–58%; (i) 3,3-dimethylacryloyl chloride, $CHCl_3$, reflux, yield: 48%; (j) (i) $AlCl_3$, toluene, 80 °C, (ii) $LiAlH_4$, THF, 0 °C to reflux, yield: 55% over two steps; (k) NCS, silica gel, $CHCl_3$, rt, yield: 74%; (l) 1,4-dibromobutane, NaH, DMF, rt, yield: 43%; (m) sodium acetylide, xylene/DMF, 40 °C, yield: 25%.

DOI: 10.1021/acs.jmedchem.9b00946
J. Med. Chem. XXXX, XXX, XXX–XXX

Table 1. HDAC1 and HDAC6 Enzymatic Evaluation of Analogues 7a–d, 11a–d, and 20a–c[a]

Cmpd	cap	CU	ZBG	IC_{50} (μM) HDAC1	IC_{50} (μM) HDAC6	SI[b]	LE[c]	LipE[d]
1a[e]	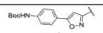			16.9	0.006	2817	0.35	6.2
7a				> 30	0.19	> 155	0.47	5.8
7b				31.5	0.075	418	0.45	5.1
7c				3.03	0.010	294	0.47	5.7
7d				2.04	0.024	85	0.41	5.7
11a				> 30	4.36	> 7	0.31	2.0
11b				11.2	0.69	16	0.36	3.3
11c				> 30	1.99	> 15	0.31	2.1
11d				> 30	1.35	> 22	0.27	1.3
20a				> 30	0.20	> 152	0.45	3.9
20b				> 30	1.98	> 15	0.38	2.5
20c				0.20	0.028	7.2	0.48	4.8
NextA[f]				2.86	0.005	572	0.46	5.7
TSA[g]	-	-	-	0.009	0.002	4.4	0.55	6.4

[a]IC_{50} values are the mean of two experiments obtained from curve-fitting of a 10-point enzymatic assay starting from 30 μM with 3-fold serial dilution against HDAC1 and HDAC6 (Reaction Biology Corp, Malvern, PA). [b]SI: HDAC6 selectivity over HDAC1. [c]LE: ligand efficiency = 1.4 × pIC_{50}/number of heavy atoms. [d]LipE: lipophilic ligand efficiency = pIC_{50} − clog $P_{o/w}$. [e]IC_{50} values were extracted from the article by Gaisina, I. N. et al., *ChemMedChem* **2016,** *11,* 81–92. [f]IC_{50} values were extracted from the article by Kozikowski, A. P. et al., *ACS Chem. Neurosci.* **2019,** *10,* 1679–1695. [g]TSA: trichostatin A.

Scheme 3. Synthetic Routes to Compounds 20a–c[a]

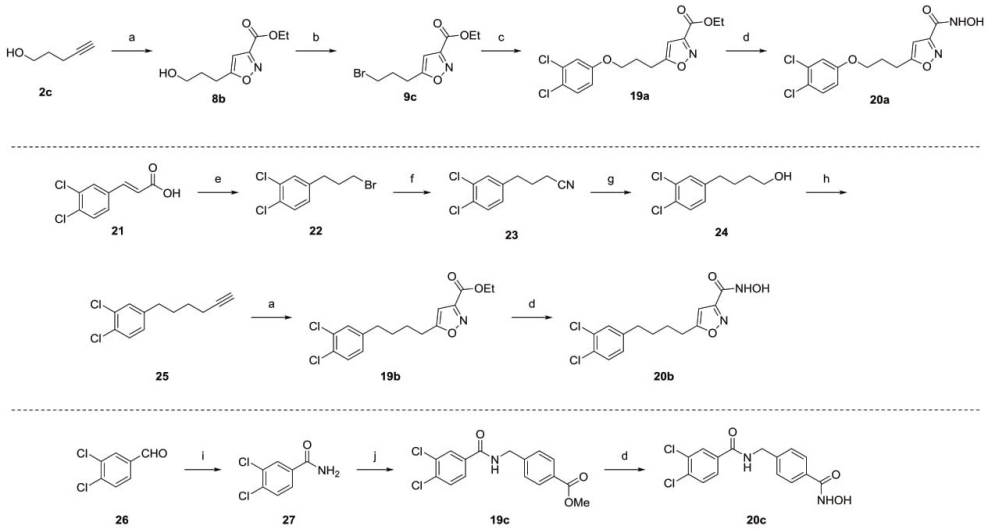

[a](a) ethyl 2-chloro-2-(hydroxyimino)acetate, $NaHCO_3$, EtOAc, 100 °C (MW), yields: 58–96%; (b) CBr_4, Ph_3P, DCM, rt, yield: 83%; (c) 3,4-dichlorophenol, Cs_2CO_3, DMF, 80 °C, yield: 80%; (d) NH_2OH (aq, 50%), NaOH, THF/MeOH (1:1), 0 °C to rt, yields: 30–40%; for **20c**, yield: 22% over three steps; (e) (i) $LiAlH_4$, THF, 0 °C to reflux, (ii) CBr_4, Ph_3P, DCM, 0 °C to rt, yield: 11% over two steps; (f) NaCN, dimethyl sulfoxide (DMSO), 100 °C, yield: 72%; (g) (i) aq NaOH, EtOH, reflux, (ii) BH_3-THF, THF, 0 °C to rt, yield: 88% over two steps; (h) (i) CBr_4, Ph_3P, DCM, rt, (ii) sodium acetylide, DMF, 40 °C, yield: 39% over two steps; (i) NH_2OH·HCl, K_2CO_3, $Cu(OAc)_2$, H_2O, reflux; (j) TFA, Et_3SiH, methyl 4-formylbenzoate, toluene, reflux.

the *N*-phenyl amides **13a–b** by treating with 3-chloropropanoyl chloride and 3,3-dimethylacryloyl chloride, respectively. Subsequently, intramolecular Friedel–Crafts cyclization under $AlCl_3$ conditions followed by the reduction of the intermediate lactam with $LiAlH_4$ afforded tetrahydroquinolines **14a–b**.[63,79]

Reductive amination of **14a–b** and the aldehyde intermediate **9b** which was prepared from **8a** by pyridinium chlorochromate (PCC) oxidation, provided the corresponding esters **10b–c**. In the end, the desired hydroxamate analogues **11b–c** were obtained using the same standard procedure as above. The

DOI: 10.1021/acs.jmedchem.9b00946
J. Med. Chem. XXXX, XXX, XXX–XXX

Table 2. HDAC Profiles of the 3,4-Dichlorophenyl Capped Compounds SS-208 and 20c, As Well As NextA[a]

Cmpd	SS-208 (7b)		20c		NextA	
Structure	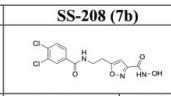		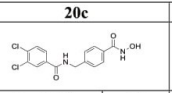		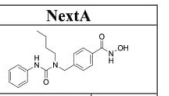	
Isoform	IC_{50} (μM)	SI[b]	IC_{50} (μM)	SI	IC_{50} (μM)	SI
HDAC1	1.39 ± 0.73	116	0.034 ± 0.003	17	0.36 ± 0.12	90
HDAC4	19.5 ± 4.2	1625	3.53 ± 0.13	1765	14.8 ± 1.7	3700
HDAC5	6.91 ± 0.29	576	3.12 ± 0.48	1560	6.62 ± 2.66	1655
HDAC6	0.012 ± 0.002	1	0.002 ± 0.0003	1	0.004 ± 0.002	1
HDAC7	8.34 ± 0.71	695	0.50 ± 0.008	250	2.43 ± 0.30	608
HDAC8	1.23 ± 0.59	103	0.92 ± 0.15	460	1.54 ± 0.76	385
HDAC9	38.2 ± 5.1	3183	3.07 ± 0.17	1535	2.0 ± 0.77	500
HDAC11	5.12 ± 1.29	427	1.05 ± 0.11	525	10.6 ± 2.2	2650

[a]IC_{50} values are the mean of two experiments ± SEM obtained from curve-fitting of a 10-point enzymatic assay starting from 100 μM with 3-fold serial dilution against the HDAC isoform. [b]SI: HDAC6 selectivity index over other HDAC isoforms.

synthetic route to the dibenz[*b*,*f*]azepine-capped analogue **11d** began with the dichlorination of **15** using *N*-chlorosuccinimide (NCS)/silica gel[80] followed by N-alkylation with 1,4-dibromobutane under NaH/DMF conditions and alkynation with sodium acetylide to provide the key dibenz[*b*,*f*]azepine-substituted alkyne **18**. Then, the building block **18** underwent 1,3-dipolar cycloaddition, and the desired isoxazole-3-hydroxamate **11d** was then obtained in the usual manner.

As a 3,4-dichlorophenyl cap on **7b** retained the HDAC6 potency and selectivity over HDAC1 (data are shown in Table 1), we further synthesized compounds **20a**–**c** in order to evaluate the effects of the amide CU and isoxazole-based ZBG. To prepare the analogue **20a** which contains an ether linker in place of the amide group, the synthetic route shown in Scheme 3 was followed. 1,3-Dipolar cycloaddition between 4-pentyn-1-ol (**2c**) and ethyl 2-chloro-2-(hydroximino)acetate generated the isoxazole ring (compound **8b**). This intermediate underwent bromination with CBr_4/Ph_3P followed by O-alkylation with 3,4-dichlorophenol under Cs_2CO_3/DMF conditions. The synthesis was completed as above to afford the desired hydroxamate **20a**. To synthesize analogue **20b** which only contains an alkyl chain rather than an amide group, the α,β-unsaturated carboxylic acid in the starting material **21** was first transformed into a bromoalkyl intermediate **22** through $LiAlH_4$ reduction and bromination with CBr_4/Ph_3P. Compound **22** was further converted to the nitrile **23** with NaCN. Subsequent hydrolysis under basic condition and borane reduction provided the butanol **24**. The alkyne **25** was obtained through bromination and alkynation under similar conditions as described above and underwent 1,3-dipolar cycloaddition and conversion to the hydroxamic acid **20b**. The synthetic route to the benzyl hydroxamate analogue **20c** started from the $Cu(OAc)_2$-catalyzed one-pot conversion of 3,4-dichlorobenzaldehyde (**26**) into 3,4-dichlorobenzamide (**27**) through a Beckmann-type rearrangement.[81] Subsequent reductive N-alkylation of the amide intermediate **27** using trifluoroacetic acid (TFA)/Et_3SiH with methyl 4-formylbenzoate led to the generation of the corresponding ester **19c**,[82] which upon standard treatment afforded the desired hydroxamate **20c**.

HDAC Isoform Inhibition. To evaluate isoform potency and selectivity of all new analogues (**7a**–**d**, **11a**–**d**, and **20a**–**c**), we first prescreened their inhibitory activity against human HDAC6 and HDAC1 in vitro (performed by Reaction Biology Corp, Malvern, PA). As illustrated in Table 1, the replacement of the phenylisoxazole cap of the parent compound **1a** with phenyl rings as in compounds **7a**–**b** led to a 12.5-fold to 32-fold decrease in inhibitory potency for HDAC6, while micromolar inhibition values against HDAC1 remained constant. Compounds **7c**–**d**, in which the cap moiety was replaced with a naphthyl or biphenyl group, retained low nanomolar inhibitory potency for HDAC6 with a concomitant decrease of the HDAC1/HDAC6 selectivity index. Notably, this replacement significantly decreased the number of heavy atoms and TPSA values compared to the hit **1a** (Table S2) and improved the ligand efficiency (LE) values beyond 0.4 while keeping the lipophilic ligand efficiency (LipE) values above 5.0 (Table 1).[83,84] The incorporation of sterically bulky caps into the molecule to form the bicyclic- or tricyclic-capped analogues **11a**–**d** resulted in a significant decrease in potency, and none of them delivered meaningful LE values (LE and LipE). The replacement of the amide moiety in **7b** with an ether (**20a**) or alkyl chain (**20b**) was also disadvantageous, as it resulted in a 3-fold to 26-fold decrease in HDAC6 potency, suggesting that the amide moiety is necessary for retaining high potency in this class. Compared to **7b**, its corresponding phenylhydroxamate analogue **20c** demonstrated about 3-fold improvement in HDAC6 potency (IC_{50} = 28 nM) and similar LE values. However, the isozyme selectivity significantly fell to around 7-fold, and the observed trend replicates finding for the **1a** and **1c** pair (Figure 2). Based on the evaluation results of LE and maintained modest potency against HDAC1, we chose compound **7b**, named SS-208, for further investigation.

To fully evaluate the advantage of isoxazole-3-hydroxamates relative to the typical phenylhydroxamate-based HDAC6 inhibitors, we assessed SS-208, **20c**, and NextA against Class I HDACs 1 and 8, Class IIa HDACs 4, 5, 7, and 9, Class IIb HDAC6, and Class IV HDAC11 in-house. The HDAC profiling against Class IIa and Class IV isoforms shows that SS-208 only exhibited micromolar potency against all these isoforms. In the side-by-side comparison with the selective HDAC6i, NextA, SS-208 exhibited similarly low nanomolar HDAC6 inhibitory activity with better selectivity over all the other tested HDAC isoforms (Table 2).

Crystallization Studies. The recently published co-crystal structures of phenylhydroxamate-based HDAC6is in complex with drHDAC6 displayed a unusual monodentate phenylhydroxamate-Zn^{2+} coordination geometry, while a bidentate coordination is generally observed for inhibitors that possess either flexible aliphatic linkers or aromatic linkers lacking a cap.[85,86] The recent findings demonstrated that the caps attached to phenylhydroxamate affect the coordination between the hydroxamates and the catalytic Zn^{2+} to be

DOI: 10.1021/acs.jmedchem.9b00946
J. Med. Chem. XXXX, XXX, XXX−XXX

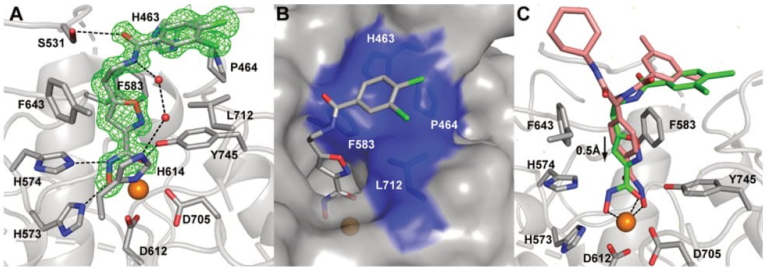

Figure 3. Crystal structure of the drHDAC6-CD2/SS-208 complex. (A) Detailed view of the substrate tunnel of HDAC6 in the complex with SS-208. $F_o - F_c$ maps (green mesh) for SS-208 are contoured at 4.0 σ and the inhibitor and selected HDAC6 residues are shown in stick representation with atoms colored grey (carbon), red (oxygen), blue (nitrogen), and green (chlorine). The active-site zinc ion and water molecules are shown as orange and red spheres, respectively. H-bonds and salt bridges are shown as dashed lines. (B) Interactions between the capping dichlorophenyl moiety and the "L1-loop pocket" formed by side chains of H463, P464, F583, and L712 (colored blue). The surface of HDAC6 is shown in a semitransparent surface representation. (C) Superposition of SS-208 and DDK-115 (PDB code: 6DVL) in the substrate tunnel of HDAC6. Carbon atoms are colored green and pink for SS-208 and DDK-115, respectively. The active-site zinc ion is coordinated in a bidentate fashion by SS-208, while the monodentate coordination is observed for DDK-115, resulting in a 0.5 Å shift of the SS-208 ring closer toward the zinc ion.

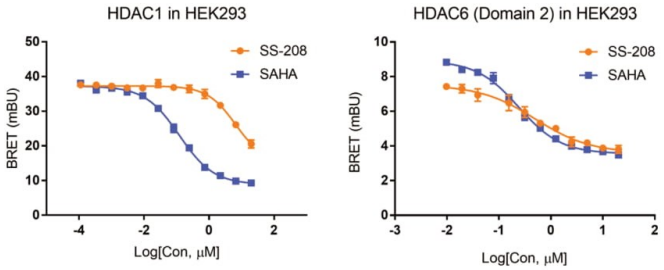

	IC_{50}, μM	
	SS-208	**SAHA**
HDAC1	6.673	0.122
HDAC6-CD2	0.504	0.241

Figure 4. SS-208 selectively inhibits HDAC6-CD2 in cells. The HDAC1 and HDAC6 (catalytic domain 2) NanoBRET target engagement assay for compound SS-208 in HEK293. IC_{50} values are the mean of four technical replicates ± SD obtained from curve-fitting of a 12-point engagement assay starting from a concentration of 20 μM with 3-fold serial dilution. SAHA was used as a positive control.

bidentate or monodentate, which is also crucial to stabilize the monodentate coordination mode that is slightly less stable (0.5 kcal/mol) than the bidentate coordination mode.[85,87] Moreover, the key residues H463, P464, F583, and L712 create an L1-loop pocket to provide a rigid binding site for hydrophobic caps. Recent research further supports that the interaction between the ligand and L1-loop pocket is critical for maintaining high selectivity against class I HDACs.[87]

To investigate the molecular basis of interactions between SS-208 and HDAC6, we solved the crystal structure of the drHDAC6-CD2/SS-208 complex to an ultra-high resolution limit of 1.15 Å. The binding of SS-208 to HDAC6 did not cause any major structural rearrangement of the enzyme as documented by the root-mean-square deviation of 0.15 Å for 300 Cα atoms between the drHDAC6/SS-208 complex and the unliganded enzyme (PDB code: 5EEM).[88] The hydroxamate functional group of SS-208 coordinates the active-site zinc ion in a canonical bidentate fashion, forming a typical five-membered chelate complex with an interatomic distance of 2.1 Å between the Zn^{2+} and each of the hydroxamate C═O and N−O groups (Figure 3A). Moreover, the hydroxamate C═O group accepts a hydrogen bond from the hydroxyl group of Y745 (2.7 Å), and the N−O− group forms hydrogen bonds with the side chains of H573 (2.6 Å) and H574 (2.5 and 2.9 Å). The isoxazole ring and the distal ethylene part of the linker are positioned within van der Waals distances from the side chains of F583, F643, and L712. The C═O group of the amide moiety establishes an interaction with S531 in a distance of 3.3 Å, and the N−H group engages in a water-mediated interaction with H614 as observed in the binding with other HDAC6is in the literature.[87] Finally, the capping dichlorophenyl ring packs against the hydrophobic patch at the entrance of the internal tunnel, the L1-loop pocket, formed by the side chains of H463, P464, F583, and L712 (Figure 3B).[87]

It is interesting to note that the bidentate zinc ion coordination reported here differs from the preferred monodentate coordination observed in drHDAC6 complexes where a phenylhydroxamate group is capped by a hydrophobic moiety of an inhibitor.[40,85,87] In our complex, the center of the isoxazole ring is shifted by 0.5 Å toward the active-site Zn^{2+},

DOI: 10.1021/acs.jmedchem.9b00946
J. Med. Chem. XXXX, XXX, XXX−XXX

and this shift stems from the bidentate coordination of the Zn^{2+} by the hydroxamate moiety (Figure 3C). This shift is likely facilitated by the presence of a "long" four-atom linker between the isoxazole ring and the capping dichlorophenyl moiety, allowing thus for the more energetically favorable bidentate hydroxamate coordination while simultaneously preserving hydrophobic interactions between the cap and the L1-loop pocket.[87]

HDAC Target Engagement Measurement in HEK293 Cells. We further assessed the potency and selectivity of SS-208 in live cells using a NanoBERT-target engagement assay to investigate its binding characteristics with HDAC1 and HDAC6 within intact cells.[89] These results performed in HEK293 are summarized in Figure 4, and suggest that SS-208 retains modest activity against HDAC1 in cells (IC_{50} = 6.67 μM), while the measured potency of SS-208 against the α-tubulin preferring deacetylase domain of HDAC6, the catalytic domain 2 (IC_{50} = 0.5 μM), indicates that SS-208 retains about 13-fold selectivity over HDAC1 in cells (418-fold enzymatic selectivity over HDAC1 in Table 1) which is comparable with our recent observation of another highly selective HDAC6i, SW-100, tested under the same conditions.[63] SW-100 showed an IC_{50} value of 2.3 nM against HDAC6 and 2273-fold selectivity over HDAC1 in the enzymatic assay, while it exhibited an IC_{50} of 0.10 μM against HDAC6-CD2 and 46-fold selectivity over HDAC1 in the cellular target engagement assay.[63] Vorinostat (SAHA), tested as a positive control, demonstrated to be potent and nonselective toward HDAC6-CD2 (IC_{50} = 0.24 μM) as well as HDAC1 (IC_{50} = 0.12 μM) (Figure 4).

Initial ADMET Properties. To evaluate the potential mutagenicity of this hydroxamate-based compound, SS-208 was incubated with two strains of *S. typhimurium* (TA98 and TA1537) in the presence and absence of mammalian microsomal enzymes (S9 mix). SS-208 did not induce ≥2-fold increases (for tester strain TA98) or ≥3-fold increases (for tester strain TA1537) in the mean number of revertant colonies at any dose levels when compared to the concurrent negative/solvent control, both in the presence and absence of the S9 mix, thus supporting the lack of mutagenicity of SS-208 under the conditions of the Ames assay (Table S3). No significant inhibition was observed in the hERG assay up to 30 μM (Figure S1). The liver microsomal stability is shown in Table 3 (half-lives of 37 and 135 min in mouse and human microsomes, respectively). This constitutes an improvement relative to the original compound **1a**. Moreover, half-lives of 22 and 135 min in mouse and human hepatocytes were determined, respectively.

Table 3. Initial ADMET Profiling of Compound SS-208[a]

Ames test (with and without S9)	TA98, TA1537	negative
hERG test (IC_{50}, μM)	HEK293 cells	>30
liver microsomal stability ($t_{1/2}$ min, with NADPH)	mouse	37
	human	135
hepatocytes stability ($t_{1/2}$ min)	mouse	22
	human	108

[a]All the ADMET assays were conducted by Pharmaron, Inc., Irvine, CA.

Inhibitory Potency of SS-208 is Comparable to NextA and Tubastatin A in Cancer Cells. As mentioned before, several selective HDAC6is are currently available for preclinical research. Among them, NextA and tubastatin A (TubA) were reported by our group.[55,56] Although these two compounds have shown outstanding in vivo antitumor effects in numerous syngeneic tumor models,[24] they were found to be Ames-positive (data are not shown). We thus wanted to compare the Ames-negative HDAC6i SS-208 with these two previously reported HDAC6is. We performed an initial screening of the in vitro activity of SS-208 by evaluating the acetylation status of α-tubulin (Ac-α-Tubulin), the best characterized physiological substrate of HDAC6. As expected, SS-208 increased Ac-α-Tubulin levels in SM1 murine melanoma (Figure 5A) and WM164 human melanoma (Figure 5B). Additionally, SS-208 had a negligible effect on the levels of acetylated histone H3 (Ac-H3) in SM1 murine melanoma cells, and these findings are comparable to the results of experiments where NextA was used (Figure 5C).

We previously observed that the selective HDAC6is NextA and TubA had similar in vitro HDAC inhibitory potency across different human and murine cancer cell lines.[28] A similar outcome was observed with SS-208, which was also comparable to the above-mentioned selective HDAC6is when tested in human PC3, human 5637, human T24, and mouse SM1 cell lines (Figure 5D). We also observed that SS-208-induced minimal cell death in the concentration range evaluated above, and these results were also comparable to NextA and TubA (Figure 5E). Importantly, we have reported that the in vivo antitumor effect of selective HDAC6is is mainly mediated by their role as modulators of antitumor immune responses and that their direct cytotoxicity toward cancer cells is minimal at concentrations lower than 5 μM.[28] Supporting these previously reported findings, we observed that SS-208 has marginal effects on viability, cytotoxicity, and apoptosis in murine SM1 melanoma cells evaluated by the multiplexed Apotox assay (Figure 5F). The absence of cytotoxic effects in cells treated with these selective HDAC6is is in sharp contrast to the effects observed with other pan-HDACis such as panobinostat (LBH589 in Figure 5F), among others, therefore removing one of the most critical side effects of nonselective HDACis or other cytotoxic anticancer drugs.

SS-208 Reduces the Expression of PD-L1 in Melanoma Cells. Our group has previously reported that the genetic and pharmacological targeting of HDAC6 affected the expression of the immunosuppressive molecule PD-L1 (CD274). The abrogation of HDAC6 activity results in the inactivation of the STAT3 pathways upon treatment with HDAC6is or knockdown of HDAC6.[50] To further evaluate if SS-208 affects the processes mentioned above, we evaluated the activation of the STAT3 pathway by assessing the phosphorylation of STAT3 after treatment with SS-208 (5 μM). The Western blot results illustrated in Figure 6A demonstrated that SS-208 efficiently reduced IL-6-mediated Y705 phosphorylation of STAT3 and the subsequent down-regulation of the PD-L1 expression. HDAC6 inhibition was evidenced by the increased levels of Ac-α-Tubulin. Further verification by qRT-PCR indicated that IL-6 significantly increased the CD274 gene expression by at least 2-fold compared to the untreated conditions, and SS-208 effectively negated the IL-6-induced CD274 gene expression suggesting that this HDAC6i regulates the PD-L1 expression at the mRNA level rather than through post-translational modifications at the protein level (Figure 6B).

DOI: 10.1021/acs.jmedchem.9b00946
J. Med. Chem. XXXX, XXX, XXX−XXX

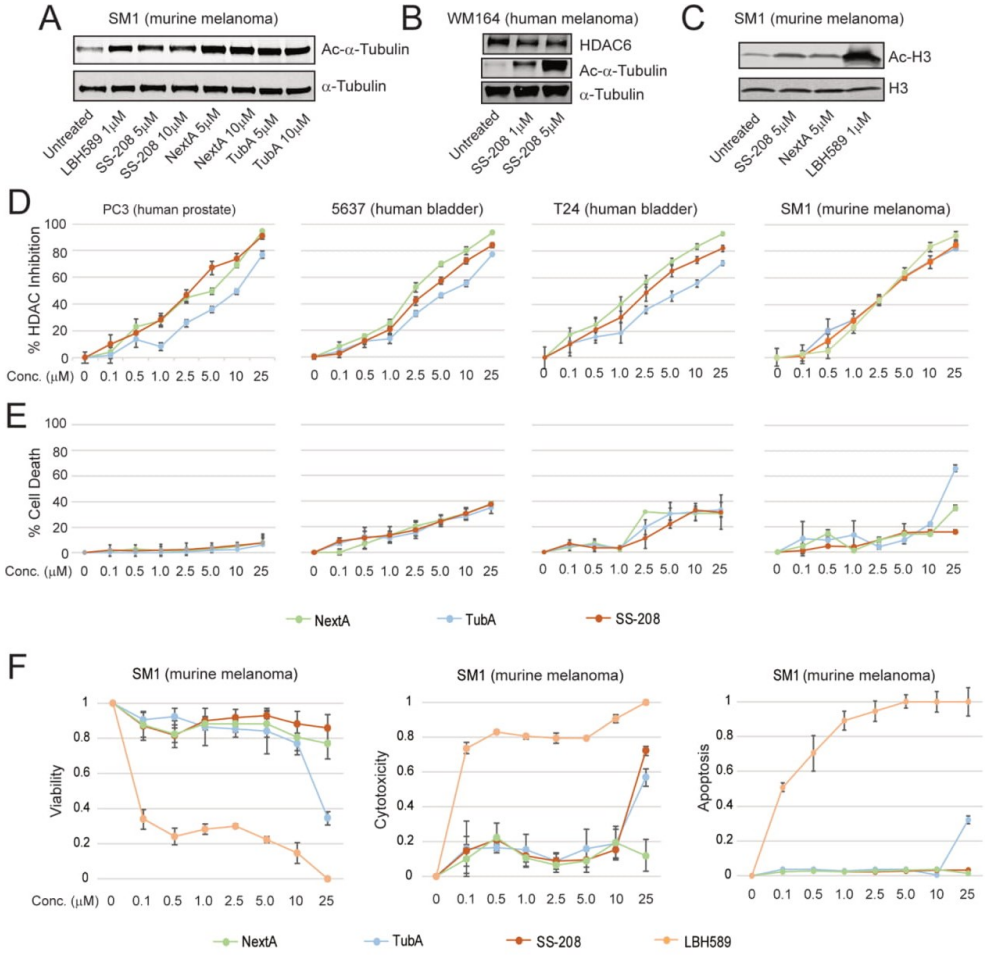

Figure 5. SS-208 activity is similar to other selective HDAC6is in cancer cells in vitro. (A) SS-208 treatment of SM1 murine melanoma cells resulted in increased Ac-α-Tubulin similar to other HDAC6is NextA and TubA. (B) Activity of HDAC6 inhibition with SS-208 was dose-dependent as indicated by the Western-blot analysis of Ac-α-Tubulin in WM164 human melanoma cells. (C) SM1 melanoma cells were treated with SS-208, NextA, or LBH589 for 24 h. The levels of Ac-H3 were evaluated by the Western-blot analysis. (D) SS-208, NextA, and TubA exhibited a similar inhibition of deacetylase activity when tested in a panel of cell lines of various tissue origins. (E) Similarly, HDAC6is did not induce cell death across the range of concentrations tested. (F) Multiplexed assay indicated that pan-HDACi, LBH589 exhibited apoptosis and cytotoxicity at concentrations as low as 100 nM, while the HDAC6is tested did not affect cell viability up to 10 μM. HDAC6is also did not induce apoptosis and cytotoxicity compared to LBH589.

SS-208 Impairs Melanoma Tumor Growth in Immunocompetent Mice. The in vivo antitumor effect of selective HDAC6is has been extensively investigated.[35,50,51] Importantly, this activity needs the presence of an intact host immune system.[28] Therefore, we wanted to evaluate whether SS-208 could also impair tumor growth in a syngeneic murine model with a functional immune system. To evaluate this possibility, we injected immunogenic murine SM1 melanoma cells subcutaneously in the flank of C57BL/6 mice and subsequently treated them with SS-208 (25 mg/kg, ip administration) or vehicle after one-week post tumor engraftment. As observed previously for other HDAC6is, the tumor growth was significantly reduced after treatment with SS-208 (Figure 7A,B), suggesting that this Ames-negative selective HDAC6i also exerts its antitumor effect by modulating the host immune system. To test this hypothesis, we evaluated the composition of different cellular components of the TME. Although we did not observe a significant infiltration of cytotoxic T cells (CD8+), their presence in the TME was slightly superior to the vehicle control (Figure 7C). Among other screened tumor-infiltrating lymphocytes, the infiltration of CD4+ T cells did not change (Figure 7D). However, the infiltration of natural killer T cells (NKT) was significantly upregulated in the SS-208 treatment arm (Figure 7E).

The antitumoral M1 macrophage phenotype has been reported to have associated with a better prognosis in several malignancies, and there is an active search for agents improving their infiltration in tumors[90] On the other hand, tumor

DOI: 10.1021/acs.jmedchem.9b00946
J. Med. Chem. XXXX, XXX, XXX−XXX

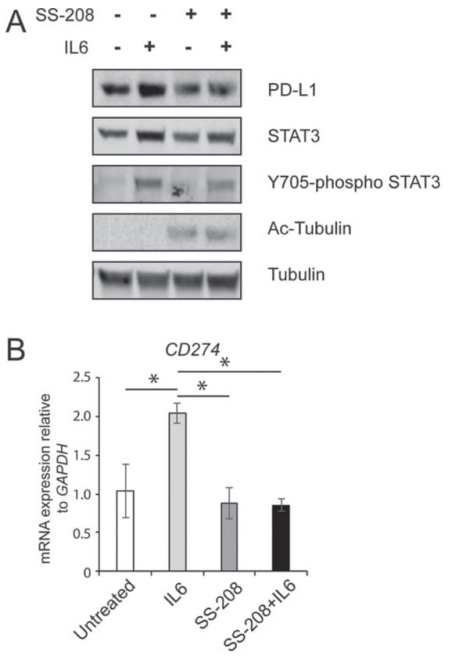

Figure 6. Immunomodulatory role of SS-208 by decreasing the expression of PD-L1 in melanoma cells. (A) SM1 murine melanoma cells were pre-treated with 5 μM of SS-208 followed by IL-6 treatment overnight and effectively reduced the expression of immunosuppressive molecule PD-L1 at the protein level. (B) SS-208 decreased IL-6 mediated STAT3 activation measured as Y705 phosphorylation and subsequently PD-L1 gene expression measured by qRT-PCR.

infiltration of pro-tumoral M2 macrophages is directly associated with a bad prognosis in cancer.[91] In previous studies from our group, we observed a significant increase in the ratio of M1 and M2 macrophages in tumors treated with selective HDAC6is but not with other nonselective inhibitors.[51] As expected, this outcome was also observed in the melanomas of the mice treated with SS-208 (Figure 7F–H), confirming that this compound possesses similar immunological properties as previously investigated NextA.[48]

■ CONCLUSIONS

We have designed and synthesized a series of HDAC6 inhibitors bearing isoxazole-3-hydroxamate instead of phenylhydroxamate as ZBG. By evaluating their inhibitory activities at HDAC isoforms, we found that: (a) the amide moiety is an important constituent of the CU to retain a high HDAC6 potency; (b) bulky caps, like napththyl and biphenyl groups, result in better HDAC6 activity but lower selectivity versus HDAC1; (c) the replacement of the corresponding phenylhydroxamate leads to a significant potency improvement against HDAC6 but the loss of hundred-fold HDAC1 selectivity. We have thus identified a novel potent and selective HDAC6i, namely, SS-208. The X-ray structure analysis of the crystallized complex of SS-208 with catalytic domain 2 from *D. rerio* HDAC6 demonstrates that: (a) the hydroxamate moiety coordinates in a distinct bidentate manner with the active-site zinc ion, forming a typical five-membered chelate complex, in contrast to the preferred monodentate coordination observed in most HDAC6 complexes with phenylhydroxamate-based inhibitors; (b) direct and indirect engagements are observed between the key amide moiety and amino acid residues in the active site that may be responsible for the ligand's nanomolar HDAC6 potency; (c) the interactions between the 3,4-dichlorophenyl cap and the L1-loop pocket is critical for high selectivity against HDAC1. Both in vitro and in vivo ADMET profiling and pharmacological observation suggest that: (a) SS-208 shows Ames-negative results under testing conditions and no significant inhibition in the hERG assay, and is more metabolically stable relative to the original compound **1a**; (b) in murine and human melanoma cells, SS-208 induces minimal cell death and exhibits marginal effects on viability, cytotoxicity, and apoptosis, while significantly increasing the levels of Ac-α-Tubulin; (c) furthermore, SS-208 efficiently reduces the IL-6-mediated Y705 phosphorylation of STAT3 and downregulates the expression of PD-L1 at the mRNA levels in melanoma cells; (d) finally, SS-208 impairs tumor growth in a murine SM1 syngeneic melanoma mouse model which is mainly mediated by immune-related antitumor activity as evidenced by the increased infiltration of CD8+ and NK+ T cells and the enhanced ratio of M1 and M2 macrophages in the TME.

■ EXPERIMENTAL SECTION

Chemistry. *General Information.* ^{1}H and ^{13}C NMR spectra were obtained on 400/101 and 500/126 MHz Bruker spectrometers, except where noted otherwise, using the solvent residual peak as the internal reference (chemical shifts: $CDCl_3$, δ 7.26/77.0; DMSO-d_6, 2.50/39.52; acetone-d_6, 2.05/29.84 and 206.26). The following abbreviations for multiplicities were used: s = singlet, d = doublet, t = triplet, q = quartet, p = pentet, m = multiplet, dd = double doublet, dt = double triplet, ddd = double–double doublet, and br s = broad singlet. TLC plates (Merck silica gel 60 F_{254}, 250 μm thickness) were used to monitor the reaction progress, and spots were visualized under UV (254 nm). High-resolution mass spectrometry (HRMS) was carried out on a Shimadzu IT-TOF instrument under the following conditions: column, ACE 3AQ (50 X 2.1 mm, id); mobile phase, 5–100% acetonitrile/water containing 0.1% formic acid at a flow rate of 0.5 mL/min for 4 min. Flash chromatography was performed on a CombiFlash Rf system (Teledyne ISCO) with silica gel cartridges. Preparative HPLC was used in the purification of all final compounds using a Shimadzu preparative LC under the following conditions: column, ACE 5AQ (150 × 21.2 mm, id); mobile phase: 5–100% acetonitrile/water containing 0.05% TFA at a flow rate of 17 mL/min for 30 min; UV detection at 254 and 280 nm. Analytical HPLC was used to determine the purity of all the final products using an Agilent 1260 series instrument under the following conditions: column, ACE 3 (150 × 4.6 mm, id); mobile phase, 5–100% acetonitrile/water containing 0.05% TFA at a flow rate of 1.0 mL/min for 25 min; UV detection at 254 nm. The purity of all the tested compounds for in vitro biological studies was >95%. The purity of SS-208 for crystallographic and in vivo studies was >98%.

2-(But-3-yn-1-yl)isoindoline-1,3-dione (**3**). To a stirred solution of 3-butyn-1-ol (**2a**, 140 mg, 2.0 mmol), phthalimide (382 mg, 2.6 mmol), and Ph_3P (682 mg, 2.6 mmol) was added DEAD (525 mg, 2.6 mmol) at 0 °C under an argon atmosphere. The resulting mixture was slowly warmed to room temperature and stirred at the same temperature for 2.5 h. Then, the reaction was quenched with H_2O and extracted with EtOAc (20 mL × 3). The combined organic extracts were washed with brine (40 mL), dried over Na_2SO_4, and concentrated under vacuum. The crude product was purified by flash chromatography (0–50% EtOAc/hexane) to afford **3** as a white powder (370 mg, 93%). ^{1}H NMR (400 MHz, $CDCl_3$): δ 7.86 (dd, J = 5.5, 3.0 Hz, 2H), 7.73 (dd, J = 5.5, 3.0 Hz, 2H), 3.89 (t, J = 7.1 Hz, 2H), 2.62 (td, J = 7.1, 2.7 Hz, 2H), 1.96 (t, J = 2.7 Hz, 1H). ^{13}C NMR

DOI: 10.1021/acs.jmedchem.9b00946
J. Med. Chem. XXXX, XXX, XXX–XXX

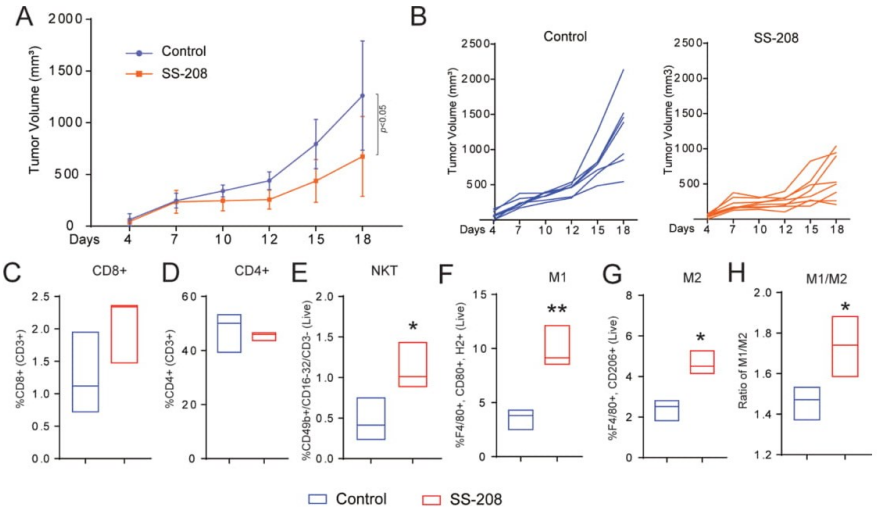

Figure 7. In vivo antitumor activity of SS-208 is mediated through the modulation of TME. (A) SS-208 treatment (25 mg/kg, ip) significantly decreased the tumor growth compared to the control group in the SM1 murine melanoma syngeneic model. (B) Tumor growth curves of individual animals in control and SS-208 treatment groups. Animals receiving SS-208 treatment consistently showed a lower tumor volume during the course of the study compared to control groups. The decrease in tumor volume in the SS-208 treatment group was associated with the infiltration of intratumoral CD8+ T-cells (C), CD4+ T-cells (D), and a significant increase in NKT-cells (E). SS-208 treatment was associated with a significant increase in antitumor M1 macrophages (F), M2 macrophages (G), and the ratio of M1/M2 (H) which is an indication of effective antitumor immunity.

(101 MHz, $CDCl_3$): δ 168.0, 134.1, 132.0, 123.4, 80.3, 70.3, 36.6, 18.4.

N-(But-3-yn-1-yl)benzamide (**5a**). General procedure A: (i) to a stirred solution of **3** (180 mg, 0.9 mmol) in MeOH (5 mL) was added hydrazine monohydrate (0.06 mL, 1.13 mmol. The resulting mixture was stirred at room temperature for 16 h. The precipitate was filtered off, and the filtrate was diluted with water (5 mL) and acidified to pH = 2 with 2 N HCl. The solution was concentrated under vacuum to afford **4** as a white powder. The crude product was used directly in the next step. (ii) To a stirred solution of **4** in DCM (5 mL) were added TEA (0.37 mL, 2.7 mmol) and benzoyl chloride (252 mg, 1.8 mmol) at 0 °C. Then, the resulting mixture was stirred at the same temperature for 30 min. The reaction was quenched with water (5 mL), and the mixture was extracted with DCM (10 mL × 3). The combined organic extracts were washed with brine (40 mL), dried over Na_2SO_4, and concentrated under vacuum. The crude product was purified by flash chromatography (0−50% EtOAc/hexane) to afford **5a** as a white powder (140 mg, 90%). ^{1}H NMR (400 MHz, acetone-d_6): δ 7.94−7.92 (m, 3H), 7.58−7.53 (m, 1H), 7.52−7.45 (m, 2H), 3.57 (td, J = 7.1, 6.0 Hz, 2H), 2.55 (td, J = 7.1, 2.7 Hz, 2H), 2.43 (t, J = 2.7 Hz, 1H).

N-(But-3-yn-1-yl)-3,4-dichlorobenzamide (**5b**)was synthesized from **3** (260 mg, 1.3 mmol) and 3,4-dichlorobenzoyl chloride (543 mg, 2.6 mmol) following general procedure A and was obtained as a colorless solid (220 mg, 70%). ^{1}H NMR (400 MHz, $CDCl_3$): δ 7.88 (d, J = 2.0 Hz, 1H), 7.60 (dd, J = 8.3, 2.1 Hz, 1H), 7.52 (d, J = 8.3 Hz, 1H), 6.41 (s, 1H), 3.61 (q, J = 6.2 Hz, 2H), 2.53 (td, J = 6.3, 2.6 Hz, 2H), 2.07 (t, J = 2.6 Hz, 1H).

Ethyl 5-(2-Benzamidoethyl)isoxazole-3-carboxylate (**6a**). General procedure B: to a solution of **5a** (140 mg, 0.8 mmol) in EtOAc (2 mL) were added $NaHCO_3$ (201 mg, 2.4 mmol) and ethyl 2-chloro-2-(hydroxyimino)acetate (367 mg, 2.4 mmol) in a microwave reaction tube. The mixture was heated at 100 °C for 1 h in a microwave reactor. After completion of the reaction, the solid was filtered off and the filtrate was concentrated under reduced pressure. The crude product was purified by flash chromatography (0−50% EtOAc/hexane) to afford **6a** as colorless oil (140 mg, 61%). ^{1}H NMR (400 MHz, $CDCl_3$): δ 7.74 (dt, J = 7.1, 1.3 Hz, 2H), 7.55−7.46 (m, 1H), 7.46−7.36 (m, 2H), 6.51 (s, 2H), 4.42 (q, J = 7.1 Hz, 2H), 3.82 (q, J = 6.4 Hz, 2H), 3.19 (t, J = 6.5 Hz, 2H), 1.40 (t, J = 7.1 Hz, 3H). ^{13}C NMR (101 MHz, $CDCl_3$): δ 172.7, 167.8, 159.9, 156.6, 134.1, 131.8, 128.7, 126.9, 102.7, 62.2, 37.9, 27.2, 14.1.

Ethyl 5-(2-(3,4-Dichlorobenzamido)ethyl)isoxazole-3-carboxylate (**6b**) was synthesized from **5b** (220 mg, 0.9 mmol) and ethyl 2-chloro-2-(hydroxyimino)acetate (408 mg, 2.7 mmol) following general procedure B and was obtained as a white solid (250 mg, 78%). ^{1}H NMR (400 MHz, DMSO-d_6): δ 8.85 (t, J = 5.5 Hz, 1H), 8.03 (d, J = 1.4 Hz, 1H), 7.82−7.71 (m, 2H), 6.76 (s, 1H), 4.34 (q, J = 7.1 Hz, 2H), 3.60 (q, J = 6.5 Hz, 2H), 3.11 (t, J = 6.7 Hz, 2H), 1.30 (t, J = 7.1 Hz, 3H). ^{13}C NMR (101 MHz, DMSO-d_6): δ 173.5, 164.2, 159.6, 156.1, 134.6, 134.2, 131.3, 130.8, 129.2, 127.5, 102.5, 61.8, 37.4, 26.3, 14.0.

Ethyl 5-(2-(2-Naphthamido)ethyl)isoxazole-3-carboxylate (**6c**). (i) **5c** was synthesized from **3** (215 mg, 1.08 mmol) and 2-naphthoyl chloride (246 mg, 1.3 mmol) following general procedure A and was obtained as a white powder (170 mg, 70%); (ii) **6c** was synthesized from **5c** (170 mg, 0.76 mmol) and ethyl 2-chloro-2-(hydroxyimino)-acetate (344 mg, 2.28 mmol) following general procedure B and was obtained as a white solid (150 mg, 58%).^{1}H NMR (400 MHz, $CDCl_3$): δ 8.25 (s, 1H), 7.86−7.77 (m, 4H), 7.57−7.45 (m, 2H), 6.90 (t, J = 5.7 Hz, 1H), 6.50 (s, 1H), 4.38 (q, J = 7.1 Hz, 2H), 3.85 (q, J = 6.5 Hz, 2H), 3.20 (t, J = 6.6 Hz, 2H), 1.36 (t, J = 7.1 Hz, 3H).

Ethyl 5-(2-(Biphenyl-3-ylcarboxamido)ethyl)isoxazole-3-carboxylate (**6d**). (i) **5d** was synthesized from **3** (215 mg, 1.08 mmol) and biphenyl-3-carbonyl chloride (280 mg, 1.3 mmol) following general procedure A and was obtained as a white powder (140 mg, 52%). (ii) **6d** was synthesized from **5d** (170 mg, 0.56 mmol) and ethyl 2-chloro-2-(hydroxyimino)acetate (255 mg, 1.69 mmol) following general procedure B and was obtained as colorless oil (100 mg, 49%). ^{1}H NMR (400 MHz, $CDCl_3$): δ 7.98 (s, 1H), 7.76−7.65 (m, 2H), 7.58−7.51 (m, 2H), 7.45−7.38 (m, 3H), 7.36−7.30 (m, 1H), 7.06 (t, J = 5.4 Hz, 1H), 6.47 (s, 1H), 4.35 (q, J = 7.1 Hz, 2H), 3.78 (q, J = 6.5 Hz, 2H), 3.14 (t, J = 6.6 Hz, 2H), 1.33 (t, J = 7.1 Hz, 3H).

DOI: 10.1021/acs.jmedchem.9b00946
J. Med. Chem. XXXX, XXX, XXX−XXX

5-(2-Benzamidoethyl)-*N*-hydroxyisoxazole-3-carboxamide (**7a**). General procedure C: in a round-bottom flask, NaOH (160 mg, 4.0 mmol) was dissolved in 50% aqueous NH_2OH (1.6 mL, approx. 50 equiv) at 0 °C. A solution of **6a** (140 mg, 0.5 mmol) in 1:1 THF/MeOH (6 mL) was added dropwise and stirring was continued for 30 min while the mixture was allowed to warm to room temperature. The solution was neutralized with 2 N HCl and extracted with EtOAc (15 mL × 3). The combined organic layers were washed with brine, dried over Na_2SO_4, and concentrated under vacuum. The crude product was purified by flash chromatography (0−10% MeOH/DCM) or preparative HPLC and lyophilized to afford **7a** as a white powder (60 mg, 43%). ^{1}H NMR (400 MHz, DMSO-d_6): δ 8.68 (t, J = 5.5 Hz, 1H), 7.81 (d, J = 7.1 Hz, 2H), 7.53 (t, J = 7.3 Hz, 1H), 7.46 (t, J = 7.3 Hz, 2H), 6.63 (s, 1H), 3.60 (q, J = 6.6 Hz, 2H), 3.09 (t, J = 6.7 Hz, 2H). ^{13}C NMR (101 MHz, DMSO-d_6): δ 172.4, 166.4, 157.4, 156.2, 134.3, 131.3, 128.3 (2C), 127.1 (2C), 101.1, 37.2, 26.3. ESI HRMS: calcd for $C_{13}H_{14}N_3O_4$ $[M + H]^+$ m/z, 276.0979; found, 276.0984.

5-(2-(3,4-Dichlorobenzamido)ethyl)-*N*-hydroxyisoxazole-3-carboxamide (7b, SS-208) was synthesized from **6b** (250 mg, 0.7 mmol) following general procedure C and was obtained as a white powder (70 mg, 29%). ^{1}H NMR (400 MHz, DMSO-d_6): δ 11.46 (s, 1H), 9.33 (s, 1H), 8.87 (t, J = 5.3 Hz, 1H), 8.04 (d, J = 1.6 Hz, 1H), 7.83−7.72 (m, 2H), 6.63 (s, 1H), 3.59 (q, J = 6.4 Hz, 2H), 3.09 (t, J = 6.8 Hz, 2H). ^{13}C NMR (101 MHz, DMSO-d_6): δ 172.3, 164.1, 157.4, 156.2, 134.5, 134.1, 131.3, 130.8, 129.1, 127.5, 101.2, 37.4, 26.1. ESI HRMS: calcd for $C_{13}H_{12}Cl_2N_3O_4$ $[M + H]^+$ m/z, 344.0205; found, 344.0198. Purity: 98.8% (254 nm).

5-(2-(2-Naphthamido)ethyl)-*N*-hydroxyisoxazole-3-carboxamide (**7c**) was synthesized from **6c** (150 mg, 0.44 mmol) following general procedure C and was obtained as a white powder (15 mg, 10%). ^{1}H NMR (400 MHz, DMSO-d_6): δ 11.45 (br s, 1H), 9.33 (br s, 1H), 8.85 (t, J = 5.2 Hz, 1H), 8.41 (s, 1H), 8.03−7.88 (m, 3H), 7.90 (d, J = 8.6 Hz, 1H), 7.63−7.57 (m, 2H), 6.66 (s, 1H), 3.66 (q, J = 6.5 Hz, 2H), 3.14 (t, J = 6.7 Hz, 2H). ESI HRMS: calcd for $C_{17}H_{16}N_3O_4$ $[M + H]^+$ m/z, 326.1135; found, 326.1137.

5-(2-([1,1′-Biphenyl]-3-ylcarboxamido)ethyl)-*N*-hydroxyisoxazole-3-carboxamide (**7d**) was synthesized from **6d** (100 mg, 0.27 mmol) following general procedure C and was obtained as an off-white powder (30 mg, 32%). ^{1}H NMR (400 MHz, DMSO-d_6): δ 11.47 (br s, 1H), 9.33 (br s, 1H), 8.81 (t, J = 5.6 Hz, 1H), 8.08 (s, 1H), 7.82 (t, J = 7.4 Hz, 2H), 7.72 (d, J = 7.4 Hz, 2H), 7.56 (t, J = 7.7 Hz, 1H), 7.50 (t, J = 7.6 Hz, 2H), 7.41 (t, J = 7.1 Hz, 1H), 6.64 (s, 1H), 3.63 (q, J = 6.5 Hz, 2H), 3.12 (t, J = 6.8 Hz, 3H). ESI HRMS: calcd for $C_{19}H_{16}N_3O_4$ $[M - H]^+$ m/z, 350.1146; found, 350.1136.

Ethyl 5-(4-Hydroxybutyl)isoxazole-3-carboxylate (**8a**) was synthesized from 5-hexyn-1-ol (**2b**, 200 mg, 2.0 mmol) and ethyl 2-chloro-2-(hydroxyimino)acetate (906 mg, 6.0 mmol) following general procedure B and was obtained as colorless oil (370 mg, 87%). ^{1}H NMR (400 MHz, $CDCl_3$): δ 6.41 (s, 1H), 4.42 (qd, J = 7.1, 1.3 Hz, 2H), 3.68 (td, J = 6.3, 1.3 Hz, 2H), 2.84 (t, J = 7.5 Hz, 2H), 1.90−1.76 (m, 2H), 1.67−1.60 (m, 2H), 1.40 (td, J = 7.1, 1.3 Hz, 3H). ^{13}C NMR (101 MHz, $CDCl_3$): δ 175.4, 160.3, 156.5, 101.7, 62.3, 62.2, 31.9, 26.6, 23.9, 14.3.

Ethyl 5-(3-Hydroxypropyl)isoxazole-3-carboxylate (**8b**) was synthesized from 4-pentyn-1-ol (**2c**, 300 mg, 3.57 mmol) and ethyl 2-chloro-2-(hydroxyimino)acetate (1.6 g, 10.7 mmol) following general procedure B and was obtained as colorless oil (680 mg, 96%). ^{1}H NMR (400 MHz, $CDCl_3$): δ 6.42 (s, 1H), 4.40 (q, J = 7.1 Hz, 2H), 3.70 (t, J = 6.1 Hz, 2H), 2.92 (t, J = 7.6 Hz, 2H), 1.97−1.88 (m, 2H), 1.38 (t, J = 7.1 Hz, 3H). ^{13}C NMR (101 MHz, $CDCl_3$): δ 175.2, 160.3, 156.5, 101.8, 62.2, 61.3, 30.2, 23.3, 14.2.

Ethyl 5-(4-Bromobutyl)isoxazole-3-carboxylate (**9a**). To a stirred solution of **8a** (100 mg, 0.47 mmol) in DCM (5 mL) were added CBr_4 (232 mg, 0.47 mmol) and Ph_3P (184 mg, 0.47 mmol) at 0 °C. Then, the resulting mixture was stirred at room temperature for 1 h. The reaction was quenched with water (5 mL) and extracted with DCM (15 mL × 3). The combined organic extracts were washed with brine (30 mL), dried over Na_2CO_3, and concentrated under vacuum. The crude product was purified by flash chromatography (0−40% EtOAc/hexane) to afford **9a** as colorless oil (90 mg, 89%).^{1}H NMR (400 MHz, $CDCl_3$): δ 6.41 (s, 1H), 4.40 (q, J = 7.1 Hz, 2H), 3.40 (t, J = 6.2 Hz, 2H), 2.83 (t, J = 6.9 Hz, 2H), 1.89−1.87 (m, 4H), 1.38 (t, J = 7.1 Hz, 3H). ^{13}C NMR (101 MHz, $CDCl_3$): δ 174.7, 160.2, 156.5, 101.8, 62.1, 32.8, 31.8, 26.0, 25.9, 14.2.

Ethyl 5-(4-Oxobutyl)isoxazole-3-carboxylate (**9b**). To a stirred solution of **8a** (150 mg, 0.70 mmol) in DCM (5 mL) was added PCC (300 mg, 1.4 mmol) at room temperature. The resulting mixture was stirred at the same temperature for 2 h. Then, the solid was filtered off and the filtrate was concentrated under vacuum. The crude product was purified by flash chromatography (0−60% EtOAc/hexane) and **9b** was obtained as colorless oil (130 mg, 88%). ^{1}H NMR (400 MHz, $CDCl_3$): δ 9.75 (t, J = 1.1 Hz, 1H), 6.40 (s, 1H), 4.38 (q, J = 7.1 Hz, 2H), 2.83 (t, J = 7.3 Hz, 2H), 2.53 (td, J = 7.1, 1.0 Hz, 2H), 2.11−1.94 (m, 2H), 1.36 (t, J = 7.1 Hz, 3H). ^{13}C NMR (101 MHz, $CDCl_3$): δ 200.9, 174.3, 160.1, 156.5, 101.9, 62.1, 42.6, 25.8, 19.8, 14.1.

Ethyl 5-(3-Bromopropyl)isoxazole-3-carboxylate (**9c**) was synthesized from **8b** (680 mg, 3.42 mmol), CBr_4 (1.70 g, 5.13 mmol), and Ph_3P (1.35 g, 5.13 mmol) using a procedure similar to that described for the synthesis of **9a** and was obtained as colorless oil (850 mg, 83%). ^{1}H NMR (400 MHz, $CDCl_3$): δ 6.46 (s, 1H), 4.42 (q, J = 7.1 Hz, 2H), 3.43 (t, J = 6.3 Hz, 2H), 3.01 (t, J = 7.3 Hz, 2H), 2.33−2.18 (m, 2H), 1.40 (t, J = 7.1 Hz, 3H). ^{13}C NMR (101 MHz, $CDCl_3$): δ 173.6, 160.1, 156.6, 102.3, 62.3, 31.9, 30.2, 25.3, 14.3.

Ethyl 5-(4-(5,6-Dichloro-1*H*-indol-1-yl)butyl)isoxazole-3-carboxylate (**10a**). To a stirred solution of **9a** (90 mg, 0.33 mmol) in DMF (3 mL) were added 5,6-dichloro-1*H*-indole (56 mg, 0.30 mmol) and Cs_2CO_3 (217 mg, 0.66 mmol) at room temperature. The resulting mixture was heated at 80 °C overnight. The reaction was quenched with sat. NH_4Cl aqueous solution (5 mL) and extracted with EtOAc (10 mL × 3). The combined organic layers were washed with brine (30 mL), dried over Na_2SO_4, and concentrated under vacuum. The crude product was purified by flash chromatography (0−30% EtOAc/hexane) to afford **10a** as colorless oil (90 mg, 80%). ^{1}H NMR (400 MHz, $CDCl_3$): δ 7.68 (s, 1H), 7.39 (s, 1H), 7.08 (d, J = 3.2 Hz, 1H), 6.42 (dd, J = 3.1, 0.7 Hz, 1H), 6.35 (s, 1H), 4.42 (q, J = 7.1 Hz, 2H), 4.09 (t, J = 6.9 Hz, 2H), 2.80 (t, J = 7.4 Hz, 2H), 1.92−1.85 (m, 2H), 1.77−1.65 (m, 2H), 1.41 (t, J = 7.1 Hz, 3H). ^{13}C NMR (101 MHz, $CDCl_3$): δ 174.5, 160.2, 156.6, 134.9, 129.7, 128.3, 125.7, 123.6, 122.1, 110.9, 101.9, 101.3, 62.3, 46.3, 29.5, 26.4, 25.0, 14.3.

Ethyl 5-(4-(6-Chloro-3,4-dihydroquinolin-1(2*H*)-yl)butyl)-isoxazole-3-carboxylate (**10b**). To a stirred solution of **9b** (130 mg, 0.62 mmol) and **14a** (104 mg, 0.62 mmol) in EtOH/AcOH (5 mL/0.5 mL) was added $NaBH(OAc)_3$ (263 mg, 1.24 mmol) at room temperature. Then, the resulting mixture was stirred at the same temperature overnight. The reaction was quenched with saturated aqueous $NaHCO_3$ solution (5 mL), and the mixture was extracted with DCM (10 mL × 3). The combined organic layers were washed with brine, dried over Na_2SO_4, and concentrated under vacuum. The crude product was purified by flash chromatography (0−20% EtOAc/hexane) to afford **11b** as colorless oil (130 mg, 58%). ^{1}H NMR (400 MHz, $CDCl_3$): δ 6.95 (dd, J = 8.7, 2.6 Hz, 1H), 6.88 (d, J = 2.6 Hz, 1H), 6.42 (d, J = 8.0 Hz, 1H), 6.41 (s, 1H), 4.43 (q, J = 7.1 Hz, 2H), 3.29−3.12 (m, 4H), 2.84 (t, J = 7.3 Hz, 2H), 2.69 (t, J = 6.3 Hz, 2H), 1.94−1.88 (m, 2H), 1.80−1.72 (m, 2H), 1.67−1.60 (m, 2H), 1.41 (t, J = 7.1 Hz, 3H). ^{13}C NMR (101 MHz, $CDCl_3$): δ 175.1, 160.2, 156.5, 143.8, 128.8, 126.8, 124.1, 120.1, 111.5, 101.7, 62.2, 51.1, 49.5, 28.1, 26.7, 25.7, 25.2, 22.1, 14.2.

Ethyl 5-(4-(6-Chloro-4,4-dimethyl-3,4-dihydroquinolin-1(2*H*)-yl)-butyl)isoxazole-3-carboxylate (**10c**) was synthesized from **9b** (130 mg, 0.62 mmol) and **14b** (121 mg, 0.62 mmol) using a procedure similar to that described for the synthesis of **10b** and was obtained as colorless oil (100 mg, 42%). ^{1}H NMR (400 MHz, $CDCl_3$): δ 7.10 (d, J = 2.6 Hz, 1H), 6.96 (dd, J = 8.8, 2.6 Hz, 1H), 6.42 (d, J = 9.5 Hz, 1H), 6.41 (s, 1H), 4.43 (q, J = 7.1 Hz, 2H), 3.32−3.19 (m, 4H), 2.85 (t, J = 7.4 Hz, 2H), 1.80−1.64 (m, 6H), 1.41 (t, J = 7.1 Hz, 3H), 1.25 (s, 6H). ^{13}C NMR (101 MHz, $CDCl_3$): δ 175.1, 160.3, 156.5, 142.5, 132.9, 126.6, 126.1, 120.3, 111.7, 101.8, 62.2, 51.3, 45.9, 36.8, 32.3, 30.6 (2C), 26.8, 25.6, 25.3, 14.3.

Ethyl 5-(4-(2,8-Dichloro-10,11-dihydro-5*H*-dibenz[*b*,*f*]azepin-5-yl)butyl)isoxazole-3-carboxylate (**10d**) was synthesized from **18**

DOI: 10.1021/acs.jmedchem.9b00946
J. Med. Chem. XXXX, XXX, XXX−XXX

(100 mg, 0.30 mmol) and ethyl 2-chloro-2-(hydroxyimino)acetate (135 mg, 0.90 mmol) following general procedure B and was obtained as light-yellow oil (100 mg, 67%). ^{1}H NMR (400 MHz, $CDCl_3$): δ 7.09−7.08 (m, 4H), 6.96−6.93 (m, 2H), 6.31 (s, 1H), 4.43 (q, J = 7.1 Hz, 2H), 3.67 (t, J = 6.6 Hz, 2H), 3.10 (s, 4H), 2.74 (t, J = 7.4 Hz, 2H), 1.76−1.59 (m, 4H), 1.41 (t, J = 7.1 Hz, 3H).

5-(4-(5,6-Dichloro-1*H*-indol-1-yl)butyl)-*N*-hydroxyisoxazole-3-carboxamide (**11a**) was synthesized from **10a** (90 mg, 0.24 mmol) following general procedure C and was obtained as an off-white powder (35 mg, 39%). ^{1}H NMR (400 MHz, DMSO-d_6): δ 11.43 (s, 1H), 9.32 (d, J = 1.6 Hz, 1H), 7.89 (s, 1H), 7.79 (s, 1H), 7.51 (d, J = 3.1 Hz, 1H), 6.51 (s, 1H), 6.46 (d, J = 3.1 Hz, 1H), 4.22 (t, J = 7.0 Hz, 2H), 2.82 (t, J = 7.5 Hz, 2H), 1.65−1.75 (m, 2H), 1.65−1.54 (m, 2H). ^{13}C NMR (101 MHz, DMSO-d_6): δ 174.3, 157.4, 156.3, 134.7, 131.3, 127.9, 123.5, 121.5, 121.4, 111.7, 100.6, 100.5, 45.2, 29.14, 25.27, 24.12. ESI HRMS: calcd for $C_{16}H_{16}N_3O_3Cl_2$ $[M + H]^+$ m/z, 368.0563; found, 368.0555.

5-(4-(6-Chloro-3,4-dihydroquinolin-1(2*H*)-yl)butyl)-*N*-hydroxyisoxazole-3-carboxa-mide (**11b**) was synthesized from **10b** (130 mg, 0.36 mmol) following general procedure C and was obtained as an off-white powder (100 mg, 79%). ^{1}H NMR (400 MHz, DMSO-d_6): δ 11.43 (s, 1H), 6.93 (dd, J = 8.7, 2.6 Hz, 1H), 6.88 (d, J = 2.7 Hz, 1H), 6.55 (s, 1H), 6.53 (d, J = 8.8 Hz, 1H), 3.29−3.16 (m, 4H), 2.84 (t, J = 7.4 Hz, 2H), 2.65 (t, J = 6.3 Hz, 2H), 1.86−1.77 (m, 2H), 1.69−1.64 (m, 2H), 1.57−1.50 (m, 2H). ^{13}C NMR (101 MHz, DMSO-d_6): δ 174.5, 157.4, 156.3, 143.8, 128.1, 126.3, 123.8, 118.1, 111.6, 100.5, 50.0, 48.5, 27.4, 25.7, 24.7, 24.4, 21.3. ESI HRMS: calcd for $C_{17}H_{21}N_3O_3Cl$ $[M + H]^+$ m/z, 350.1266; found, 350.1256.

5-(4-(6-Chloro-4,4-dimethyl-3,4-dihydroquinolin-1(2*H*)-yl)butyl)-*N*-hydroxyisoxazo-le-3-carboxamide (**11c**) was synthesized from **10c** (100 mg, 0.28 mmol) following general procedure C and was obtained as an off-white powder (100 mg, 94%).^{1}H NMR (400 MHz, DMSO-d_6): δ 11.43 (s, 1H), 7.07 (d, J = 2.7 Hz, 1H), 6.94 (dd, J = 8.7, 2.6 Hz, 1H), 6.55 (s, 1H), 6.54 (d, J = 9.0 Hz, 1H), 3.28−3.21 (m, 4H), 2.84 (t, J = 7.3 Hz, 2H), 1.71−1.46 (m, 6H), 1.19 (s, 6H). ^{13}C NMR (101 MHz, DMSO-d_6): δ 174.5, 163.0, 157.4, 142.5, 132.5, 126.2, 125.3, 118.4, 111.9, 100.5, 50.2, 44.7, 40.2, 39.9, 39.7, 39.5, 39.3, 39.1, 38.9, 36.0, 31.8, 30.2 (2C), 25.6, 24.6, 24.5. ESI HRMS: calcd for $C_{19}H_{24}N_3O_3Cl$ $[M + H]^+$ m/z, 378.1579; found, 378.1576.

5-(4-(2,8-Dichloro-10,11-dihydro-5*H*-dibenz[*b*,*f*]azepin-5-yl)-butyl)-*N*-hydroxyisoxa-zole-3-carboxamide (**11d**) was synthesized from **10d** (100 mg, 0.20 mmol) following general procedure C and was obtained as a white powder (30 mg, 34%). ^{1}H NMR (400 MHz, $CDCl_3$): δ 7.09−7.07 (m, 4H), 6.95−6.92 (m, 2H), 6.37 (s, 1H), 3.66 (t, J = 6.5 Hz, 2H), 3.09 (s, 4H), 2.72 (t, J = 7.4 Hz, 2H), 1.76−1.68 (m, 2H), 1.63−1.57 (m, 2H); ^{13}C NMR (101 MHz, $CDCl_3$): δ 175.2, 156.0, 154.0, 146.3 (2C), 135.7 (2C), 129.7 (2C), 127.9 (2C), 126.4 (2C), 121.2 (2C), 100.7, 50.0, 31.7 (2C), 26.8, 26.7, 24.8. ESI HRMS: calcd for $C_{22}H_{22}Cl_2N_3O_3$ $[M + H]^+$ m/z, 446.1033; found, 446.1030.

3-Chloro-*N*-(4-chlorophenyl)propanamide (**13a**). To a round-bottom flask charged with 4-chloroaniline (**12**, 5.0 g, 39.4 mmol) in acetone (50 mL) was added 3-chloropropanoyl chloride (1.9 mL, 19.7 mmol) at room temperature. The resulting mixture was allowed to stir for 1 h under reflux conditions. The mixture was cooled to room temperature, quenched with 2 N HCl (30 mL), and extracted with EtOAc (25 mL × 3). The combined organic layers were washed with brine (20 mL), dried over Na_2SO_4, and concentrated under vacuum. **13a** was obtained as an off-white powder (4.6 g, 54%) and used directly in the next step without further purification. ^{1}H NMR (400 MHz, $CDCl_3$): δ 7.56 (br s, 1H), 7.46 (d, J = 8.7 Hz, 2H), 7.28 (d, J = 8.8 Hz, 2H), 3.87 (t, J = 6.3 Hz, 2H), 2.81 (t, J = 6.3 Hz, 2H). ^{13}C NMR (101 MHz, $CDCl_3$): δ 167.9, 136.0, 129.8, 129.1 (2C), 121.4 (2C), 40.4, 39.8.

N-(4-Chlorophenyl)-3-methylbut-2-enamide (**13b**). To a round-bottom flask charged with 4-chloroaniline (**12**, 1.27 g, 10.0 mmol) in $CHCl_3$ (20 mL) was added 3,3-dimethylacryloyl chloride (1.18 g, 10.0 mmol). The resulting mixture was heated to reflux for 2 h. The mixture was cooled to room temperature and quenched with 2 N HCl (20 mL), and then extracted with EtOAc (20 mL × 3). The combined organic layers were washed with brine (20 mL), dried over Na_2SO_4, and concentrated under vacuum. The crude product was purified by flash chromatography (0−80% EtOAc/hexane) to afford **13b** as a white powder (1.00 g, 48%). ^{1}H NMR (400 MHz, $CDCl_3$): δ 7.54 (br s, 1H), 7.47 (d, J = 8.1 Hz, 2H), 7.22 (d, J = 8.8 Hz, 2H), 5.70 (s, 1H), 2.19 (s, 3H), 1.86 (s, 3H). ^{13}C NMR (101 MHz, $CDCl_3$): δ 165.2, 154.0, 136.8, 128.8 (4C), 121.0, 118.4, 27.3, 20.0.

6-Chloro-1,2,3,4-tetrahydroquinoline (**14a**). (i) In a three-necked flask charged with **13a** (4.6 g, 21.1 mmol) under an argon atmosphere was added $AlCl_3$ (5.47 g, 42.2 mmol) at 140 °C. The resulting mixture was stirred at the same temperature for 12 h. Then, the reaction was cautiously quenched with 1 N HCl (20 mL) at 0 °C, and the mixture was extracted with EtOAc (30 mL × 3). The combined organic extracts were washed with brine (20 mL), dried over Na_2SO_4, and concentrated under vacuum. The crude product was purified by flash chromatography (0−80% EtOAc/hexane) to afford the lactam intermediate as a white powder (3.1 g, 17.1 mmol). (ii) To a stirred solution of $LiAlH_4$ (1.95 g, 51.4 mmol) in THF (30 mL) were added dropwise a solution of the lactam intermediate (3.1 g, 17.1 mmol) in THF (20 mL) at 0 °C. The resulting mixture was stirred at the same temperature for 20 min and then heated at reflux for an additional 1 h. The reaction was subsequently quenched with water (2.0 mL), 5 N NaOH (2.0 mL), and water (10 mL). The resulting precipitate was filtered off and washed with EtOAc (20 mL × 3). The filtrate was washed with brine (20 mL), dried over Na_2SO_4, and concentrated under vacuum. **14a** was obtained as colorless oil (2.43 g, 70% over two steps) and used directly in the next step without further purification. ^{1}H NMR (400 MHz, $CDCl_3$): δ 6.93−6.86 (m, 2H), 6.38 (d, J = 8.0 Hz, 1H), 3.77 (br s, 1H), 3.33−3.15 (m, 2H), 2.72 (t, J = 6.4 Hz, 2H), 1.94−1.88 (m, 2H). ^{13}C NMR (101 MHz, $CDCl_3$): δ 143.2, 128.8, 126.3, 122.7, 120.9, 114.9, 41.7, 26.7, 21.6.

6-Chloro-4,4-dimethyl-1,2,3,4-tetrahydroquinoline (**14b**). (i) To a round-bottom flask charged with **13b** (1.0 g, 4.78 mmol) in Toluene (15 mL) was added $AlCl_3$ (2.50 g, 19.1 mmol) at room temperature. The resulting mixture was heated at 80 °C for 2 h. Then, the reaction was cautiously quenched with 1 N HCl (10 mL) at 0 °C, and the mixture was extracted with EtOAc (15 mL × 3). The combined organic layers were washed with brine (20 mL), dried over Na_2SO_4, and concentrated under vacuum. The crude product was purified by flash chromatography (0−80% EtOAc/hexane) to afford the lactam intermediate as a brown powder (640 mg, 64%); (ii) to a stirred solution of $LiAlH_4$ (250 mg, 6.60 mmol) in THF (10 mL) was dropwise added the lactam intermediate (460 mg, 2.20 mmol) in THF (20 mL) at 0 °C. The resulting mixture was stirred at the same temperature for 20 min and then heated to reflux conditions for an additional 1 h. The reaction was subsequently quenched with water (0.5 mL), 5 N NaOH (0.5 mL), and water (2.5 mL). The resulting precipitate was filtered off and washed with EtOAc (20 mL × 3). The filtrate was washed with brine (20 mL), dried over Na_2SO_4, and concentrated under vacuum. The crude product was purified by flash chromatography (0−20% EtOAc/hexane) to afford compound **14b** as colorless oil (370 mg, 86%). ^{1}H NMR (400 MHz, DMSO-d_6): δ 7.05 (d, J = 2.5 Hz, 1H), 6.83 (dd, J = 8.6, 2.5 Hz, 1H), 6.44 (d, J = 8.6 Hz, 1H), 5.91 (br s, 1H), 3.21−3.12 (m, 2H), 1.61−1.53 (m, 2H), 1.20 (s, 6H). ^{13}C NMR (101 MHz, DMSO-d_6): δ 143.1, 130.5, 125.9, 125.3, 118.3, 114.8, 37.0, 36.0, 31.5, 30.3 (2C).

2,8-Dichloro-10,11-dihydro-5*H*-dibenz[*b*,*f*]azepine (**16**). To a stirred solution of 10,11-dihydro-5*H*-dibenz[*b*,*f*]azepine (**15**, 500 mg, 2.56 mmol) in $CHCl_3$ (75 mL) was added at room temperature predried silica gel (10 g, 2 g per mmol of NCS). The mixture was stirred gently, and the reaction vessel covered with foil to exclude light. NCS (685 mg, 5.12 mmol) was then added portion-wise over 1 h at room temperature. The mixture was stirred at the same temperature overnight. After completion of the reaction, excess silica gel was removed by vacuum filtration. The filtrate was washed with water and brine, dried over Na_2SO_4, and concentrated under reduced pressure. The crude product was purified by flash chromatography using (0−10% EtOAc/hexane) to afford **16** as a white solid (500 mg, 74%). ^{1}H NMR (400 MHz, $CDCl_3$): δ 7.04−7.02 (m, 4H), 6.65 (d, J = 6.2 Hz, 2H), 5.93 (s, 1H), 3.02 (s, 4H).

DOI: 10.1021/acs.jmedchem.9b00946
J. Med. Chem. XXXX, XXX, XXX−XXX

2,8-Dichloro-5-(hex-5-yn-1-yl)-10,11-dihydro-5*H*-dibenzo[*b*,*f*]-azepine (**18**). (i) To a stirred solution of **16** (300 mg, 1.15 mmol) in DMF (5 mL) was slowly added NaH (60%, 140 mg, 3.45 mmol). The mixture was stirred at room temperature for 15 min, followed by a dropwise addition of 1,4-dibromobutane (364 mg, 1.7 mmol). The mixture was stirred at room temperature for 1 h. After completion of the reaction, 1 N HCl aqueous solution was added to adjust the pH to 6−7. Then, the solution was extracted with EtOAc (10 mL × 3). The combined organic layers were washed with brine, dried over Na_2SO_4, and concentrated under reduced pressure. The crude product was purified by flash chromatography (0−5% EtOAc/hexane) to afford **17** as colorless oil (200 mg, 43%). (ii) To a stirred solution of **17** (200 mg, 0.5 mmol) in xylene/DMF (2/2 mL) was added a sodium acetylide suspension (0.2 mL, 18 wt % slurry in xylene) under an argon atmosphere at room temperature. Then, the mixture was stirred at 40 °C overnight. After completion, the reaction solution was quenched with water (10 mL), and the mixture was extracted with EtOAc (10 mL × 3). The combined organic layers were washed with brine, dried over Na_2SO_4, and concentrated under reduced pressure. The crude product was purified by flash chromatography (0−5% EtOAc/hexane) to afford **18** (100 mg, 25%) as colorless oil. ^{1}H NMR (400 MHz, $CDCl_3$): δ 7.09−7.07 (m, 4H), 6.97 (d, J = 9.0 Hz, 2H), 3.67 (t, J = 6.8 Hz, 2H), 3.10 (s, 4H), 2.14 (td, J = 7.0, 2.6 Hz, 2H), 1.89 (t, J = 2.6 Hz, 1H), 1.67−1.64 (m, 2H), 1.55−1.51 (m, 2H).

Ethyl 5-(3-((3,4-Dichlorophenyl)amino)propyl)isoxazole-3-carboxylate (**19a**) was synthesized from **9c** (464 mg, 2.85 mmol) and 3,4-dichlorophenol (850 mg, 3.41 mmol) using a procedure similar to that described for the synthesis of **10a** and was obtained as colorless oil (490 mg, 80%). ^{1}H NMR (400 MHz, $CDCl_3$): δ 7.28 (d, J = 8.9 Hz, 1H), 6.94 (d, J = 2.8 Hz, 1H), 6.71 (dd, J = 8.9, 2.9 Hz, 1H), 6.43 (s, 1H), 4.41 (q, J = 7.1 Hz, 2H), 3.96 (t, J = 5.9 Hz, 2H), 3.00 (t, J = 7.5 Hz, 2H), 2.26−2.08 (m, 2H), 1.38 (t, J = 7.1 Hz, 3H). ^{13}C NMR (101 MHz, $CDCl_3$): δ 174.3, 160.1, 157.7, 156.5, 132.9, 130.8, 124.2, 116.4, 114.5, 102.0, 66.9, 62.2, 27.0, 23.4, 14.2.

Ethyl 5-(4-(3,4-Dichlorophenyl)butyl)isoxazole-3-carboxylate (**19b**) was synthesized from **25** (18 mg, 0.1 mmol) following general procedure B and was obtained as colorless oil (20 mg, 58%). ^{1}H NMR (400 MHz, $CDCl_3$): δ 7.34 (d, J = 8.2 Hz, 1H), 7.25 (d, J = 2.0 Hz, 1H), 6.99 (dd, J = 8.2, 2.0 Hz, 1H), 6.40 (s, 1H), 4.55−4.46 (m, 2H), 2.83 (t, J = 7.3 Hz, 2H), 2.61 (t, J = 7.4 Hz, 2H), 1.78−1.64 (m, 4H).

5-(3-((3,4-Dichlorophenyl)amino)propyl)-*N*-hydroxyisoxazole-3-carboxamide (**20a**) was synthesized from **19a** (160 mg, 0.47 mmol) following general procedure C and was obtained as a white powder (65 mg, 40%). ^{1}H NMR (400 MHz, DMSO-d_6): δ 11.45 (s, 1H), 9.33 (s, 1H), 7.51 (d, J = 8.9 Hz, 1H), 7.23 (d, J = 2.9 Hz, 1H), 6.96 (dd, J = 8.9, 2.9 Hz, 1H), 6.60 (s, 1H), 4.06 (t, J = 6.1 Hz, 2H), 2.96 (t, J = 7.5 Hz, 2H), 2.15−2.03 (m, 2H). ^{13}C NMR (101 MHz, DMSO-d_6): δ 173.8, 157.9, 157.5, 156.3, 131.6, 131.0, 122.4, 116.4, 115.5, 100.7, 67.2, 40.2, 39.9, 39.7, 39.5, 39.3, 39.1, 38.9, 26.4, 22.6. ESI HRMS: calcd for $C_{13}H_{13}Cl_2N_2O_4$ $[M + H]^+$ m/z, 331.0247; found, 331.0244.

5-(4-(3,4-Dichlorophenyl)butyl)-*N*-hydroxyisoxazole-3-carboxamide (**20b**) was synthesized from **19b** (50 mg, 0.15 mmol) following general procedure C and was obtained as an off-white powder (15 mg, 30%). ^{1}H NMR (400 MHz, $CDCl_3$): δ 7.34 (d, J = 8.1 Hz, 1H), 7.24 (s, 1H), 6.98 (d, J = 7.7 Hz, 1H), 6.45 (s, 1H), 2.82 (t, J = 7.2 Hz, 2H), 2.60 (t, J = 7.2 Hz, 2H), 1.78−1.61 (m, 4H). ^{13}C NMR (101 MHz, $CDCl_3$): δ 175.2, 169.0, 156.2, 141.9, 132.3, 130.3, 130.3, 129.9, 127.8, 100.8, 34.6, 30.3, 26.8, 26.5. ESI HRMS: calcd for $C_{14}H_{15}Cl_2N_2O_3$ $[M + H]^+$ m/z, 329.0454; found, 329.0456.

3,4-Dichloro-*N*-(4-(hydroxycarbamoyl)benzyl)benzamide (**20c**). (i) To a stirred suspension of 3,4-dichlorobenzaldehyde (**26**, 1.04 g, 6.0 mmol) in water (20 mL) NH_2OH·HCl (0.42 g, 6.0 mmol) and K_2CO_3 (0.83 g, 6.0 mmol) were added, followed by the addition of $Cu(OAc)_2$ (20 mg, 0.12 mmol). The reaction mixture was heated to reflux for 6 h. After completion of the reaction, the solution was extracted with EtOAc (20 mL × 3). The combined organic layers were washed with brine, dried over Na_2SO_4, and concentrated under vacuum. The crude product was washed with Et_2O to afford amide intermediate **27** as a white powder (0.80 g, 70%). (ii) To a suspension of 3,4-dichlorobenzamide (**27**, 0.80 g, 4.25 mmol) and methyl 4-formylbenzoate (232 mg, 1.41 mmol) in toluene (10 mL) was added TFA (325 μL, 4.25 mmol) and triethylsilane (677 μL, 4.25 mmol) at room temperature. The resulting mixture was heated to reflux overnight. After completion of the reaction, the solution was extracted with EtOAc (20 mL × 3). The combined organic layers were washed with brine, dried over Na_2SO_4, and concentrated under vacuum. The crude product **19c** containing excess dichlorobenzamide (∼800 mg) was advanced in the next step without further purification. (iii) Compound **20c** was synthesized from the crude compound **19c** (∼800 mg) following general procedure C and was obtained as an off-white powder (150 mg, 31% over two steps). ^{1}H NMR (500 MHz, DMSO-d_6): δ 11.17 (s, 1H), 9.27 (t, J = 6.0 Hz, 1H), 8.99 (s, 1H), 8.13 (d, J = 2.1 Hz, 1H), 7.87 (dd, J = 8.4, 2.1 Hz, 1H), 7.78 (d, J = 8.4 Hz, 1H), 7.71 (d, J = 8.0 Hz, 2H), 7.38 (d, J = 8.0 Hz, 2H), 4.51 (d, J = 5.9 Hz, 2H). ^{13}C NMR (126 MHz, DMSO-d_6): δ 164.0, 164.0, 142.4, 134.5, 134.1, 131.4, 131.3, 130.8, 129.2, 127.6, 127.2 (2C), 126.9 (2C), 42.6. ESI HRMS: calcd for $C_{15}H_{13}Cl_2N_2O_3$ $[M + H]^+$ m/z, 339.0298; found, 339.0306.

4-(3-Bromopropyl)-1,2-dichlorobenzene (**22**). (i) A suspension of $LiAlH_4$ (262 mg, 6.9 mmol) in THF (23 mmol, 0.3 M solution) was prepared in an ice bath and under an argon atmosphere. To this suspension was added dropwise a THF solution (8 mL) of 3,4-dichlorocinnamic acid (**21**, 500 mg, 2.3 mmol). After the addition of the substrate solution, the resulting mixture was left to warm to room temperature while stirring. Then, it was heated to reflux for 5 h. The reaction was quenched with water (0.3 mL), 5 N NaOH (0.3 mL), and water (1.5 mL), the precipitate was filtered off, and the filtrate was extracted with EtOAc (10 mL × 3). The organic layers were washed with brine, dried over Na_2SO_4, and concentrated under vacuum. The crude product was purified by flash chromatography (0−50% EtOAc/hexane) to afford the intermediate alcohol as colorless oil (80 mg, 17%). (ii) To a stirred solution of the intermediate (80 mg, 0.40 mmol) in DCM (5 mL) were added CBr_4 (194 mg, 0.6 mmol) and Ph_3P (160 mg, 0.6 mmol) at 0 °C. Then, the resulting mixture was stirred at room temperature for 1 h. The reaction was quenched with water (5 mL), extracted with DCM (10 mL × 3). The combined organic extracts were washed with brine (30 mL), dried over Na_2SO_4, and concentrated under vacuum. The crude product was purified by flash chromatography (0−20% EtOAc/hexane) to afford **22** as colorless oil (70 mg, 65%). ^{1}H NMR (400 MHz, $CDCl_3$): δ 7.36 (d, J = 8.2 Hz, 1H), 7.29 (d, J = 2.0 Hz, 1H), 7.04 (dd, J = 8.2, 2.1 Hz, 1H), 3.38 (t, J = 6.4 Hz, 2H), 2.79−2.70 (m, 2H), 2.19−2.08 (m, 2H). ^{13}C NMR (101 MHz, $CDCl_3$): δ 140.8, 132.4, 130.5, 130.4, 130.2, 128.0, 33.7, 33.1, 32.5.

4-(3,4-Dichlorophenyl)butanenitrile (**23**). To a solution of **22** (70 mg, 0.26 mmol) in DMSO (3 mL) were added NaCN (115 mg, 2.36 mmol) at room temperature. Then, the resulting mixture was heated at 100 °C for 1 h. The mixture was diluted with water (5 mL) and extracted with EtOAc (10 mL × 3). The combined organic extracts were washed with aqueous $FeSO_4$ solution (10 mL) and brine (10 mL), dried over Na_2SO_4, and concentrated under vacuum. Compound **23** was obtained as yellow oil (40 mg, 72%) and used directly into the next step without further purification. ^{1}H NMR (400 MHz, $CDCl_3$): δ 7.37 (dd, J = 8.2, 0.8 Hz, 1H), 7.28 (d, J = 1.2 Hz, 1H), 7.03 (dd, J = 8.2, 1.5 Hz, 1H), 2.75 (t, J = 7.5 Hz, 2H), 2.34 (t, J = 7.0 Hz, 2H), 1.96 (p, J = 7.1 Hz, 2H). ^{13}C NMR (101 MHz, $CDCl_3$): δ 140.0, 132.6, 130.6, 130.4 (2C, overlapping), 127.9, 119.1, 33.5, 26.6, 16.4.

4-(3,4-Dichlorophenyl)butan-1-ol (**24**). (i) To a stirred solution of **23** (40 mg, 0.19 mmol) in EtOH (1 mL) was added 50% w/v aq NaOH (1 mL) at room temperature. The resulting mixture was heated at 80 °C for 3 h. Then, the mixture was diluted with water (5 mL) and extracted with EtOAc (10 mL × 3). The aqueous layer was separated and acidified with 2 N HCl to pH = 3−4, then extracted with EtOAc (10 mL × 3). The combined organic layers were washed with brine (30 mL), dried over Na_2SO_4, and concentrated under vacuum. The crude carboxylic acid product was obtained as a pink solid (40 mg, 90%) and used directly in the next step without further purification. (ii) To a stirred solution of the carboxylic acid (40 mg,

DOI: 10.1021/acs.jmedchem.9b00946
J. Med. Chem. XXXX, XXX, XXX−XXX

0.17 mmol) in THF (3 mL) was added BF_3·THF (1 M in THF, 0.34 mL) at 0 °C after 5 min. The resulting mixture was allowed to warm to room temperature overnight. The reaction was quenched with 1 N NaOH, and the mixture was extracted with EtOAc (10 mL × 3). The combined organic layers were washed with water (30 mL) and brine (30 mL), dried over Na_2SO_4, and concentrated under vacuum. **24** was obtained as colorless oil (40 mg, 98%) and used directly in the next step without further purification. ^{1}H NMR (400 MHz, $CDCl_3$): δ 7.33 (d, J = 8.2 Hz, 1H), 7.27 (d, J = 1.8 Hz, 1H), 7.01 (dd, J = 8.2, 1.8 Hz, 1H), 3.66 (t, J = 6.3 Hz, 2H), 2.60 (t, J = 7.5 Hz, 2H), 1.74−1.64 (m, 2H), 1.62−1.55 (m, 2H), 1.53 (br s, 1H). ^{13}C NMR (101 MHz, $CDCl_3$): δ 142.6, 132.2, 130.3, 130.2, 129.7, 127.9, 62.6, 34.8, 32.1, 27.3.

1,2-Dichloro-4-(hex-5-yn-1-yl)benzene (**25**). (i) To a stirred solution of **24** (40 mg, 0.18 mmol) in DCM (3 mL) were added CBr_4 (90 mg, 0.27 mmol) and Ph_3P (70 mg, 0.27 mmol) at 0 °C. Then, the resulting mixture was stirred at room temperature for 1 h. The reaction was quenched with water (5 mL) and extracted with DCM (10 mL × 3). The combined organic layers were washed with brine (30 mL), dried over Na_2SO_4, and concentrated under vacuum. The crude product was purified by flash chromatography (0−20% EtOAc/hexane) to afford the intermediate bromide as colorless oil (20 mg, 40%). (ii) To a stirred solution of the bromide (20 mg, 0.07 mmol) in DMF (2 mL) was added a sodium acetylide suspension (18 wt % slurry in xylene, 0.03 mL) under an argon atmosphere. The resulting mixture was stirred at 40 °C overnight. The reaction was quenched with water (5 mL), extracted with EtOAc (10 mL × 3). The combined organic layers were washed with brine (30 mL), dried over Na_2SO_4, and concentrated under vacuum. **25** was obtained as colorless oil (18 mg, 98%) and used directly in the next step without further purification. ^{1}H NMR (400 MHz, $CDCl_3$): δ 7.33 (d, J = 8.2 Hz, 1H), 7.28−7.25 (m, 1H), 7.01 (dd, J = 8.2, 2.0 Hz, 1H), 2.59 (t, J = 7.7 Hz, 2H), 2.22 (td, J = 7.0, 2.6 Hz, 2H), 1.95 (t, J = 2.6 Hz, 1H), 1.74−1.70 (m, 2H), 1.58−1.51 (m, 2H). ^{13}C NMR (101 MHz, $CDCl_3$): δ 142.4, 132.2, 130.3, 130.2, 129.7, 127.9, 84.0, 68.6, 34.5, 30.0, 27.8, 18.2.

HDAC 1 and 6 Enzymatic Assay Procedure. HDAC inhibition assays in Table 1 were performed by the Reaction Biology Corporation (Malvern, PA) using human full-length recombinant HDAC1 and 6, isolated from a baculovirus expression system in Sf9 cells. An acetylated, fluorogenic peptide derived from residues 379−382 of p53 (RHKKAc, 50 μM) was used as the substrate in the assays. The reaction buffer contained: 50 mM Tris·HCl pH 8.0, 137 mM NaCl, 2.7 mM KCl, 1 mM $MgCl_2$, 1 mg/mL BSA, and a final concentration of 1% DMSO. The enzyme was added into wells of the reaction plate, and stock solutions of compounds were distributed into the enzyme mixture by acoustic technology (Echo550 instrument; nanoliter range). The plates were spun down and pre-incubated for 5−10 min. The substrate was then delivered to all reaction wells to initiate the reaction, which was incubated for 2 h at 30 °C. After incubation, developer and trichostatin A (TSA) were added to quench the reaction and generate fluorescence. Kinetic measurements were then taken for 1.5 h at 15 min intervals to ensure that the development was complete. Endpoint readings were taken for analysis after the development reached a plateau. Dose response curves were generated, and the IC_{50} value for each compound was extrapolated from the generated plots (10-point IC_{50} curves were generated using a 3-fold serial dilution pattern starting at 30 μM).

Expression and Purification of HDACs1, 4−9, and 11. Large scale expression of human HDACs was carried out in HEK293/T17 cells essentially as described previously.[92,93] Briefly, transiently transfected cells were harvested three days post transfection and the cell pellets resuspended in a lysis buffer (50 mM Tris, 150 mM NaCl, 10 mM KCl, 2 mM $MgCl_2$, 10% glycerol, 0.2% NP-40, 2 units/mL benzonase, pH 8) supplemented with a cocktail of protease inhibitors (Roche, Basel, Switzerland). The cells were lysed by sonication (30 W; 3 × 20 s) on ice and the cell lysate cleared by centrifugation at 40 000g for 30 min at 4 °C. Recombinant fusion HDAC proteins were purified via Strep-Tactin affinity chromatography (IBA, Göttingen, Germany) with the elution buffer comprising 50 mM HEPES, 100 mM NaCl, 50 mM KCl, 10% glycerol, and 3 mM desthiobiotin, pH 7.5. Purified proteins were concentrated to 1 mg/mL, aliquoted, flash-frozen in liquid nitrogen and stored at −80 °C until further use.

Determination of Inhibitory Activity Against HDACs1, 4−9, and 11. IC_{50} values in Table 2 were determined using a fluorescence-based assay with 10 μM Ac-GAK(Ac)-AMC (HDAC 1, 6) or 10 μM Boc-Lys(TFA)-AMC (HDAC 4, 5, 7, 8, 9, 11) as a substrate.[94] Briefly, individual HDACs were pre-incubated with dilution series of tested inhibitors (0−100 μM) in a 384-well plate in the total volume of 40 μL for 10 min at 37 °C in reaction buffer comprising 50 mM HEPES, 140 mM NaCl, 10 mM KCl, 1 mM TCEP, 0.1% BSA, pH 7.4. The deacetylation reaction was started by the addition of 10 μL of a 10 μM substrate into the HDAC/inhibitor mixture. Following the 30 min incubation at 37 °C, the reaction was terminated by the addition of 25 μL of the trypsin solution (4 mg/mL). Fluorescence development by trypsin was carried out at 37 °C for 15 and 60 min for the Ac-GAK(Ac)-AMC and Boc-Lys(TFA)-AMC substrate, respectively. Released aminomethylcoumarin was quantified using a CLARIOstar fluorimeter with the excitation and emission wavelengths set to 365 and 440 nm, respectively. A nonlinear regression analysis was employed to calculate IC_{50} values using GraphPad Prism software (10-point IC_{50} curves were generated using a 3-fold serial dilution pattern starting at 100 μM). Reactions without the enzyme or the inhibitor were used to define 0 and 100% of the HDAC activity, respectively.

drHDAC6 Expression and Purification. The second catalytic domain of HDAC6 from *D. rerio* (drHDAC6; amino acids 440−798) was expressed and purified essentially as described previously.[88] Briefly, the synthetic gene encoding HDAC6 was recombined into a Gateway expression plasmid in frame with the TEV-cleavable His-MBP N-terminal tag. The fusion protein was expressed in *Escherichia coli* BL21-Codon plus (DE3)-RIPL at 16 °C overnight. The purification protocol comprised the HisTrap HP affinity step (GE Healthcare, Chicago, IL, USA), removal of the tag by the TEV protease, affinity purification on an amylose resin (New England Biolabs, Ipswitch, MA, USA), ion-exchange chromatography on HiTrap Q sepharose (GE Healthcare), and size-exclusion chromatography on a HiLoad Superdex 75 pg column (GE Healthcare; mobile phase: 50 mM HEPES, 100 mM KCl, 5% glycerol, 1 mM TCEP, pH 7.5) as the final step. The purity of the final protein preparation was >98% as determined by sodium dodecyl sulphate-polyacrylamide gel electrophoresis and purified drHDAC6-CD2 was concentrated to 10 mg/mL, aliquoted, flash-frozen in liquid nitrogen and stored at −80 °C until further use.

Crystallization and Data Collection. The drHDAC6 stock solution was mixed with 1/20 volume of the SS-208 solution (80 mM in DMSO), and the crystallization droplets were prepared by combining 1 μL of the complex solution with 1 μL of a reservoir solution containing 19% PEG 3350 (Sigma-Aldrich), 0.2 M KSCN (Hampton research), 0.1 M Bis-Tris (Sigma-Aldrich) at pH 6.5. To bolster the nucleation step, the droplets were streak-seeded using the seed stock prepared from crystals of the HDAC6/SAHA complex using a Crystal Crusher (Hampton Research). The crystals were grown by the hanging drop vapor diffusion method at 283 K. Diffraction quality crystals were vitrified in liquid nitrogen from the mother liquor supplemented with 20% (v/v) glycerol. The diffraction data were collected from a single crystal at 90 K using synchrotron radiation at a Bessy II beamline MX 14.2 (Berlin, Germany) equipped with a Pilatus 2M detector at an X-ray wavelength of 0.92 Å. Data processing was performed with the XDSAPP software package.[95]

Structure Determination and Refinement. The difference Fourier method was used to determine the structure of the drHDAC6-CD2/SS-208 complex using the drHDAC6/TSA complex (PDB code: 5EEK) without the inhibitor and water molecules as a starting model.[88] Iterative refinement and model building cycles were performed using Refmac 5.8. and Coot, respectively.[96,97] Ligand topologies and coordinates were generated with AceDRG[98] and the inhibitor was fitted into the $|F_o| - |F_c|$ electron density maps in the final stages of the refinement. Approximately 2500 randomly selected reflections were kept aside for cross-validation (Rfree) during the

DOI: 10.1021/acs.jmedchem.9b00946
J. Med. Chem. XXXX, XXX, XXX−XXX

refinement process. The final model was validated using the MolProbity server.[99] The data collection and structure refinement statistics are summarized in the Table S4.

Cell Transfection, Treatments, and BRET Measurements. NanoBRET target engagement was performed against HDAC6 (CD2) and HDAC1 according to the manufacturer's protocol (Promega) in HEK293 cells (ATCC). HEK293 cells were transfected with plasmid constructs encoding HDAC6 (CD2)-NanoLuc and HDAC1-NanoLuc as described previously.[89] HDAC6 (CD2)-NanoLuc encoded a GSSGAIA linker between HDAC (CD2) and NanoLuc, and HDAC1−NanoLuc encoded a SWTWEGNKWTWK linker between HDAC1 and NanoLuc. NanoBRET HDAC tracer (Promega) was added to a final concentration of 250 and 1000 nM for HDAC6 (CD2) and HDAC1, respectively, immediately prior to testing compound addition. Tracer concentrations were selected for each HDAC such that tracer occupancy did not impart a shift in the observed compound IC_{50} value. The serially diluted test compounds were then added to the cells and allowed to equilibrate for 2 h prior to BRET measurements. To measure BRET, a NanoBRET NanoGlo Substrate-(Promega) and Extracellular NanoLuc inhibitor was added per the manufacturer's protocol, and filtered luminescence was measured on a GloMax Discover luminometer equipped with a 450 nm BP filter (donor) and 610 nm LP filter (acceptor), using a 0.5 s integration time. Milli-BRET units (mBU) are the BRET values × 1000. Competitive displacement data were then graphed with GraphPad Prism software using a 3-parameter curve fit with the following equation (equation).

$$Y = \text{bottom} + (\text{top-bottom})/[1 + 10^{(X-\log IC_{50})}]$$

Mice. Experiments involving mice were performed in accordance with approved protocols by the Institutional Care and Use Committee (IACUC) at The George Washington University (Protocol A354). The C57BL/6 mice were obtained from the Charles River Laboratories (Wilmington, Massachusetts, USA). All the in vivo studies performed used tumor cells passaged in vivo (mouse to mouse) a minimum of five times before the tumor challenge experiment. Once the in vivo passaged cells were obtained, the mice were injected subcutaneously with 1.0×10^6 melanoma cells suspended in 100 μL 1× phosphate buffered saline (PBS) (Corning, 21-040-CV). Treatment started once tumors were palpable or as indicated in particular experiments. The mice were treated intraperitoneally with SS-208 (25 mg/kg) or vehicle control depending on the randomly assigned treatment group (10 female mice per group, 4−6 weeks old). The control mice were injected with 100 μL 1× PBS as the vehicle control. The mice were treated five days a week until tumors in the control group reached maximum size according to our IACUC protocol. Tumor volume was calculated using caliper measurements by the formula $L \times W2/2$.

All animal studies were done with consideration for toxicity in relation to each individual agent and using a dose that was previously verified through in vivo testing. However, we routinely monitored for early signs of toxicity. A particular focus was given to mortality, body weight, and food consumption. At the end-point postmortem evaluation, using gross visual examination of organs, was done for each condition.

Cell Culture. In vivo tumors: SM1 cells were originally obtained from the laboratory of Dr. A. Ribas at the University of California Los Angeles.[100] SM1 tumor cells were passaged in vivo directly from mouse to mouse for at least five passages. Tumors were grown and selected for optimal and consistent growth rate. When preparing cells for subcutaneous injection, mice with a tumor burden measuring approximately 7 mm × 7 mm were euthanized. Tumors were extracted and processed under sterile conditions. A cell count was used to adjust the cell concentration to 1.0×10^6 per 100 μL of PBS, indicative of the volume per mouse injection. These cells were immediately injected into the experimental mice, as described above. The cells in excess from the tumor processing were frozen in 90% fetal bovine serum (Serum Source, FB02-500HI) with 10% DMSO (Sigma-Aldrich, D2650) and stored in liquid nitrogen for future experiments.

HDACis for Cellular Studies. SS-208 was kept as a stock solution of 10 mg/mL and diluted with a buffer provided by the manufacturer to the concentration used for each particular experiment. NextA was provided by StarWise Therapeutics LLC. TubA (S8049) was purchased from Selleckchem. The pan-HDACi LBH589 (50-148-338) was purchased from Biotang Inc.

Cellular Viability and Apoptosis Assays. Using a ApoTox-Glo Triplex Assay (Promega, G6321) viability and apoptosis were measured. The SM1 cells were treated with individual HDACis along with the recommended assay controls. Pan-HDACi, LBH589 was also used as a control on all plates. Following the manufacturer's protocol, viability/cytotoxicity reagents were added, and fluorescence was measured at specific wavelengths—that is, 400Ex/505Em (viability) and 485Ex/520Em (cytotoxicity). Next, the Caspase 3/7 reagent was added, and luminescence was measured at Lm578 (apoptosis). The measurements were collected using a SpectraMax 3i multi-mode microplate reader.

Cellular HDAC Inhibition. Using HDAC-Glo I/II Assay (Promega, G6420) Cells were plated at a density of 10 000 cells per/well overnight in a white, flat clear bottom 96 well plate. After 24 h, the plate was then treated with the compounds of interest (NextA, TubA, and SS-208) at the desired concentrations and incubated at 37 °C and 5% CO_2 for 1 h. After incubation with the compounds, the developer is added to the substrate, mixed, and added directly to the plate, following the manufactured protocol. Immediately after plating, the plate was read for an hour and 15 min with a reading done every 2 min, using the SpectraMax 3i multi-mode plate reader.

Flow Cytometry. Tumor cells were immediately processed into single cell suspensions for analysis by flow cytometry. The first panel for flow cytometry was to analyze the expression of immune cell surface markers. These cells were stained with phycoerythrin (PE)-conjugated antibodies in a 96-well format. The antibodies were purchased from BD Biosciences (San Jose, California, USA), Biolegend (San Diego, California, USA), and eBioscience (San Diego, California, USA). Tumor cells were stained with antimouse CD274 (PD-L1) (BD Biosciences, 558091), antimouse CD 273 (PD-L2) (Biolegend, 107205), antimouse CD276 (B7-H3) (Biolegend, 124507), antimouse B7-H4 (Biolegend, 139405), antimouse Galactin-9 (Biolegend, 137903), antimouse CD252 (OX40-L), antimouse CD275 (ICOS-L) (eBioscience, 12-5985-81), antimouse MHC I (H-2Kb) (eBioscience, 12-5958-80), or antimouse MHC II (I-A/I-E) (eBioscience, 12-5321-81). After staining for 30 min at room temperature, the cells were washed at least three times with 1× PBS and resuspended in FACS buffer.

The second panel for flow cytometry was designed to measure the activity and infiltration of Natural Killer (NK) and T-cells. The following antibodies were used: PerCP/Cy5.5 antimouse CD3 (T-cells) (Biolegend, 100218), Alexa Fluor 488 antimouse CD4 (CD4+ T cells) (Biolegend, 100423), PE/Cy7 antimouse CD8a (CD8+ T cells) (Biolegend, 100766), APC/Fire 750 antimouse CD49b (NK cells) (Biolegend, 108922), Brilliant Violet 421 antimouse CD25 (T-cell activation) (Biolegend, 102034), and Brilliant Violet 785 antimouse CD45.2 (T-cell activation) (Biolegend, 109839). Finally, the third flow cytometry panel measured the activity and infiltration of myeloid cells using the following markers: Brilliant Violet 421 antimouse/human C11b (Macrophage) (Biolegend, 101236), APC antimouse CD80 (M1) (Biolegend, 104714), PE/Cy7 antimouse CD206 MMR (M2) (Biolegend, 141720), Brilliant Violet 630 antimouse CD11c (mDC) (Biolegend, 117339), APC/Fire 750 antimouse CD45.2 (MDSC) (Biolegend, 109852), PE antimouse CD123 [IL-3 receptor (IL-3Rα)] (Biolegend, 106005), Brilliant Violet 603 antimouse Ly-6G/Ly-6C (MDSC) (Biolegend, 108440), FITC antimouse H 2 (M2) (Biolegend, 125508), and Brilliant Violet 785 antimouse F4/80 (Macrophage) (Biolegend, 123141). After staining for 30 min at room temperature, the cells were washed with 1× PBS, similar to the first panel. The samples were fixed with Life Technologies IC Fixation Buffer (FB001) from ThermoFisher

DOI: 10.1021/acs.jmedchem.9b00946
J. Med. Chem. XXXX, XXX, XXX−XXX

Scientific (Waltham, Massachusetts, USA) according to the manufacturer's protocol and resuspended in FACS buffer.

To determine viability, all flow cytometry panels used LIVE/DEAD Fixable Aqua Dead Cell Stain (L34957) from ThermoFisher Scientific. The samples were run in a BD Celesta cell analyzer, recording at least 30 000 events. The results were analyzed using FlowJo software 10.4.

Quantitative Real-Time PCR. SM1 murine melanoma cells were plated in a 6-well plate. The cells were serum starved overnight followed by pretreatment with 5 μM SS-208 for 1 h. Subsequently, treatment with recombinant murine IL-6 (Biolegend, San Diego, CA 92121) at 30 ng/mL was performed for overnight. Following the manufacturer's instructions, total RNA was extracted from the cells using the Trizol (Life Technologies, Carlsbad, CA, 92008). The samples were processed immediately or stored at −80 °C. Quantification of RNA was done using a ND-1000 NanoDrop spectrophotometer (NanoDrop Technologies, Inc., Wilmington, Delaware). The 260/280 ratios were routinely over 1.9. sample cDNA was produced using a iScript cDNA synthesis kit (Bio-Rad, 1708891). Target mRNA was quantified using an iQ SYBR green Supermix (Bio-Rad, 1708882). Primers targeting PD-L1 and GAPDH for qRT-PCR were purchased from Invitrogen (Waltham, Massachusetts, USA) and the sequences are listed in the previous publication.[51] Cycling conditions were used as per manufacturer's instructions. Single product amplification was confirmed by the melting curve analysis, and primer efficiency was near 100% in all the experiments performed. Quantification is expressed in arbitrary units, and target mRNA levels were normalized to GAPDH expression using the method described by Pfaffl[101] using Microsoft Excel Software (Microsoft, Redmond, WA).

Immunoblotting. Cells were lysed in RIPA buffer (Pierce, 89900) with a 1× protease and phosphatase inhibitor (Pierce, A32961). Lysates were sonicated in a Bioruptor (Diagenode, Denville, NJ, USA) in a 4 °C water bath for 8 min (8 cycles of 30 s on, 30 s off). The protein concentration was determined using a Pierce BCA protein assay kit (Thermo Fisher Scientific, 23225) according to the manufacturer's protocol. The samples were mixed with a NuPAGE LDS 4× loading gel (NP0007) and NuPAGE 10× reducing agent (NP0009), then placed on a heating block at 100 °C. Next, the samples were loaded onto 4−20% (BioRad, 4561093) or 10% gels (BioRad, 4561033) and transferred to LF PVDF (BioRad, 170-4274). The membranes were blocked with LI-COR Biosciences (Lincoln, Nebraska, USA) Odyssey blocking buffer (927-40100). The bands were detected using an Azure Biosystems (Dublin, California, USA) imaging system c600. The antibodies used for immunoblotting included: PD-L1 (ProSci, 4059), PD-L2 (ProSci, 4063), total STAT3 (Cell Signal, 12640), phosphor-STAT3 (Y705) (Cell Signal, 9138), α-Tubulin (Cell Signaling, 3873), Ac-α-Tubulin (Cell Signaling, 3971), histone H3 (Cell Signaling 3638), Ac-histone H3 (Cell Signaling 9649S), and HDAC6 (Assay Biotech C0226). The bands were analyzed using ImageJ (NIH).

Statistical Analysis and Reproducibility. The experiments were done in triplicate unless otherwise noted. The analysis was done using unpaired *t*-tests with significance at $p < 0.05$ and the Kaplan−Meier survival curves using GraphPad Prism 7. All analyses of cell viability, apoptosis, and cytotoxicity were completed using Microsoft Excel Software (Microsoft, Redmond, WA).

■ ASSOCIATED CONTENT

Supporting Information

The Supporting Information is available free of charge on the ACS Publications website at DOI: 10.1021/acs.jmedchem.9b00946.

Additional data on the Ames test and the hERG assay, crystallization data collection, and refinement statistics, and physicochemical properties, ^{1}H NMR spectra, and ^{13}C NMR spectra for compounds **7a−d**, **11a−d**, and **20a−c** (PDF)

Molecular formula strings including screening data (CSV)

Accession Codes

Atomic coordinates and corresponding structure factors for the drHDAC6-CD2/SS-208 complex have been deposited at the Protein Data Bank as the 6R0K entry.

■ AUTHOR INFORMATION

Corresponding Authors

*E-mail: akozikowski@starwisetrx.com. Phone: +1-773-793-5866 (A.P.K.).

*E-mail: avillagra@email.gwu.edu. Phone: +1-202-994-9547 (A.V.).

ORCID

Sida Shen: 0000-0002-0295-2545

Mauricio T. Tavares: 0000-0002-4400-7787

Guiping Zhang: 0000-0001-9818-4773

Cyril Bařinka: 0000-0003-2751-3060

Present Addresses

¶Departments of Chemistry, Center for Molecular Innovation and Drug Discovery, and Center for Developmental Therapeutics, Northwestern University, Evanston, Illinois 60208, United States.

▽Department of Chemistry, Scripps Research, Jupiter, Florida 33458, United States.

Author Contributions

S.S. and M.H. contributed equally to this paper. A.V. and A.P.K. conceived the original idea, initiated the project, and oversaw all the chemical, biological, and in vivo experimental designs and data analysis. S.S. designed and synthesized compounds, oversaw all the experimental design, analyzed data, and wrote the manuscript with assistance from the other authors. M.H., S.N., and T.K. designed and performed all biological and in vivo experimental designs, analyzed data, and contributed to the manuscript writing. J.P. crystallized the drHDAC6/SS-208 complex; K.U. solved, refined, and analyzed the drHDAC6/SS-208 X-ray structure; C.B. determined IC_{50} values of HDAC isoforms, analyzed data, and contributed to manuscript writing. M.T.T. and G.Z. assisted the scale-up work of SS-208 and assisted in the preparation of the manuscript. C.A.Z. designed and performed the cellular HDAC target engagement assay; M.B.R. oversaw the experimental design and data analyses of the target engagement study and assisted in the preparation of the manuscript.

Notes

The authors declare no competing financial interest.

■ ACKNOWLEDGMENTS

Funded by NIH R21 CA184612-01 and Melanoma Research Foundation CDA Grant Award (A.V.); NIH R01NS079183, R43HD093464, and R41AG058283 (A.P.K.). Additionally, this work was in part supported by the CAS (RVO: 86652036), the Czech Science Foundation (15-19640S), the MEYS CR (CIISB for Biocev: LM2015043), the Grant Agency of Charles University (project number: 1558218), and project BIOCEV (CZ.1.05/1.1.00/02.0109) from the ERDF (C.B.). We would like to acknowledge the important technical contributions and advice of Kimberlyn Acklin, MS, SCYM (ASCP), at The George Washington University Flow Cytometry Core Facility and Bethany Rentz, RVT, at The George Washington University Office of Animal Research. We

Q

thank Petra Baranova and Barbora Havlinova for excellent technical assistance and Lucia Motlova for helping with crystallization experiments. We also thank Dr. Werner Tueckmantel for proofreading the article and providing comments. We acknowledge the Helmholtz-Zentrum Berlin for the allocation of synchrotron radiation beamtime at the MX14.2 beamline and the support by the project CALIPSOplus (grant agreement 730872) from the EU Framework Programme for Research and Innovation HORIZON 2020.

■ ABBREVIATIONS

ADMET, absorption, distribution, metabolism, excretion, and toxicity; TPSA, topological polar surface area; MW, molecular weight; hERG, human Ether-à-go-go related gene; DEAD, diethyl azodicarboxylate; PCC, pyridinium chlorochromate; NCS, *N*-chlorosuccinimide; TFA, trifluoroacetic acid; DMF, *N*,*N*-dimethylformamide; DMSO, dimethyl sulfoxide; DCM, dichloromethane; DCE, 1,2-dichloroethane; THF, tetrahydrofuran; PD-L1/2, programmed death-ligand 1/2; PD-1, programmed cell death-1; CTLA-4, cytotoxic T-lymphocyte-associated protein 4; MHC, major histocompatibility complex; CD25/40/80, cluster of differentiation 25/40/80

■ REFERENCES

(1) Stone, A.; Cooper, J.; Koenig, K. L.; Golfinos, J. G.; Oratz, R. A comparison of survival rates for treatment of melanoma metastatic to the brain. *Cancer Invest.* **2004**, *22*, 492−497.
(2) Miranda, E. P. Management of cutaneous melanoma. *N. Engl. J. Med.* **2004**, *351*, 2770−2771.
(3) Luke, J. J.; Flaherty, K. T.; Ribas, A.; Long, G. V. Targeted agents and immunotherapies: optimizing outcomes in melanoma. *Nat. Rev. Clin. Oncol.* **2017**, *14*, 463−482.
(4) Livingstone, E.; Zimmer, L.; Vaubel, J.; Schadendorf, D. BRAF, MEK and KIT inhibitors for melanoma: adverse events and their management. *Chin. Clin. Oncol.* **2014**, *3*, 29.
(5) Waterhouse, P.; Penninger, J. M.; Timms, E.; Wakeham, A.; Shahinian, A.; Lee, K. P.; Thompson, C. B.; Griesser, H.; Mak, T. W. Lymphoproliferative disorders with early lethality in mice deficient in Ctla-4. *Science* **1995**, *270*, 985−988.
(6) Polkowska, M.; Ekk-Cierniakowski, P.; Czepielewska, E.; Kozłowska-Wojciechowska, M. Efficacy and safety of BRAF inhibitors and anti-CTLA4 antibody in melanoma patients-real-world data. *Eur. J. Clin. Pharmacol.* **2018**, *75*, 329−334.
(7) Robert, C.; Schachter, J.; Long, G. V.; Arance, A.; Grob, J. J.; Mortier, L.; Daud, A.; Carlino, M. S.; McNeil, C.; Lotem, M.; Larkin, J.; Lorigan, P.; Neyns, B.; Blank, C. U.; Hamid, O.; Mateus, C.; Shapira-Frommer, R.; Kosh, M.; Zhou, H.; Ibrahim, N.; Ebbinghaus, S.; Ribas, A. Pembrolizumab versus Ipilimumab in Advanced Melanoma. *N. Engl. J. Med.* **2015**, *372*, 2521−2532.
(8) Weber, J.; Mandala, M.; Del Vecchio, M.; Gogas, H. J.; Arance, A. M.; Cowey, C. L.; Dalle, S.; Schenker, M.; Chiarion-Sileni, V.; Marquez-Rodas, I.; Grob, J.-J.; Butler, M. O.; Middleton, M. R.; Maio, M.; Atkinson, V.; Queirolo, P.; Gonzalez, R.; Kudchadkar, R. R.; Smylie, M.; Meyer, N.; Mortier, L.; Atkins, M. B.; Long, G. V.; Bhatia, S.; Lebbé, C.; Rutkowski, P.; Yokota, K.; Yamazaki, N.; Kim, T. M.; de Pril, V.; Sabater, J.; Qureshi, A.; Larkin, J.; Ascierto, P. A. Adjuvant Nivolumab versus Ipilimumab in Resected Stage III or IV Melanoma. *N. Engl. J. Med.* **2017**, *377*, 1824−1835.
(9) Wolchok, J. D.; Chiarion-Sileni, V.; Gonzalez, R.; Rutkowski, P.; Grob, J.-J.; Cowey, C. L.; Lao, C. D.; Wagstaff, J.; Schadendorf, D.; Ferrucci, P. F.; Smylie, M.; Dummer, R.; Hill, A.; Hogg, D.; Haanen, J.; Carlino, M. S.; Bechter, O.; Maio, M.; Marquez-Rodas, I.; Guidoboni, M.; McArthur, G.; Lebbé, C.; Ascierto, P. A.; Long, G. V.; Cebon, J.; Sosman, J.; Postow, M. A.; Callahan, M. K.; Walker, D.; Rollin, L.; Bhore, R.; Hodi, F. S.; Larkin, J. Overall survival with combined nivolumab and ipilimumab in advanced melanoma. *N. Engl. J. Med.* **2017**, *377*, 1345−1356.
(10) O'Sullivan Coyne, G.; Madan, R. A.; Gulley, J. L. Nivolumab: promising survival signal coupled with limited toxicity raises expectations. *J. Clin. Oncol.* **2014**, *32*, 986−988.
(11) O'Donnell, J. S.; Smyth, M. J.; Teng, M. W. Acquired resistance to anti-PD1 therapy: checkmate to checkpoint blockade? *Genome Med.* **2016**, *8*, 111.
(12) Gide, T. N.; Wilmott, J. S.; Scolyer, R. A.; Long, G. V. Primary and acquired resistance to immune checkpoint inhibitors in metastatic melanoma. *Clin. Cancer Res.* **2018**, *24*, 1260−1270.
(13) Datta, M.; Coussens, L. M.; Nishikawa, H.; Hodi, F. S.; Jain, R. K. Reprogramming the tumor microenvironment to improve immunotherapy: emerging strategies and combination therapies. *Am. Soc. Clin. Oncol. Educ. Book* **2019**, *39*, 165−174.
(14) Kowal, J.; Kornete, M.; Joyce, J. A. Re-education of macrophages as a therapeutic strategy in cancer. *Immunotherapy* **2019**, *11*, 677−689.
(15) Voorwerk, L.; Slagter, M.; Horlings, H. M.; Sikorska, K.; van de Vijver, K. K.; de Maaker, M.; Nederlof, I.; Kluin, R. J. C.; Warren, S.; Ong, S.; Wiersma, T. G.; Russell, N. S.; Lalezari, F.; Schouten, P. C.; Bakker, N. A. M.; Ketelaars, S. L. C.; Peters, D.; Lange, C. A. H.; van Werkhoven, E.; van Tinteren, H.; Mandjes, I. A. M.; Kemper, I.; Onderwater, S.; Chalabi, M.; Wilgenhof, S.; Haanen, J. B. A. G.; Salgado, R.; de Visser, K. E.; Sonke, G. S.; Wessels, L. F. A.; Linn, S. C.; Schumacher, T. N.; Blank, C. U.; Kok, M. Immune induction strategies in metastatic triple-negative breast cancer to enhance the sensitivity to PD-1 blockade: the TONIC trial. *Nat. Med.* **2019**, *25*, 920−928.
(16) Choi, J.; Gyamfi, J.; Jang, H.; Koo, J. S. The role of tumor-associated macrophage in breast cancer biology. *Histol. Histopathol.* **2018**, *33*, 133−145.
(17) Kim, H. J.; Bae, S. C. Histone deacetylase inhibitors: molecular mechanisms of action and clinical trials as anti-cancer drugs. *Am. J. Transl. Res.* **2011**, *3*, 166−179.
(18) Li, T.; Zhang, C.; Hassan, S.; Liu, X.; Song, F.; Chen, K.; Zhang, W.; Yang, J. Histone deacetylase 6 in cancer. *J. Hematol. Oncol.* **2018**, *11*, 111.
(19) Ganai, S. A. Histone deacetylase inhibitors modulating non-epigenetic players: the novel mechanism for small molecule based therapeutic intervention. *Curr. Drug Targets* **2018**, *19*, 593−601.
(20) Glozak, M. A.; Sengupta, N.; Zhang, X.; Seto, E. Acetylation and deacetylation of non-histone proteins. *Gene* **2005**, *363*, 15−23.
(21) Li, Y.; Seto, E. HDACs and HDAC inhibitors in cancer development and therapy. *Cold Spring Harbor Perspect. Med.* **2016**, *6*, a026831.
(22) Eckschlager, T.; Plch, J.; Stiborova, M.; Hrabeta, J. Histone deacetylase inhibitors as anticancer drugs. *Int. J. Mol. Sci.* **2017**, *18*, No. E1414.
(23) Landreville, S.; Agapova, O. A.; Matatall, K. A.; Kneass, Z. T.; Onken, M. D.; Lee, R. S.; Bowcock, A. M.; Harbour, J. W. Histone deacetylase inhibitors induce growth arrest and differentiation in uveal melanoma. *Clin. Cancer Res.* **2012**, *18*, 408−416.
(24) Clawson, G. A. Histone deacetylase inhibitors as cancer therapeutics. *Ann. Transl. Med.* **2016**, *4*, 287.
(25) Shen, L.; Orillion, A.; Pili, R. Histone deacetylase inhibitors as immunomodulators in cancer therapeutics. *Epigenomics* **2016**, *8*, 415−428.
(26) Hornig, E.; Heppt, M. V.; Graf, S. A.; Ruzicka, T.; Berking, C. Inhibition of histone deacetylases in melanoma-a perspective from bench to bedside. *Exog. Dermatol.* **2016**, *25*, 831−838.
(27) Woods, D. M.; Sodre, A. L.; Villagra, A.; Sarnaik, A.; Sotomayor, E. M.; Weber, J. HDAC inhibition upregulates PD-1 ligands in melanoma and augments immunotherapy with PD-1 blockade. *Cancer Immunol. Res.* **2015**, *3*, 1375−1385.
(28) Woan, K. V.; Lienlaf, M.; Perez-Villaroel, P.; Lee, C.; Cheng, F.; Knox, T.; Woods, D. M.; Barrios, K.; Powers, J.; Sahakian, E.; Wang, H. W.; Canales, J.; Marante, D.; Smalley, K. S. M.; Bergman, J.; Seto, E.; Kozikowski, A.; Pinilla-Ibarz, J.; Sarnaik, A.; Celis, E.; Weber, J.;

DOI: 10.1021/acs.jmedchem.9b00946
J. Med. Chem. XXXX, XXX, XXX−XXX

Sotomayor, E. M.; Villagra, A. Targeting histone deacetylase 6 mediates a dual anti-melanoma effect: enhanced antitumor immunity and impaired cell proliferation. *Mol. Oncol.* **2015**, *9*, 1447−1457.
(29) Roche, J.; Bertrand, P. Inside HDACs with more selective HDAC inhibitors. *Eur. J. Med. Chem.* **2016**, *121*, 451−483.
(30) Guerriero, J. L.; Sotayo, A.; Ponichtera, H. E.; Castrillon, J. A.; Pourzia, A. L.; Schad, S.; Johnson, S. F.; Carrasco, R. D.; Lazo, S.; Bronson, R. T.; Davis, S. P.; Lobera, M.; Nolan, M. A.; Letai, A. Class IIa HDAC inhibition reduces breast tumours and metastases through anti-tumour macrophages. *Nature* **2017**, *543*, 428−432.
(31) Lee, J.-H.; Yao, Y.; Mahendran, A.; Ngo, L.; Venta-Perez, G.; Choy, M. L.; Breslow, R.; Marks, P. A. Creation of a histone deacetylase 6 inhibitor and its biological effects. *Proc. Natl. Acad. Sci. U.S.A.* **2015**, *112*, 12005−12010.
(32) Hsieh, H.-Y.; Chuang, H.-C.; Shen, F.-H.; Detroja, K.; Hsin, L.-W.; Chen, C.-S. Targeting breast cancer stem cells by novel HDAC3-selective inhibitors. *Eur. J. Med. Chem.* **2017**, *140*, 42−51.
(33) Hideshima, T.; Mazitschek, R.; Qi, J.; Mimura, N.; Tseng, J.-C.; Kung, A. L.; Bradner, J. E.; Anderson, K. C. HDAC6 inhibitor WT161 downregulates growth factor receptors in breast cancer. *Oncotarget* **2017**, *8*, 80109−80123.
(34) Lee, H.-Y.; Nepali, K.; Huang, F.-I.; Chang, C.-Y.; Lai, M.-J.; Li, Y.-H.; Huang, H.-L.; Yang, C.-R.; Liou, J.-P. (N-Hydroxycarbonylbenylamino)quinolines as selective histone deacetylase 6 inhibitors suppress growth of multiple myeloma in vitro and in vivo. *J. Med. Chem.* **2018**, *61*, 905−917.
(35) Tavares, M. T.; Shen, S.; Knox, T.; Hadley, M.; Kutil, Z.; Bařinka, C.; Villagra, A.; Kozikowski, A. P. Synthesis and pharmacological evaluation of selective histone deacetylase 6 inhibitors in melanoma models. *ACS Med. Chem. Lett.* **2017**, *8*, 1031−1036.
(36) Ruijter, A. J. M. d.; Gennip, A. H. v.; Caron, H. N.; Kemp, S.; Kuilenburg, A. B. P. v. Histone deacetylases (HDACs): characterization of the classical HDAC family. *Biochem. J.* **2003**, *370*, 737−749.
(37) Haberland, M.; Montgomery, R. L.; Olson, E. N. The many roles of histone deacetylases in development and physiology: implications for disease and therapy. *Nat. Rev. Genet.* **2009**, *10*, 32−42.
(38) Matthias, P.; Yoshida, M.; Khochbin, S. HDAC6 a new cellular stress surveillance factor. *Cell Cycle* **2008**, *7*, 7−10.
(39) Imai, Y.; Maru, Y.; Tanaka, J. Action mechanisms of histone deacetylase inhibitors in the treatment of hematological malignancies. *Cancer Sci.* **2016**, *107*, 1543−1549.
(40) Miyake, Y.; Keusch, J. J.; Wang, L.; Saito, M.; Hess, D.; Wang, X.; Melancon, B. J.; Helquist, P.; Gut, H.; Matthias, P. Structural insights into HDAC6 tubulin deacetylation and its selective inhibition. *Nat. Chem. Biol.* **2016**, *12*, 748−754.
(41) Faria Freitas, M.; Cuendet, M.; Bertrand, P. HDAC inhibitors: a 2013-2017 patent survey. *Expert Opin. Ther. Pat.* **2018**, *28*, 365−381.
(42) Clinical trials for ACY-1215. https://clinicaltrials.gov/ct2/results?term=ACY-1215&Search=Search (accessed Mar 15, 2019).
(43) Clinical trials for ACY-241. https://clinicaltrials.gov/ct2/results?term=ACY-241&Search=Search (accessed Mar 15, 2019).
(44) Fukada, M.; Hanai, A.; Nakayama, A.; Suzuki, T.; Miyata, N.; Rodriguiz, R. M.; Wetsel, W. C.; Yao, T.-P.; Kawaguchi, Y. Loss of deacetylation activity of Hdac6 affects emotional behavior in mice. *PLoS One* **2012**, *7*, No. e30924.
(45) Jochems, J.; Boulden, J.; Lee, B. G.; Blendy, J. A.; Jarpe, M.; Mazitschek, R.; Van Duzer, J. H.; Jones, S.; Berton, O. Antidepressant-like properties of novel HDAC6-selective inhibitors with improved brain bioavailability. *Neuropsychopharmacology* **2014**, *39*, 389−400.
(46) d'Ydewalle, C.; Krishnan, J.; Chiheb, D. M.; Van Damme, P.; Irobi, J.; Kozikowski, A. P.; Berghe, P. V.; Timmerman, V.; Robberecht, W.; Van Den Bosch, L. HDAC6 inhibitors reverse axonal loss in a mouse model of mutant HSPB1-induced Charcot-Marie-Tooth disease. *Nat. Med.* **2011**, *17*, 968−974.
(47) Liu, J.; Gu, J.; Feng, Z.; Yang, Y.; Zhu, N.; Lu, W.; Qi, F. Both HDAC5 and HDAC6 are required for the proliferation and metastasis of melanoma cells. *J. Transl. Med.* **2016**, *14*, 7.
(48) Liu, J.; Luan, W.; Zhang, Y.; Gu, J.; Shi, Y.; Yang, Y.; Feng, Z.; Qi, F. HDAC6 interacts with PTPN1 to enhance melanoma cells progression. *Biochem. Biophys. Res. Commun.* **2018**, *495*, 2630−2636.
(49) Peng, U.; Wang, Z.; Pei, S.; Ou, Y.; Hu, P.; Liu, W.; Song, J. ACY-1215 accelerates vemurafenib induced cell death of BRAF-mutant melanoma cells via induction of ER stress and inhibition of ERK activation. *Oncol. Rep.* **2017**, *37*, 1270−1276.
(50) Lienlaf, M.; Perez-Villarroel, P.; Knox, T.; Pabon, M.; Sahakian, E.; Powers, J.; Woan, K. V.; Lee, C.; Cheng, F.; Deng, S.; Smalley, K. S. M.; Montecino, M.; Kozikowski, A.; Pinilla-Ibarz, J.; Sarnaik, A.; Seto, E.; Weber, J.; Sotomayor, E. M.; Villagra, A. Essential role of HDAC6 in the regulation of PD-L1 in melanoma. *Mol. Oncol.* **2016**, *10*, 735−750.
(51) Knox, T.; Sahakian, E.; Banik, D.; Hadley, M.; Palmer, E.; Noonepalle, S.; Kim, J.; Powers, J.; Gracia-Hernandez, M.; Oliveira, V.; Cheng, F.; Chen, J.; Barinka, C.; Pinilla-Ibarz, J.; Lee, N. H.; Kozikowski, A.; Villagra, A. Selective HDAC6 inhibitors improve anti-PD-1 immune checkpoint blockade therapy by decreasing the anti-inflammatory phenotype of macrophages and down-regulation of immunosuppressive proteins in tumor cells. *Sci. Rep.* **2019**, *9*, 6136.
(52) Huang, P.; Almeciga-Pinto, I.; Jarpe, M.; van Duzer, J. H.; Mazitschek, R.; Yang, M.; Jones, S. S.; Quayle, S. N. Selective HDAC inhibition by ACY-241 enhances the activity of paclitaxel in solid tumor models. *Oncotarget* **2017**, *8*, 2694−2707.
(53) Santo, L.; Hideshima, T.; Kung, A. L.; Tseng, J.-C.; Tamang, D.; Yang, M.; Jarpe, M.; van Duzer, J. H.; Mazitschek, R.; Ogier, W. C.; Cirstea, D.; Rodig, S.; Eda, H.; Scullen, T.; Canavese, M.; Bradner, J.; Anderson, K. C.; Jones, S. S.; Raje, N. Preclinical activity, pharmacodynamic, and pharmacokinetic properties of a selective HDAC6 inhibitor, ACY-1215, in combination with bortezomib in multiple myeloma. *Blood* **2012**, *119*, 2579−2589.
(54) Zhang, Y.; Ying, J. B.; Hong, J. J.; Li, F. C.; Fu, T. T.; Yang, F. Y.; Zheng, G. X.; Yao, X. J.; Lou, Y.; Qju, Y.; Xue, W. W.; Zhu, F. How does chirality determine the selective inhibition of histone deacetylase 6? A lesson from trichostatin A enantiomers based on molecular dynamics. *ACS Chem. Neurosci.* **2019**, *10*, 2467−2480.
(55) Butler, K. V.; Kalin, J.; Brochier, C.; Vistoli, G.; Langley, B.; Kozikowski, A. P. Rational design and simple chemistry yield a superior, neuroprotective HDAC6 inhibitor, tubastatin A. *J. Am. Chem. Soc.* **2010**, *132*, 10842−10846.
(56) Bergman, J. A.; Woan, K.; Perez-Villarroel, P.; Villagra, A.; Sotomayor, E. M.; Kozikowski, A. P. Selective histone deacetylase 6 inhibitors bearing substituted urea linkers inhibit melanoma cell growth. *J. Med. Chem.* **2012**, *55*, 9891−9899.
(57) Strebl, M. G.; Campbell, A. J.; Zhao, W.-N.; Schroeder, F. A.; Riley, M. M.; Chindavong, P. S.; Morin, T. M.; Haggarty, S. J.; Wagner, F. F.; Ritter, T.; Hooker, J. M. HDAC6 Brain Mapping with [18F]Bavarostat Enabled by a Ru-Mediated Deoxyfluorination. *ACS Cent. Sci.* **2017**, *3*, 1006−1014.
(58) De Vreese, R.; Van Steen, N.; Verhaeghe, T.; Desmet, T.; Bougarne, N.; De Bosscher, K.; Benoy, V.; Haeck, W.; Van Den Bosch, L.; D'Hooghe, M. Synthesis of benzothiophene-based hydroxamic acids as potent and selective HDAC6 inhibitors. *Chem. Commun.* **2015**, *51*, 9868−9871.
(59) Shen, S.; Benoy, V.; Bergman, J. A.; Kalin, J. H.; Frojuello, M.; Vistoli, G.; Haeck, W.; Van Den Bosch, L.; Kozikowski, A. P. Bicyclic-capped histone deacetylase 6 inhibitors with improved activity in a model of axonal Charcot-Marie-Tooth disease. *ACS Chem. Neurosci.* **2016**, *7*, 240−258.
(60) Lee, H.-Y.; Fan, S.-J.; Huang, F.-I.; Chao, H.-Y.; Hsu, K.-C.; Lin, T. E.; Yeh, T.-K.; Lai, M.-J.; Li, Y.-H.; Huang, H.-L.; Yang, C.-R.; Liou, J.-P. 5-Aroylindoles act as selective histone deacetylase 6 inhibitors ameliorating Alzheimer's disease phenotypes. *J. Med. Chem.* **2018**, *61*, 7087−7102.
(61) De Vreese, R.; Galle, L.; Depetter, Y.; Franceus, J.; Desmet, T.; Van Hecke, K.; Benoy, V.; Van Den Bosch, L.; D'hooghe, M.

DOI: 10.1021/acs.jmedchem.9b00946
J. Med. Chem. XXXX, XXX, XXX−XXX

Synthesis of potent and selective HDAC6 inhibitors bearing a cyclohexane- or cycloheptane-annulated 1,5-benzothiazepine scaffold. *Chem.—Eur. J.* **2017**, *23*, 128−136.
(62) De Vreese, R.; Depetter, Y.; Verhaeghe, T.; Desmet, T.; Benoy, V.; Haeck, W.; Van Den Bosch, L.; D'hooghe, M. Synthesis and SAR assessment of novel Tubathian analogs in the pursuit of potent and selective HDAC6 inhibitors. *Org. Biomol. Chem.* **2016**, *14*, 2537−2549.
(63) Kozikowski, A. P.; Shen, S.; Pardo, M.; Tavares, M. T.; Szarics, D.; Benoy, V.; Zimprich, C. A.; Kutil, Z.; Zhang, G.; Bařinka, C.; Robers, M. B.; Van Den Bosch, L.; Eubanks, J. H.; Jope, R. S. Brain penetrable histone deacetylase 6 inhibitor SW-100 ameliorates memory and learning impairments in a mouse model of Fragile X Syndrome. *ACS Chem. Neurosci.* **2018**, *10*, 1679−1695.
(64) Vögerl, K.; Ong, N.; Senger, J.; Herp, D.; Schmidtkunz, K.; Marek, M.; Müller, M.; Bartel, K.; Shaik, T. B.; Porter, N. J.; Robaa, D.; Christianson, D. W.; Romier, C.; Sippl, W.; Jung, M.; Bracher, F. Synthesis and biological investigation of phenothiazine-based benzhydroxamic acids as selective histone deacetylase 6 inhibitors. *J. Med. Chem.* **2019**, *62*, 1138−1166.
(65) Wang, X.-X.; Wan, R.-Z.; Liu, Z.-P. Recent advances in the discovery of potent and selective HDAC6 inhibitors. *Eur. J. Med. Chem.* **2018**, *143*, 1406−1418.
(66) De Vreese, R.; D'Hooghe, M. Synthesis and applications of benzohydroxamic acid-based histone deacetylase inhibitors. *Eur. J. Med. Chem.* **2017**, *135*, 174−195.
(67) Schlimme, S.; Hauser, A.-T.; Carafa, V.; Heinke, R.; Kannan, S.; Stolfa, D. A.; Cellamare, S.; Carotti, A.; Altucci, L.; Jung, M.; Sippl, W. Carbamate prodrug concept for hydroxamate HDAC inhibitors. *ChemMedChem* **2011**, *6*, 1193−1198.
(68) Senger, J.; Melesina, J.; Marek, M.; Romier, C.; Oehme, I.; Witt, O.; Sippl, W.; Jung, M. Synthesis and biological investigation of oxazole hydroxamates as highly selective histone deacetylase 6 (HDAC6) inhibitors. *J. Med. Chem.* **2016**, *59*, 1545−1555.
(69) Zhu, J.; Mo, J.; Lin, H.-z.; Chen, Y.; Sun, H.-p. The recent progress of isoxazole in medicinal chemistry. *Bioorg. Med. Chem.* **2018**, *26*, 3065−3075.
(70) Sysak, A.; Obmińska-Mrukowicz, B. Isoxazole ring as a useful scaffold in a search for new therapeutic agents. *Eur. J. Med. Chem.* **2017**, *137*, 292−309.
(71) Gaisina, I. N.; Tueckmantel, W.; Ugolkov, A.; Shen, S.; Hoffen, J.; Dubrovskyi, O.; Mazar, A.; Schoon, R. A.; Billadeau, D.; Kozikowski, A. P. Identification of HDAC6-selective inhibitors of low cancer cell cytotoxicity. *ChemMedChem* **2016**, *11*, 81−92.
(72) Kozikowski, A. P.; Tapadar, S.; Luchini, D. N.; Kim, K. H.; Billadeau, D. D. Use of the nitrile oxide cycloaddition (NOC) reaction for molecular probe generation: a new class of enzyme selective histone deacetylase inhibitors (HDACIs) showing picomolar activity at HDAC6. *J. Med. Chem.* **2008**, *51*, 4370−4373.
(73) Tapadar, S.; He, R.; Luchini, D. N.; Billadeau, D. D.; Kozikowski, A. P. Isoxazole moiety in the linker region of HDAC inhibitors adjacent to the Zn-chelating group: effects on HDAC biology and antiproliferative activity. *Bioorg. Med. Chem. Lett.* **2009**, *19*, 3023−3026.
(74) Daina, A.; Michielin, O.; Zoete, V. SwissADME: a free web tool to evaluate pharmacokinetics, drug-likeness and medicinal chemistry friendliness of small molecules. *Sci. Rep.* **2017**, *7*, 42717.
(75) Shen, S.; Kozikowski, A. P. Why Hydroxamates May Not Be the Best Histone Deacetylase Inhibitors-What Some May Have Forgotten or Would Rather Forget? *ChemMedChem* **2016**, *11*, 15−21.
(76) Simoni, D.; Invidiata, F. P.; Rondanin, R.; Grimaudo, S.; Cannizzo, G.; Barbusca, E.; Porretto, F.; D'Alessandro, N.; Tolomeo, M. Structure−Activity Relationship Studies of Novel Heteroretinoids: Induction of Apoptosis in the HL-60 Cell Line by a Novel Isoxazole-Containing Heteroretinoid. *J. Med. Chem.* **1999**, *42*, 4961−4969.
(77) Segretti, M. C. F.; Vallerini, G. P.; Brochier, C.; Langley, B.; Wang, L.; Hancock, W. W.; Kozikowski, A. P. Thiol-based potent and selective HDAC6 inhibitors promote tubulin acetylation and T-regulatory cell suppressive function. *ACS Med. Chem. Lett.* **2015**, *6*, 1156−1161.
(78) Lv, W.; Zhang, G.; Barinka, C.; Eubanks, J. H.; Kozikowski, A. P. Design and synthesis of mercaptoacetamides as potent, selective, and brain permeable histone deacetylase 6 inhibitors. *ACS Med. Chem. Lett.* **2017**, *8*, 510−515.
(79) Parmenon, C.; Guillard, J.; Caignard, D.-H.; Hennuyer, N.; Staels, B.; Audinot-Bouchez, V.; Boutin, J.-A.; Dacquet, C.; Ktorza, A.; Viaud-Massuard, M.-C. 4,4-Dimethyl-1,2,3,4-tetrahydroquinoline-based PPARα/γ agonists. Part I: Synthesis and pharmacological evaluation. *Bioorg. Med. Chem. Lett.* **2008**, *18*, 1617−1622.
(80) Elliott, E.-C.; Regan, S. L.; Maggs, J. L.; Bowkett, E. R.; Parry, L. J.; Williams, D. P.; Park, B. K.; Stachulski, A. V. Haloarene derivatives of carbamazepine with reduced bioactivation liabilities: 2-monohalo and 2,8-dihalo derivatives. *J. Med. Chem.* **2012**, *55*, 9773−9784.
(81) Martínez-Asencio, A.; Yus, M.; Ramón, D. J. Copper(II) acetate-catalyzed one-pot conversion of aldehydes into primary amides through a Beckmann-type rearrangement. *Tetrahedron* **2012**, *68*, 3948−3951.
(82) Dubé, D.; Scholte, A. A. Reductive N-alkylation of amides, carbamates and ureas. *Tetrahedron Lett.* **1999**, *40*, 2295−2298.
(83) Hopkins, A. L.; Groom, C. R.; Alex, A. Ligand efficiency: a useful metric for lead selection. *Drug Discovery Today* **2004**, *9*, 430−431.
(84) Johnson, T. W.; Gallego, R. A.; Edwards, M. P. Lipophilic efficiency as an important metric in drug design. *J. Med. Chem.* **2018**, *61*, 6401−6420.
(85) Porter, N. J.; Mahendran, A.; Breslow, R.; Christianson, D. W. Unusual zinc-binding mode of HDAC6-selective hydroxamate inhibitors. *Proc. Natl. Acad. Sci. U.S.A.* **2017**, *114*, 13459−13464.
(86) Porter, N. J.; Wagner, F. F.; Christianson, D. W. Entropy as a driver of selectivity for inhibitor binding to histone deacetylase 6. *Biochemistry* **2018**, *57*, 3916−3924.
(87) Porter, N. J.; Osko, J. D.; Diedrich, D.; Kurz, T.; Hooker, J. M.; Hansen, F. K.; Christianson, D. W. Histone deacetylase 6-selective inhibitors and the influence of capping groups on hydroxamate-zinc denticity. *J. Med. Chem.* **2018**, *61*, 8054−8060.
(88) Hai, Y.; Christianson, D. W. Histone deacetylase 6 structure and molecular basis of catalysis and inhibition. *Nat. Chem. Biol.* **2016**, *12*, 741−747.
(89) Robers, M. B.; Dart, M. L.; Woodroofe, C. C.; Zimprich, C. A.; Kirkland, T. A.; Machleidt, T.; Kupcho, K. R.; Levin, S.; Hartnett, J. R.; Zimmerman, K.; Niles, A. L.; Ohana, R. F.; Daniels, D. L.; Slater, M.; Wood, M. G.; Cong, M.; Cheng, Y.-Q.; Wood, K. V. Target engagement and drug residence time can be observed in living cells with BRET. *Nat. Commun.* **2015**, *6*, 10091.
(90) Mills, C. D.; Lenz, L. L.; Harris, R. A. A Breakthrough: macrophage-directed cancer immunotherapy. *Cancer Res.* **2016**, *76*, 513−516.
(91) Yang, L.; Zhang, Y. Tumor-associated macrophages: from basic research to clinical application. *J. Hematol. Oncol.* **2017**, *10*, 58.
(92) Skultetyova, L.; Ustinova, K.; Kutil, Z.; Novakova, Z.; Pavlicek, J.; Mikesova, J.; Trapl, D.; Baranova, P.; Havlinova, B.; Hubalek, M.; Lansky, Z.; Barinka, C. Human histone deacetylase 6 shows strong preference for tubulin dimers over assembled microtubules. *Sci. Rep.* **2017**, *7*, 11547.
(93) Kutil, Z.; Novakova, Z.; Meleshin, M.; Mikesova, J.; Schutkowski, M.; Barinka, C. Histone deacetylase 11 is a fatty-acid deacylase. *ACS Chem. Biol.* **2018**, *13*, 685−693.
(94) Wu, H.; Yang, K.; Zhang, Z.; Leisten, E. D.; Li, Z.; Xie, H.; Liu, J.; Smith, K. A.; Novakova, Z.; Barinka, C.; Tang, W. Development of multi-functional histone deacetylase 6 degraders with potent anti-myeloma activity. *J. Med. Chem.* **2019**, *62*, 7042−7057.
(95) Sparta, K. M.; Krug, M.; Heinemann, U.; Mueller, U.; Weiss, M. S. Xdsapp2.0. *J. Appl. Crystallogr.* **2016**, *49*, 1085−1092.
(96) Vagin, A. A.; Steiner, R. A.; Lebedev, A. A.; Potterton, L.; McNicholas, S.; Long, F.; Murshudov, G. N. REFMAC5 dictionary:

DOI: 10.1021/acs.jmedchem.9b00946
J. Med. Chem. XXXX, XXX, XXX−XXX

organization of prior chemical knowledge and guidelines for its use. *Acta Crystallogr., Sect. D: Biol. Crystallogr.* **2004**, *60*, 2184−2195.
(97) Emsley, P.; Lohkamp, B.; Scott, W. G.; Cowtan, K. Features and development ofCoot. *Acta Crystallogr., Sect. D: Biol. Crystallogr.* **2010**, *66*, 486−501.
(98) Long, F.; Nicholls, R. A.; Emsley, P.; Gražulis, S.; Merkys, A.; Vaitkus, A.; Murshudov, G. N. AceDRG: a stereochemical description generator for ligands. *Acta Crystallogr., Sect. D: Struct. Biol.* **2017**, *73*, 112−122.
(99) Chen, V. B.; Arendall, W. B.; Headd, J. J.; Keedy, D. A.; Immormino, R. M.; Kapral, G. J.; Murray, L. W.; Richardson, J. S.; Richardson, D. C. MolProbity: all-atom structure validation for macromolecular crystallography. *Acta Crystallogr., Sect. D: Biol. Crystallogr.* **2010**, *66*, 12−21.
(100) Koya, R. C.; Mok, S.; Otte, N.; Blacketor, K. J.; Comin-Anduix, B.; Tumeh, P. C.; Minasyan, A.; Graham, N. A.; Graeber, T. G.; Chodon, T.; Ribas, A. BRAF inhibitor vemurafenib improves the antitumor activity of adoptive cell immunotherapy. *Cancer Res.* **2012**, *72*, 3928−3937.
(101) Pfaffl, M. W. A new mathematical model for relative quantification in real-time RT-PCR. *Nucleic Acids Res.* **2001**, *29*, No. e45.

DOI: 10.1021/acs.jmedchem.9b00946
J. Med. Chem. XXXX, XXX, XXX−XXX

3 Discussion and conclusions

Being connected to various disorders in humans, HDAC6 has drawn attention to the investigation of its functions and role in the cell. HDAC6 regulates a myriad of molecular processes through the deacetylase domains and the ubiquitin-binding domain. HDAC6 increases cell motility by α-tubulin and cortactin deacetylation. The functionality of the ubiquitin-binding domain is critical for the HDAC6-regulated cell responses to stress. Being a multidomain protein, it is likely that each domain of HDAC6 may fulfill its own function and be responsible for interaction with various partners. The knowledge of the exact function of each separate domain will broaden our understanding of the HDAC6 function and involvement in regulatory mechanisms.

During the last two decades, HDAC6 has been studied by numerous research groups, however, the information about HDAC6 preference for different tubulin forms as well as kinetic analysis is missing. While the enzymatic properties of α-TAT, for a major tubulin acetylase, on tubulin and microtubule substrates have been elucidated in detail, the same information about HDAC6 is virtually absent. For this reason, the detailed kinetic study and the mechanism of HDAC6 interaction with tubulin and its polymer (microtubules) were addressed by our work and publications presented in the thesis.

It was shown by Hubbert et al. in 2002 that mouse HDAC6 deacetylates assembled, but not free tubulin (27). However, several controversial studies reported HDAC6 preference for tubulin vs microtubules with no quantitative data presented to evaluate substrate preferences. Matsuyama et al., have shown the deacetylation of tubulin dimers by mouse HDAC6 (73). At the same time, North et al. reported that HDAC6 deacetylates tubulin dimers as well as microtubules (149). It is worth noticing that in these studies either partially purified HDAC6 or different truncated HDAC6 orthologs (murine/zebrafish) were typically used leading thus to inconsistencies in the published data (150). To avoid this issue, we have used untagged human wild type HDAC6 in our studies. The enzymatic activity of purified HDAC6 was tested and compared with the ones described in the literature. The K_m values were in good accord with the literature (31,151,152). The IC_{50} values for HDAC6 inhibitors SAHA (153), trichostatin A (TSA), and Nexturastat A (154) were determined and also fitted well to ones already published.

Furthermore, we have performed a detailed kinetic analysis of tubulin and tubulin polymers deacetylation by HDAC6. HDAC6 showed a preference for free tubulin dimers over microtubules with the deacetylation rate 1500-fold higher – 0.6 mol/mol*s and 0.0004 mol/mol*s, respectively. Miyake et al. observed a 2.5-fold difference in the deacetylation rate while using HDAC6 catalytic core in their assay (151). This difference in the deacetylation rate may suggest the importance of domains outside the catalytic core in the recognition of tubulin dimers and microtubules as a substrate. Additionally, this supports the hypothesis about opposing substrate preferences of HDAC6 and αTAT1.

Several different tubulin polymers were prepared and tested to see whether the HDAC6 preference for tubulin dimers is mainly caused by the accessibility of the acetylated αK40 loop. The

deacetylation rate of Dolastatin-10 rings and Zn-sheets was 100-fold and 750-fold slower than of free tubulin dimers. These findings suggest that both lateral and longitudinal interactions in the polymerized tubulin lattice are crucial for HDAC6 recognition and deacetylation.

The K40 is located in the flexible loop comprised of 20 amino acids evolutionary conserved in tubulin from different species. The impact of neighboring amino acids of the αK40 loop on HDAC6 substrate recognition has not been described. The HDAC6 deacetylation of the T3–T19 peptides, derived from conserved αK40 loop sequence, clearly shows that amino acids beyond positions P−1 and P+1 around the central lysine are not critical for the recognition of the peptidic substrates by HDAC6. This finding indicates that the enzyme is rather promiscuous at the peptide level and such promiscuity has been also observed in experiments using human acetylome microarrays (155). Consequently, sequential and/or structural motifs away from the central lysine and their interactions with residues outside the active pocket of HDAC6 might be of critical importance to define substrate specificity at the protein level (156). This is supported by findings that H20-21 loops and the H25 helix of HDAC6 are important for the α-tubulin recognition (151). The unique position of H20-21 loops and the H25 helix in DD2 are critical for the substrate recognition, as the replacement of the loops impaired the HDAC6 deacetylation activity on α-tubulin (151). Moreover, due to the special conformation of the loop following the H25 helix, HDAC6 uniquely possesses a large open basis (∼14 Å wide) that provides the selectivity for Nexturastat A and TSA (151). Therefore, there is a clear difference between the recognition and deacetylation of peptidic substrates and tubulin dimers.

The mechanism of microtubule deacetylation remains an unanswered question up-to-now. It has been reported that αTAT1 acetylates microtubules evenly via entering their lumen without tip preference or lattice breakage (157). Other studies have shown that αTAT1 can enter microtubule-lumen through bends and breaks of the microtubule-lattice, but does not move efficiently inside the microtubules (158). Furthermore, the mobility of αTAT1 in the microtubule lumen is controlled by the affinity of αTAT1 for its binding sites, which are highly concentrated there (158). The absence of such information about HDAC6 inspired us to shed light on this question. Using TIRF microscopy, we have visualized the direct interaction of HDAC6 and microtubules showing its fast kinetics and uniform binding without tip preferences suggesting its binding to microtubules' outer surface than entering the lumen of microtubules. We have shown that the binding pattern of HDAC6 corresponds with the deacetylation pattern. Further analysis has shown that the deacetylation of microtubules by HDAC6 is linear in time. At the same time, however, it is still not clear how microtubules are deacetylated by HDAC6 and if HDAC6 can enter microtubule lumen. These questions warrant further studies.

Consequently, we assume that obtained data support the hypothesis of αTAT1 and HDAC6 being the main tubulin acetylase and deacetylase, respectively. The preference of HDAC6 for free tubulin instead of assembled microtubules, leads to pronounced acetylation of stable long-living microtubules, supporting the idea of acetylation as an age marker for microtubules (157).

A desire to understand the mechanism of HDAC6 tubulin/microtubule interactions led us to the question “what is the interacting interface of both molecules?”.

HDAC6, as well as the majority of eukaryotic proteins, contains both structured and disordered regions (159). Up-to-now, a lot of efforts have been invested in studying the role of DD2 and BUZ domains, which have a compact fold. However, much less is known about other domains, especially intrinsically disordered regions – the N-terminal domain and the SE14 domain. The investigations are mainly focused on catalytic core domains, although it is very likely that N- and C-terminal regions play particularly important roles in substrate recognition. It was already shown that the acetylation of lysines outside the catalytic core of HDAC1 (K432, K438, K439, and K441) attenuates its deacetylation activity (160).

In our study, we show that the N-terminal intrinsically disordered region of HDAC6 is mediating interactions with tubulin/microtubules. It is known that the N-terminus harbors NES and NLS as well as two lysine-rich clusters. We have discovered that the acetylation status of lysine clusters of the N-terminus of HDAC6 is critical for its interactions with tubulin/microtubules. By point-mutations of each of these clusters, we have identified the second cluster to be crucial for HDAC6 binding to tubulin. In total, HDAC6 harbors 5 lysine clusters located along its sequence which can be acetylated by p300 thus regulating its function (26). The remaining three lysine-rich sites are located in the DD2 domain and the SE14 domain and have no impact on HDAC6 interaction with tubulin. However, they may be critical in other HDAC6 physiological functions. For example, the SE14 domain has been reported to be responsible for the stable retention of human HDAC6 in the cytoplasm (25).

The detailed analysis of the HDAC6 N-terminus revealed its high phylogenetic conservation and pronounced cationic character. We proved that HDAC6/tubulin interactions are based on ionic attraction forces and promoted by positively charged lysines of HDAC6 and negatively charged tubulin/microtubule surface. As the N-terminus is conserved among species, interactions of HDAC6 orthologs (*D.rerio* and *Mus musculus*) with microtubules were shown as well. The role of positively charged lysines has been corroborated by suing the HDAC6 mutant with lysines replaced by arginines in the second cluster had similar to WT deacetylase activity in eukaryotic cells. This suggests, that HDAC6 tubulin/microtubules interactions are triggered not by a specific sequential motif, but rather by overall charge. This notion was supported by testing of a scrambled sequence of the MBD, which was bound to microtubules with the same affinity as the WT. The N-terminus of HDAC6 orthologs contains 11 to 16 positively charged amino acids. However, species from *D.rerio* to *H.sapiens* have these amino acids organized into patches. It is interesting to note that some HDAC6 orthologs, such as *Penaeus vannamei*, *Ascaris lumbricoides* and *Nephila clavipes* do not show cationic character but rather neutral (pI = ~6.0, calculated from the sequence). It remains an open question of whether patch organization of lysines is critical for the regulation of HDAC6 interaction with tubulin and possible with other substrates. The knowledge of exact mechanisms of HDAC6 interaction with certain substrates

might help us to design HDAC6-specific compounds that could selectively block the deacetylation of a certain chosen (defined) substrate.

Generally, pan-inhibitors of HDACs show antitumor activity through inhibiting proliferation and improving immune responses (107). The HDAC protein family is a therapeutic target for cancer treatment and the FDA-approved nonselective inhibitors are used nowadays (vorinostat, romidepsin, panobinostat, belinostat, and chidamide) (161). HDACs affect multiple targets in the cell, thus it is important to understand the exact role of individual HDACs in pathological processes and to develop isoform-specific HDAC inhibitors. Off-targeting other HDAC proteins might cause organism dysfunctions – for example, HDAC1-null mice die before 10.5 days having severe proliferation defects (162), lethal defects appear after deletion of *hdac1* in zebrafish (163). It has been shown that conditional HDAC1 deletion in the heart, brain, and the muscles was tolerated in mice most likely due to redundancy with HDAC2, but the global deletion of HDAC1 and HDAC2 resulted in lethal phenotypes (162). So, the main obstacle in the development of new HDAC6 inhibitors is to ensure their high selectivity together with good pharmacokinetic profile, low toxicity, and minimal adverse effects.

Melanoma is the most dangerous type of skin cancer with high metastasis, rapid disease progression, and high mortality (164,165). Last five years, advanced-stage melanoma patients are treated using immunotherapy because this approach has shown longer overall survival. It has been shown that HDAC6 is highly expressed and required for melanoma cell proliferation and metastasis, therefore two partially selective HDAC6 inhibitors (ricolinostat and citarinostat) were used in clinical trials through monotherapy or combinatorial approach (166). In prior studies, it has been shown that anti-PD1 monoclonal antibodies appeared to be less toxic and more acceptable for melanoma treatment. Moreover, the selective pharmacological inhibition of HDAC6 downregulates the PD-L1 expression and is important for the immune checkpoint blockade (167,168). Recently it was discovered that the combination of selective HDAC6 inhibitor Nexturastat A and PD-1 immune blockade improved antitumor immune response and was much more effective than monotherapy (148). Being a promising melanoma therapy, we aimed to develop a highly selective HDAC6 inhibitor with a good pharmacologic profile.

The novel highly selective inhibitor was discovered harboring isoxazole moiety as a zinc-binding group – SS-208. This isoxazole-3-hydroxamate-based inhibitor has been selected based on the ligand efficiency evaluation and modest potency against HDAC1. Compared with the selective HDAC6 inhibitor Nexturastat A, the SS-208 inhibitor exhibited similar nanomolar inhibitory activity. The advantage of the SS-208 inhibitor is in its higher selectivity over all other HDAC isoforms (minimum 100-fold difference in IC_{50} values) associated with less adverse effects.

SS-208 in a complex with the catalytic domain 2 of HDAC6 from *D.rerio* was crystallized and the structure was solved to an ultra-high resolution limit of 1.15 Å. It showed that the SS-208 inhibitor has bidentate coordination of the active-site zinc ion that differs from typical a monodentate coordination

observed for phenylhydroxamate-based inhibitors (169). The bidentate coordination is typically observed when the inhibitor contains either flexible aliphatic linkers or aromatic linkers lacking the cap (170). The bidentate coordination mode is more stable than the monodentate coordination mode (171). Moreover, the inhibitor did not cause major structural rearrangements of the active tunnel of HDAC6. Consequently, the SS-208 inhibitor showed the same HDAC inhibitory potency as Nexturastat A and Tubastatin A across human and murine cancer cell lines *in vitro*. It is worth mentioning that the M1 macrophage phenotype is associated with a better prognosis and the M2 macrophage infiltration is associated with a bad prognosis in cancer (172,173). Moreover, while treating mice with the SS-208 inhibitor, the increased ratio of M1 and M2 macrophages has been observed. Altogether these findings prove that SS-208 impairs tumor growth by mediating immune-related antitumor activity having similar immunological properties as previously mentioned Nexturastat A (174).

To summarize the thesis, I have demonstrated the importance of HDAC6 as the main tubulin deacetylase, regulating a myriad of cellular processes. It is apparent that HDAC6 recruits various proteins and can be regulated through the interaction with them. Therefore, the research may aim at the identification of HDAC6 interaction with its partners and at the rational design of inhibitors that interrupt protein-protein interactions, for example, the inhibitors targeting tubulin deacetylation. In the publications included in this thesis, we addressed several aspects of HDAC6 functioning - from HDAC6-mediated tubulin deacetylation to the development of HDAC6-specific inhibitors.

We thoroughly analyzed the kinetics of tubulin deacetylation and visualized the interaction of HDAC6 with microtubules with their subsequent deacetylation. Next, we analyzed these interactions at the single-molecule level and determined the affinity of HDAC6 to tubulin and microtubules. Furthermore, we have designed a highly selective HDAC6 inhibitor with good pharmacological properties and the ability to mediate immune-related antitumor activity. Overall, the work presented here contributed to the growing pool of knowledge on HDAC6, its mechanism of interaction with tubulin, and its prominence as a therapeutic target.

References

1. Taunton, J., Hassig, C. A., and Schreiber, S. L. (1996) A mammalian histone deacetylase related to the yeast transcriptional regulator Rpd3p. *Science* **272**, 408-411
2. Gray, S. G., Eriksson, T., and Ekstrom, T. J. (1999) Methylation, gene expression and the chromatin connection in cancer (review). *Int J Mol Med* **4**, 333-350
3. Berger, S. L. (2007) The complex language of chromatin regulation during transcription. *Nature* **447**, 407-412
4. Shahbazian, M. D., and Grunstein, M. (2007) Functions of site-specific histone acetylation and deacetylation. *Annu Rev Biochem* **76**, 75-100
5. Abel, T., and Zukin, R. S. (2008) Epigenetic targets of HDAC inhibition in neurodegenerative and psychiatric disorders. *Curr Opin Pharmacol* **8**, 57-64
6. Joshi, P., Greco, T. M., Guise, A. J., Luo, Y., Yu, F., Nesvizhskii, A. I., and Cristea, I. M. (2013) The functional interactome landscape of the human histone deacetylase family. *Mol Syst Biol* **9**, 672
7. Blander, G., and Guarente, L. (2004) The Sir2 family of protein deacetylases. *Annu Rev Biochem* **73**, 417-435
8. Bertrand, P. (2010) Inside HDAC with HDAC inhibitors. *Eur J Med Chem* **45**, 2095-2116
9. Gregoretti, I. V., Lee, Y. M., and Goodson, H. V. (2004) Molecular evolution of the histone deacetylase family: functional implications of phylogenetic analysis. *J Mol Biol* **338**, 17-31
10. Fischle, W., Kiermer, V., Dequiedt, F., and Verdin, E. (2001) The emerging role of class II histone deacetylases. *Biochem Cell Biol* **79**, 337-348
11. Valenzuela-Fernandez, A., Cabrero, J. R., Serrador, J. M., and Sanchez-Madrid, F. (2008) HDAC6: a key regulator of cytoskeleton, cell migration and cell-cell interactions. *Trends Cell Biol* **18**, 291-297
12. Lahm, A., Paolini, C., Pallaoro, M., Nardi, M. C., Jones, P., Neddermann, P., Sambucini, S., Bottomley, M. J., Lo Surdo, P., Carfi, A., Koch, U., De Francesco, R., Steinkuhler, C., and Gallinari, P. (2007) Unraveling the hidden catalytic activity of vertebrate class Ila histone deacetylases. *P Natl Acad Sci USA* **104**, 17335-17340
13. Gao, L., Cueto, M. A., Asselbergs, F., and Atadja, P. (2002) Cloning and functional characterization of HDAC11, a novel member of the human histone deacetylase family. *J Biol Chem* **277**, 25748-25755
14. Mahlknecht, U., Schnittger, S., Landgraf, F., Schoch, C., Ottmann, O. G., Hiddemann, W., and Hoelzer, D. (2001) Assignment of the human histone deacetylase 6 gene (HDAC6) to X chromosome p11.23 by in situ hybridization. *Cytogenet Cell Genet* **93**, 135-136
15. Voelter-Mahlknecht, S., and Mahlknecht, U. (2003) Cloning and structural characterization of the human histone deacetylase 6 gene. *Int J Mol Med* **12**, 87-93
16. Verdel, A., and Khochbin, S. (1999) Identification of a new family of higher eukaryotic histone deacetylases. Coordinate expression of differentiation-dependent chromatin modifiers. *J Biol Chem* **274**, 2440-2445
17. Grozinger, C. M., Hassig, C. A., and Schreiber, S. L. (1999) Three proteins define a class of human histone deacetylases related to yeast Hda1p. *Proc Natl Acad Sci U S A* **96**, 4868-4873
18. Barlow, A. L., van Drunen, C. M., Johnson, C. A., Tweedie, S., Bird, A., and Turner, B. M. (2001) dSIR2 and dHDAC6: two novel, inhibitor-resistant deacetylases in Drosophila melanogaster. *Exp Cell Res* **265**, 90-103
19. Yang, X. J., and Gregoire, S. (2005) Class II histone deacetylases: from sequence to function, regulation, and clinical implication. *Mol Cell Biol* **25**, 2873-2884
20. Zhuang, Y., Nguyen, H. T., Lasky, J. A., Cao, S., Li, C., Hu, J., Guo, X., Burow, M. E., and Shan, B. (2010) Requirement of a novel splicing variant of human histone deacetylase 6 for TGF-beta1-mediated gene activation. *Biochem Biophys Res Commun* **392**, 608-613
21. Uhlen, M., Fagerberg, L., Hallstrom, B. M., Lindskog, C., Oksvold, P., Mardinoglu, A., Sivertsson, A., Kampf, C., Sjostedt, E., Asplund, A., Olsson, I., Edlund, K., Lundberg, E., Navani, S., Szigyarto, C. A., Odeberg, J., Djureinovic, D., Takanen, J. O., Hober, S., Alm, T., Edqvist, P. H., Berling, H., Tegel, H., Mulder, J., Rockberg, J., Nilsson, P., Schwenk, J. M., Hamsten, M., von Feilitzen, K., Forsberg, M., Persson, L., Johansson, F., Zwahlen, M., von

Heijne, G., Nielsen, J., and Ponten, F. (2015) Proteomics. Tissue-based map of the human proteome. *Science* **347**, 1260419
22. Saji, S., Kawakami, M., Hayashi, S., Yoshida, N., Hirose, M., Horiguchi, S., Itoh, A., Funata, N., Schreiber, S. L., Yoshida, M., and Toi, M. (2005) Significance of HDAC6 regulation via estrogen signaling for cell motility and prognosis in estrogen receptor-positive breast cancer. *Oncogene* **24**, 4531-4539
23. Lee, Y. S., Lim, K. H., Guo, X., Kawaguchi, Y., Gao, Y., Barrientos, T., Ordentlich, P., Wang, X. F., Counter, C. M., and Yao, T. P. (2008) The cytoplasmic deacetylase HDAC6 is required for efficient oncogenic tumorigenesis. *Cancer Res* **68**, 7561-7569
24. Verdel, A., Curtet, S., Brocard, M. P., Rousseaux, S., Lemercier, C., Yoshida, M., and Khochbin, S. (2000) Active maintenance of mHDA2/mHDAC6 histone-deacetylase in the cytoplasm. *Curr Biol* **10**, 747-749
25. Bertos, N. R., Gilquin, B., Chan, G. K., Yen, T. J., Khochbin, S., and Yang, X. J. (2004) Role of the tetradecapeptide repeat domain of human histone deacetylase 6 in cytoplasmic retention. *J Biol Chem* **279**, 48246-48254
26. Liu, Y., Peng, L., Seto, E., Huang, S., and Qiu, Y. (2012) Modulation of histone deacetylase 6 (HDAC6) nuclear import and tubulin deacetylase activity through acetylation. *J Biol Chem* **287**, 29168-29174
27. Hubbert, C., Guardiola, A., Shao, R., Kawaguchi, Y., Ito, A., Nixon, A., Yoshida, M., Wang, X. F., and Yao, T. P. (2002) HDAC6 is a microtubule-associated deacetylase. *Nature* **417**, 455-458
28. Zhang, Y., Li, N., Caron, C., Matthias, G., Hess, D., Khochbin, S., and Matthias, P. (2003) HDAC-6 interacts with and deacetylates tubulin and microtubules in vivo. *Embo J* **22**, 1168-1179
29. Zhang, Y., Gilquin, B., Khochbin, S., and Matthias, P. (2006) Two catalytic domains are required for protein deacetylation. *J Biol Chem* **281**, 2401-2404
30. Haggarty, S. J., Koeller, K. M., Wong, J. C., Grozinger, C. M., and Schreiber, S. L. (2003) Domain-selective small-molecule inhibitor of histone deacetylase 6 (HDAC6)-mediated tubulin deacetylation. *Proc Natl Acad Sci U S A* **100**, 4389-4394
31. Zou, H., Wu, Y., Navre, M., and Sang, B. C. (2006) Characterization of the two catalytic domains in histone deacetylase 6. *Biochem Biophys Res Commun* **341**, 45-50
32. Osko, J. D., and Christianson, D. W. (2019) Structural Basis of Catalysis and Inhibition of HDAC6 CD1, the Enigmatic Catalytic Domain of Histone Deacetylase 6. *Biochemistry-Us* **58**, 4912-4924
33. Kawaguchi, Y., Kovacs, J. J., McLaurin, A., Vance, J. M., Ito, A., and Yao, T. P. (2003) The deacetylase HDAC6 regulates aggresome formation and cell viability in response to misfolded protein stress. *Cell* **115**, 727-738
34. Bertos, N. R., Wang, A. H., and Yang, X. J. (2001) Class II histone deacetylases: structure, function, and regulation. *Biochem Cell Biol* **79**, 243-252
35. Boyault, C., Gilquin, B., Zhang, Y., Rybin, V., Garman, E., Meyer-Klaucke, W., Matthias, P., Muller, C. W., and Khochbin, S. (2006) HDAC6-p97/VCP controlled polyubiquitin chain turnover. *Embo J* **25**, 3357-3366
36. Hook, S. S., Orian, A., Cowley, S. M., and Eisenman, R. N. (2002) Histone deacetylase 6 binds polyubiquitin through its zinc finger (PAZ domain) and copurifies with deubiquitinating enzymes. *Proc Natl Acad Sci U S A* **99**, 13425-13430
37. Seigneurin-Berny, D., Verdel, A., Curtet, S., Lemercier, C., Garin, J., Rousseaux, S., and Khochbin, S. (2001) Identification of components of the murine histone deacetylase 6 complex: link between acetylation and ubiquitination signaling pathways. *Mol Cell Biol* **21**, 8035-8044
38. Carolina dos S. Passos, N. D., Yun Choi, Robert E. Cohen, Remo Perozzo, Alessandra Nurisso, Claudia A. Simões-Pires,. (2017) Methods for addressing the protein-protein interaction between histone deacetylase 6 and ubiquitin. *bioRxiv*
39. Ouyang, H., Ali, Y. O., Ravichandran, M., Dong, A., Qiu, W., MacKenzie, F., Dhe-Paganon, S., Arrowsmith, C. H., and Zhai, R. G. (2012) Protein aggregates are recruited to aggresome by histone deacetylase 6 via unanchored ubiquitin C termini. *J Biol Chem* **287**, 2317-2327
40. Hai, Y., and Christianson, D. W. (2016) Histone deacetylase 6 structure and molecular basis of catalysis and inhibition. *Nat Chem Biol* **12**, 741-747

41. Aldana-Masangkay, G. I., and Sakamoto, K. M. (2011) The role of HDAC6 in cancer. *J Biomed Biotechnol* **2011**, 875824
42. Destaing, O., Saltel, F., Gilquin, B., Chabadel, A., Khochbin, S., Ory, S., and Jurdic, P. (2005) A novel Rho-mDia2-HDAC6 pathway controls podosome patterning through microtubule acetylation in osteoclasts. *J Cell Sci* **118**, 2901-2911
43. Boyault, C., Sadoul, K., Pabion, M., and Khochbin, S. (2007) HDAC6, at the crossroads between cytoskeleton and cell signaling by acetylation and ubiquitination. *Oncogene* **26**, 5468-5476
44. Lucas, R. M., Bauer, C. S., Chinnaiya, K., Schwartzentruber, A. l., MacDonald, R., Collins, M. O., Aasly, J. O., Br ├┐ nstad, G., Ferraiuolo, L., Mortiboys, H., and Vos, K. J. D. (2019) LRRK2-mediated phosphorylation of HDAC6 regulates HDAC6-cytoplasmic dynein interaction and aggresome formation. *bioRxiv*, 554881
45. Atabakhsh, E., Bryce, D. M., Lefebvre, K. J., and Schild-Poulter, C. (2009) RanBPM Has Proapoptotic Activities That Regulate Cell Death Pathways in Response to DNA Damage. *Mol Cancer Res* **7**, 1962-1972
46. Salemi, L. M., Almawi, A. W., Lefebvre, K. J., and Schild-Poulter, C. (2014) Aggresome formation is regulated by RanBPM through an interaction with HDAC6. *Biol Open* **3**, 418-430
47. Salemi, L. M., Maitland, M. E. R., Yefet, E. R., and Schild-Poulter, C. (2017) Inhibition of HDAC6 activity through interaction with RanBPM and its associated CTLH complex. *BMC Cancer* **17**, 460
48. Liu, L. T., Chang, H. C., Chiang, L. C., and Hung, W. C. (2003) Histone deacetylase inhibitor up-regulates RECK to inhibit MMP-2 activation and cancer cell invasion. *Cancer Res* **63**, 3069-3072
49. Parab, S., Shetty, O., Gaonkar, R., Balasinor, N., Khole, V., and Parte, P. (2015) HDAC6 deacetylates alpha tubulin in sperm and modulates sperm motility in Holtzman rat. *Cell Tissue Res* **359**, 665-678
50. Zhang, X., Yuan, Z., Zhang, Y., Yong, S., Salas-Burgos, A., Koomen, J., Olashaw, N., Parsons, J. T., Yang, X. J., Dent, S. R., Yao, T. P., Lane, W. S., and Seto, E. (2007) HDAC6 modulates cell motility by altering the acetylation level of cortactin. *Mol Cell* **27**, 197-213
51. Chen, S., Owens, G. C., Makarenkova, H., and Edelman, D. B. (2010) HDAC6 regulates mitochondrial transport in hippocampal neurons. *PLoS One* **5**, e10848
52. Kalinski, A. L., Kar, A. N., Craver, J., Tosolini, A. P., Sleigh, J. N., Lee, S. J., Hawthorne, A., Brito-Vargas, P., Miller-Randolph, S., Passino, R., Shi, L., Wong, V. S. C., Picci, C., Smith, D. S., Willis, D. E., Havton, L. A., Schiavo, G., Giger, R. J., Langley, B., and Twiss, J. L. (2019) Deacetylation of Miro1 by HDAC6 blocks mitochondrial transport and mediates axon growth inhibition. *J Cell Biol* **218**, 1871-1890
53. Riolo, M. T., Cooper, Z. A., Holloway, M. P., Cheng, Y., Bianchi, C., Yakirevich, E., Ma, L., Chin, Y. E., and Altura, R. A. (2012) Histone deacetylase 6 (HDAC6) deacetylates survivin for its nuclear export in breast cancer. *J Biol Chem* **287**, 10885-10893
54. Hansen, B. K., Gupta, R., Baldus, L., Lyon, D., Narita, T., Lammers, M., Choudhary, C., and Weinert, B. T. (2019) Analysis of human acetylation stoichiometry defines mechanistic constraints on protein regulation. *Nat Commun* **10**
55. Kim, S. C., Sprung, R., Chen, Y., Xu, Y. D., Ball, H., Pei, J. M., Cheng, T. L., Kho, Y., Xiao, H., Xiao, L., Grishin, N. V., White, M., Yang, X. J., and Zhao, Y. M. (2006) Substrate and functional diversity of lysine acetylation revealed by a proteomics survey. *Mol Cell* **23**, 607-618
56. Choudhary, C., Kumar, C., Gnad, F., Nielsen, M. L., Rehman, M., Walther, T. C., Olsen, J. V., and Mann, M. (2009) Lysine acetylation targets protein complexes and co-regulates major cellular functions. *Science* **325**, 834-840
57. Zhang, Y., Zhang, M., Dong, H., Yong, S., Li, X., Olashaw, N., Kruk, P. A., Cheng, J. Q., Bai, W., Chen, J., Nicosia, S. V., and Zhang, X. (2009) Deacetylation of cortactin by SIRT1 promotes cell migration. *Oncogene* **28**, 445-460
58. Gupta, M. P., Samant, S. A., Smith, S. H., and Shroff, S. G. (2008) HDAC4 and PCAF bind to cardiac sarcomeres and play a role in regulating myofilament contractile activity. *J Biol Chem* **283**, 10135-10146

59. Arakawa, Y., Cordeiro, J. V., and Way, M. (2007) F11L-mediated inhibition of RhoA-mDia signaling stimulates microtubule dynamics during Vaccinia virus infection. *Cell Host Microbe* **1**, 213-226
60. Tien, S. C., and Chang, Z. F. (2014) Oncogenic Shp2 disturbs microtubule regulation to cause HDAC6-dependent ERK hyperactivation. *Oncogene* **33**, 2938-2946
61. Guo, D., Song, X. H., Guo, T. F., Gu, S. G., Chang, X. L., Su, T., Yang, X. H., Liang, B., and Huang, D. Y. (2018) Vimentin acetylation is involved in SIRT5-mediated hepatocellular carcinoma migration. *Am J Cancer Res* **8**, 2453-2466
62. Simonsson, M., Heldin, C. H., Ericsson, J., and Gronroos, E. (2005) The balance between acetylation and deacetylation controls Smad7 stability. *Journal of Biological Chemistry* **280**, 21797-21803
63. Kume, S., Haneda, M., Kanasaki, K., Sugimoto, T., Araki, S., Isshiki, K., Isono, M., Uzu, T., Guarente, L., Kashiwagi, A., and Koya, D. (2007) SIRT1 inhibits transforming growth factor beta-induced apoptosis in glomerular mesangial cells via Smad7 deacetylation. *J Biol Chem* **282**, 151-158
64. Sadoul, K., Boyault, C., Pabion, M., and Khochbin, S. (2008) Regulation of protein turnover by acetyltransferases and deacetylases. *Biochimie* **90**, 306-312
65. Wang, X. J., Taplick, J., Geva, N., and Oren, M. (2004) Inhibition of p53 degradation by Mdm2 acetylation. *Febs Lett* **561**, 195-201
66. Saito, M., Hess, D., Eglinger, J., Fritsch, A. W., Kreysing, M., Weinert, B. T., Choudhary, C., and Matthias, P. (2019) Acetylation of intrinsically disordered regions regulates phase separation. *Nat Chem Biol* **15**, 51-+
67. Borgas, D., Chambers, E., Newton, J., Ko, J., Rivera, S., Rounds, S., and Lu, Q. (2016) Cigarette Smoke Disrupted Lung Endothelial Barrier Integrity and Increased Susceptibility to Acute Lung Injury via Histone Deacetylase 6. *Am J Respir Cell Mol Biol* **54**, 683-696
68. Watabe, M., and Nakaki, T. (2011) Protein kinase CK2 regulates the formation and clearance of aggresomes in response to stress. *J Cell Sci* **124**, 1519-1532
69. Deribe, Y. L., Wild, P., Chandrashaker, A., Curak, J., Schmidt, M. H., Kalaidzidis, Y., Milutinovic, N., Kratchmarova, I., Buerkle, L., Fetchko, M. J., Schmidt, P., Kittanakom, S., Brown, K. R., Jurisica, I., Blagoev, B., Zerial, M., Stagljar, I., and Dikic, I. (2009) Regulation of epidermal growth factor receptor trafficking by lysine deacetylase HDAC6. *Sci Signal* **2**, ra84
70. Williams, K. A., Zhang, M., Xiang, S., Hu, C., Wu, J. Y., Zhang, S., Ryan, M., Cox, A. D., Der, C. J., Fang, B., Koomen, J., Haura, E., Bepler, G., Nicosia, S. V., Matthias, P., Wang, C., Bai, W., and Zhang, X. (2013) Extracellular signal-regulated kinase (ERK) phosphorylates histone deacetylase 6 (HDAC6) at serine 1035 to stimulate cell migration. *J Biol Chem* **288**, 33156-33170
71. Lafarga, V., Aymerich, I., Tapia, O., Mayor, F., Jr., and Penela, P. (2012) A novel GRK2/HDAC6 interaction modulates cell spreading and motility. *Embo J* **31**, 856-869
72. Novakova, Z., Wozniak, K., Jancarik, A., Rais, R., Wu, Y., Pavlicek, J., Ferraris, D., Havlinova, B., Ptacek, J., Vavra, J., Hin, N., Rojas, C., Majer, P., Slusher, B. S., Tsukamoto, T., and Barinka, C. (2016) Unprecedented Binding Mode of Hydroxamate-Based Inhibitors of Glutamate Carboxypeptidase II: Structural Characterization and Biological Activity. *J Med Chem* **59**, 4539-4550
73. Matsuyama, A., Shimazu, T., Sumida, Y., Saito, A., Yoshimatsu, Y., Seigneurin-Berny, D., Osada, H., Komatsu, Y., Nishino, N., Khochbin, S., Horinouchi, S., and Yoshida, M. (2002) In vivo destabilization of dynamic microtubules by HDAC6-mediated deacetylation. *Embo J* **21**, 6820-6831
74. Sadoul, K., and Khochbin, S. (2016) The growing landscape of tubulin acetylation: lysine 40 and many more. *Biochem J* **473**, 1859-1868
75. Portran, D., Schaedel, L., Xu, Z. J., Thery, M., and Nachury, M. V. (2017) Tubulin acetylation protects long-lived microtubules against mechanical ageing. *Nat Cell Biol* **19**, 391-+
76. Xu, Z. J., Schaedel, L., Portran, D., Aguilar, A., Gaillard, J., Marinkovich, M. P., Thery, M., and Nachury, M. V. (2017) Microtubules acquire resistance from mechanical breakage through intralumenal acetylation. *Science* **356**, 328-332
77. Nogales, E., Whittaker, M., Milligan, R. A., and Downing, K. H. (1999) High-resolution model of the microtubule. *Cell* **96**, 79-88

78. Cai, D. W., McEwen, D. P., Martens, J. R., Meyhofer, E., and Verhey, K. J. (2009) Single Molecule Imaging Reveals Differences in Microtubule Track Selection Between Kinesin Motors. *Plos Biol* **7**
79. Dompierre, J. P., Godin, J. D., Charrin, B. C., Cordelieres, F. P., King, S. J., Humbert, S., and Saudou, F. (2007) Histone deacetylase 6 inhibition compensates for the transport deficit in Huntington's disease by increasing tubulin acetylation. *J Neurosci* **27**, 3571-3583
80. Sudo, H., and Baas, P. W. (2010) Acetylation of Microtubules Influences Their Sensitivity to Severing by Katanin in Neurons and Fibroblasts. *J Neurosci* **30**, 7215-7226
81. Akella, J. S., Wloga, D., Kim, J., Starostina, N. G., Lyons-Abbott, S., Morrissette, N. S., Dougan, S. T., Kipreos, E. T., and Gaertig, J. (2010) MEC-17 is an alpha-tubulin acetyltransferase. *Nature* **467**, 218-U111
82. Shida, T., Cueva, J. G., Xu, Z., Goodman, M. B., and Nachury, M. V. (2010) The major alpha-tubulin K40 acetyltransferase alphaTAT1 promotes rapid ciliogenesis and efficient mechanosensation. *Proc Natl Acad Sci U S A* **107**, 21517-21522
83. Ohkawa, N., Sugisaki, S., Tokunaga, E., Fujitani, K., Hayasaka, T., Setou, M., and Inokuchi, K. (2008) N-acetyltransferase ARD1-NAT1 regulates neuronal dendritic development. *Genes Cells* **13**, 1171-1183
84. Grant, P. A., Eberharter, A., John, S., Cook, R. G., Turner, B. M., and Workman, J. L. (1999) Expanded lysine acetylation specificity of Gcn5 in native complexes. *J Biol Chem* **274**, 5895-5900
85. Shida, T., Cueva, J. G., Xu, Z. J., Goodman, M. B., and Nachury, M. V. (2010) The major alpha-tubulin K40 acetyltransferase alpha TAT1 promotes rapid ciliogenesis and efficient mechanosensation. *P Natl Acad Sci USA* **107**, 21517-21522
86. Zhang, Y., Kwon, S., Yamaguchi, T., Cubizolles, F., Rousseaux, S., Kneissel, M., Cao, C., Li, N., Cheng, H. L., Chua, K., Lombard, D., Mizeracki, A., Matthias, G., Alt, F. W., Khochbin, S., and Matthias, P. (2008) Mice lacking histone deacetylase 6 have hyperacetylated tubulin but are viable and develop normally. *Mol Cell Biol* **28**, 1688-1701
87. Chu, C. W., Hou, F. J., Zhang, J. M., Phu, L., Loktev, A. V., Kirkpatrick, D. S., Jackson, P. K., Zhao, Y. M., and Zou, H. (2011) A novel acetylation of beta-tubulin by San modulates microtubule polymerization via down-regulating tubulin incorporation. *Mol Biol Cell* **22**, 448-456
88. Kovacs, J. J., Murphy, P. J., Gaillard, S., Zhao, X., Wu, J. T., Nicchitta, C. V., Yoshida, M., Toft, D. O., Pratt, W. B., and Yao, T. P. (2005) HDAC6 regulates Hsp90 acetylation and chaperone-dependent activation of glucocorticoid receptor. *Mol Cell* **18**, 601-607
89. Murphy, P. J., Morishima, Y., Kovacs, J. J., Yao, T. P., and Pratt, W. B. (2005) Regulation of the dynamics of hsp90 action on the glucocorticoid receptor by acetylation/deacetylation of the chaperone. *J Biol Chem* **280**, 33792-33799
90. Bali, P., Pranpat, M., Bradner, J., Balasis, M., Fiskus, W., Guo, F., Rocha, K., Kumaraswamy, S., Boyapalle, S., Atadja, P., Seto, E., and Bhalla, K. (2005) Inhibition of histone deacetylase 6 acetylates and disrupts the chaperone function of heat shock protein 90: a novel basis for antileukemia activity of histone deacetylase inhibitors. *J Biol Chem* **280**, 26729-26734
91. Scroggins, B. T., Robzyk, K., Wang, D. X., Marcu, M. G., Tsutsumi, S., Beebe, K., Cotter, R. J., Felts, S., Toft, D., Karnitz, L., Rosen, N., and Neckers, L. (2007) An acetylation site in the middle domain of Hsp90 regulates chaperone function. *Mol Cell* **25**, 151-159
92. Kekatpure, V. D., Dannenberg, A. J., and Subbaramaiah, K. (2009) HDAC6 modulates Hsp90 chaperone activity and regulates activation of aryl hydrocarbon receptor signaling. *J Biol Chem* **284**, 7436-7445
93. Wu, H., and Parsons, J. T. (1993) Cortactin, an 80/85-Kilodalton Pp60(Src) Substrate, Is a Filamentous Actin-Binding Protein Enriched in the Cell Cortex. *J Cell Biol* **120**, 1417-1426
94. Li, Y., Zhang, X. W., Polakiewicz, R. D., Yao, T. P., and Comb, M. J. (2008) HDAC6 is required for epidermal growth factor-induced beta-catenin nuclear localization. *Journal of Biological Chemistry* **283**, 12686-12690
95. Nelson, W. J., and Nusse, R. (2004) Convergence of Wnt, beta-catenin, and cadherin pathways. *Science* **303**, 1483-1487

96. Liu, C., Li, Y., Semenov, M., Han, C., Baeg, G. H., Tan, Y., Zhang, Z., Lin, X., and He, X. (2002) Control of beta-catenin phosphorylation/degradation by a dual-kinase mechanism. *Cell* **108**, 837-847
97. Parmigiani, R. B., Xu, W. S., Venta-Perez, G., Erdjument-Bromage, H., Yaneva, M., Tempst, P., and Marks, P. A. (2008) HDAC6 is a specific deacetylase of peroxiredoxins and is involved in redox regulation. *Proc Natl Acad Sci U S A* **105**, 9633-9638
98. Inoue, A., Yoshida, N., Omoto, Y., Oguchi, S., Yamori, T., Kiyama, R., and Hayashi, S. (2002) Development of cDNA microarray for expression profiling of estrogen-responsive genes. *J Mol Endocrinol* **29**, 175-192
99. Yu, X. W., Guo, S. P., Song, W. H., Xiang, T. X., Yang, C. C., Tao, K., Zhou, L., Cao, Y. J., and Liu, S. C. (2017) Estrogen receptor a (ER alpha) status evaluation using RNAscope in situ hybridization: a reliable and complementary method for IHC in breast cancer tissues. *Hum Pathol* **61**, 121-129
100. Zhang, Z. H., Yamashita, H., Toyama, T., Sugiura, H., Omoto, Y., Ando, Y., Mita, K., Hamaguchi, M., Hayashi, S., and Iwase, H. (2004) HDAC6 expression is correlated with better survival in breast cancer. *Clin Cancer Res* **10**, 6962-6968
101. Sakuma, T., Uzawa, K., Onda, T., Shiiba, M., Yokoe, H., Shibahara, T., and Tanzawa, H. (2006) Aberrant expression of histone deacetylase 6 in oral squamous cell carcinoma. *Int J Oncol* **29**, 117-124
102. Bradbury, C. A., Khanim, F. L., Hayden, R., Bunce, C. M., White, D. A., Drayson, M. T., Craddock, C., and Turner, B. M. (2005) Histone deacetylases in acute myeloid leukaemia show a distinctive pattern of expression that changes selectively in response to deacetylase inhibitors. *Leukemia* **19**, 1751-1759
103. Zhang, S. L., Zhu, H. Y., Zhou, B. Y., Chu, Y., Huo, J. R., Tan, Y. Y., and Liu, D. L. (2019) Histone deacetylase 6 is overexpressed and promotes tumor growth of colon cancer through regulation of the MAPK/ERK signal pathway. *Oncotargets Ther* **12**, 2409-2419
104. Wickstrom, S. A., Masoumi, K. C., Khochbin, S., Fassler, R., and Massoumi, R. (2010) CYLD negatively regulates cell-cycle progression by inactivating HDAC6 and increasing the levels of acetylated tubulin. *Embo J* **29**, 131-144
105. Blandino, G., Levine, A. J., and Oren, M. (1999) Mutant p53 gain of function: differential effects of different p53 mutants on resistance of cultured cells to chemotherapy. *Oncogene* **18**, 477-485
106. Ryu, H. W., Shin, D. H., Lee, D. H., Choi, J., Han, G., Lee, K. Y., and Kwon, S. H. (2017) HDAC6 deacetylates p53 at lysines 381/382 and differentially coordinates p53-induced apoptosis. *Cancer Lett* **391**, 162-171
107. Woan, K. V., Lienlaf, M., Perez-Villaroel, P., Lee, C., Cheng, F., Knox, T., Woods, D. M., Barrios, K., Powers, J., Sahakian, E., Wang, H. W., Canales, J., Marante, D., Smalley, K. S. M., Bergman, J., Seto, E., Kozikowski, A., Pinilla-Ibarz, J., Sarnaik, A., Celis, E., Weber, J., Sotomayor, E. M., and Villagra, A. (2015) Targeting histone deacetylase 6 mediates a dual anti-melanoma effect: Enhanced antitumor immunity and impaired cell proliferation. *Mol Oncol* **9**, 1447-1457
108. Fortin, N. J., Agster, K. L., and Eichenbaum, H. B. (2002) Critical role of the hippocampus in memory for sequences of events. *Nat Neurosci* **5**, 458-462
109. Simoes-Pires, C., Zwick, V., Nurisso, A., Schenker, E., Carrupt, P. A., and Cuendet, M. (2013) HDAC6 as a target for neurodegenerative diseases: what makes it different from the other HDACs? *Mol Neurodegener* **8**, 7
110. Perez, M., Santa-Maria, I., Gomez de Barreda, E., Zhu, X., Cuadros, R., Cabrero, J. R., Sanchez-Madrid, F., Dawson, H. N., Vitek, M. P., Perry, G., Smith, M. A., and Avila, J. (2009) Tau--an inhibitor of deacetylase HDAC6 function. *J Neurochem* **109**, 1756-1766
111. Govindarajan, N., Rao, P., Burkhardt, S., Sananbenesi, F., Schluter, O. M., Bradke, F., Lu, J., and Fischer, A. (2013) Reducing HDAC6 ameliorates cognitive deficits in a mouse model for Alzheimer's disease. *EMBO Mol Med* **5**, 52-63
112. Su, M., Shi, J. J., Yang, Y. P., Li, J., Zhang, Y. L., Chen, J., Hu, L. F., and Liu, C. F. (2011) HDAC6 regulates aggresome-autophagy degradation pathway of alpha-synuclein in response to MPP+-induced stress. *J Neurochem* **117**, 112-120

113. Du, G. P., Liu, X. A., Chen, X. P., Song, M., Yan, Y., Jiao, R. J., and Wang, C. C. (2010) Drosophila Histone Deacetylase 6 Protects Dopaminergic Neurons against alpha-Synuclein Toxicity by Promoting Inclusion Formation. *Mol Biol Cell* **21**, 2128-2137
114. Jiang, Q., Ren, Y., and Feng, J. (2008) Direct binding with histone deacetylase 6 mediates the reversible recruitment of parkin to the centrosome. *J Neurosci* **28**, 12993-13002
115. Iwata, A., Riley, B. E., Johnston, J. A., and Kopito, R. R. (2005) HDAC6 and microtubules are required for autophagic degradation of aggregated huntingtin. *J Biol Chem* **280**, 40282-40292
116. Hahnen, E., Hauke, J., Trankle, C., Eyupoglu, I. Y., Wirth, B., and Blumcke, I. (2008) Histone deacetylase inhibitors: possible implications for neurodegenerative disorders. *Expert Opin Investig Drugs* **17**, 169-184
117. Finnin, M. S., Donigian, J. R., Cohen, A., Richon, V. M., Rifkind, R. A., Marks, P. A., Breslow, R., and Pavletich, N. P. (1999) Structures of a histone deacetylase homologue bound to the TSA and SAHA inhibitors. *Nature* **401**, 188-193
118. Ago, T., Liu, T., Zhai, P., Chen, W., Li, H., Molkentin, J. D., Vatner, S. F., and Sadoshima, J. (2008) A redox-dependent pathway for regulating class II HDACs and cardiac hypertrophy. *Cell* **133**, 978-993
119. Lombardi, P. M., Cole, K. E., Dowling, D. P., and Christianson, D. W. (2011) Structure, mechanism, and inhibition of histone deacetylases and related metalloenzymes. *Curr Opin Struct Biol* **21**, 735-743
120. Maolanon, A. R., Madsen, A. S., and Olsen, C. A. (2016) Innovative Strategies for Selective Inhibition of Histone Deacetylases. *Cell Chem Biol* **23**, 759-768
121. Dowling, D. P., Gantt, S. L., Gattis, S. G., Fierke, C. A., and Christianson, D. W. (2008) Structural studies of human histone deacetylase 8 and its site-specific variants complexed with substrate and inhibitors. *Biochemistry-Us* **47**, 13554-13563
122. Miller, T. A., Witter, D. J., and Belvedere, S. (2003) Histone deacetylase inhibitors. *J Med Chem* **46**, 5097-5116
123. Kosugi, H., Ito, M., Yamamoto, Y., Towatari, M., Ito, M., Ueda, R., Saito, H., and Naoe, T. (2001) In vivo effects of a histone deacetylase inhibitor, FK228, on human acute promyelocytic leukemia in NOD / Shi-scid/scid mice. *Jpn J Cancer Res* **92**, 529-536
124. Sasakawa, Y., Naoe, Y., Inoue, T., Sasakawa, T., Matsuo, M., Manda, T., and Mutoh, S. (2003) Effects of FK228, a novel histone deacetylase inhibitor, on tumor growth and expression of p21 and c-myc genes in vivo. *Cancer Lett* **195**, 161-168
125. Elbeltagi, H. M., Martens, A. C. M., Lelieveld, P., Haroun, E. A., and Hagenbeek, A. (1993) Acetyldinaline - a New Oral Cytostatic Drug with Impressive Differential Activity against Leukemic-Cells and Normal Stem-Cells - Preclinical Studies in a Relevant Rat Model for Human Acute Myelocytic-Leukemia. *Cancer Research* **53**, 3008-3014
126. Suzuki, T., Ando, T., Tsuchiya, K., Fukazawa, N., Saito, A., Mariko, Y., Yamashita, T., and Nakanishi, O. (1999) Synthesis and histone deacetylase inhibitory activity of new benzamide derivatives. *J Med Chem* **42**, 3001-3003
127. Jaboin, J., Wild, J., Hamidi, H., Khanna, C., Kim, C. J., Robey, R., Bates, S. E., and Thiele, C. J. (2002) MS-27-275, an inhibitor of histone deacetylase, has marked in vitro and in vivo antitumor activity against pediatric solid tumors. *Cancer Res* **62**, 6108-6115
128. Saito, A., Yamashita, T., Mariko, Y., Nosaka, Y., Tsuchiya, K., Ando, T., Suzuki, T., Tsuruo, T., and Nakanishi, O. (1999) A synthetic inhibitor of histone deacetylase, MS-27-275, with marked in vivo antitumor activity against human tumors. *Proc Natl Acad Sci U S A* **96**, 4592-4597
129. Komatsu, Y., Tomizaki, K. Y., Tsukamoto, M., Kato, T., Nishino, N., Sato, S., Yamori, T., Tsuruo, T., Furumai, R., Yoshida, M., Horinouchi, S., and Hayashi, H. (2001) Cyclic hydroxamic-acid-containing peptide 31, a potent synthetic histone deacetylase inhibitor with antitumor activity. *Cancer Res* **61**, 4459-4466
130. Furumai, R., Komatsu, Y., Nishino, N., Khochbin, S., Yoshida, M., and Horinouchi, S. (2001) Potent histone deacetylase inhibitors built from trichostatin A and cyclic tetrapeptide antibiotics including trapoxin. *Proc Natl Acad Sci U S A* **98**, 87-92
131. Breslow, R., Belvedere, S., and Gershell, L. (2000) Development of cytodifferentiating agents for cancer chemotherapy. *Helv Chim Acta* **83**, 1685-1692

132. Arrowsmith, C. H., Bountra, C., Fish, P. V., Lee, K., and Schapira, M. (2012) Epigenetic protein families: a new frontier for drug discovery. *Nat Rev Drug Discov* **11**, 384-400
133. Prior, R., Van Helleputte, L., Klingl, Y. E., and Van Den Bosch, L. (2018) HDAC6 as a potential therapeutic target for peripheral nerve disorders. *Expert Opin Ther Tar* **22**, 993-1007
134. Kuendgen, A., Schmid, M., Schlenk, R., Knipp, S., Hildebrandt, B., Steidl, C., Germing, U., Haas, R., Dohner, H., and Gattermann, N. (2006) The histone deacetylase (HDAC) inhibitor valproic acid as monotherapy or in combination moth all-trans retinoic acid in patients with acute myeloid leukemia. *Cancer-Am Cancer Soc* **106**, 112-119
135. Negmeldin, A. T., and Pflum, M. K. H. (2017) The structural requirements of histone deacetylase inhibitors: SAHA analogs modified at the C5 position display dual HDAC6/8 selectivity. *Bioorg Med Chem Lett* **27**, 3254-3258
136. Scuto, A., Kirschbaum, M., Kowolik, C., Kretzner, L., Juhasz, A., Atadja, P., Pullarkat, V., Bhatia, R., Forman, S., Yen, Y., and Jove, R. (2008) The novel histone deacetylase inhibitor, LBH589, induces expression of DNA damage response genes and apoptosis in Ph- acute lymphoblastic leukemia cells. *Blood* **111**, 5093-5100
137. Plumb, J. A., Finn, P. W., Williams, R. J., Bandara, M. J., Romero, M. R., Watkins, C. J., La Thangue, N. B., and Brown, R. (2003) Pharmacodynamic response and inhibition of growth of human tumor xenografts by the novel histone deacetylase inhibitor PXD101. *Mol Cancer Ther* **2**, 721-728
138. Furumai, R., Matsuyama, A., Kobashi, N., Lee, K. H., Nishiyama, M., Nakajima, H., Tanaka, A., Komatsu, Y., Nishino, N., Yoshida, M., and Horinouchi, S. (2002) FK228 (depsipeptide) as a natural prodrug that inhibits class I histone deacetylases. *Cancer Res* **62**, 4916-4921
139. Zhang, L., Zhang, J., Jiang, Q. X., Zhang, L., and Song, W. G. (2018) Zinc binding groups for histone deacetylase inhibitors. *J Enzym Inhib Med Ch* **33**, 714-721
140. Tatamiya, T., Saito, A., Sugawara, T., and Nakanishi, O. (2004) Isozyme-selective activity of the HDAC inhibitor MS-275. *Cancer Research* **64**, 567-567
141. Suraweera, A., O'Byrne, K. J., and Richard, D. J. (2018) Combination Therapy With Histone Deacetylase Inhibitors (HDACi) for the Treatment of Cancer: Achieving the Full Therapeutic Potential of HDACi. *Front Oncol* **8**
142. Codd, R. (2008) Traversing the coordination chemistry and chemical biology of hydroxamic acids. *Coordin Chem Rev* **252**, 1387-1408
143. Drummond, D. C., Noble, C. O., Kirpotin, D. B., Guo, Z., Scott, G. K., and Benz, C. C. (2005) Clinical development of histone deacetylase inhibitors as anticancer agents. *Annu Rev Pharmacol Toxicol* **45**, 495-528
144. Diedrich, D., Hamacher, A., Gertzen, C. G., Alves Avelar, L. A., Reiss, G. J., Kurz, T., Gohlke, H., Kassack, M. U., and Hansen, F. K. (2016) Rational design and diversity-oriented synthesis of peptoid-based selective HDAC6 inhibitors. *Chem Commun (Camb)* **52**, 3219-3222
145. Zhang, Y., Ying, J. B., Hong, J. J., Li, F. C., Fu, T. T., Yang, F. Y., Zheng, G. X., Yao, X. J., Lou, Y., Qiu, Y. Q., Xue, W. W., and Zhu, F. (2019) How Does Chirality Determine the Selective Inhibition of Histone Deacetylase 6? A Lesson from Trichostatin A Enantiomers Based on Molecular Dynamics. *Acs Chem Neurosci* **10**, 2467-2480
146. Senger, J., Melesina, J., Marek, M., Romier, C., Oehme, I., Witt, O., Sippl, W., and Jung, M. (2016) Synthesis and Biological Investigation of Oxazole Hydroxamates as Highly Selective Histone Deacetylase 6 (HDAC6) Inhibitors. *J Med Chem* **59**, 1545-1555
147. Sysak, A., and Obminska-Mrukowicz, B. (2017) Isoxazole ring as a useful scaffold in a search for new therapeutic agents. *Eur J Med Chem* **137**, 292-309
148. Knox, T., Sahakian, E., Banik, D., Hadley, M., Palmer, E., Noonepalle, S., Kim, J., Powers, J., Gracia-Hernandez, M., Oliveira, V., Cheng, F. D., Chen, J., Barinka, C., Pinilla-Ibarz, J., Lee, N. H., Kozikowski, A., and Villagra, A. (2019) Selective HDAC6 inhibitors improve anti-PD-1 immune checkpoint blockade therapy by decreasing the anti-inflammatory phenotype of macrophages and down-regulation of immunosuppressive proteins in tumor cells. *Sci Rep-Uk* **9**
149. North, B. J., Marshall, B. L., Borra, M. T., Denu, J. M., and Verdin, E. (2003) The human Sir2 ortholog, SIRT2, is an NAD+-dependent tubulin deacetylase. *Mol Cell* **11**, 437-444
150. Zhao, Z., Xu, H., and Gong, W. (2010) Histone deacetylase 6 (HDAC6) is an independent deacetylase for alpha-tubulin. *Protein Pept Lett* **17**, 555-558

151. Miyake, Y., Keusch, J. J., Wang, L., Saito, M., Hess, D., Wang, X., Melancon, B. J., Helquist, P., Gut, H., and Matthias, P. (2016) Structural insights into HDAC6 tubulin deacetylation and its selective inhibition. *Nat Chem Biol* **12**, 748-754
152. Schultz, B. E., Misialek, S., Wu, J., Tang, J., Conn, M. T., Tahilramani, R., and Wong, L. (2004) Kinetics and comparative reactivity of human class I and class IIb histone deacetylases. *Biochemistry-Us* **43**, 11083-11091
153. Lai, M. J., Huang, H. L., Pan, S. L., Liu, Y. M., Peng, C. Y., Lee, H. Y., Yeh, T. K., Huang, P. H., Teng, C. M., Chen, C. S., Chuang, H. Y., and Liou, J. P. (2012) Synthesis and biological evaluation of 1-arylsulfonyl-5-(N-hydroxyacrylamide)indoles as potent histone deacetylase inhibitors with antitumor activity in vivo. *J Med Chem* **55**, 3777-3791
154. Bergman, J. A., Woan, K., Perez-Villarroel, P., Villagra, A., Sotomayor, E. M., and Kozikowski, A. P. (2012) Selective histone deacetylase 6 inhibitors bearing substituted urea linkers inhibit melanoma cell growth. *J Med Chem* **55**, 9891-9899
155. Kutil, Z., Skultetyova, L., Rauh, D., Meleshin, M., Snajdr, I., Novakova, Z., Mikesova, J., Pavlicek, J., Hadzima, M., Baranova, P., Havlinova, B., Majer, P., Schutkowski, M., and Barinka, C. (2019) The unraveling of substrate specificity of histone deacetylase 6 domains using acetylome peptide microarrays and peptide libraries. *FASEB J* **33**, 4035-4045
156. Riester, D., Hildmann, C., Grunewald, S., Beckers, T., and Schwienhorst, A. (2007) Factors affecting the substrate specificity of histone deacetylases. *Biochem Biophys Res Commun* **357**, 439-445
157. Szyk, A., Deaconescu, A. M., Spector, J., Goodman, B., Valenstein, M. L., Ziolkowska, N. E., Kormendi, V., Grigorieff, N., and Roll-Mecak, A. (2014) Molecular Basis for Age-Dependent Microtubule Acetylation by Tubulin Acetyltransferase. *Cell* **157**, 1405-1415
158. Coombes, C., Yamamoto, A., McClellan, M., Reid, T. A., Plooster, M., Luxton, G. W., Alper, J., Howard, J., and Gardner, M. K. (2016) Mechanism of microtubule lumen entry for the alpha-tubulin acetyltransferase enzyme alphaTAT1. *Proc Natl Acad Sci U S A* **113**, E7176-E7184
159. Dunker, A. K., Lawson, J. D., Brown, C. J., Williams, R. M., Romero, P., Oh, J. S., Oldfield, C. J., Campen, A. M., Ratliff, C. R., Hipps, K. W., Ausio, J., Nissen, M. S., Reeves, R., Kang, C. H., Kissinger, C. R., Bailey, R. W., Griswold, M. D., Chiu, M., Garner, E. C., and Obradovic, Z. (2001) Intrinsically disordered protein. *J Mol Graph Model* **19**, 26-59
160. Qiu, Y., Zhao, Y., Becker, M., John, S., Parekh, B. S., Huang, S., Hendarwanto, A., Martinez, E. D., Chen, Y., Lu, H., Adkins, N. L., Stavreva, D. A., Wiench, M., Georgel, P. T., Schiltz, R. L., and Hager, G. L. (2006) HDAC1 acetylation is linked to progressive modulation of steroid receptor-induced gene transcription. *Mol Cell* **22**, 669-679
161. Eckschlager, T., Plch, J., Stiborova, M., and Hrabeta, J. (2017) Histone Deacetylase Inhibitors as Anticancer Drugs. *Int J Mol Sci* **18**
162. Montgomery, R. L., Davis, C. A., Potthoff, M. J., Haberland, M., Fielitz, J., Qi, X., Hill, J. A., Richardson, J. A., and Olson, E. N. (2007) Histone deacetylases 1 and 2 redundantly regulate cardiac morphogenesis, growth, and contractility. *Genes Dev* **21**, 1790-1802
163. Yamaguchi, M., Tonou-Fujimori, N., Komori, A., Maeda, R., Nojima, Y., Li, H., Okamoto, H., and Masai, I. (2005) Histone deacetylase 1 regulates retinal neurogenesis in zebrafish by suppressing Wnt and Notch signaling pathways. *Development* **132**, 3027-3043
164. Douglas, J. G., and Sondak, V. K. (2004) RE: A comparison of survival rates for treatment of melanoma metastatic to the brain. *Cancer Invest* **22**, 643-644
165. Miranda, E. P. (2004) Management of cutaneous melanoma. *New Engl J Med* **351**, 2770-2771
166. Liu, J., Gu, J., Feng, Z., Yang, Y., Zhu, N., Lu, W., and Qi, F. (2016) Both HDAC5 and HDAC6 are required for the proliferation and metastasis of melanoma cells. *J Transl Med* **14**, 7
167. Lienlaf, M., Perez-Villarroel, P., Knox, T., Pabon, M., Sahakian, E., Powers, J., Woan, K. V., Lee, C., Cheng, F., Deng, S., Smalley, K. S. M., Montecino, M., Kozikowski, A., Pinilla-Ibarz, J., Sarnaik, A., Seto, E., Weber, J., Sotomayor, E. M., and Villagra, A. (2016) Essential role of HDAC6 in the regulation of PD-L1 in melanoma. *Molecular Oncology* **10**, 735-750
168. Crosby, T., Fish, R., Coles, B., and Mason, M. (2018) Systemic treatments for metastatic cutaneous melanoma (vol 6, CD011123, 2018). *Cochrane Db Syst Rev*
169. Freitas, M. F., Cuendet, M., and Bertrand, P. (2018) HDAC inhibitors: a 2013-2017 patent survey. *Expert Opin Ther Pat* **28**, 365-381

170. Porter, N. J., Mahendran, A., Breslow, R., and Christianson, D. W. (2017) Unusual zinc-binding mode of HDAC6-selective hydroxamate inhibitors. *Proc Natl Acad Sci U S A* **114**, 13459-13464
171. Porter, N. J., Osko, J. D., Diedrich, D., Kurz, T., Hooker, J. M., Hansen, F. K., and Christianson, D. W. (2018) Histone Deacetylase 6-Selective Inhibitors and the Influence of Capping Groups on Hydroxamate-Zinc Denticity. *J Med Chem* **61**, 8054-8060
172. Yang, L., and Zhang, Y. (2017) Tumor-associated macrophages: from basic research to clinical application. *J Hematol Oncol* **10**
173. Mills, C. D., Lenz, L. L., and Harris, R. A. (2016) A Breakthrough: Macrophage-Directed Cancer Immunotherapy. *Cancer Research* **76**, 513-516
174. Liu, J. Q., Luan, W. J., Zhang, Y., Gu, J. Y., Shi, Y. D., Yang, Y. W., Feng, Z. H., and Qi, F. Z. (2018) HDAC6 interacts with PTPN1 to enhance melanoma cells progression. *Biochem Bioph Res Co* **495**, 2630-2636